TEXTURAL AND MICROSTRUCTURAL CHANGES DURING WARM ROLLING OF AN EXTRA LOW CARBON AND TWO INTERSTITIAL FREE STEELS

by

ARUNANSU HALDAR

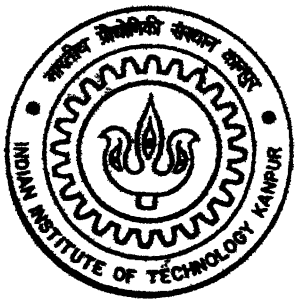

Department of Materials and Metallurgical Engineering
INDIAN INSTITUTE OF TECHNOLOGY KANPUR

June, 2001

TEXTURAL AND MICROSTRUCTURAL CHANGES DURING WARM ROLLING OF AN EXTRA LOW CARBON AND TWO INTERSTITIAL FREE STEELS

A Thesis Submitted

in Partial Fulfilment of the Requirements

for the degree of

DOCTOR OF PHILOSOPHY

by

ARUNANSU HALDAR

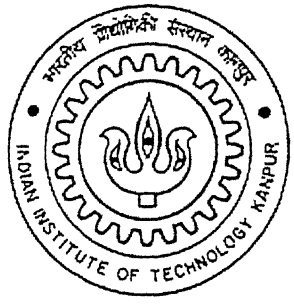

Department of Materials and Metallurgical Engineering
INDIAN INSTITUTE OF TECHNOLOGY KANPUR

June, 2001

Certificate

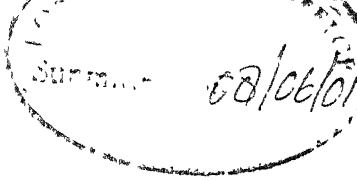

It is certified that the work contained in the thesis entitled **"Textural and Microstructural Changes During Warm Rolling of an Extra Low Carbon and Two Interstitial Free Steels"**, has been carried out by Arunansu Haldar (Roll No. 9620671) under our supervision. This work has not been submitted elsewhere for a degree.

Date : 31st May, 2001

(Professor R.K. Ray)

Department of Materials and Metallurgical Engineering
Indian Institute of Technology
Kanpur - 208016

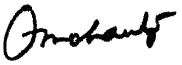

(Dr. O.N. Mohanty)

Chief, R&D Division
Tata Steel
Jamshedpur - 831007

Certificate

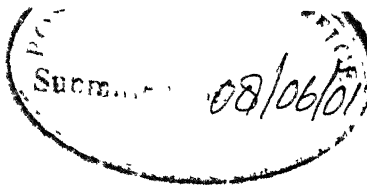

It is certified that the work contained in the thesis entitled **"Textural and Microstructural Changes During Warm Rolling of an Extra Low Carbon and Two Interstitial Free Steels"**, has been carried out by Arunansu Haldar (Roll No. 9620671) under our supervision. This work has not been submitted elsewhere for a degree.

Date : 31st May, 2001

(Professor R.K. Ray)

Department of Materials and Metallurgical Engineering
Indian Institute of Technology
Kanpur - 208016

(Dr. O.N. Mohanty)

Chief, R&D Division
Tata Steel
Jamshedpur - 831007

Dedicated to my
Parents, wife and daughter

Acknowledgements

At the outset I would like to tender my deepest reverence and most sincere gratitude to my teacher and thesis supervisor Prof. R.K. Ray for his earnest involvement, competent guidance and lively impetus, without which this work could not have seen the light of the day. It would be befitting to mention that he is also a friend and philosopher to me. He was very careful not only to my research work, but also at every moment of my stay at the campus of IIT, Kanpur. I want to show my sincere regards to such a great personality.

I also gratefully express my sincere gratitude to Prof. O.N. Mohanty, Chief of R&D Division, Tata Steel and my co- supervisor, for his sincere guidance and cooperation at various stages of this work. Without his co-operation this work could not have been completed.

It is worth mentioning that this work could not have taken this shape unless the Management of Tata Steel would allow and support me for this work. It is the management of Tata Steel, to whom I am greatly indebted for giving me this great opportunity for pursuing higher study. I personally also want to express my sincere gratitude to Dr. T. Mukherjee, Executive Director, Tata Steel and Dr. Amit Chatterjee, G.M. (Technical), Tatasteel, who were instrumental behind this research project.

I also sincerly remember the the management of SAIL, R&D and particularly Mr. D.Sengupta for providing experimental rolling mill and taking special care in carrying out precision rolling experiment for this work. I am grateful to Prof. G. Gottstein, Director of *Institute fur Allgemeine Metallkunde und Metallphysik. RWTH, Aachhen, Germany*, for his kind help and cooperation for complete texture measurements for this work. I sincerely thank Prof. R.I. Ganguly, Dr. R.C Behera and Dr. A.K. Panda of REC, Rourkella for their kind support. My thanks are also due to Prof. P.R. Ramchandra Rao, Director, NML, Jamshedpur for providing TEM facility for this work. I am personally grateful to Mr. Samar Das of NML for his kind help in carrying out TEM work.

I want to specially thank Mr. V. Kumar, Crystal Growth Laboratory, IIT Kanpur for his untiring support through out my stay at IIT, Kanpur. Without his help this work could not have been completed.

I also sincerely acknowledge the help and support given by Mr. A.J. Khan in carrying out metallography work. Special thanks are also due to A.K.Verma, Pankaj, Munnaji, Jana, Samantada, Vikram, Gopal and Sumit and others for their constant cooperation and help during this work.

I want to thank Prof. R.I. Ganguly, Prof. R.C. Behera of REC Rourkella, for their kind help in carrying out so many experiments of my work.

This occasion is perfectly befitting to acknowledge specially Samit and Rajib, who had always been so kind on me to take special interest in doing major preparation work for the thesis. Simply words are not sufficient to acknowledge their kind help at every moments of my stay at IIT, Kanpur. I specially acknowledge Samit, who was always been a source of my energy at IITK, without his support, almost at every step, my work would not have been completed. My association with them will be ever-cherishable memory in my life.

My sincere thanks due to also Surajit, Santosh , Kesta, Ani, and our Btop group, for their kind help and support in making my stay at hall V ever memorable. I will really miss their association and specially the cooking at B top when I go out of this campus. Thanks are due to also Sandip. Arindam, Sanjoy, Mukut and Pada, for their help at various stages of my work.

This is the right occasion to remember with reverence the sacrifices encouragement and moral supports of my parents, my wife Nupur and daughter Shalmoli, who always remained behind the scene but was stead fast in providing me every sort of support and inspiration through out this work without which I would not have reached this stage.

Arunansu Haldar

Contents

List of Figures

List of Tables

Synopsis

An attempt has been made in the present investigation to study the microstructural and textural changes which occur in an extra low carbon (ELC) steel and two interstitial free (IF) steels after warm rolling and after subsequent recrystallisation annealinng.

The steels were soaked at two different temperatures - 1150 ^{o}C (in the γ range) and 830 ^{o}C (in the α range) and then subjected to warm rolling in single pass using wedge-shaped samples. Bar-shaped specimens were soaked at 1150 ^{o}C, followed by multipass rolling. Here three different rolling schedules were chosen in which different amounts of rolling reductions were given in the γ and in the α range, keeping total amounts of reduction in the three schedules nearly constant. In schedule 1 most of the reduction was given in the γ regime, while lesser amount of reduction in γ and greater amount in α were given in schedule 2. In schedule 3 the entire amount of deformation was given in the α regime in a number of passes. Four different finish rolling temperatures - 800 ^{o}C, 700 ^{o}C, 600 ^{o}C and 500 ^{o}C were used in both single pass and multipass rolling schedules. All the warm rolled steels were further subjected to recrystallisation annealing at 775 ^{o}C for 25 minutes.

The microstructures of the different warm rolled and annealed samples were characterised using optical, scanning electron (SEM) and transmission electron microscopy (TEM). Profusion of deformation bands (DB) formed in all three steels after warm rolling. The densities of deformation bands were carefully measured in all warm rolled samples

and the normalised dislocation densities were determined from relevant hardness values. Flow stress curves for different samples were generated from hot compression test data. Crystallographic textures were determined from all the warm rolled and annealed materials by calculating the orientation distribution functions (ODFs) from a number of pole figures. The texture data have been plotted in the form of φ_1 sections, $\varphi_2 = 45^{O}$ sections and the α, γ, η, ζ, and ε fibre plots.

The analysis of the flow stress data indicates that the high temperature γ phase undergoes both dynamic recovery and recrystallisation, whereas dynamic recovery seems to be the predominant relaxation process in ferrite when warm rolled in the upper α range such as 800 ^{O}C and 700 ^{O}C. Post dynamic static relaxation processes occur during the interpass holding times in multipass rolling. Microstructural observations broadly corroborate the above findings.

After single pass rolling, the ELC steel shows the highest density of deformation bands at 500 ^{O}C FRT. The DB density in this steel decreases rapidly with increasing FRT, becoming nearly zero at an FRT of 800 ^{O}C. The samples soaked at higher temperature of 1150 ^{O}C show slightly higher DB densities than the ones soaked at the lower temperature of 830 ^{O}C. In general, the ELC steel samples show rather low DB densities after multipass rolling, the samples of schedule 3 showing higher DB density than those subjected to the other two schedules. The two IF steels do not show any wide variation in DB density with steel composition, soaking temperature or FRT, both after single and after multipass

rolling. The multipass rolled samples show slightly lower DB density values than the single pass rolled samples.

The deformation bands appear to make a series of angles with the rolling direction, starting from rather low angles going up to ~ ± 35 ^{o}. Deformation bands with angles up to ± 25 ^{o} constitute nearly 80 to 90 percent of the cumulative frequency. These band angles do not show any significant correlation with steel composition, soaking temperature, FRT or the relative amounts of deformation given in the γ and α ranges during multipass rolling.

All three steels, single pass as well as multipass rolled, exhibit the highest values of normalised dislocation density at the FRT of 500 ^{o}C. The high value decreases rapidly with increasing FRT. The rate of this decrease is slower in the two IF steels than in the ELC grade. The single pass rolled samples, in general, show higher levels of normalised dislocation densities as compared to the multipass rolled samples.

The ELC steel displays overall sharp textures and high intensities of the γ fibre after single pass rolling at the FRTs of 500 ^{o}C and 600 ^{o}C. The γ fibre intensity reduces to near zero at higher FRTs. Moderately strong γ fibres develop in both the IF steels after single pass rolling at all the four FRTs. It appears that a high value of the γ fibre intensity is directly related to a high value of the deformation band density, and vice versa.

Recrystallisation annealing leads to a drastic reduction of γ fibre intensity in the

ELC steel; by contrast, annealing treatment sharpens the γ fibre intensities in both the warm rolled IF steels.

In all the three steels, multipass rolling generally does not produce as sharp overall textures and γ fibres as are obtained after single pass rolling. Among the three steels, the least sharp texture develops in the ELC grade. Although slight improvements in the γ fibre sharpness after the post warm rolling annealing occur in the two IF steels, the effect of annealing has been found to be insignificant in the ELC steel. The maximum enhancement of the γ fibre intensity is achieved in schedule 3 of the multipass rolling process, where the entire deformation is given in the α temperature regime in several passes.

Of the two IF steels, the Ti enriched composition (steel 3) develops an overall sharper texture and γ fibre intensities, specially after single pass rolling, and these improve further in intensity after the recrystallisation annealing. From the alloy stoichiometry point of view it has been found out that the Nb enriched (steel 2) steel may not be fully stabilised with respect to carbon, while the Ti enriched steel has a fully stabilised composition. This difference is expected to manifest itself in terms of a higher concentration of free carbon solute atoms in the ferrite, in case of the Nb enriched steel, and this could be responsible for the development of weaker γ fibres in this steel as compared to the Ti enriched one. The development of very poor γ fibre intensities in the fully processed ELC steel is presumably due to the presence of a significantly higher concentration of free solute carbon atoms, due to the absence of strong carbide formers, such as Ti or Nb.

Many aspects of the physical metallurgy of warm rolling of steels are not quite clear yet and further detailed investigations are required to understand the underlying principles of strong γ fibre texture development in these steels. In the course of the present investigation it has been felt that a promising line of attack would be to try to understand the precise character of the deformation bands produced during warm rolling and their effects on the development of textures. Orientations belonging to the γ fibre are known to nucleate within the deformation bands during recrystallisation annealing. Evidently much further work is necessary in this direction.

CHAPTER 1
INTRODUCTION

1. Introduction

In the cc nventional industrial practice of production of deep drawable thin strips, hot rolling is usually carried out in the high temperature austenitic region. The hot rolled product is subsequently cold rolled and finally annealed to produce strips of required gauges. For the purpose of saving energy during the whole process an alternative could be to look into the feasibility of producing thin strips right from the hot rolling mill. In fact, over the last decade or so it has been realized that substantial benefit can be obtained by operating the hot strip mill at temperatures 70 ^{o}C or more below the normal austenitic region. The practice of rolling in the upper ferritic region instead of in the austenitic region has been termed as **Warm Rolling** or, alternatively, **Ferritic Rolling.** In fact, rapid development of warm rolling techniques has shown that it is quite possible to produce so-called thin-gauge hot strips well within the thickness ranges of cold strips [Figure 1.1] (1). In conventional austenitic hot rolling of deep drawable steels, hot strips thinner than 1.8 mm can not be produced. This underlines the importance to opt for ferritic rolling by shifting the finish rolling down to the ferritic temperature regime.

Substantial research activities have so far been carried out to understand the metallurgy of hot and cold rolling. Several review papers have already been published on this subject (2 - 5). By contrast, the physical metallurgy involved during warm rolling is not yet fully understood. Changing the rolling temperature from "hot" to "warm" regime may lead to significant changes in deformation characterstistics of the low and ultra low carbon and IF steels (6). This is illustrated in

the Figure 1.2 (1), which is a plot of flow stress as a function of deformation temperature. Although, as expected, flow stress increases uniformly with decreasing temperature of deformation in the hot rolling region (i.e. temperatures over 900 ^{o}C), during warm deformation a sudden change in flow stress behaviour becomes quite apparent. This means that taking care of the mill load during phase transformation along with the proper draft distribution during rolling, particularly at the finishing stands, plays a critical role in terms of smooth operation of the mill. The comparison of conventional austenitic and ferritic rolling is shown in Figure 1.3. There are always some advantages to be gained in rolling in ferritic region as opposed to in the austenitic region. These include energy savings due to initially lower rolling load in ferritic region and most evidently due to the lowering of required reheating temperature, which leads to increased throughput of furnace and achievement of smaller austenite grain size due to reduced AlN dissolution. A further advantage of low temperature rolling is related to a significant reduction in work roll wear as well as improved picklability due to low oxidation with a different scale morphology. As reported (1, 6), lowering of rolling temperatures down to ferritic regime may lead to energy savings of 20 % with respect to the final product. An understanding of phase transformation as well as deformation and recrystallisation behaviour of ferrite is essential in order to capitalize on the ferrite rolling process to produce various ranges of desired hot band properties.

Only in the recent past there has been some important research activity on the physical metallurgy of the warm rolling process and the development of textures and microstructures during warm rolling and subsequent annealing (6 - 10). In spite of

these, many aspects of warm rolling are not clear yet and there is scope for further research activity on various aspects of this process. The present work was undertaken to carry out a detailed study of the textural and microstructural changes during warm rolling of an extra low carbon (ELC) and two interstitial free (IF) steels. In this work an attempt has been made to investigate the effects of a few compositional and processing variables on the structural and textural changes of the three steels with a view to compare and contrast their behaviour vis-à-vis warm rolling and annealing texture development and attendant structural changes.

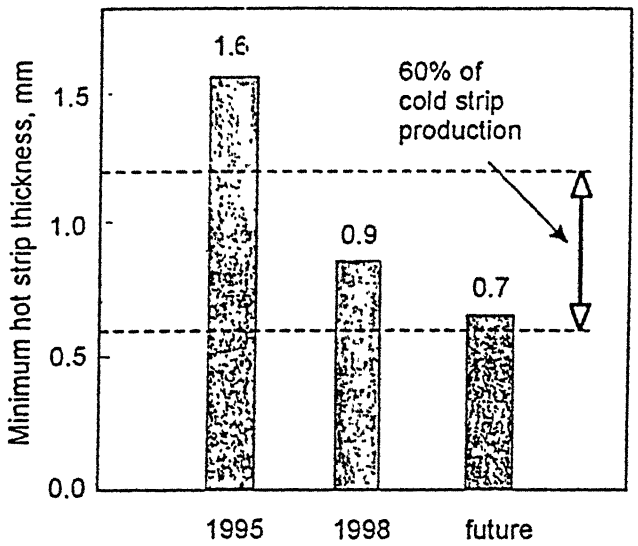

Figure 1.1 : Minimum hot strip thicknesses as a potential substitution of cold strip (1).

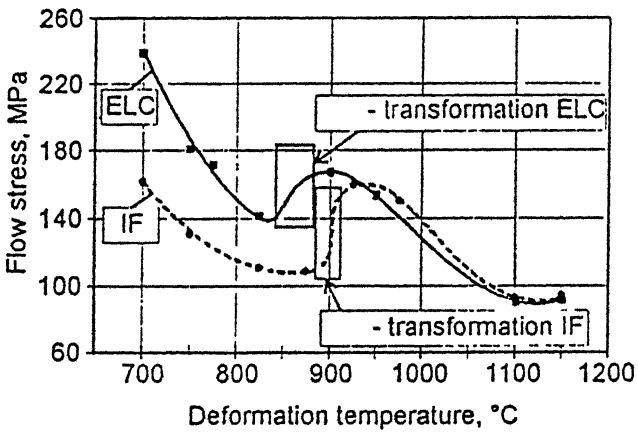

Figure 1.2 : Flow stress for the strain $\varepsilon = 0.8$ of an ELC and IF steel over the range of deformation temperature (1).

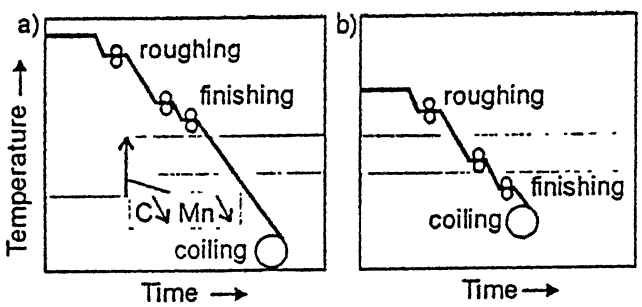

Figure 1.3 : Comparison of conventional austenitic (a) and ferritic (b) rolling (1).

CHAPTER 2
LITERATURE

2. Literature

2.1 Warm rolling

2.1.1 Phase transformation

For a particular steel, the temperature at which austenite to ferrite transformation takes place, determines the ferritic rolling temperature regime. The equilibrium phase diagram, as shown in Figure 2.1, clearly indicates that full ferritic region for ultra low carbon steels exists below 900 ^{o}C. The Figure 1.2 also shows that γ to α transformation is completely terminated at 860 ^{o}C in an IF steel and at 810 ^{o}C in ELC steel (1). In addition to cooling rate, the state of austenite prior to cooling plays critical role in determining the precise transformation temperature (11). However, only a marginal effect of cooling rate on transformation temperature is observed in IF steels because of their ultra low levels of carbon and other alloying elements (12). Industrially warm rolling is generally carried out when the microstructure contains more than 90% of ferrite and rolling is finished at around 800^{o}C or below (1, 6, 13, 14).

2.1.2 Deformation behaviour of ferrite

2.1.2.1 Influence of austenite

In actual warm rolling there would always be a significant amount of austenite present during the early stages of rolling. This will have important consequences on the flow stress and softening behaviour of ferrite. According to Saito (15), the flow stress of ferrite/austenite microstructure can be conveniently described as the weighted average of the individual flow stresses of both the phases. Figure 2.2 shows the correlation between flow stress and transformed fraction of ferrite.

2.1.2.2 Influence of dynamic strain ageing

Substantial amount of work has been carried out to model the high temperature flow stress of austenite as a function of strain, strain rate, and temperature (16, 17). Such extensive models for warm rolling conditions are not easily available. It may be pointed out here that it becomes difficult to predict the flow stress in warm rolling regime

because of complications arising out of phase transformation, presence of solute carbon and due to dynamic strain ageing (DSA) at lower temperatures.

Dynamic strain ageing is a well known phenomenon to occur in steels in presence of carbon in the temperature region of 200 to 300 ^{o}C (9, 18, 19) and is manifested by a flow stress peak. This phenomenon will be at its peak when the diffusivity of carbon atoms matches the velocity of the dislocations. Figure 2.3 (6) shows the influence of DSA on flow stress of two steels at two strain rates indicating a distinct flow stress peak due to DSA for low carbon steel and negative strain rate sensitivity ($m = \log\sigma/\log\dot{\varepsilon}$) in the vicinity of low temperature (DSA) peak. It also shows that an increase in strain rate shifts the temperature vs. flow stress curve to higher temperature (19).

Figure 2.4 shows the effect of temperature on strain rate sensitivity for a few steel compositions (6). At high deformation temperatures, steels containing solute carbon display unusually high rate sensitivities. On the contrary, at lower temperatures, the presence of solute carbon gives a reverse effect and leads to negative rate sensitivities (9, 20). These effects are absent in the steels which do not contain solute C or N, as in the IF steels where C and N are scavenged out by Ti and /or Nb. Hence DSA flow stress peak, characteristic of low carbon steels, can not be observed in IF steels. That the DSA effect arises due to the presence of interstitial atoms and their interaction with mobile dislocations at the deformation temperatures is supported by the work of Barnett and Jonas (6, 9, 20, 21) and Glen (22), who observed that addition of chromium to low carbon steels lowers their abnormally high rate sensitivity to levels similar to those of IF steels. It has been demonstrated that DSA has a considerable effect on the development of the deformed structure during warm rolling as well as on the evolution of texture during annealing.

2.1.2.3 Dynamic relaxation processes

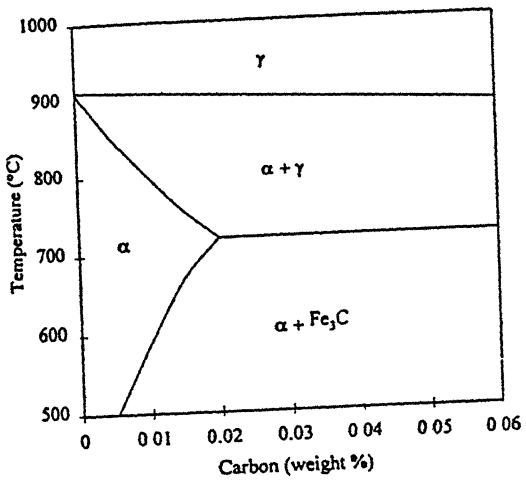

Figure 2.1 : Fe-C phase diagram covering the temperatures and steel compositions applicable for LC and ELC steels (6).

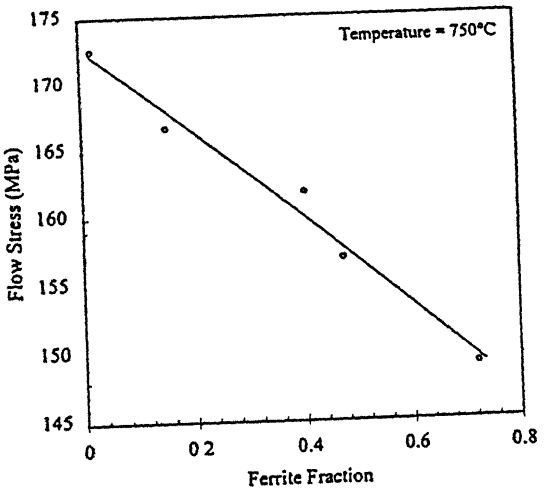

Figure 2.2 : Linear relationship between Ferrite fraction and flow stress at constant deformation temperature of 750 ^{o}C in a LC steel (15).

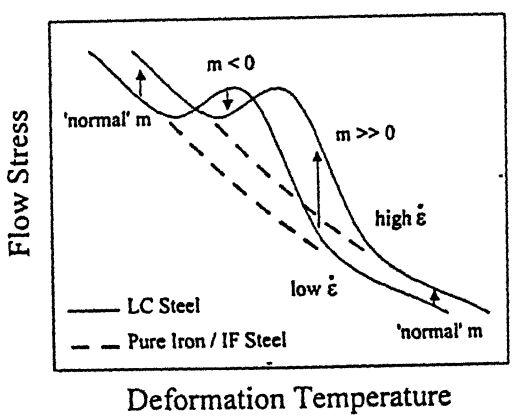

Figure 2.3 : Schematic representation of Temperature vs. flow stress data for two strain rates.The peak in the LC steel curves is a consequence of dynamic strain ageing (6).

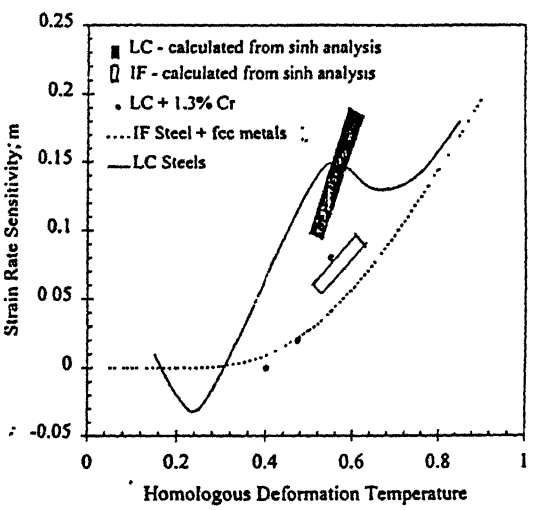

Figure 2.4 : Influence of homologous temperature on strain rate sensitivity (m) for a number of materials (6).

At elevated temperatures, the dynamic softening processes operative in the ferrite, which has high stacking fault energy, have been identified as dynamic recovery (DRC) (23 - 25) as well as dynamic recrystallisation (DRX) (23, 26 - 3.).

Glover and Sellars (23) observed that as in case of austenite dynamic restoration processes take place in the ferrite of vacuum melted and zone-refined iron at high temperatures. They observed that at temperature ranging from 500°C to 880°C, dynamic recovery is the main restoration process in pure iron over a wide range of strain rates when the Zener-Holloman parameter (Z) is greater than a critical value. Below this value dynamic recrystallisation takes place once a critical strain is exceeded. This transition in restoration process occurs at higher values of Z in the higher purity materials. Langner and Bleck (12) also confirmed that dynamic recovery is the only high temperature restoration process in low carbon, ultra low carbon and IF steels and this is not affected by the soaking temperature. In a ferritic stainless steel with high SFE, Belyakov et al. (32) also observed mainly dynamic recovery in ferrite after compression up to a true strain of 1.0 at 600 ^{o}C and at the strain rates of 10^{-2} s^{-1} to 4 x 10^{-4} s^{-1}. However, the formation of new equiaxed grains with low to high angle misorientations within microband clusters led them to believe that there is an element of "apparent" dynamic recrystallisation also.

On the basis of TEM and micro-texture measurements, Mastubara et al (26) and Tsuji et al (33) suggested the occurrence of dynamic recrystallisation (DRX) of ferrite in a Ti added IF steel. However, they further observed that the drop in stress in stress-strain curve was rather small during DRX in ferrite, which is quite different from DRX in austenite. These studies clearly indicate that a transition from DRC to DRX behaviour occurs in ferrite during high temperature deformation. The Figure 2.5 illustrates this transition behaviour (6), which seems to occur at stress levels of around 30-50 MPa. Using the experimental results of above authors Barnett and Jonas (6) constructed a deformation map, which depicts the deformation conditions that give rise to the transition stress for the dynamic restoration processes [Fig. 2.6]. It is quite evident from this figure that DRX can not possibly occur in the actual warm rolling condition in the hot strip mill

where the strain rates may vary between 20 and 200 s^{-1} within the temperature range of 600 - 850^{o}C.

Several workers (27 - 29, 34, 35) have reported that the DRX process occurs in ferrite under experimental parameters, which lie well within the DRC region [Fig. 2.6]. In all these observations strains in excess of 3.0 were involved. According to Barnett and Jonas (6) this sort of DRX may be considered as a kind of recovery process by means of which a structure consisting of low angle boundaries is gradually converted into high angle misorientations. However, the high strains at which such processes would be operative, put these outside the conditions likely to be encountered during commercial warm rolling.

2.2 Microstructure and texture in warm rolled steels

The application of warm rolled materials will involve recrystallisation at a later stage for possible benefit in the mechanical properties. The course of recrystallisation will be, of course, determined significantly by the deformed state. The most important features of the deformed state are : (i) the stored energy /dislocation density, which is the driving force for recrystallisation, (ii) the inhomogeneity of the dislocation substructure , which will affect the nucleation and growth during recrystallisation and (iii) the deformation texture, which will determine the orientations of the recrystallised grains in the bulk material.

2.2.1 Stored energy/dislocation density

Warm rolled ferrite will show predominantly a recovered microstructure since mostly dynamic recovery takes place over a wide range of temperatures (23, 36). The dislocation density in warm rolled steels has been estimated by several workers (9, 37, 38) using various techniques like hardness measurements, X-ray line broadening and TEM analysis. The major finding from these works is that DSA leads to an appreciable increase in dislocation density, specially in low carbon steels. This is reflected in a higher value of dislocation density and stored energy in LC steels as compared to the IF steels, at lower deformation temperatures (9). The dislocation density in warm rolled structures

is present largely as recovered subgrains having sizes varying between 6 μm to ~ 1μm (23, 26, 36, 39, 40).

2.2.2 Inhomogeneity of the substructure

The microstructure of warm rolled steels often display band like features which are elongated at an angle to the rolling direction (9, 41). Similar features are also commonly observed in cold rolled fcc and bcc materials (32, 42 - 54). These features have been labelled by various workers as deformation bands (DB), micro bands (MB), shear bands (SB) etc. In fact, such bands that have a ± 20-35^{O} inclinations to the rolling plane have been shown to play a significant role in the metallurgy of warm rolled steels (6, 9). Since these bands are usually contained within deformed grains, Barnett and Jonas (6) have termed them " in-grain shear bands ". For the purpose of the present review the term deformation band (DB) will be used while referring to such features.

Deformation banding is a process in which different regions of a deforming crystal gradually rotate to different orientations as deformation proceeds. According to Lee et al.(42), one cause for banding is the reduction of total work for plastic deformation through a relaxation of the deformation constraints. It is assumed that total work for the slip required by deformation banding will be less than that for homogeneous deformation, as latent hardening is expected to increase the critical resolved shear stress (CRSS) of all slip systems other than the primary slip system. The major factors which may be taken as a criteria for deformation banding are orientation, grain size and strain.

An insight into the occurrence of these bands can be had by looking into the factors that promote flow localisation. During deformation the tendency for flow to localise depends on the work hardening rate and strain rate sensitivity (55). Flow localisation is enhanced when either of these factors is negative. Negative work hardening can be caused by an unstable dislocation substucture, a strain path change or deformation heating (6). DSA is known to cause negative strain rate sensitivity (19). Since DSA is very much prevalent in low carbon (LC) steels, but not in IF steels, the

density of deformation band should be higher in LC than in the IF steels, specially at lower temperatures of deformation.

The presence of the deformation bands has been shown to cause fragmentation of the warm rolled microstructure (56). Thus a significant difference in the orientation homogeneity of the substructure of warm rolled LC and IF steels is quite expected. As observed by Barnett (56) the misorientations in an IF steel have been found to be almost an order of magnitude greater than those seen in a LC steel [Fig. 2.7]. The inhmogeneities referred to above are expected to have a strong impact on the bulk deformation texture as well as on the nucleation aspect of recrystallisation. Formation of orientation gradients in deformed grains has also been observed by Senuma et al.(8). Barnett and Jonas (6) have suggested that this observation can be rationalised on the basis of the effect of DSA on strain rate sensitivity and of rate sensitivity on deformation band frequency and grain fragmentation.

2.2.3 Warm rolling texture

The textures of warm rolled steels are quite similar to those of cold rolled materials (7, 8, 9). The main texture components here are (i) the γ fibre (<111>|| ND) and (ii) a partial α fibre (<110>|| RD), the former being much sharper in intensity in IF steels than in LC steels (8). These two components are also the two major texture components observed after cold rolling of ferritic steels. According to Barnett and Jonas (9), increasing the warm rolling temperature increases the texture sharpness in the LC grade steels [Fig. 2.8]. Similar observation was also made by Matsuoka et al. (57), who noted that the sharpness of warm rolled texture increased more rapidly with rolling temperature in a > 30 ppm C grade than in a 10 ppm C steel.

Barnett and Jonas (6, 9) tried to rationalise their observed effect of temperature of deformation on the sharpness of warm rolled texture of LC grade in terms of the density of deformation bands (in-grain shear bands, according to them) at that particular temperature. They argued that since this density is very low in the 700 ^{o}C deformed material, there has been much less fragmentation of the grains caused by deformation

bands and hence a sharper texture was obtained. The much less marked differences in the texture sharpness observed for an IF steel, deformed at two different temperatures (Fig. 2.8), presumably arise from the almost similar deformation band densities at the two temperatures in the IF steel. Tomitz and Kasper (1,58), from their simulation of strip rolling process for the production of thin and ultra thin hot strips, have shown that a lower finishing temperature during warm rolling leads to a sharper γ and α fibre in both ELC and IF steels. These results are at variance with what Barnett and Jonas (6, 9) have reported.

As in hot rolling and cold rolling, lubrication has a pronounced effect on texture development during warm rolling. High level of friction, in absence of lubrication, leads to the development of significant amount of shear strain near the surface region of the sheet and hence a significant texture inhomogeneity across the thickness of the material (59). Figure 2.9 shows a plot of the intensities of {111} and {110} components as a function of distance from the strip surface. It is clear from this plot that the Goss orientations {011}<100> is dominant in the surface, as this is a stable orientation for shear in the rolling direction (60). The effect of friction in causing through thickness inhomogeneity is not that prominent in hot rolled steels, since post rolling phase transformation tends to randomise the texture. The phenomenon of texture inhomogeneity due to frictional effect at the surface of the strip has a major impact on the subsequent recrystallisation texture development.

2.3 Microstructure and texture of warm rolled and annealed steels

2.3.1 Static relaxation processes

In warm rolling static relaxation (softening) of ferrite can occur during the interpass delay time. Further static softening takes place when the warm rolled material is subsequently annealed. The process may be quite complicated in IF steels because of the precipitation of carbides, carbonitrides and carbosulphides at different stages of rolling.

2.3.1.1 Interpass softening

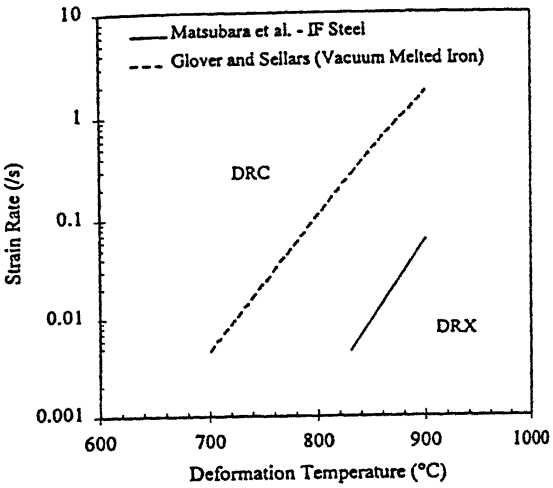

Figure 2.5 : Deformation map distinguishing between the regions of operation of dynamic recovery (DRC) and dynamic recrystallisation [DRX] (6, 23, 26).

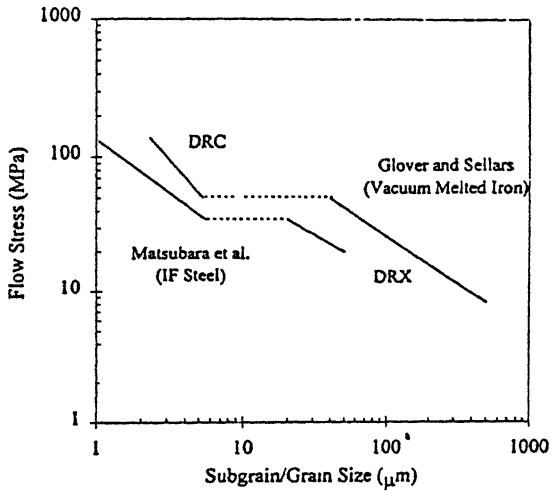

Figure 2.6 : Deformation map showing the transition from a DRC to a DRX structure (6,23,26)

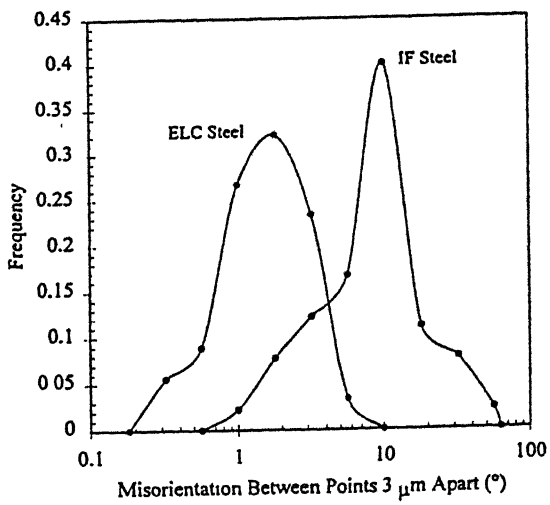

Figure 2.7 : Comparison of the fragmentation (misorientation) in warm deformed grains in an IF and an ELC steel (56).

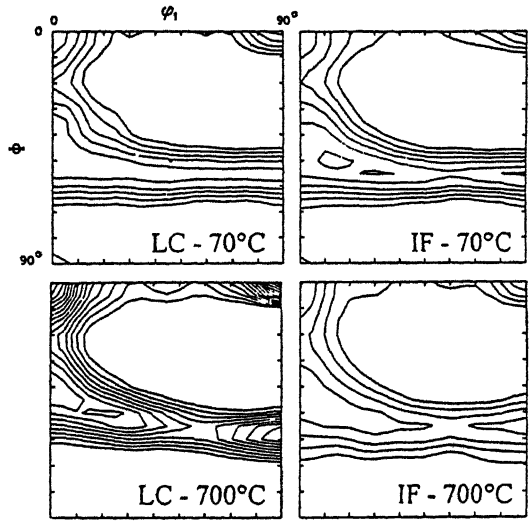

Figure 2.8 : Deformation textures of a LC steel and an IF steel after cold and warm rolling (9).

Langner and Bleck (12), compared recrystallisation kinetics of ferrite and austenite in low carbon (0.022% C) and ultra low carbon (0.006%C) steels using multi-stroke compression test. The static recrystallisation of austenite was found to be very fast at 1000 ^{o}C, in comparison to ferrite at 700 ^{o}C for both the steels. Recovery was found to be the dominant feature in ferrite softening up to almost 100 seconds of interpass time. Increasing strain and strain rates have a positive effect in accelerating the softening kinetics, where as softening is retarded by increasing the initial austenite grain size. In the small interpass time during industrial hot strip mill rolling, only static recovery is therefore expected to take place.

According to Barnett and Jonas (6, 9), some degree of interpass recrystallisation may actually occur in both LC and IF grades for rolling temperatures above ~ 800 ^{o}C. They came to conclusion after extrapolation of data contained in Figure 2.10, showing the influence of strain rate on the time to 50% recrystallisation in an IF and two LC grade steels. Barnett (61) has postulated a rough model for the time to 50% recrystallisation of ferrite in LC steels in the absence of significant effects of AlN precipitation. However, considerable further work is required in this area to take care of the influence of concurrent precipitation of AlN. In case of IF steel the precipitation, both in austenite and ferrite (62,63), will play very significant role during softening of ferrite. Detailed study so far by various authors (62 - 66) indicates that Ti is responsible for forming TiN, TiS, $Ti_4C_2S_4$ and carbonitrides and Nb mainly forms carbides and carbonitrides. The importance of the occurrence of precipitation during interpass time on post dynamic softening of a Ti - Nb IF steel has also been highlighted by Cetlin et al. (67).

Figure 2.11 (63) shows the calculated precipitation start time, $t_{0.05}$ and the static recrystallisation start time, $t_{0.05x}$, in ferrite region for a Nb rich Ti-Nb IF steel based on a modified Dutta and Sellars' model (68). This figure shows that at a temperature of approximately 700 ^{o}C and above recrystallisation will occur before precipitation initiates. When the temperature is lower than 675 ^{o}C, precipitation will occur earlier than recrystallisation and therefore recrystallisation will be retarded significantly. Huang et al,

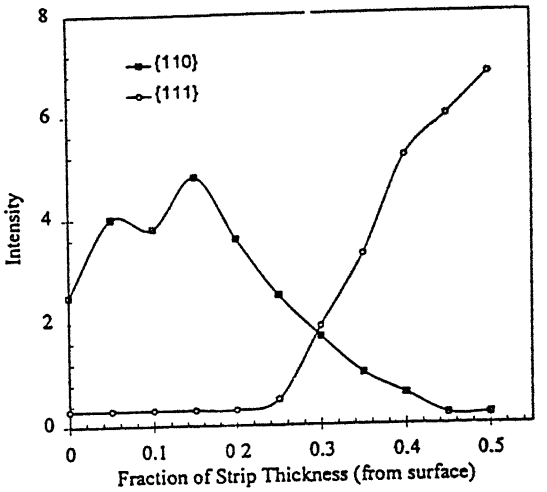

Figure 2.9 : Variation of rolling texture through sheet thickness of an IF steel due to friction effects (59).

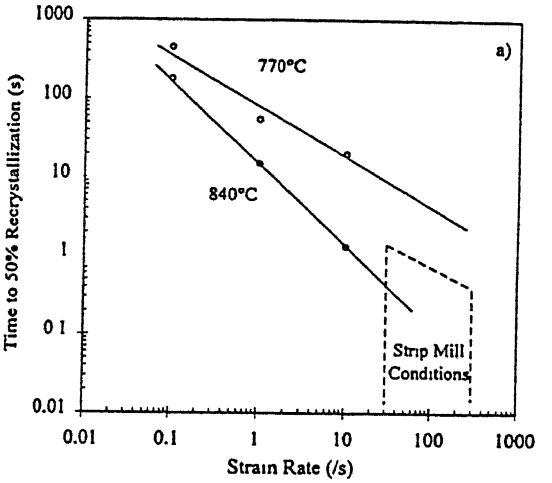

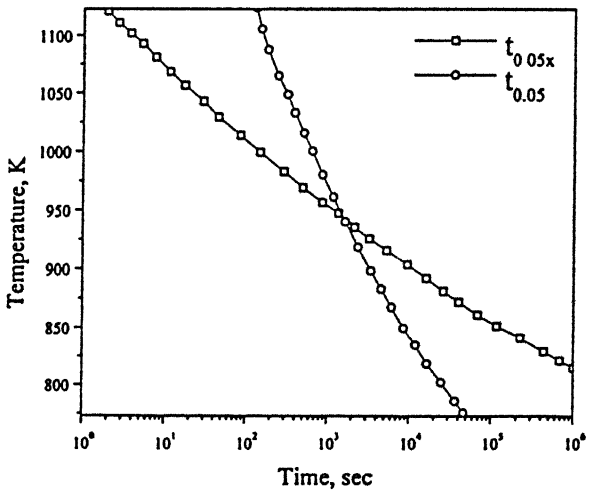

Figure 2.11 : Calculated precipitation start time ($t_{0.05}$) and static recrystallisation start time ($t_{0.05x}$) in ferrite region for two IF steels (63)

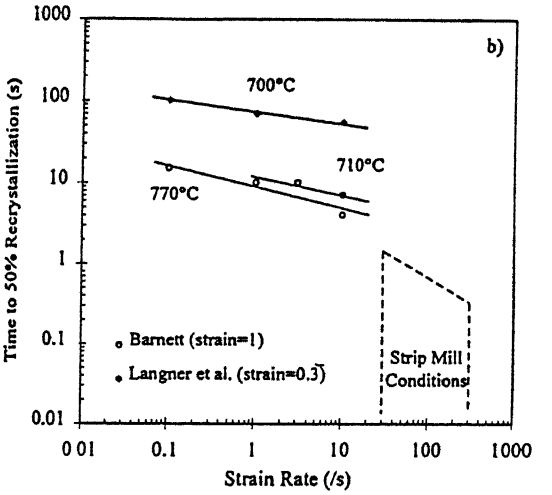

Figure 2.10 : Influence of strain rate on 50% static recrystallisation for a) an IF steel and b) two LC grades steels (6).

(63) also stated that the above inference is consistent with their micrstructural observations.

2.3.1.2 Static softening during annealing

Researches have revealed a distinct difference between the behaviour of IF and LC steels, so far as kinetics of recrystallisation during annealing is concerned. The times for 50% recrystallisation during annealing of an IF and a LC grade, which were subjected to single pass rolling (65% reduction) followed by isothermal annealing at 700 ^{o}C, are shown in Figure 2.12. From this figure it is clearly evident that the IF steel displays slower recrystallisation kinetics than LC steel. The reason for this difference could be due to the fact that IF grades typically contain a higher density of fine precipitates as compared to LC steels. The presence of solute carbon in LC steel can also play a large role in this respect (10).

The above Figure also clearly illustrates that the influence of temperature of warm rolling on the recrystallisation kinetics is much more significant in LC steel than in the IF steel. At lower temperatures of deformation in the LC steel, DSA is most active and therefore in presence of solute C the dislocation density after rolling will be very high, thereby increasing the driving force for recrystallisation. This will ensure that the kinetics of recrystallisation of the warm rolled and cold rolled LC steel will not be much different. However, the effect of DSA will not be felt at higher temperatures of deformation, say at 700 ^{o}C, where the rate of recrystallisation will be approximately 1½ orders of magnitude slower as compared with rolling at room temperature (10). Since the rolling temperature has considerably less influence on the annealing of IF materials, these grades therefore lend themselves more readily to the replacement of cold by warm rolled products.

The statically recrystallised grain size is influenced by the deformation temperature to a much greater extent in the LC steel than in the IF [Fig. 2.13]. For lower deformation temperatures, the IF steel shows a coarser recrystallised grain size than the LC grade. This effect is reversed for higher warm rolling temperatures, as shown in the above Figure. Barnett and Jonas (6) have tried to explain this observation on the basis of

the difference in the deformation band (in-grain shear band) density in the LC and IF steels as a function of warm rolling temperature.

2.3.2 Recrystallisation textures

As in case of deformation texture, there exists a through - thickness inhomogeneity in the recrystallisation texture also which develops in warm rolled steels after annealing.

2.3.2.1 Texture development on the mid-plane

The recrysrtallisation texture is influenced by the rolling temperature to a greater extent in LC grades than in the IF steels (10). In IF steels the <111>ND (γ fibre) is dominant after annealing for all the rolling temperatures (10). On the other hand, γ fibre intensity in LC steels decreases with increasing rolling temperatures and disappears completely after recrystallisation when rolled at 700^{o}C (10). Similar behaviour was also observed by Tomitz and Kasper (1, 58) in an ELC steel and by Senuma et.al (8) in a LC steel. Figure 2.14 shows typically the effect of rolling temperature on the recrystallisation texture for both IF and LC steels.

Barnett (IJ_3) and others (69, 70) observed that the deformation bands (in-grain shear bands) in the IF steels act as the nucleation sites for {111} oriented nuclei. Duggan et al (71,72) observed a similar type of nucleation in a cold rolled ELC steel. Similar observations have been reported by other workers also (69,70). It is therefore appears that deformation bands in adequate density must be present in warm rolled steels so that {111} texture of sufficient intensity forms during subsequent recrystallisation. It is known that in cold rolled steels which contain a high level of solute carbon during rolling, heavy deformation banding is detrimental to the formation of {111} texture during annealing (5). It is necessary to reconcile these two observed contradictory effects of deformation banding on annealing texture development in steels. It would be interesting to mention here the results obtained by Matsuoka et al.(57) who investigated the effect of deformation temperature on {111} intensity after recrystallisation in steels of two different solute carbon levels, namely 10 ppm and > 30 ppm [Fig. 2.15]. This Figure

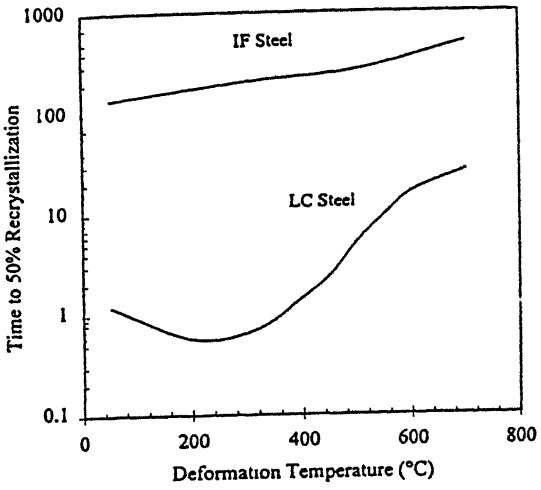

Figure 2.12 : Influence of deformation temperature on the time to 50 % recrystallisation at 700 °C for an IF steel and a LC steel (10).

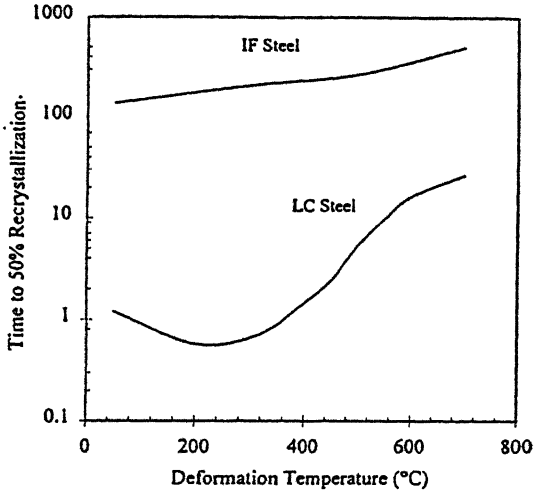

Figure 2.13 : Influence of rolling temperature on the recrystallised grain sizes (10) for the steels referred to Fig. 2.12.

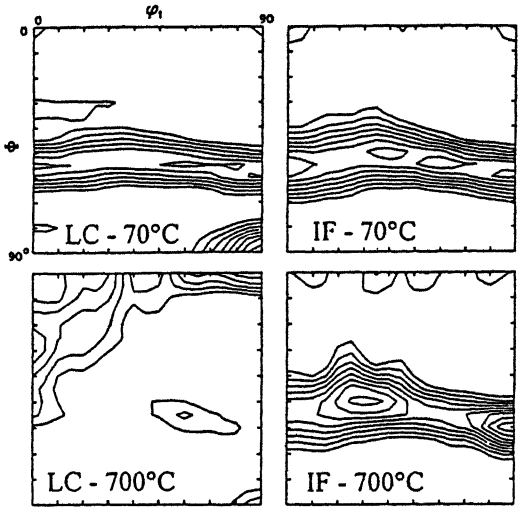

Figure 2.14 : Recrystallisation textures [$\varphi_2 = 45^{\circ}$ ODF section] corresponding to an IF steel and a LC steel (10).

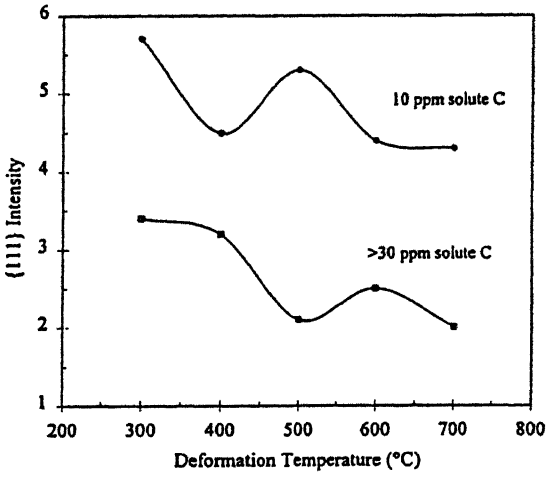

Figure 2.15 : Influence of rolling temperature on {111} recrystallisation texture intensity for two steels of different carbon levels (57).

shows that for all deformation temperatures, the steel with 10 ppm solute carbon shows a significantly higher intensity of the {111} component than the steel with >30 ppm solute carbon. Barnett and Jonas (6,9), in an effort to rationalise these effects on the basis of difference in the density of deformation bands (in-grain shear bands) in the two steels, suggested that the trough in the curve at 500 ^{o}C for the higher carbon steels corresponds to the DSA flow stress peak at the strain rate used, which would lead to a much severe intensity of the deformation bands in that steel. In the low carbon steel, for comparable deformation temperature, there will not be any DSA effect and therefore the density of the deformation bands will be lower than in the other steel, and this possibly reflected in a higher intensity of {111} texture in the former. If their arguments are accepted, the question automatically arises as to what should be the optimum density of deformation banding to yield a high intensity of the {111} texture component after recrystallisation. Presumably, the answer is not a straightforward one and there is a need to study the possible interaction of solute carbon and density of deformation banding as a function of deformation temperature, strain rate and level of deformation during warm rolling.

It would be interesting at this stage to refer to the work carried by Senuma et al.(8) who studied the recrystallisation texture development after warm rolling in a LC and an IF steel. They observed that the main component of the recrystallisation texture in the LC steel was {113}<110> while <111> ND (γ fibre) is the major component in the IF steel. They have tried to explain these differences on the basis of the influence of carbon in solution on crystal rotation at the nucleation sites. They concluded that the different recrystallisation textures formed in the above two steels can be explained by the difference in the preferential nucleation sites and in the local crystal rotation in the vicinity of grain boundaries.

2.3.2.2 Texture development on the surface

During rolling the friction between the rolls and the strip surface within the roll bite induces texture inhomogeneity across the strip thickness. This is now well established in a variety of fcc metals and alloys (72 - 76) and cold rolled LC and IF steels (6, 77 - 80). Similar effects of friction are also observed in plain carbon and IF steels

during warm rolling (59, 81). Figure 2.16 displays the effect of friction on the development of the {111} and {110} components of the recrystallisation texture in an IF steel warm rolled with and without lubrication. It is quite clear that proper lubrication drastically reduces the through-thickness texture inhomogeneity and at the same time produces a sharp and uniform {111} texture, which is desirable for good deep drawability. The adverse impact of friction during warm rolling on the formability properties have been reported by several other workers also (82 - 84). Matsuoka et al.(81, 84) and Senuma et al.(70) recommend that warm rolling should be carried out a at a friction coefficient below 0.15 in order to achieve high and uniform {111} intensity along the thickness.

2.4 Industrial warm rolling practice and new innovations

Warm rolling is now used in a large number of steel industries for full-scale production. This is because the benefits that accrue from this type of rolling can be enormous. The main advantages experienced by the industry is not only operational cost savings but also the wide range of products which can be rolled industrially by this process. Barnett and Jonas (6) have compiled a list of products which can be produced with advantage by using the warm rolling practice and the benefits that can be realised therefrom. These results, in the form of two tables, are reproduced in Tables 2.1 and 2.2 below. It can be seen from Table 2.1 that warm rolling can help to produce a range of steel products starting from a basic CQ grade to super deep drawing quality(SDDQ) grades.

It is worth mentioning here that the annual production of ferritically rolled steel grades in Cockerill and Sambre, Belgium was as high as 500, 000 tons in 1999. About 20% reduction in electric power consumption was achieved by them for ferritically rolled products. Producing thinner hot rolled products not only give advantage in cold rolling mill but also in the pickling line. Thus warm rolling helps in reducing the thickness of the scale layer to a significantly larger extent, and the steel gets pickled faster than hot rolled products. Brown et al. (85) in their simulation study, have shown that scale layers less than 2 μm in thickness will form during warm rolling, and this is almost five fold less

than in conventional rolling. The other benefits, in this case, are realized in the cost and rate of production. Cold rolling and annealing after warm rolling may further widen the application of warm rolling (6, 13, 86, 87, 88).

A very recent laboratory study by Tomitz et al.(1, 5, 89) shows that warm rolling can be a very innovative process in producing varieties of hot rolled thin gauge strips, which may be able to replace 90% of the existing cold rolled products in future. Under the simulated conditions they have observed that control of parameters like reheating temperature, finish rolling temperature, coiling temperature and the amount of cold deformation (of ferritically rolled strips) are very critical to get the actual benefit of warm rolling. They indicated that various deep drawable thin-gauge strips of IF steel can be produced by varying these parameters, as shown in Figure 2.17

Thus the warm rolling process can pave the way of producing very thin and super formable IF steel strips substituting so many cold rolled grades. But ultra low plain carbon steels can not give any major benefit in this process other than giving a soft hot strip with poor formability ($r_m < 1.0$).

Table 2.1. Different types of warm rolled products (6)

Sl. no	Type	Product	Grade	Coiling temperature	Pre-anneal	Cold roll	Anneal	Galv.
1	Hot band	CQ	LC	High	-	-	-	-
2	"	CQ-DDQ	LC-IF	Low	-	-	Yes	(yes)
3	Cold band	CQ-DQ	LC	High	-	Yes	Yes	(yes)
4	"	CQ-DQ	LC-IF	Low	-	Yes	Yes	(yes)
5	"	DQ-SDDQ	IF	Low	Yes	Yes	Yes	(yes)

Table 2.2. Benefits that can be realised from warm rolling (6)

	Products	Comments
Warm rolling		
Increased furnace throughput	All	Only if using low reheating temperatures
Less energy usage	"	"
Less scale loss	"	"
Less damage to slabs	"	"
Reduced roll wear	"	Less roll changes, higher productivity
Less water on run out table	1,3	Only for high coiling temperatures
Less streaking (Ti-IF steels)	2,4,5	Only if using low reheat temperatures
Thinner gauge	All	Where heat loss limits gauge
Pickling		
Increased throughput	All	Due to thinner scale layer
Increased throughput	3	Only if hot band gauge is increased
Less acid usage	All	-
As warm rolled products		
Softer	1	Only for high coiling temperatures
Higher r - value	2	Only if using lubrication
Non - ageing	1,2	Only if using low reheat temperatures
Cold rolling		
Lower rolling loads	3, (4)	Mostly for high coiling temperatures
Increased throughput	3	"
Less roll wear	3	"
Cold rolled products		
Higher r - value	5	Only if using lubrication in warm rolling
Softer grade	3	Only for high coiling temperatures

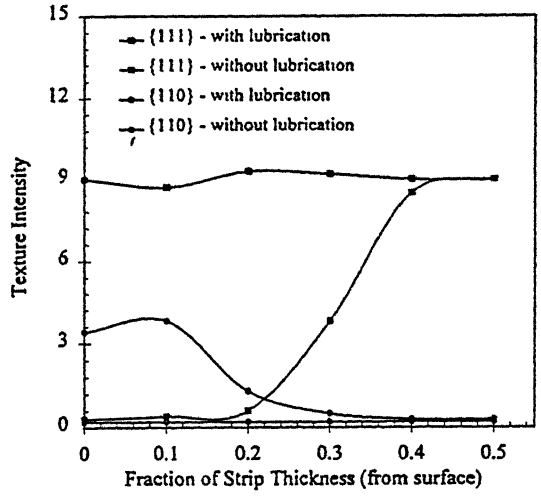

Fig. 2.16 Influence of lubrication on the {111} and {110} texture intensities of a warm rolled and annealed IF steel (59).

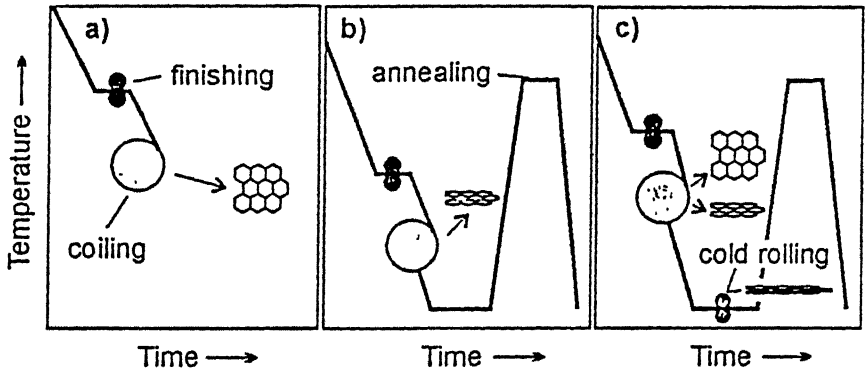

Fig. 2.17 Three different warm rolling process routes for production of a) soft hot strip b) hard hot strip additionally annealed and c) cold strip made of a ferritic rolled strip (1).

CHAPTER 3
EXPERIMENTAL

3. Experimental

3.1 Steels used for this study

Two interstitial free (IF) steels and one extra low carbon (ELC) steel were selected for the present investigation. The compositions of the steels are given in Table 3.1. All the steels were prepared in BF-LD-CC-HSM route. RH-degassar was used to achieve ultra low levels of interstitials. The starting materials for this investigation were transfer bar samples taken after roughing rolling in the hot strip mill (HSM).

Table 3.1 Chemical composition (wt %) of the steels

Steel	C	Mn	S	P	Si	Al	Ti	Nb	O_2	N_2
1	0.007	0.11	0.010	0.010	0.003	0.043	-	-	12 ppm	50 ppm
2	0.003	0.10	0.010	0.012	0.008	0.44	0.020	0.037	10 ppm	30 ppm
3	0.003	0.11	0.009	0.012	0.008	0.050	0.054	0.014	8 ppm	32 ppm

3.2 Phase transformation

In order to determine the warm rolling regime, continuous cooling transformation (CCT) diagrams for the three steels were determined using Gleeble-1500 thermo-mechanical simulator. Hollow samples of 6-10 mm outside diameter and wall thickness of 1 mm were used for this purpose. The samples were re-heated to 1150 ^{o}C and were kept at that temperature for 10 minutes for homogenisation before cooling started. The samples were first cooled to 950 ^{o}C at a cooling rate of 5 ^{o}C s^{-1} and then further cooled to room temperature at constant cooling rates ranging from 0.5 ^{o}C s^{-1} to 100 ^{o}C s^{-1}. The transformation start and finish temperatures were determined from dilatometric data and

then superimposed on the respective cooling curves. In addition to determining the CCT diagrams, The transformation start (Ac_1) and finish temperatures (Ac_3) were also determined during heating cycles at just three heating rates of 0.5 $^{o}C\ s^{-1}$, 1 $^{o}C\ s^{-1}$ and 5 $^{o}C\ s^{-1}$.

3.3 Hot deformation

Flow stress curves were determined for all three steels in the austenitic as well as ferritic regions by hot compression testing at a constant strain rate of 0.1 s^{-1}. Gleeble 1500 thermo-mechanical simulator was used for uniaxial hot compression testing, using samples of 10 mm diameter and 15 mm height. Initially all the samples were homogenized at 1150 ^{o}C for 10 minutes and cooled to room temperature at a cooling rate of 3 $^{o}C\ s^{-1}$, in order to achieve uniform starting microstructure. Then all the samples were again heated to 1150 ^{o}C and soaked for 10 minutes followed by cooling to test temperatures (1050 ^{o}C to 500 ^{o}C) at cooling rate of 5 $^{o}C\ s^{-1}$. Isothermal deformation was given up to a pre-determined true strain of 0.75 at a constant strain rate of 0.1 s^{-1}. The samples were then cooled to room temperature at a constant cooling rate of 10 $^{o}C\ s^{-1}$.

A second series of samples were also soaked in the ferritic region at the temperature of 830 ^{o}C and then cooled to test temperatures varying between 800 ^{o}C to 500 ^{o}C at intervals of 100 ^{o}C followed by isothermal compression at a strain rate similar to that for the first series of samples.

3.4 Warm rolling

Both single pass and multipass rolling experiments were carried out using a 170 tons experimental two high rolling mill having roll diameter of 350 mm. An ester based industrial oil was used as lubricant. For single pass rolling bar shaped samples were used, whereas wedge shaped specimens were used for multipass rolling. The shapes and dimensions of the two types of samples are shown in Figure 3.1.

Before the actual experiments, dummy rolling, both in single pass and multipass were carried out with embedded thermocouples (mineral insulated K-type having total diameter of 2 mm) in order to determine the actual temperatures attained during rolling. Surface temperatures of the samples were also measured using an infrared pyrometer at a fixed emissivity of 0.85. The temperatures, as measured by pyrometers and thermocouples, were plotted in the form of graph (Fig. 3.2) to be used later to determine the actual temperatures during final rolling experiments which were performed using the pyrometer only. The measured temperature profiles at the surface as well as at the center of bar shaped specimens are shown in Figure 3.3. The temperature gap between the surface and the core of the bar was observed to increase gradually and was as high as 50 ^{o}C at the later stage of rolling and cooling. Not much variation in temperature at different locations of the wedge shaped samples was noticed during rolling (Fig. 3.4).

3.4.1 Single pass rolling

Single pass rolling was carried out with wedge shaped samples in order to get proper bite during rolling. Due to load limitations in the rolling mill, reduced width was used for rolling at 500 ^{o}C. Two soaking temperatures 1150 ^{o}C and 830 ^{o}C were used and

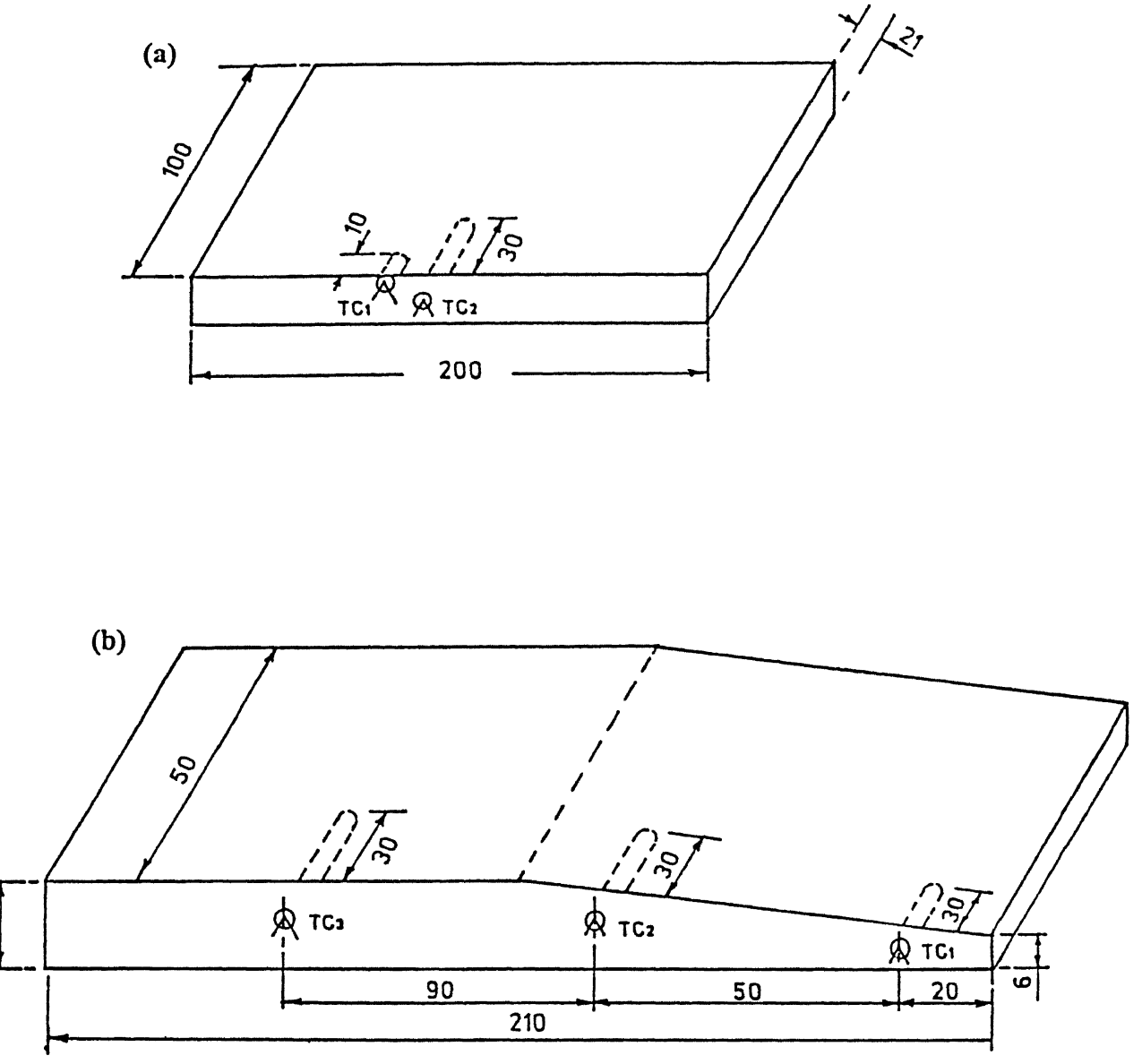

Figure 3.1 : The shapes and dimensions (mm) of two types of samples used for (a) multipass rolling and (b) single pass rolling.

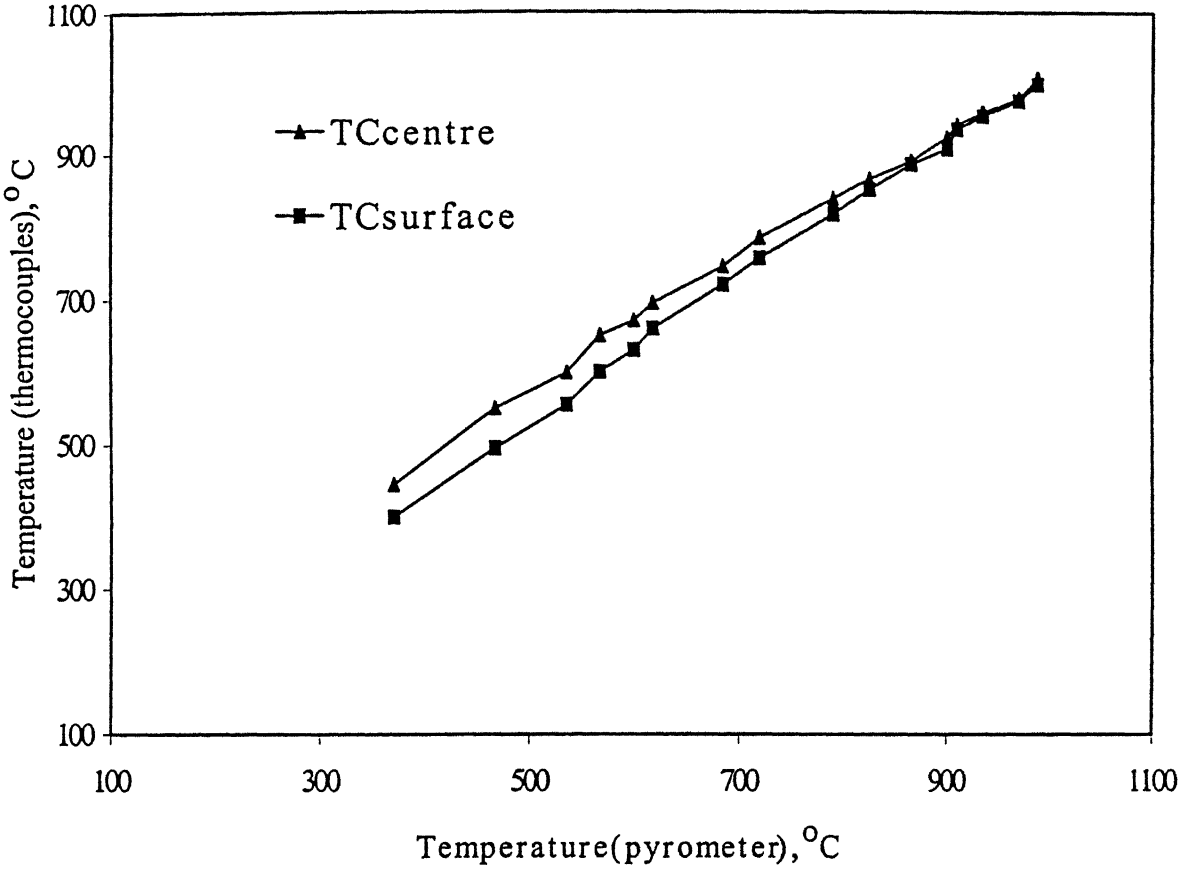

Figure 3.2 : Correlation between the temperatures measured by thermcouples (TC) and the pyrometer.

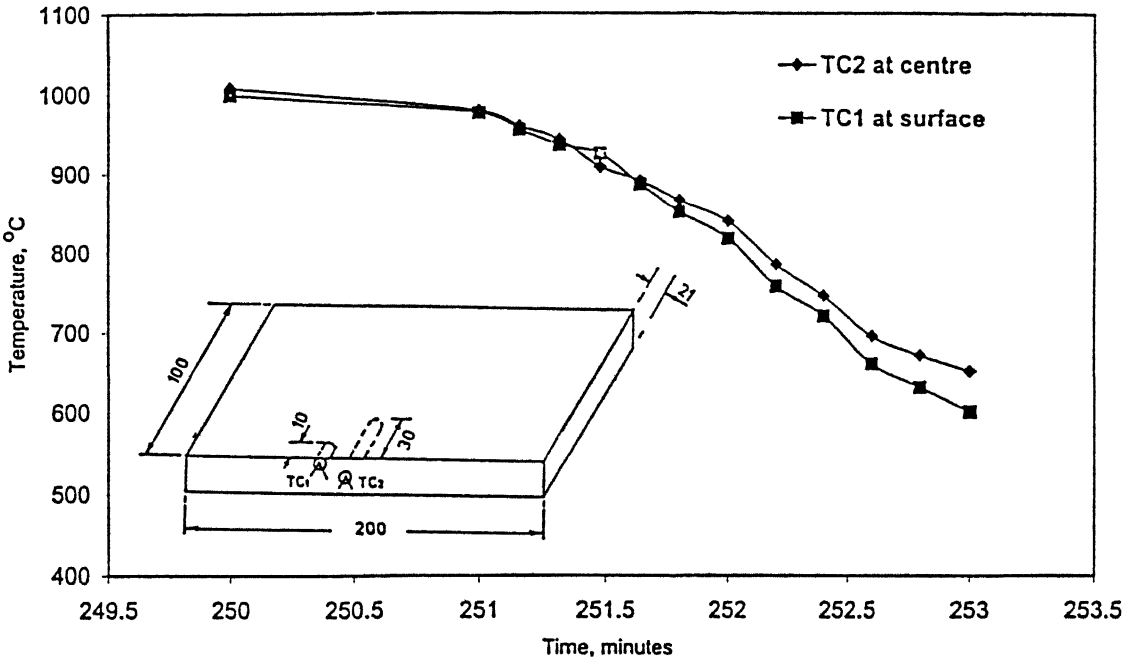

Figure 3.3 : Temperature profiles measured by the thermocouples at the surface (TC1) and the center (TC2) of the samples during multipass rolling (dummy).

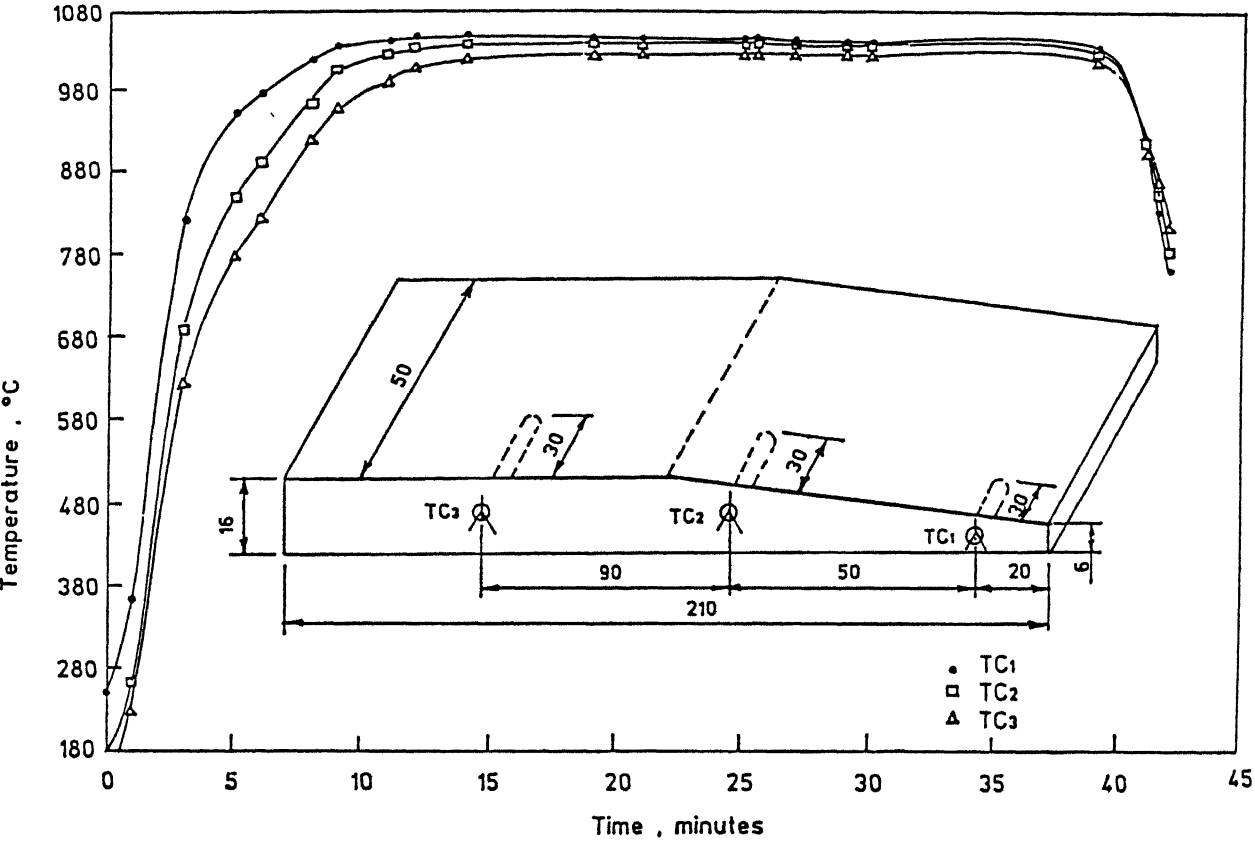

Figure 3.4 : Temperature profile at different locations of the wedge shaped sample during heating, soaking and the single pass rolling (dummy).

the soaking time in each case was 45 minutes. After soaking the bars were kept in air and then rolled in order to arrive at the desired finish rolling temperatures (FRT) of 800 ^{o}C, 700 ^{o}C, 600 ^{o}C and 500 ^{o}C. The total amount of the deformation given at each temperature was ~ 80%. The rolling speed used was 11-12 m min^{-1}. After rolling all the samples were air cooled to room temperature.

3.4.2 Multipass rolling

The relative amounts of deformation in the γ and α temperature ranges were varied according to three different schedules: Schedule 1, 2 and 3. The details of the three schedules are shown in Figure 3.5 (a) to (c). In the first schedule the starting material was given ~ 71 % reduction in the γ region and the resulting material was subjected to further ~ 33% deformation in the α region. These relative amounts of deformation were ~ 42% and ~ 66.6 % in the second and 0% and ~80 % in the third schedule. The total amount of deformation in each schedule was maintained at ~ 80 % as far as practicable. For multipass rolling the soaking was always carried out at 1150 ^{o}C for 45 minutes. Uni-directional rolling of the bar was always maintained during the different passes. The interpass delay times varied between 10 seconds to 60 seconds. After completion of the rolling the warm rolled materials were allowed to cool in the air.

3.5 Annealing treatment

All the warm rolled samples from the three steels (single as well as multi-pass rolling) were annealed in a salt bath furnace at a temperature of 775 ^{o}C for 25 minutes. The heating rate during annealing was maintained at around 8-10 ^{o}C s^{-1}. After annealing

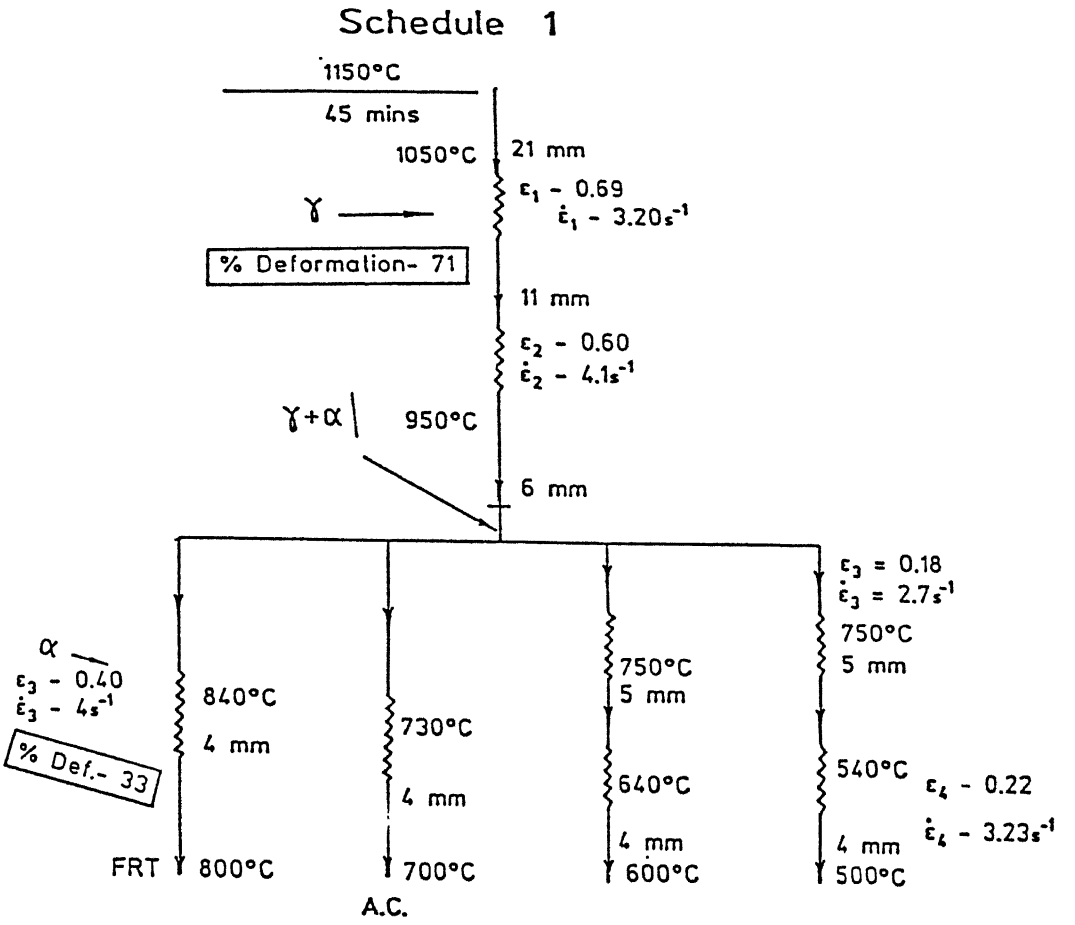

Figure 3.5(a) : Schematic representation of the schedule 1 followed during multipass rolling.

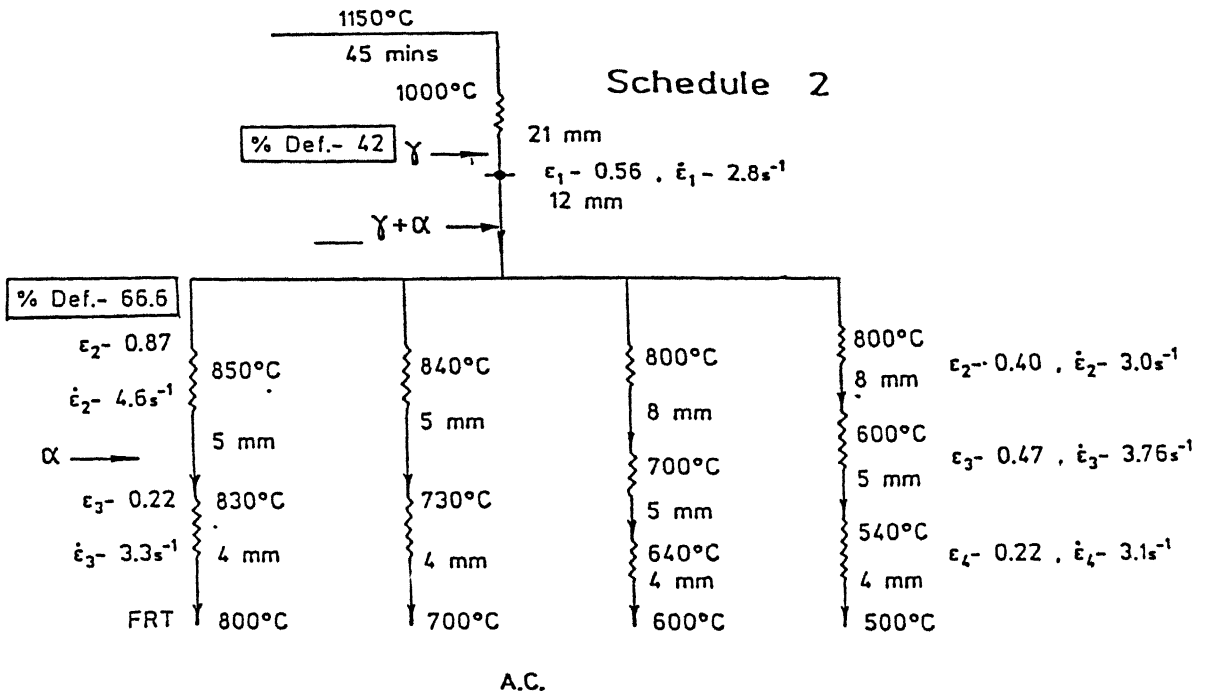

Figure 3.5(b) : Schematic representation of the schedule 2 followed during multipass rolling.

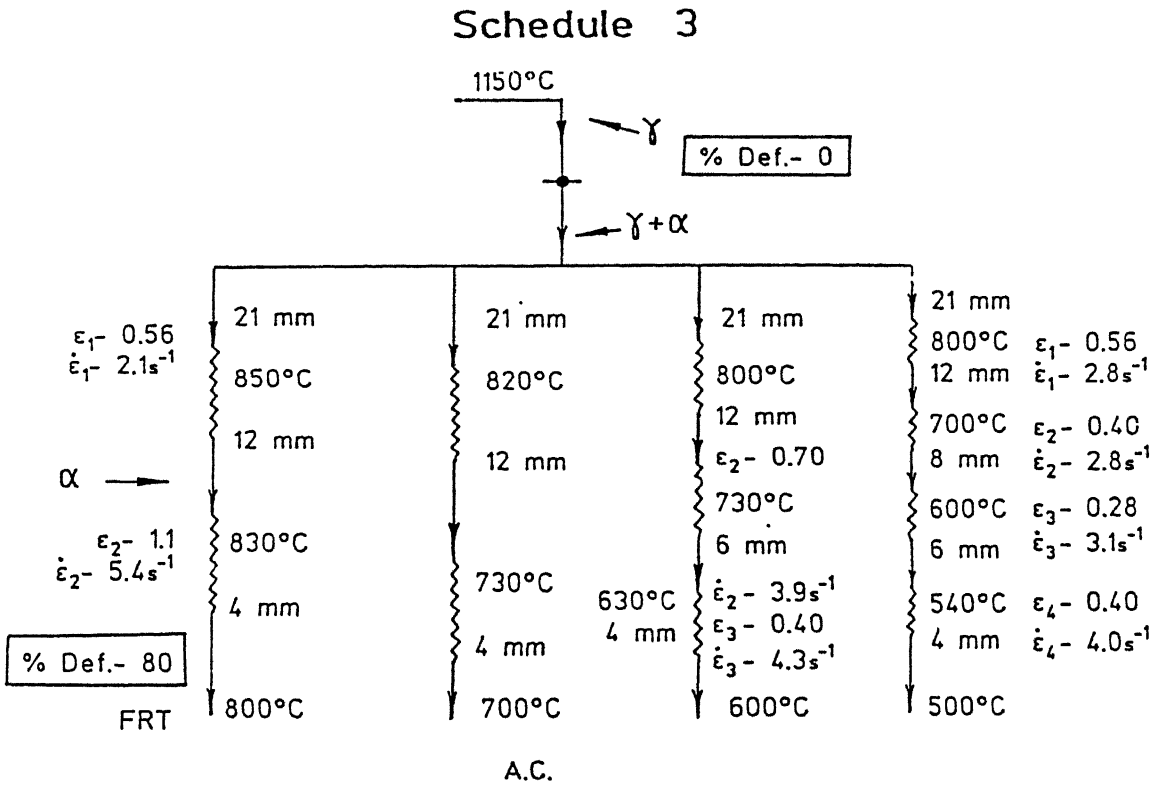

Figure 3.5(c) : Schematic representation of the schedule 3 followed during multipass rolling.

all the samples were quenched in water.

3.6 Dislocation density measurements

The dislocation densities (relative) of different rolled samples were estimated from the measured hardness values (Vicker's, 5 kg load) of the initially soaked (prior to rolling) and the rolled materials. These values were measured from the central parts of longitudinal sections of the specimens. A total of at least five measurements were carried out on each sample and the average value was then considered. The difference in the hardness values of a material at the above two different stages was then determined and this value was squared. This is supposed to be proportional to the dislocation density of the rolled material. It may be pointed out here that Vicker's hardness values vary linearly with the flow stress (36) and flow stress difference arising from the change in dislocation density is proportional to the square root of dislocation density (90).

3.7 Optical microscopy

Optical microscopy was carried out from the starting soaked materials to measure the initial grain sizes and also to reveal the deformation band densities of warm rolled samples. For this purpose etching of the samples was carried out with Nital reagent having a series of concentrations (0.5-5%). Sometimes double and deep etching was done in order to get a clear view of the bands. Even then the deformation bands, sometimes, could not be detected properly under the optical microscope. Point counting method was used to determine the percent area of deformation bands in all the rolled samples. In this method the deformation bands were considered as second phase during counting. A minimum of

500 counts was taken for each sample. A Ziess Exoplan optical microscope was used for this purpose.

3.8 Scanning electron microscopy (SEM)

In a large number of samples optical microscopy could not clearly reveal the deformation bands. Those samples were investigated using a SEM. The longitudinal sections of the samples were used in order to get a better view of the bands. A JEOL JXA 6400 scanning electron microscope operated at an accelerating voltage of 15 to 25 KV was used for this purpose.

3.9 Transmission electron microscopy (TEM)

A selected number of warm rolled as well as annealed samples were studied under TEM to bring out detailed information on the substructural features. The samples were subjected to an initial chemical thinning using a solution of ortho-phosphoric acid and hydrogen peroxide in the ratio of 30:70. These samples were then mechanically thinned down from both sides to 0.1 mm thickness by manual polishing on emery papers. These were electropolished in an electrolytic solution of acetic acid and perchloric acid (80:20) to remove the disturbed surface layers from both sides. Discs of 3 mm were punched out of the thin slices and these were then electrolytically polished by a twin jet electropolisher using a mixture of glacial acetic acid and perchloric acid (80:20) as electrolyte, using 60-70 V at a temperature of about 12 ^{o}C. TEM studies were carried out in a Phillips CM 200 electron microscope with an operating voltage of 200 KV. As far as practicable the thin discs were taken from the mid-thickness regions of the strips.

3.10 Measurement and representation of texture

Crystallographic texture of a rolled polycrystalline sheet metal is represented as {hkl}<uvw>, where {hkl} set of planes is parallel to the rolling plane and <uvw> set of directions is along the rolling direction. Crystallographic textures were measured from the mid-thickness planes of the rolled and heat treated samples. Specimens of the size 24 mm x 14 mm were cut from as rolled and heat treated sheets for this purpose. Initially a little less than half of the total thickness was removed from one of the flat surfaces of the specimens by coarse grinding. The samples were then polished metallographically up to diamond polishing stage. This was followed by electropolishing in an electrolytic solution of glacial acetic acid and perchloric acid (80:20) to remove the disturbed surface layers.

The {110}, {200}, {211} and {113} pole figures were determined by Schulz reflection using Mo K_α radiation with a zirconium filter in a fully computerized texture goniometer. Intensity levels of the pole figures were determined by comparison with the intensity obtained from a solid specimen of pure iron, which had been randomised by repeated deformation and annealing. Orientation distribution functions (ODFs) were calculated from the measured pole figures using the technique developed by Bunge (91).

In this method the orientation of a crystallite in a polycrystalline specimen is specified with respect to the specimen co-ordinate system by the three Eulerian angles φ_1, φ and φ_2. A function known as orient distribution function, f(g), which represents the

relative intensity of orientations, is computed in the form of a series expansion of generalised spherical harmonics calculated from the pole figure data.

The Cartesian Euler angle space, with three dimensional orientation distribution function within, is normally represented, for BCC materials, in the form of sections φ_1= constant (φ_1= 0,5,10, ..., 90^O). Most of the important crystallographic orientations for BCC materials appear in these sections.

From the ODF data the following fibres were plotted:

(i) f(g) versus ϕ for $\varphi_1 = 0^O$, $\varphi_2 = 45^O$ (α fibre)

(ii) f(g) versus φ_1 for $\phi = 55^O$, $\varphi_2 = 45^O$ (γ fibre)

(iii) f(g) versus ϕ for $\varphi_1 = 0^O$, $\varphi_2 = 0^O$ (η fibre)

(iv) f(g) versus φ_1 for $\phi = 45^O$, $\varphi_2 = 0^O$ (ζ fibre) and

(v) f(g) versus ϕ for $\varphi_1 = 90^O$, $\varphi_2 = 45^O$ (ε fibre)

Since the major fibres are located in $\varphi_2 = 45^O$ section, this particular section was also generated in all cases from the ODFs.

Figures 3.6 (a) and (b) represent an isometric view of the three-dimensional Eulerian space and a $\varphi_2 = 45^O$ section containing γ and α fibre orientations, commonly encountered in steels.

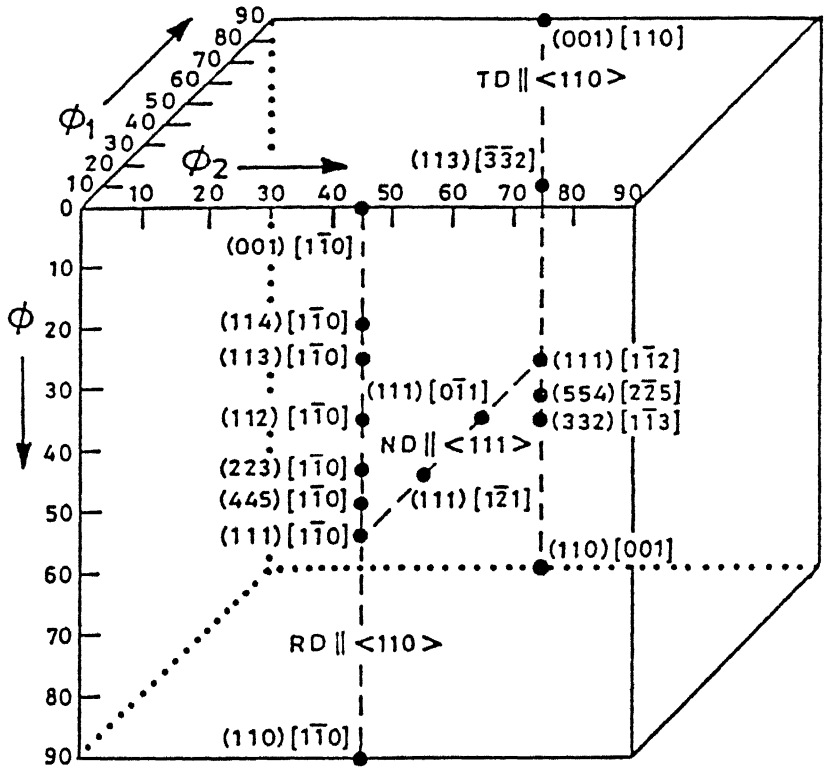

Figure 3.6(a) : Isometric view of the three dimensional Euler space showing locations of ideal orientations.

CHAPTER 4
RESULTS

4. Results

4.1 Initial materials

The average grain sizes of the three steels, soaked at 1150 ^{o}C and 830 ^{o}C, have been measured from their respective microstructures. These are given in a tabular form in Table 4.1 below.

Table 4.1 Average grain sizes of initial materials

Steel	Grain sizes (μm) of initial materials	
	Soaked at 1150 ^{o}C	Soaked at 830 ^{o}C
1	81	70
2	75	50
3	120	78

4.2 Continuous cooling transformation (CCT) diagrams

CCT diagrams for all the three steels were determined after soaking at 1150 ^{o}C and at cooling rates ranging from 0.5 ^{o}C s^{-1} to 100 ^{o}C s^{-1} [Fig. 4.1 (a) to (c)]. The transformation start and finish temperatures have been marked on the corresponding cooling rate curves. The three regimes, γ, $\gamma + \alpha$ and α have been properly marked on each diagram. Using these as guidelines, the four finish rolling temperatures in α, namely 800 ^{o}C, 700 ^{o}C, 600 ^{o}C and 500 ^{o}C were chosen. The cooling rates experienced before rolling started lay between 1 - 2 ^{o}C s^{-1}.

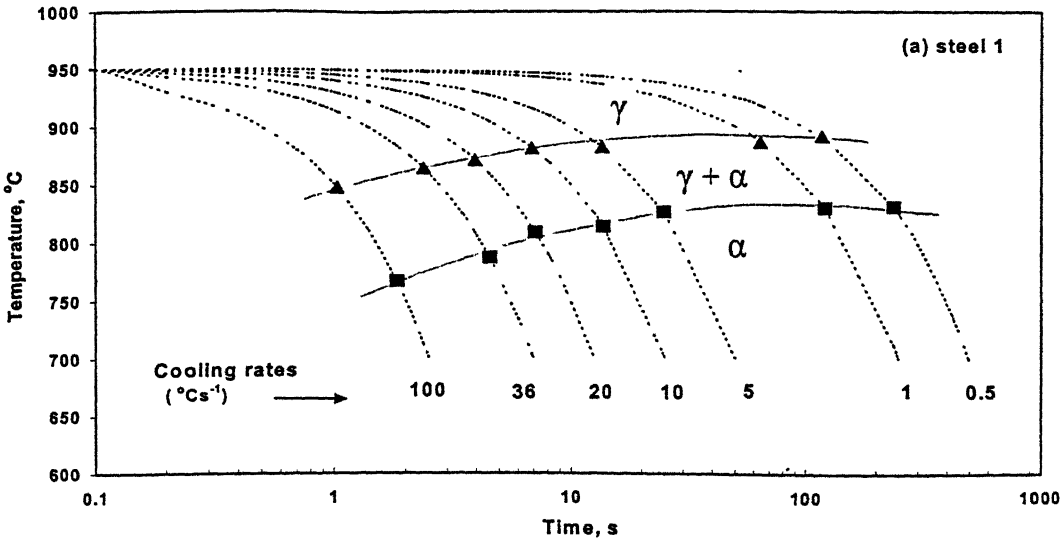

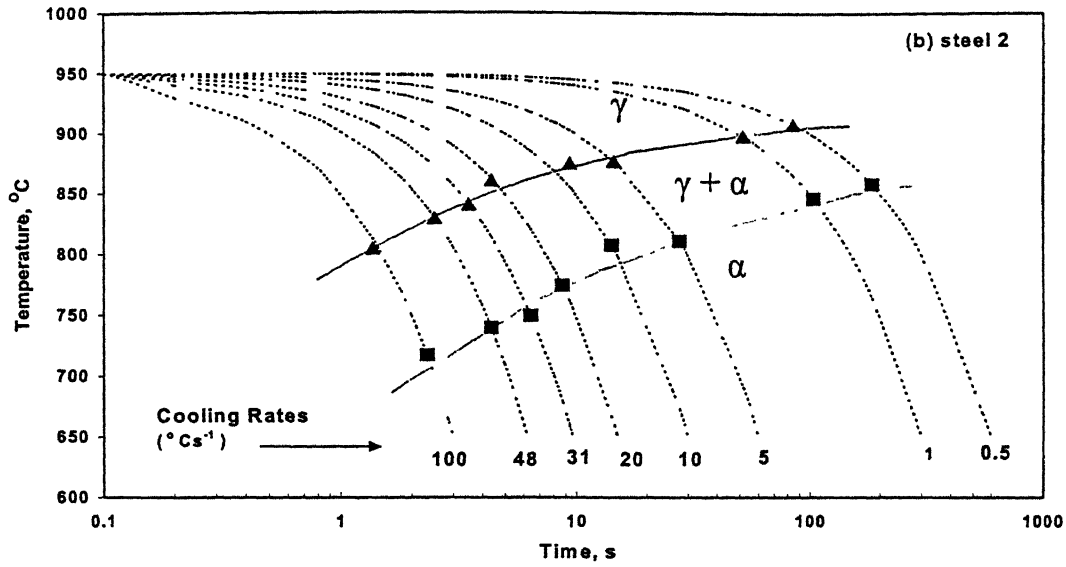

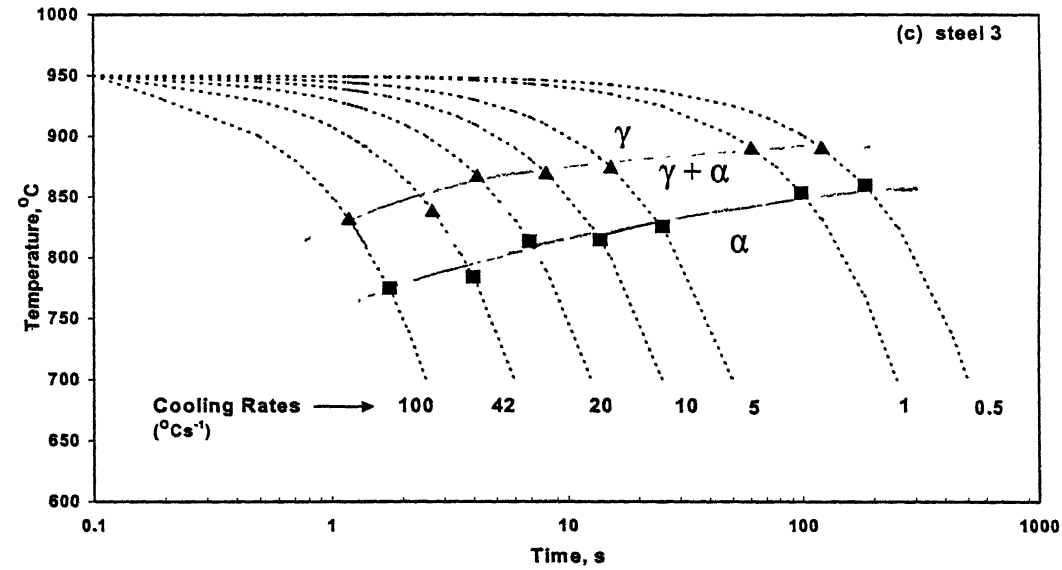

Figure 4.1 : CCT diagrams of three steels

The transformation start and finish temperatures were also determined during the heating cycle, using heating rates of 0.5 $^{O}C\ s^{-1}$, 1 $^{O}C\ s^{-1}$ and 5 $^{O}C\ s^{-1}$. The measured Ac_1 and Ac_3 temperatures have been shown in tabular form in Table 4.2. The average heating rates during soaking was measured as ~ 2 $^{O}C\ s^{-1}$.

Table 4.2 Transformation temperatures during heating

Steel	Heating rate, $^{O}C\ s^{-1}$					
	0.5		1		5	
	Ac_1 (^{O}C)	Ac_3 (^{O}C)	Ac_1 (^{O}C)	Ac_3 (^{O}C)	Ac_1 (^{O}C)	Ac_3 (^{O}C)
1	850	901	856	905	868	906
2	890	908	891	910	892	916
3	870	916	881	922	909	935

It is clear from the Table 4.2 that at the soaking temperature of 830 ^{O}C, all the three steels will be in the ferritic regime.

4.3 Hot deformation study

4.3.1 Steel 1

The flow stress (true stress-true strain) diagrams of steel 1 (soaked at 1150 ^{O}C), as measured over a range of temperatures from 1050 ^{O}C to 500 ^{O}C are shown in Fgure 4.2 (a). In the austenite region (1050 ^{O}C - 950 ^{O}C) the flow stress value increases with decrease in temperature. Evidence of dynamic recrystallisation can be seen in these flow stress curves, which display prominent peaks in stress after which a steady state is attained. In the

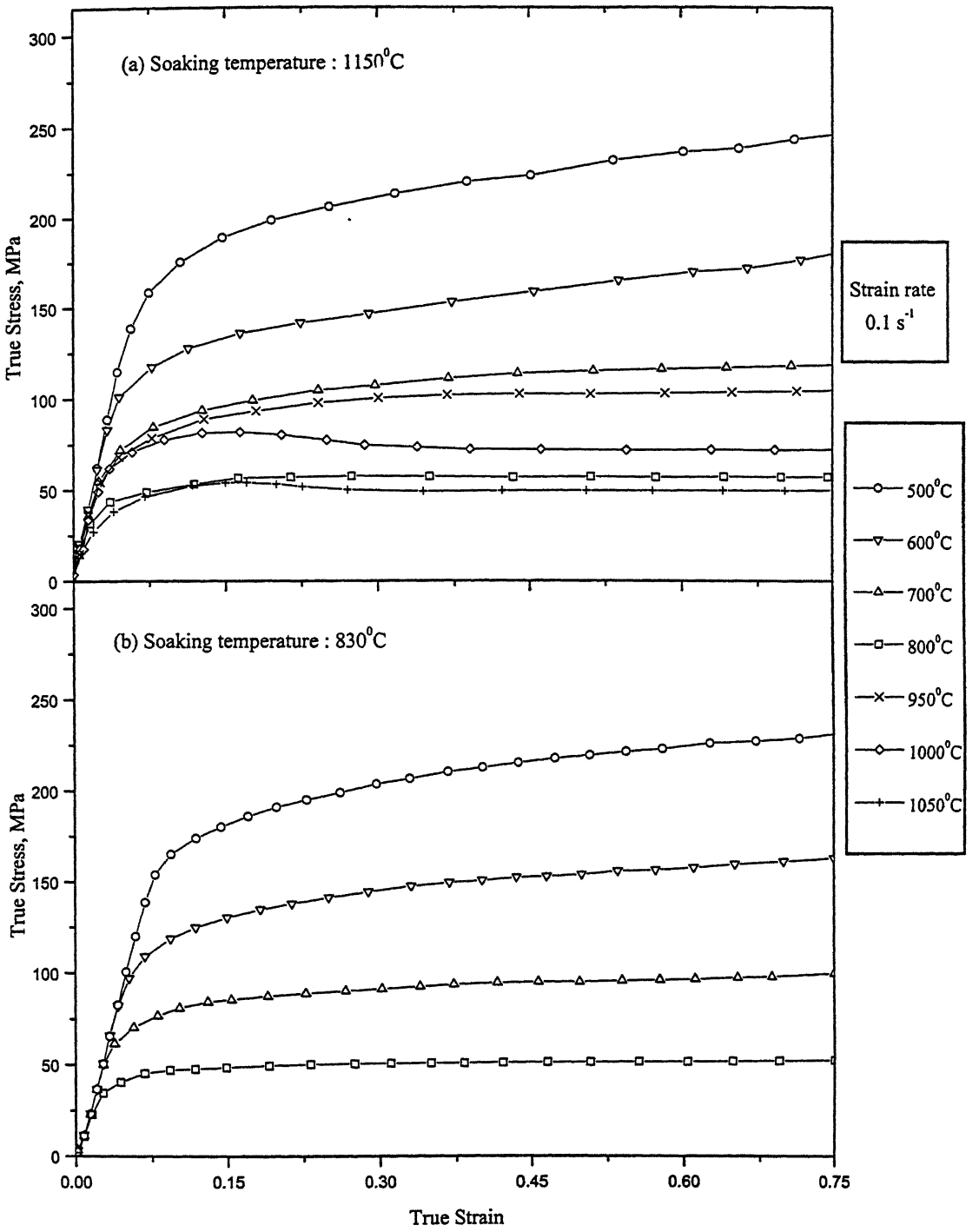

Figure 4.2 : Stress - strain curves of steel 1 at various temperatures.

ferritic range, the flow stress value at 800 ^{o}C was observed to be the lowest and the relevant curve lies close to that for the 1050 ^{o}C plot. The flow stress plots for ferrite at 800 ^{o}C and 700 ^{o}C show distinct signs of a dynamic restoration (recovery) process, as a result of which a steady state is reached at the strain levels of 0.20 and 0.40 at 800 ^{o}C and 700 ^{o}C respectively. The flow stress curves are still rising after a true strain of 0.75 for both the 600 ^{o}C and 500 ^{o}C plots.

The flow stress (true stress - true strain) plots for steel 1 (soaked at 830 ^{o}C), as measured over a wide range of temperatures from 800 ^{o}C to 500 ^{o}C are shown in Figure 4.2 (b). As in the case of the previous set, a steady state is achieved at strain levels of 0.21 and 0.43 at temperatures 800 ^{o}C and 700 ^{o}C respectively, due to dynamic restoration process. However the flow curves at 600 ^{o}C and 500 ^{o}C indicate higher work hardening.

The data in Figure 4.2 (a) were replotted as flow stress versus reciprocal of deformation temperature, at six strain levels, and these are displayed in Figure 4.3 (a). In the austenitic region at all the strain levels the flow stress values increased with decrease in temperature, after which it suddenly dropped due to phase transformation from austenite to ferrite. The flow stress values again increased with decrease in temperature in the ferritic region.

4.3.2 Steel 2

The flow stress diagrams of steel 2 (soaked at 1150 ^{o}C) showed a behaviour similar to those of steel 1 [Fig.4.4 (a)]. As in the previous steel, in the austenitic region the flow

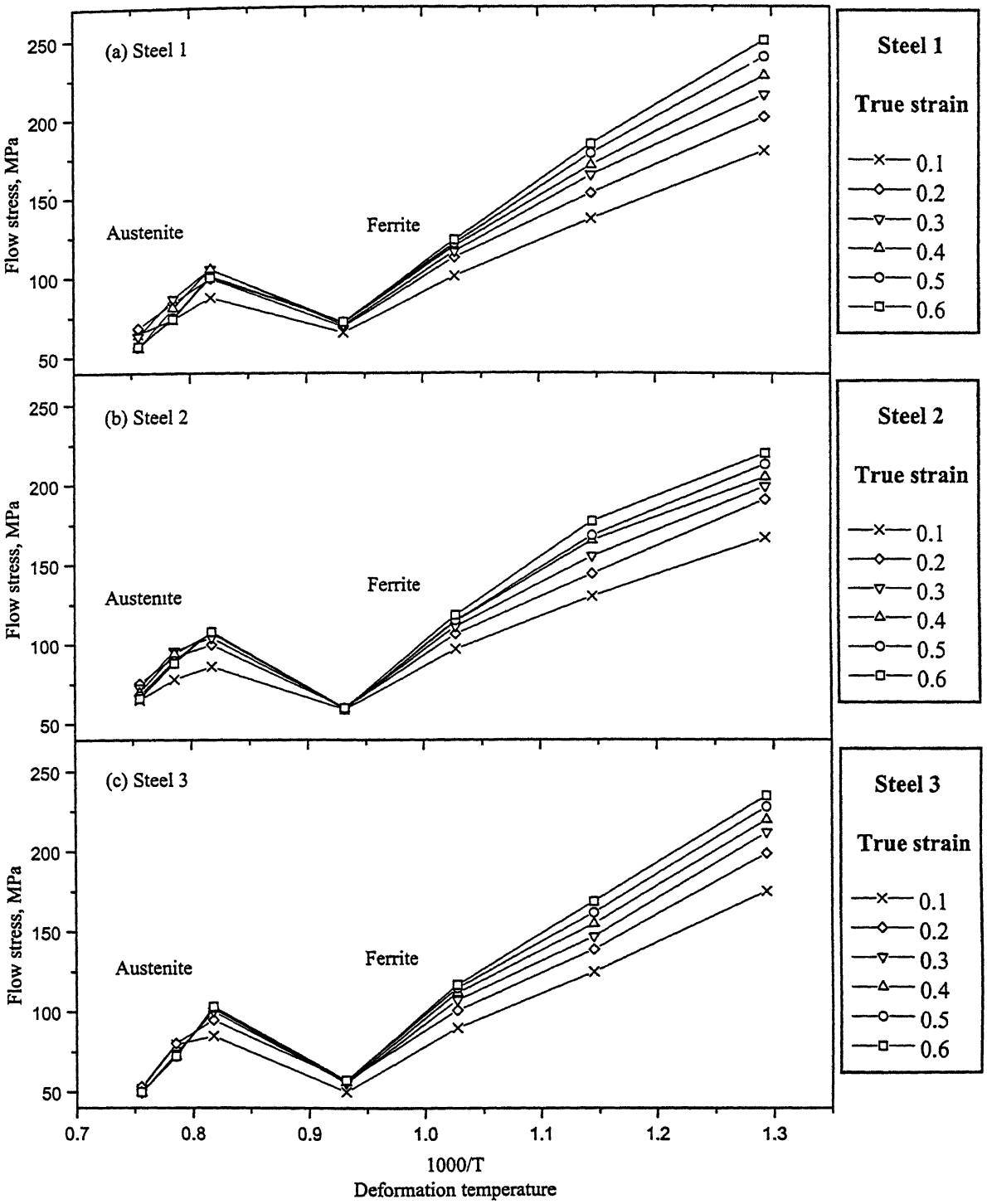

Figure 4.3 : Flow stress versus reciprocal of deformation temperature plots for three steels.

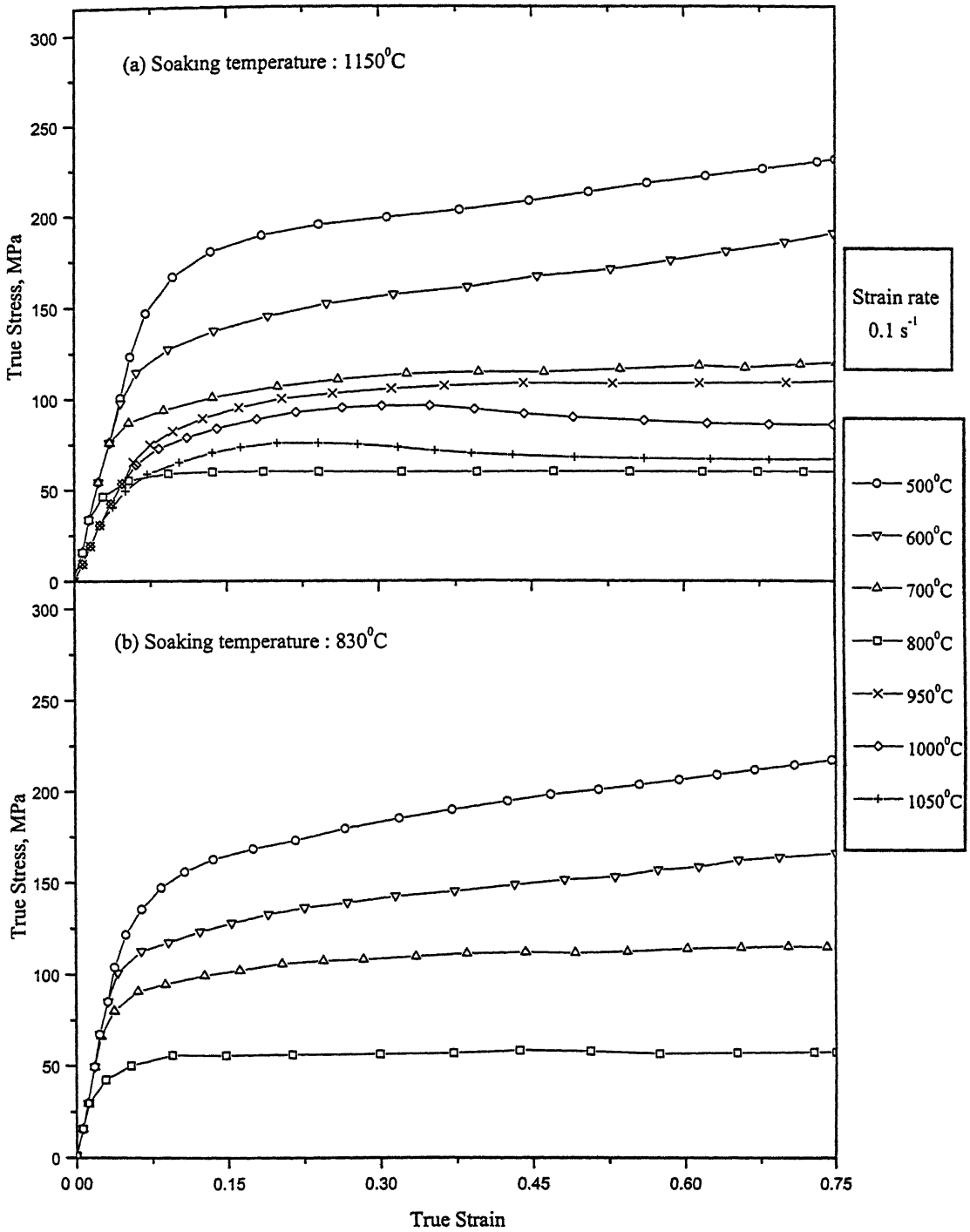

Figure 4.4 : Stress - strain curves of steel 2 at various temperatures.

stress decreases with increase in temperature. Perceptible dynamic flow softening (recrystallisation) is observed at 1050 ^{o}C, 1000 ^{o}C and 950 ^{o}C. In the ferritic region, steady state flow (due to dynamic recovery) is achieved at and beyond the strain levels of 0.18 and 0.39 at 800 ^{o}C and 700 ^{o}C respectively. The flow stress curves at 600 ^{o}C and 500 ^{o}C do not show any dynamic softening up to a true strain of 0.75.

Evidence of dynamic recovery can be clearly seen in the flow curves of steel 2 (soaked at 830 ^{o}C) at 800 ^{o}C and 700 ^{o}C. The steady state is achieved at the strains of 0.27 and 0.47 at these two temperatures respectively [Fig.4.4 (b)]. The flow stress plots at 600 ^{o}C and 500 ^{o}C show a steadily rising trend even up to a strain of 0.75.

The plots of flow stress versus reciprocal of deformation temperature at different strain levels for steel 2 [Fig. 4.3 (b)] show behaviour very similar to those for steel 1.

4.3.3 Steel 3

The flow stress diagrams of steel 3 (soaked at 1150 ^{o}C) measured at temperatures between 1050 ^{o}C and 500 ^{o}C, are shown in Figure 4.5(a). As in the case of the steels 1 and 2, here also, in the austenitic region (1050 ^{o}C to 950 ^{o}C) the flow stress value increases with decrease in temperature. Signs of dynamic recrystallisation can be clearly seen in all these three low stress curves. The flow stress plots for ferrite at 800 ^{o}C and 700 ^{o}C show evidences of dynamic recovery, whereas the plots at 600 ^{o}C and 500 ^{o}C show a rising trend even after a true strain beyond 0.75.

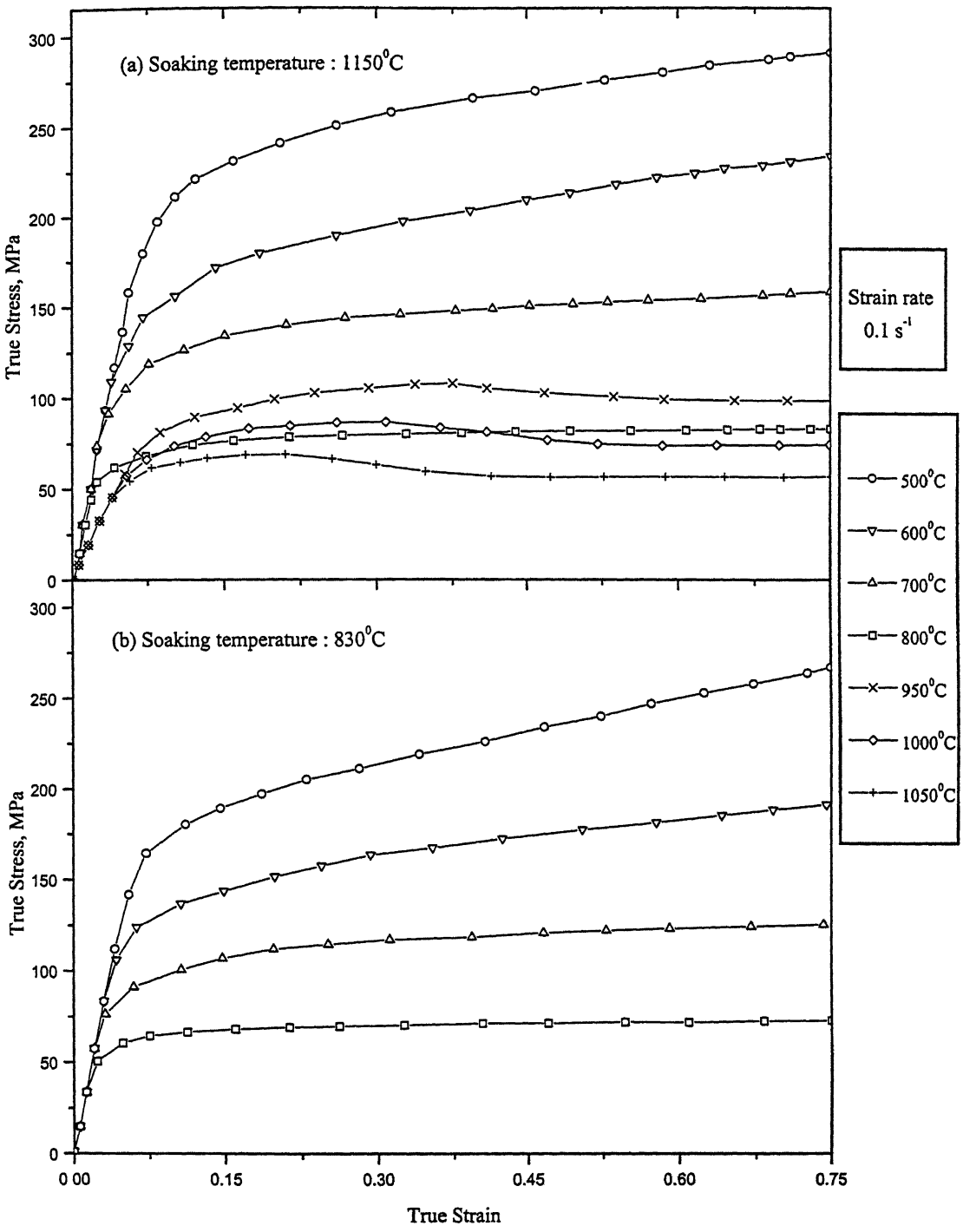

Figure 4.5 : Stress - strain curves of steel 3 at various temperatures.

The flow stress diagrams of steel 3 (soaked at 830 ^{o}C) as displayed in Figure 4.5 (b) show trends similar to steel 2.

The plots of the flow stress versus the reciprocal of the deformation temperature for steel 3 at various strain levels are shown in Figure 4.3 (c) The nature of these plots are very similar to the corresponding plots of steel 2.

4.4. Microstructural characterisation of warm rolled steels

All the three warm rolled steels display a large density of deformation bands (in-grain shear bands) after rolling under various conditions. In view of their great importance in the microstructural and textural evolution in these steels, an attempt has been made to characterise these bands using optical and scanning electron microscopy. In addition, the dislocation densities of the warm rolled steels were also measured. Finally, selected number of thin foils made from all the three steels were carefully examined in a transmission electron microscope (TEM) in order to have a clear idea of their substructural features.

4.4.1. Deformation bands

The deformed microstructures of the warm rolled steels generally consist of ferrite grains, with a large fraction of them containing deformation bands. These bands appear as approximately parallel lines within grains. Etching of the bands was sometimes found to be difficult, particularly in case of the IF steels. Examples of banded grains in the ELC steel (steel 1) are shown typically in Figures 4.6. (a) – (f). A comparison of Figure 4.6(a) and

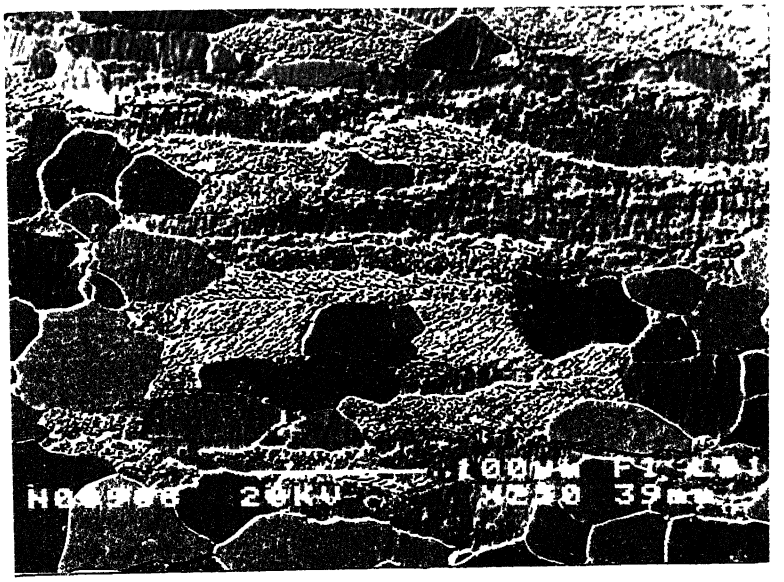

(a) FRT : 800 ^{o}C

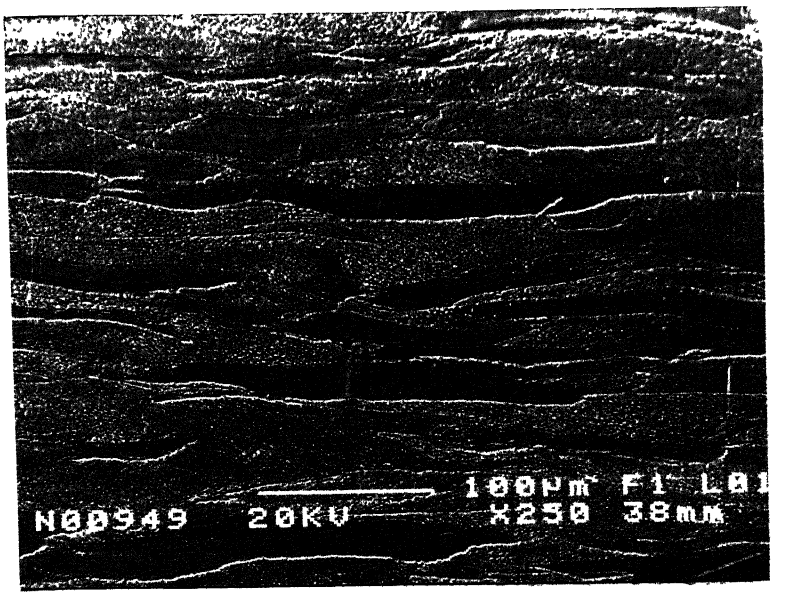

(b) FRT : 600 ^{o}C

RD ⟶

Figure 4.6 (a) and (b) : Typical microstructures of steel 1 after single pass rolling [after soaking at 1150 ^{o}C].

(c) FRT : 500 ^{O}C

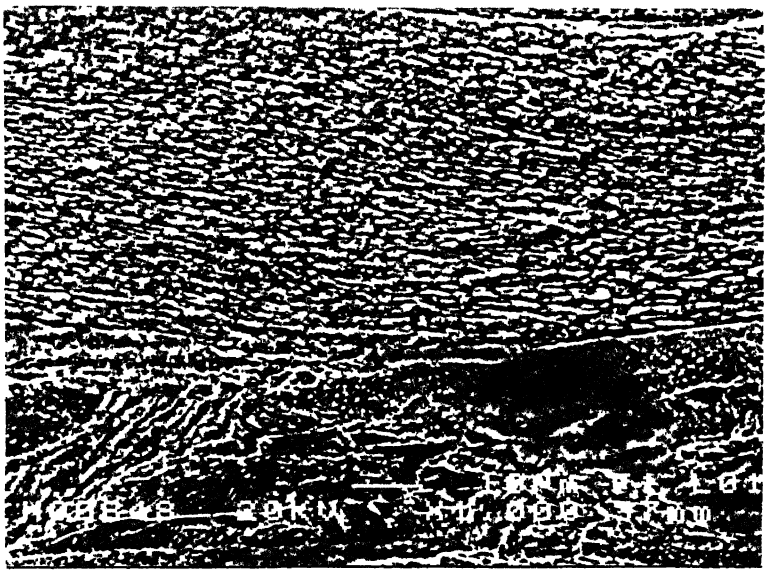

(d) FRT : 500 ^{O}C

RD ⟶

Figure 4.6 (c) and (d) : Typical microstructures of steel 1 after single pass rolling [after soaking at 830 ^{O}C].

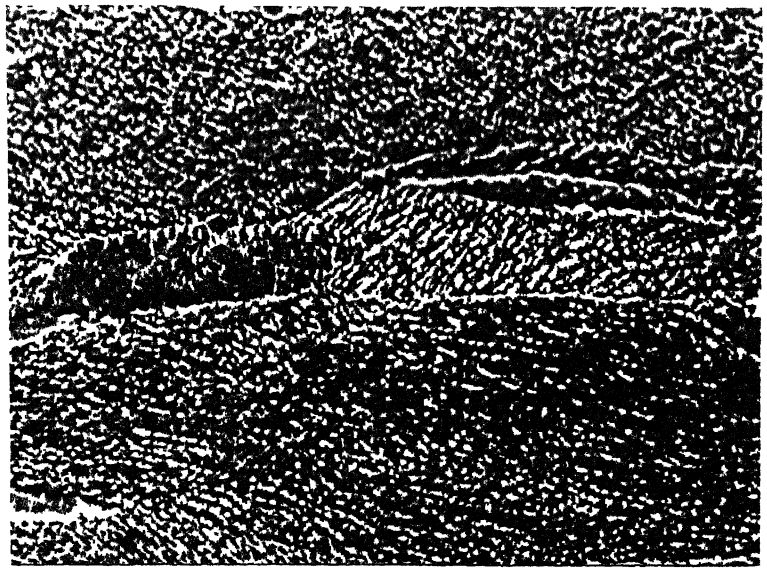

(e) FRT : 600 ^{o}C

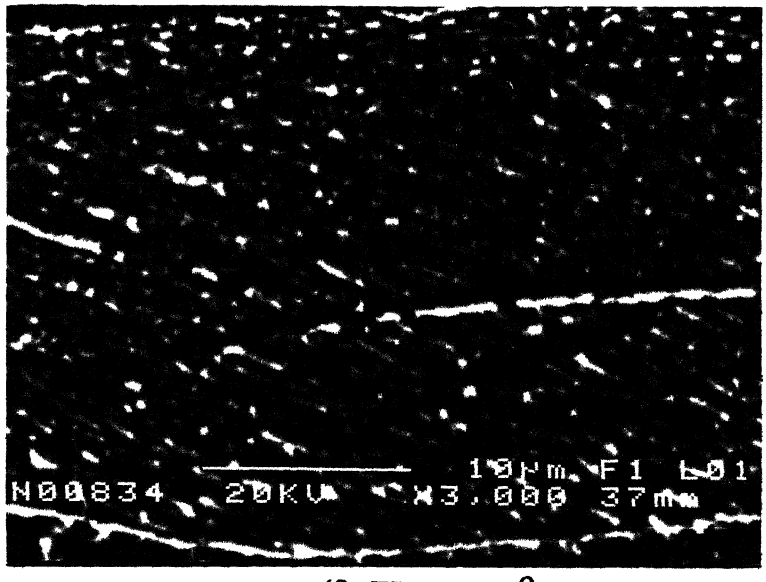

(f) FRT : 500 ^{o}C

RD ⟶

Figure 4.6 (e) and (f) : Typical microstructures of steel 1 after single pass rolling [after soaking at 830 ^{o}C].

Figure 4.6(b) shows clearly that the ferrite grains are polygonal in shape when the FRT is high (800 ^{o}C) whereas deformed and elongated ferrite grains are obtained at lower FRT (600 ^{o}C). Higher magnification micrographs clearly reveal the individual bands [Fig.4.6 (c)]. It has been observed that the bands are inclined at various angles ranging from ~ 16^{o} to as high as ~ 32^{o} with the rolling direction. Sometimes bands nearly parallel to the rolling direction are also seen [Fig.4.6 (d)]. In many cases, in the ELC steel, the bands appear rather discontinuous [Fig. 4.6(e)]. At some places the bands appear to have the same physical orientation across a grain boundary [Fig. 4.6(f)]. Presumably these are the macroscopic shear bands having much larger flow localisation.

All the above examples of deformation bands were taken from the single pass rolled steel 1. The density of deformation bands in the multipass rolled materials in steel 1 has been found to be significantly less than in the single pass rolled samples. In fact, in the multipass rolled steel 1, polygonal grain structure has been obtained for the samples with higher FRTs such as 800 ^{o}C and 700 ^{o}C, while typical deformed structures were revealed by the samples finish rolled at lower temperatures, such as 500 ^{o}C. This was found to be true for schedules 1 and 2 of multipass rolling. These differences are shown typically in Figures 4.7 (a) and (b). On the other hand, after rolling under schedule 3, even samples with the higher FRT (700 ^{o}C) show a deformed structure only, the elongated grains showing hardly any deformation band inside.

Quantitative measurement of the degree of banding in each sample was obtained by assuming the banded regions as a second phase and then measuring the area percent of the

100 μm

(a) FRT : 800 °C

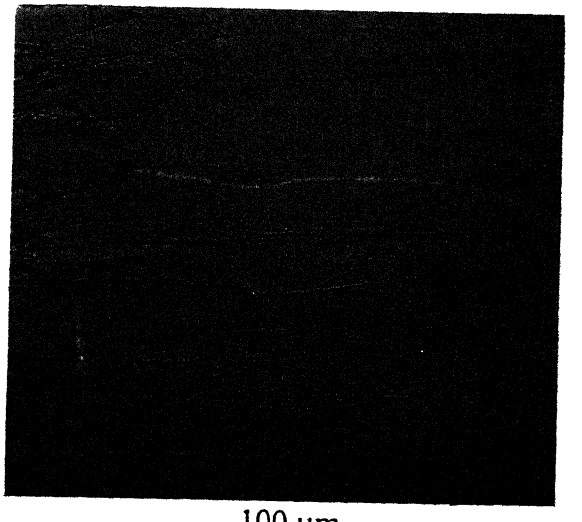

100 μm

(b) FRT : 500 °C

RD ⟶

Figure 4.7 (a) and (b) : Optical micrographs showing typical microstructures of steel 1 after multipass rolling under schedule 2.

bands by a simple point counting technique. Figure 4.8 (a) displays plots of % area of deformation bands versus FRT during single pass rolling for two different soaking temperatures in case of steel 1. Evidently, the density of deformation bands is substantially high when FRT is low and it decreases rapidly with increase in FRT and then ultimately becomes effectively zero for an FRT of 800^0C. The samples, which were soaked at higher temperature of 1150^0C, show significantly larger density of DB than the samples soaked at 830^0C. The variation of % area of DB with FRT for multipass rolling [Fig 4.8 (d)] follows the same trend as in Figure 4.8 (a), however, here the densities of DB, in general, are substantially lower than in the previous case. Out of the three schedules, the samples, which were rolled according to schedule 3, show higher densities of DB than those treated under schedules 1 and 2.

Typical banded structures for the IF steels 2 and 3 are depicted in Figures 4.9 (a)–(d), for both single pass and multipass rolling. As in case of the ELC steel 1, the bands in these steels also make angles ranging between ~ 16^O to ~ 32^O with the rolling direction. The % area of deformation bands versus FRT plots [Fig. 4.8 (b) and (e)] for steel 2 show clearly that the density of DB remains within a narrow band of ~ 25 - 30 % over a range of FRT s from 500 – 700 ^{O}C, above which there appears to be a perceptible increase. The samples with a soaking temperature of 1150 ^{O}C in general, show a higher value of DB density than the ones with a soaking temperature of 830 ^{O}C. The densities of DB in samples treated under all the three schedules of multipass rolling are very much the same and their values hardly change with the FRT [Fig.4.8 (e)]. For steel 3 the trends of the % area of DB versus FRT plots for both single pass and multi pass rolling [Fig. 4.8 (c) and

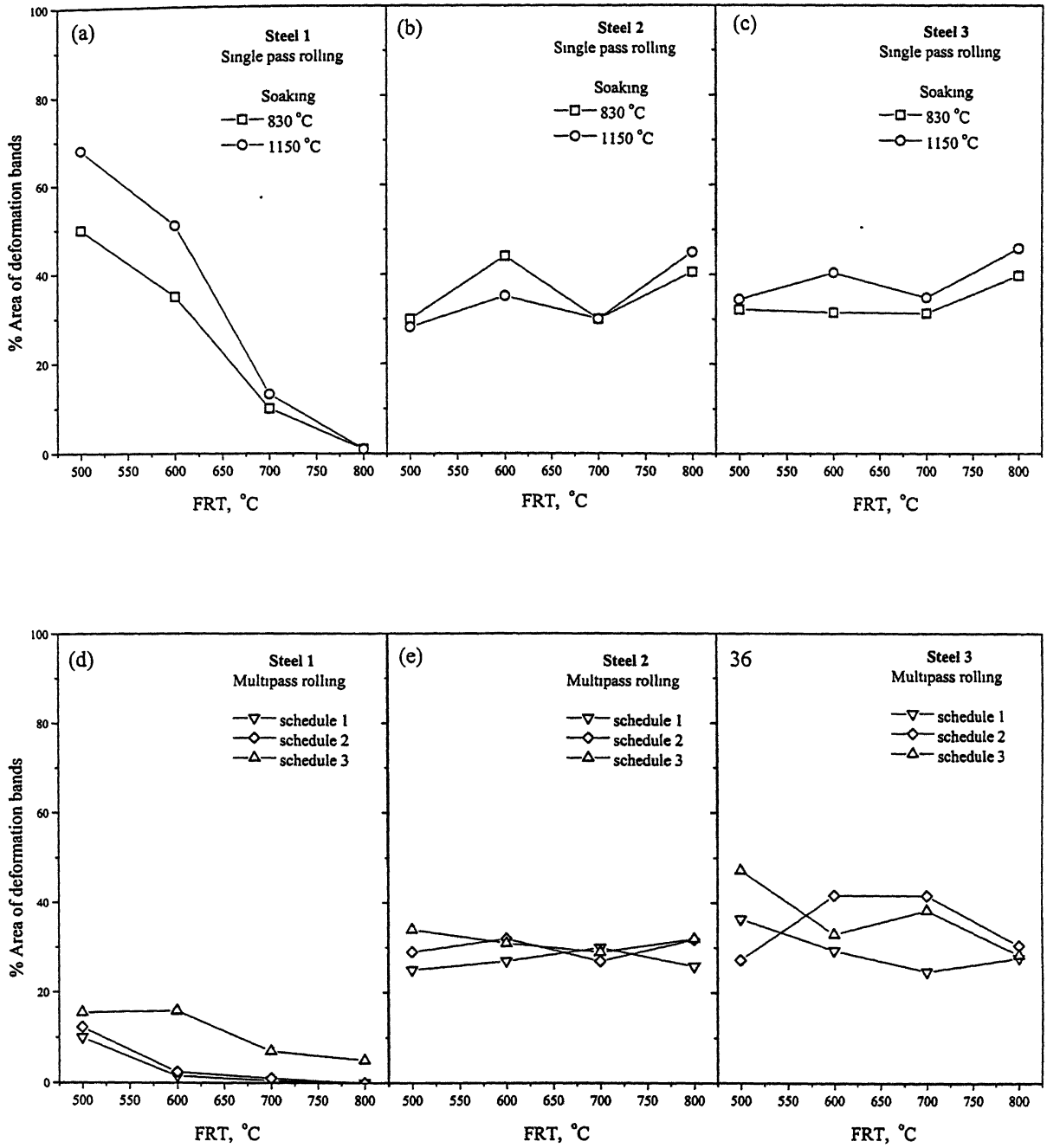

Figure 4.8 : Effect of FRT on % area of deformation bands for three steels during single pass (a, b, c) and multipass (d, e, f) rolling.

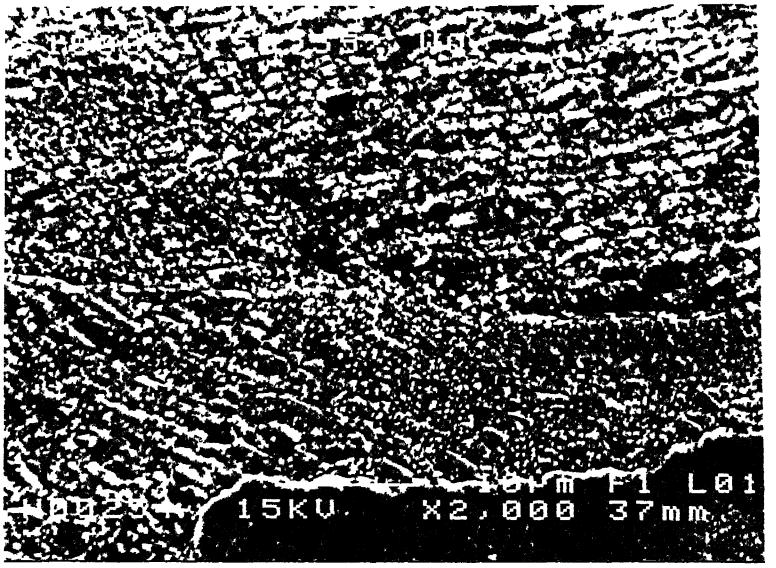

(a) FRT : 800 ^{o}C

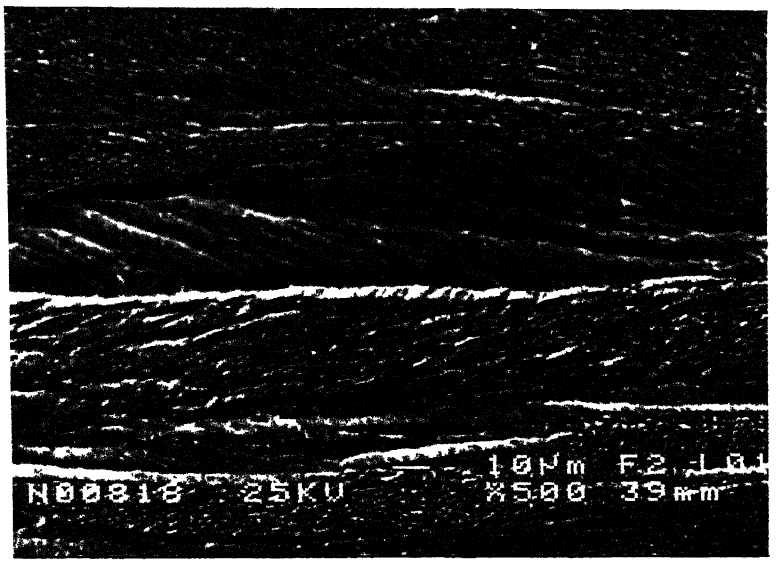

(b) FRT : 500 ^{o}C

RD ⟶

Figure 4.9 (a) and (b) : Typical microstructures of steel 2 after (a) single pass rolling [after soaking at 1150 ^{o}C] and (b) multi pass rolling [schedule 3].

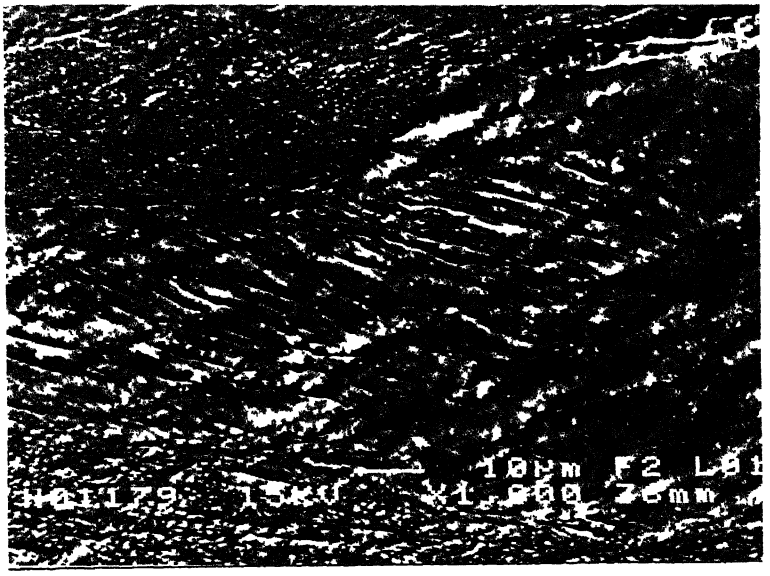

(c) FRT : 500 ^{o}C

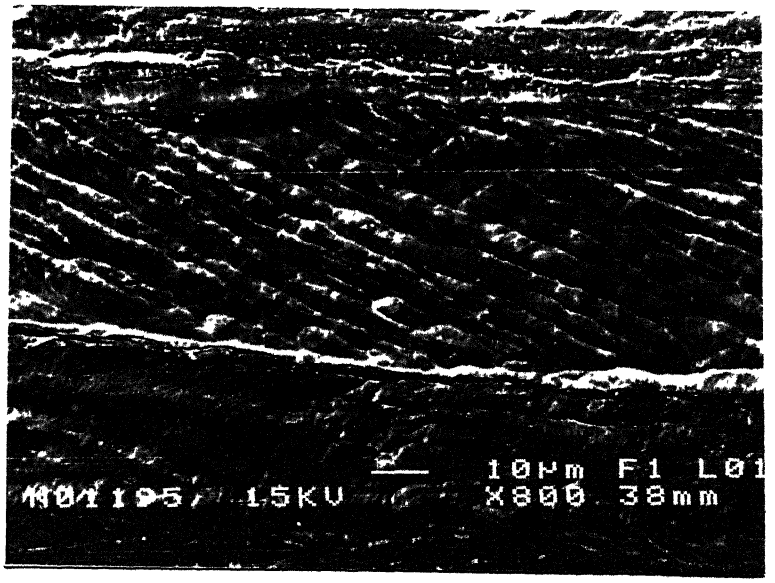

(d) FRT : 700 ^{o}C

RD ⟶

Figure 4.9 (c) and (d) : Typical microstructures of steel 3 after (c) single pass rolling [after soaking at 830 ^{o}C] and (d) multi pass rolling [schedule 2].

(f)] appear very much similar to the corresponding plots for steel 2. The only difference is that the values of % area of DB in the three schedules vary within a much wider band compared to the samples of steel 2.

The typical mean and standard deviation of deformation band orientations with respect to the rolling direction, for all the three steels, under different conditions, are given in Tables 4.3 and 4.4. It is quite clear from this table that no specific pattern of variation of DB orientation angles with rolling direction emerges as functions of steel composition, type of rolling deformation, soaking temperature or FRT. This aspect is also apparent from the plots of cumulative distribution of DB angles to the rolling direction, as shown in Figures 4.10(a) - (d).

4.4.2. Dislocation density

The dislocation densities in samples from all the steels, after warm rolling at different temperatures, were estimated from their hardness values and these are displayed in Figures 4.11(a) to (f). The calculated densities were normalised by dividing the values by the highest value encountered. Figure 4.11(a) shows that for steel 1, the normalised dislocation density for the 1150 ^{o}C soaked materials are always higher than those for the 830 ^{o}C soaked samples. In fact amongst all the samples, the one which was single pass rolled with an FRT of 500 ^{o}C, shows the highest dislocation density. As expected, the dislocation density decreases rapidly with increase in FRT. The dislocation density versus FRT plots for all the three schedules during multipass rolling of steel 1 [Fig. 4.11(d)] also shows a similar behaviour. Figure 4.11(b) displays the plot of normalised dislocation

Table 4.3 Mean and standard deviation of deformation band angles with respect to the rolling direction [single pass rolling]

Steel 1				
	Soaking at 1150 ^{O}C		Soaking at 830 ^{O}C	
FRT (^{O}C)	Mean deformation band angle to RD (^{O})		Mean deformation band angle to RD (^{O})	
800	-	-	-	-
700	-	-	-	-
600	27.9 ± 12.0	-18.9 ± 6.5	30.8 ± 7.5	-21.8 ± 9.6
500	23.7 ± 6.2	-15.4 ± 6.9	22.9 ± 6.2	-22.9 ± 4.4
Steel 2				
800	16.4 ± 12.3	-16.9 ± 6.7	-	-
700	-	-23.1 ± 8.9	24.7 ± 6.8	-34.4 ± 8.3
600	11.8 ± 2.6	-25.8 ± 7.3	24.3 ± 9.5	-27.3 ± 8.9
500	18.6 ± 9.8	-24.5 ± 3.9	22.9 ± 6.7	-20.0 ± 10.4
Steel 3				
800	23.9 ± 8.4	-19.5 ± 5.3	19.5 ± 3.7	-20.5 ± 7.6
700	-	-	-	-
600	17.1 ± 7.2	-18.5 ± 3.3	21.9 ± 12.8	-23.4 ± 5.4
500	16.6 ± 8.7	-18.7 ± 1.0	24.4 ± 4.9	-21.2 ± 4.9

Table 4.4 Mean and standard deviation of deformation band angles with respect to the rolling direction during multipass rolling

Steel 2						
	Schedule 1		Schedule 2		Schedule 3	
FRT (^{O}C)	Mean deformation band angle to RD (^{O})		Mean deformation band angle to RD (^{O})		Mean deformation band angle to RD (^{O})	
800	12.7 ± 10.5	-12.2 ± 7.6	28.8 ± 4.4	-34.5 ± 5.0	-	-
700	25.9 ± 6.4	-24.3 ± 6.1	33.9 ± 1.4	-33.7 ± 7.2	-	-
600	-	-	-	-	20.2 ± 5.0	-21.7 ± 3.8
500	32.7 ± 2.2	-22.8 ± 23	28.6 ± 2.5	-33.0 ± 3.1	20.6 ± 5.6	-
Steel 3						
800	29.6 ± 9.5	-26.2 ± 6.3	18.2 ± 4.3	-26.9 ± 8.6	23.1 ± 4.9	-18.0 ± 1.7
700	-	-	28.5 ± 6.0	-23.3 ± 4.9	-	-
600	29.1 ± 4.0	-25.0 ± 5.3	22.4 ± 4.0	-21.1 ± 4.2	23.7 ± 5.8	-14.4 ± 1.6
500	30.5 ± 4.9	-27.3 ± 5.1	31.5 ± 4.6	-22.5 ± 4.4	-	-

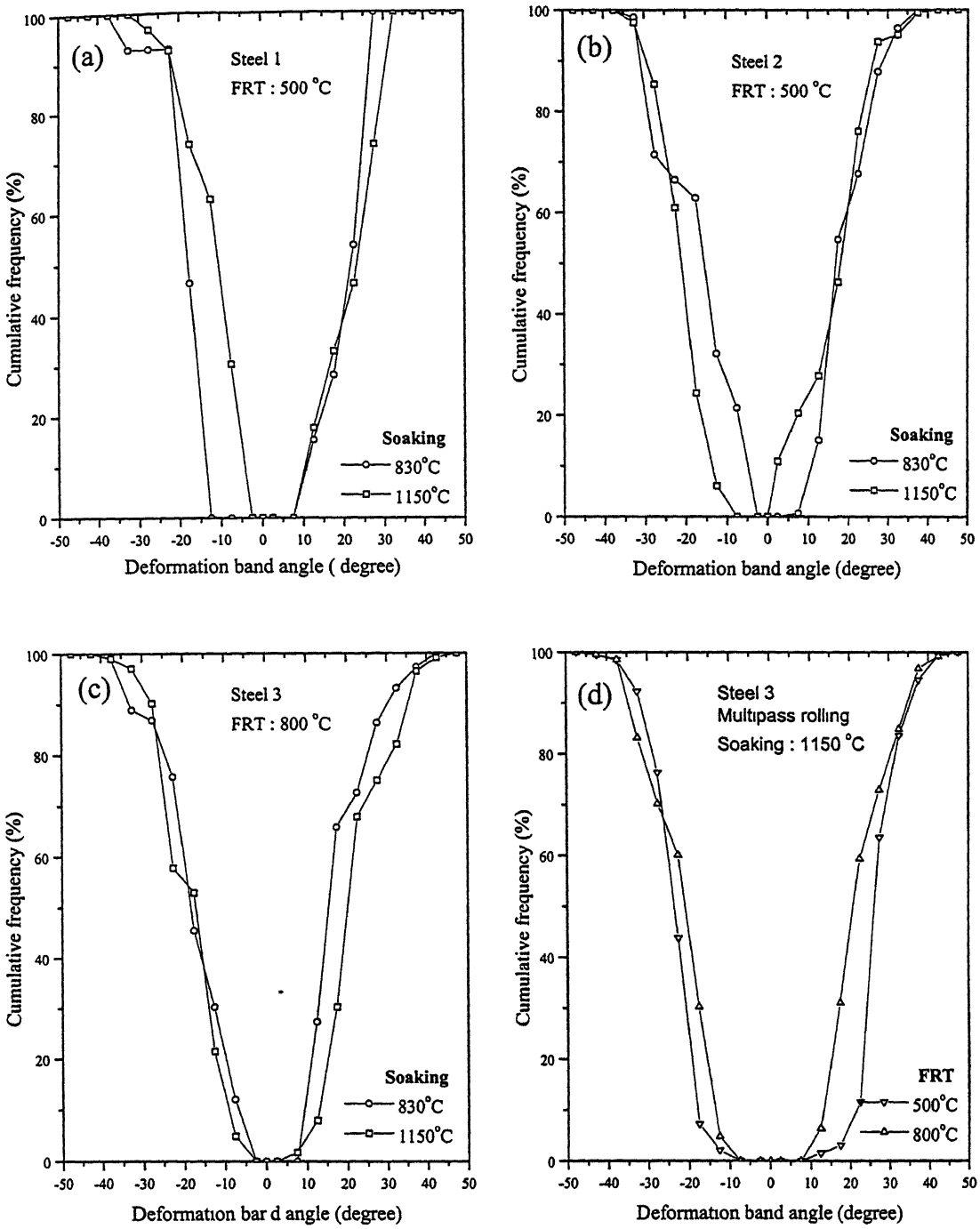

Figure 4.10 : Typical cumulative distributions of deformation band angles to the rolling directions in three steels.

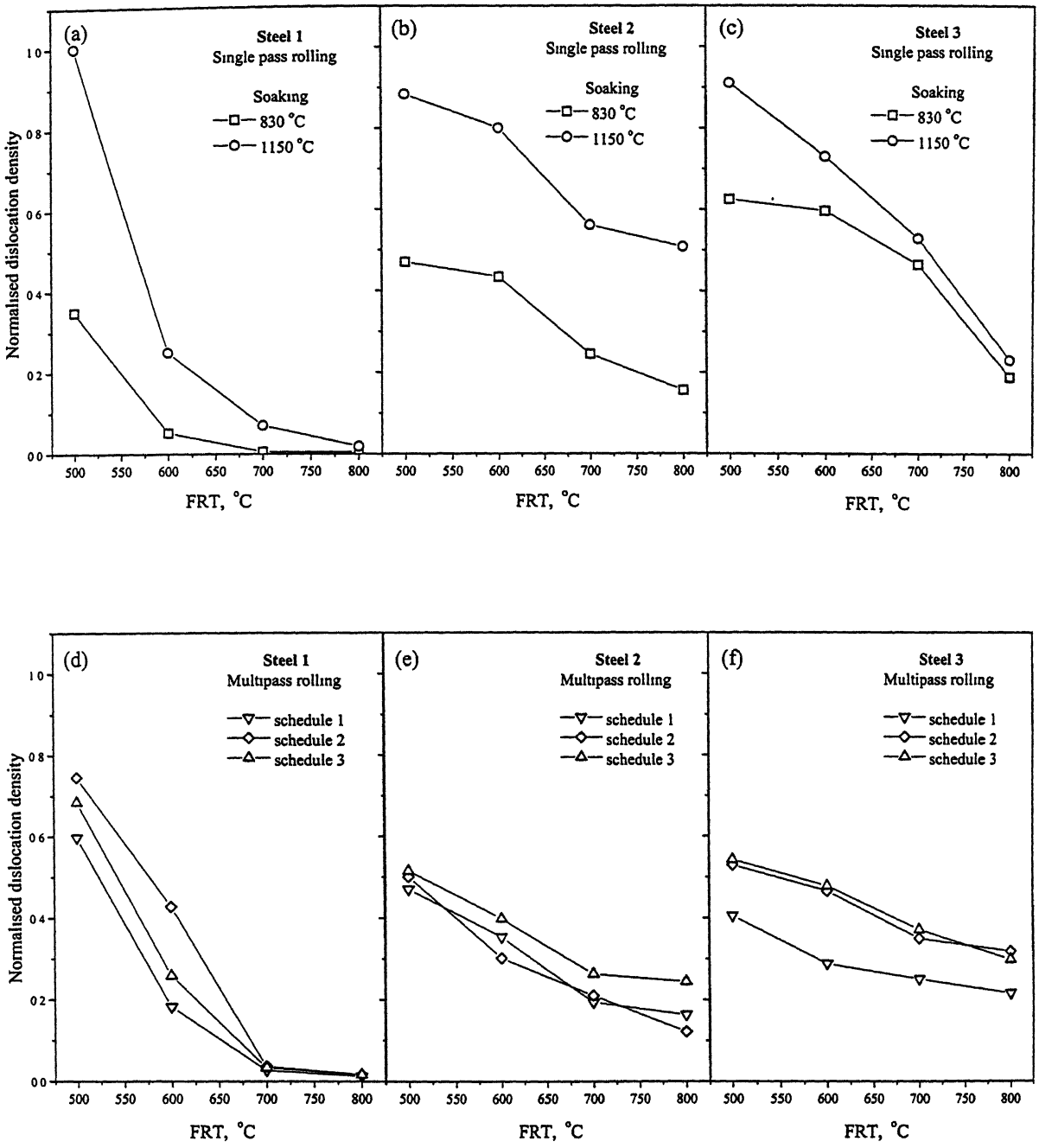

Figure 4.11: Effect of FRT on normalised dislocation density for three steels during single pass (a, b, c) and multipass (d, e, f) rolling.

density versus FRT for single pass rolled steel 2 for two different soaking temperatures. As in case of steel 1, here also the 1150 ^{o}C soaked samples show a much higher dislocation density as compared to those soaked at 830 ^{o}C, at all the FRT s. In fact, in this steel the decrease in dislocation density with increase in FRT is less drastic as compared to steel 1.The multipass rolled samples of steel 2, for all the three schedules, also show a behaviour similar to the samples of steel 1[Fig. 4.11(e)]. However, the decrease of dislocation density with increasing FRT is much less drastic here than in samples for steel 1. The plots [Fig.4.11(c) and (f)] of normalised dislocation density versus FRT, for both single pass and multipass rolled samples of steel 3, are very much similar to those obtained for steel 2. The most important difference between these plots for the ELC steel on one hand and the IF steels on the other, is that whereas the normalised dislocation density becomes almost zero at an FRT of 700^{0}C for the ELC steel, it has a substantial value in the IF steels right upto the highest FRT, namely 800^{0}C.

4.4.3 Substructural features

As mentioned earlier, a limited number of thin foils were prepared for transmission electron microscopy from all the three steels, subjected to single pass rolling. The foils were all made from the rolling plane section.

Fig. 4.12(a) shows a typical TEM micrograph of steel 1, soaked at 1150 ^{o}C and finish rolled at 500 ^{o}C. The microstructure here consists of highly dislocated cells and looks very much like a cold rolled structure. Sometimes the cells show signs of fine precipitation [Fig.4.12 (b)]. Evidence of subgrain formation, characteristic of a dynamic

(a) FRT : 500 ^{o}C

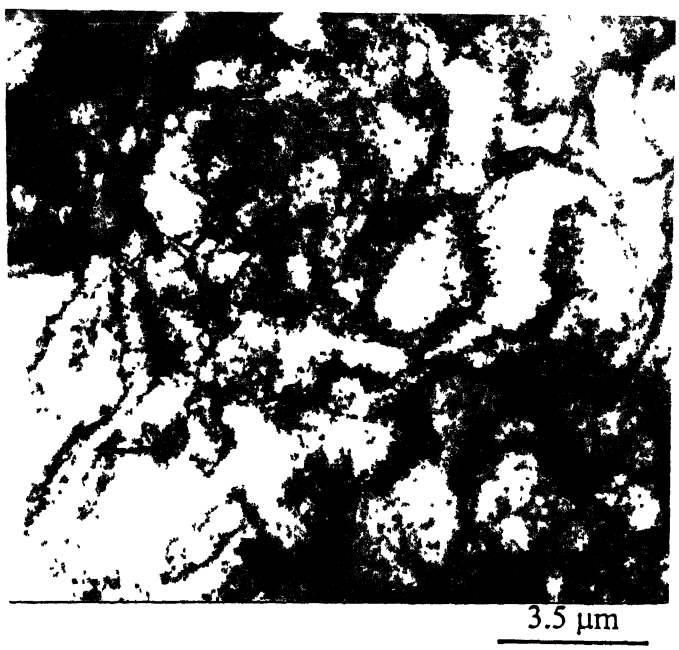

(b) FRT : 500 ^{o}C

Figure 4.12 (a) and (b) : TEM micrographs showing (a) dislocated cells and (b) fine precipitates along with dislocated cells in steel 1 [single pass rolling after soaking at 1150 ^{o}C].

restoration process, can also be seen at a few places [Fig.4.12(c)]. At a few places band like structures are also seen [Fig.4.12 (d)]. Cells with very high dislocation density at the cell boundaries but fewer dislocations inside are seen in the thin foils made from 830 ^{o}C soaked sample of steel 1, finish rolled at 500 ^{o}C [Fig.4.12 (e)]. The microstructure from a deformation banded region [Fig.4.12 (f)] show a fine cell structure, with signs of recovery in a few of them.

The TEM micrographs taken from the 1150 ^{o}C soaked steel 2, finish rolled at 800 ^{o}C, typically show a structure full of recovered subgrains, with a low dislocation density inside, and somewhat higher dislocation density at the subgrain boundaries [Fig.4.13 (a)]. A highly recovered and banded microstructure can also be seen at a few places [Fig.4.13 (b)]. By contrast, the sample finish rolled at 500 ^{o}C shows a profusion of cells with a high dislocation density, a structure similar to that of a cold rolled steel [Fig.4.13(c)]. Similar substructures are also obtained in thin foils of the same steel, soaked at 830 ^{0}C and finish rolled at 500 ^{o}C [Fig.4.13 (d)]. Some amount of recovery can be clearly seen within a few cells.

A typical microstructure of steel 3, soaked at 830 ^{o}C and finish rolled at 500 ^{o}C, consists of a highly dislocated cell structure [Fig.414 (a)], some of the cells clearly showing signs of recovery [Fig.4.14 (b)].

4.4.4 Microstructures of heat treated steels

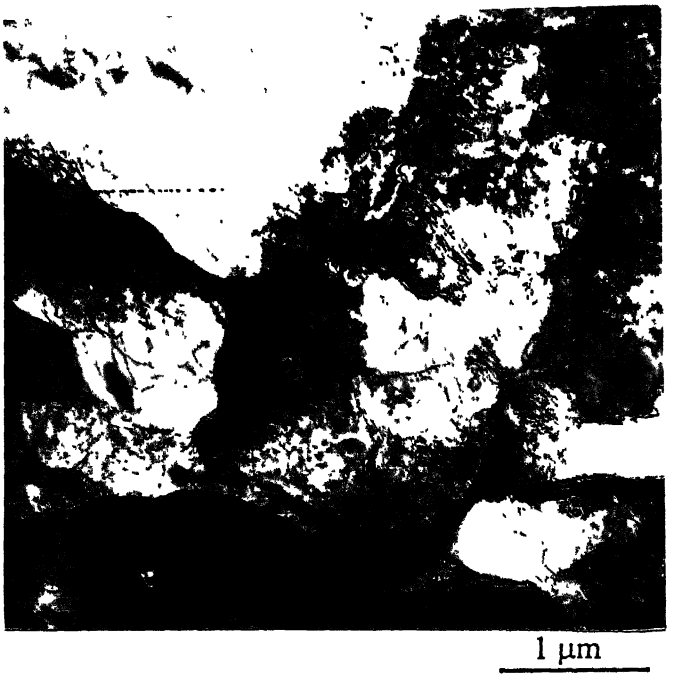

(c) FRT : 500 ^{O}C

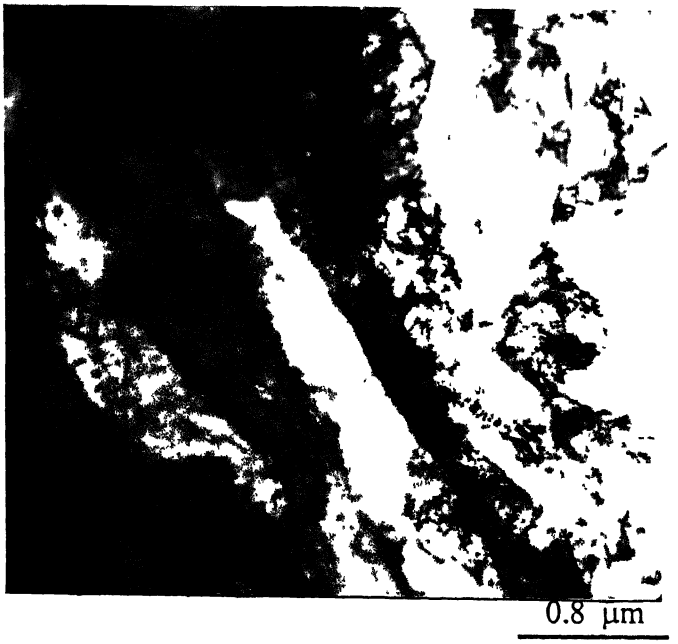

(d) FRT : 500 ^{O}C

Figure 4.12 (c) and (d) : TEM micrographs showing (c) sub grain formation and (d) banded like structure in steel 1 [single pass rolling after soaking at 1150 ^{O}C].

(e) FRT : 500 ^{o}C

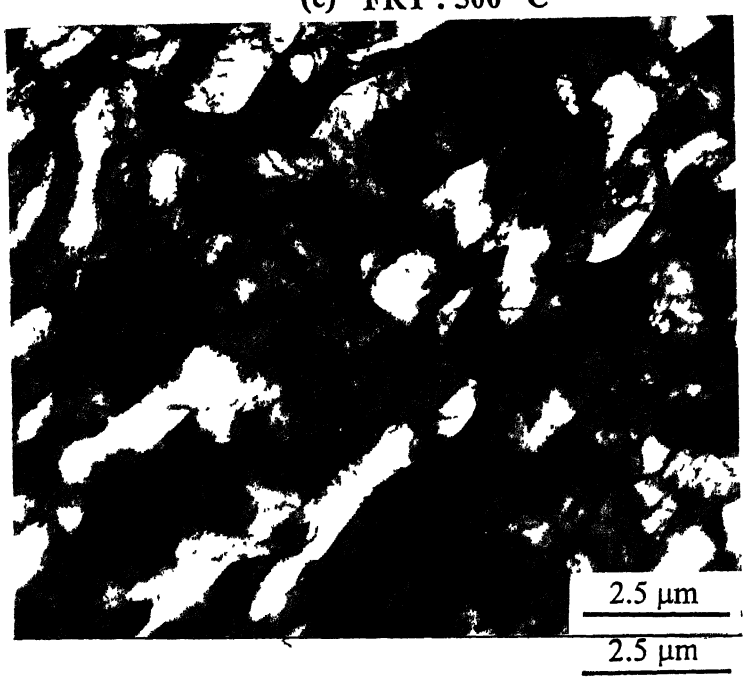

(f) FRT : 500 ^{o}C

Figure 4.12 (e) and (f) : TEM micrographs showing (e) cells with very high dislocation density at the cell boundaries and (f) deformation bands with fine cell structure in steel 1 [single pass rolling after soaking at 830 ^{o}C].

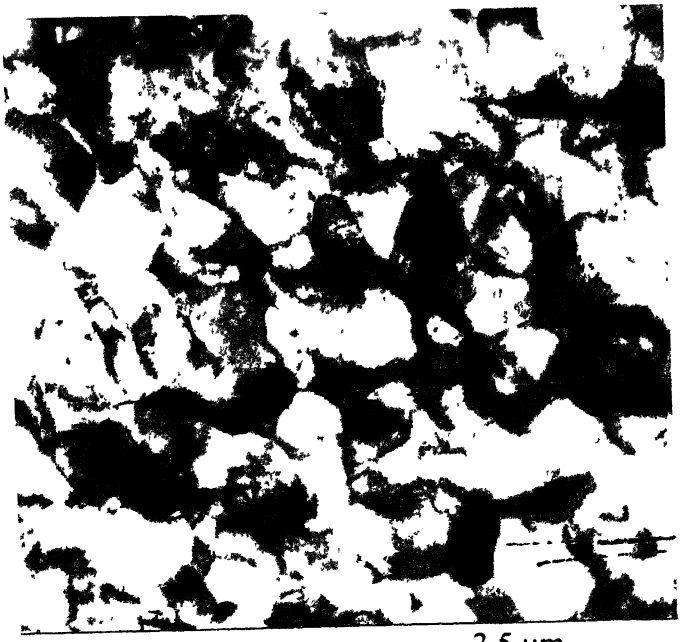

(a) FRT : 800 ^{o}C

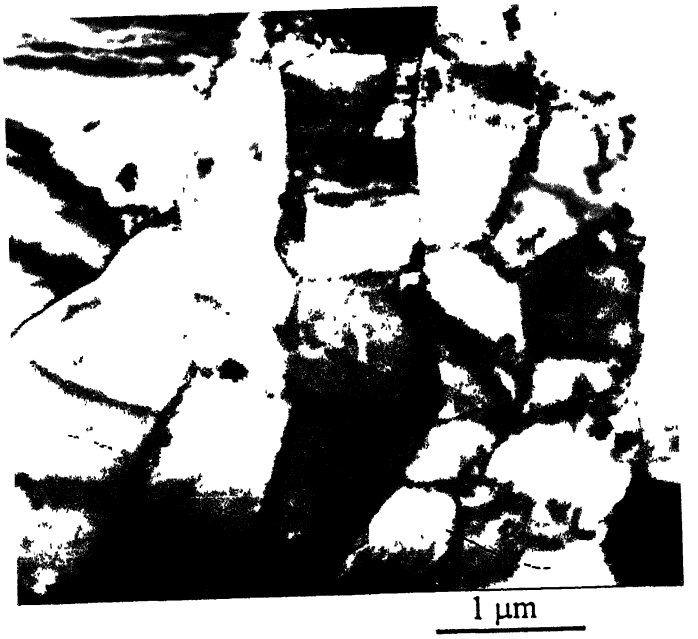

(b) FRT : 800 ^{o}C

Figure 4.13 (a) and (b) : TEM micrographs showing (a) recovered subgrains and (b) recovered subgrains with bands in steel 2 (single pass rolling after soaking at 1150 ^{o}C).

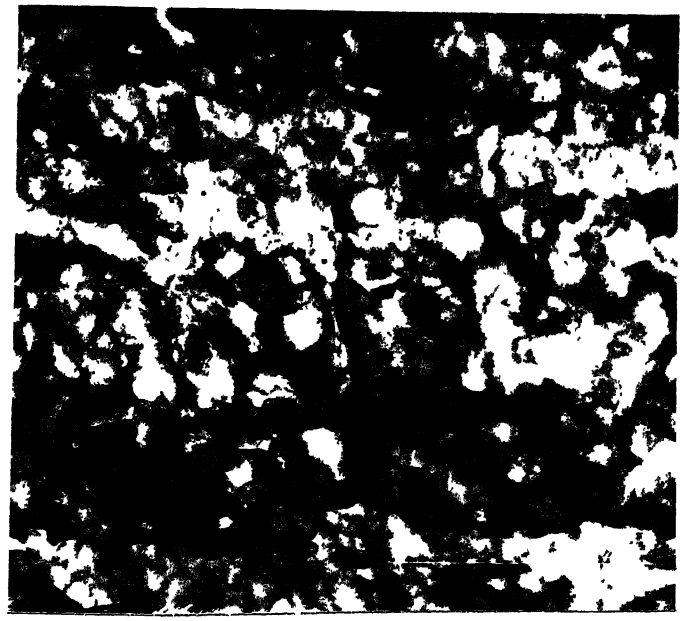

(c) FRT : 500 ^{o}C

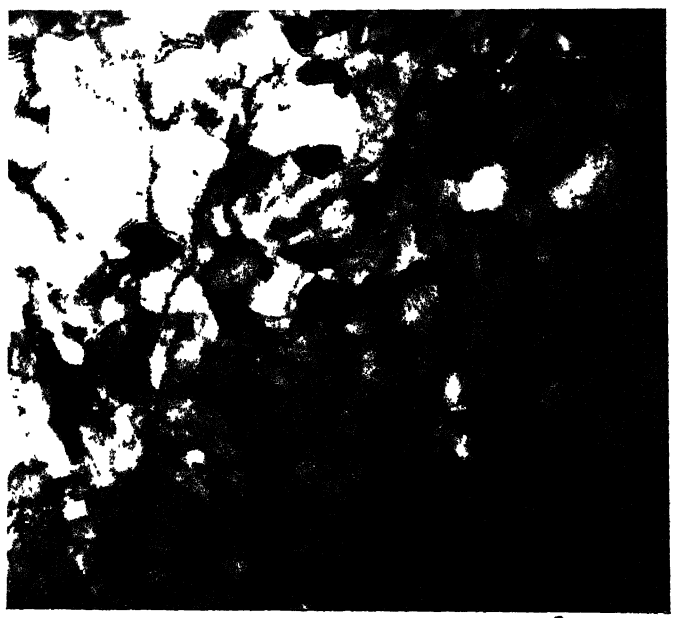

(d) FRT : 500 ^{o}C

Figure 4.13 (c) and (d) : TEM micrographs showing highly dislocated sub-structures formed steel 2 after single pass rolling at the FRT of 500 ^{o}C after soaking at 1150 ^{o}C (c) and 830 ^{o}C (d).

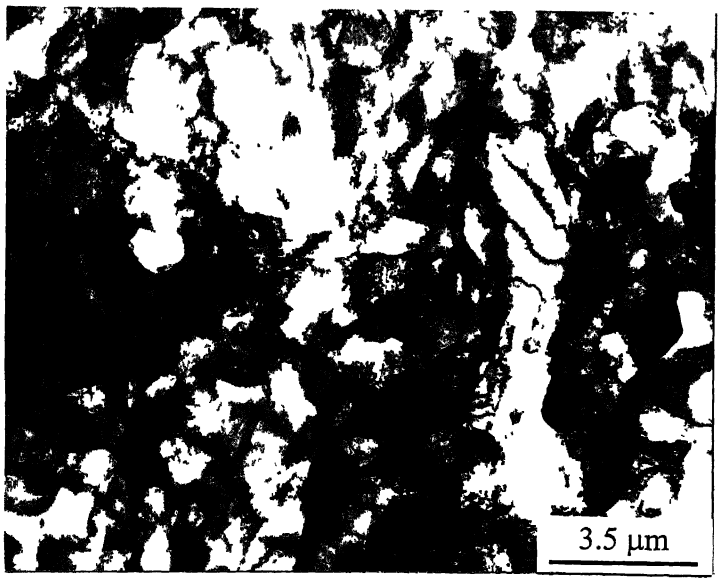

3.5 μm

(a) FRT : 500 °C

1 μm

(b) FRT : 500 °C

Figure 4.14 : TEM micrographs showing highly dislocated structures formed in steel 3 after single pass rolling at the FRT of 500 °C [after soaking at 830 °C].

The optical microstructures of the heat treated steels, previously finish rolled at 500 ^{o}C, 600 ^{o}C, 700 ^{o}C and 800 ^{o}C under various rolling schedules show fully recrystallised structures. A set of micrographs, illustrating the changes in microstructure for various FRT s for the ELC steel 1 and one of the IF compositions, namely steel 2, are displayed in Figures 4.15(a) -(d) and Figures 4.16 (a) – (d).

TEM micrographs taken from thin foils of a few heat treated samples are given below. Although optical micrographs have invariably shown highly recrystallised microstructures, recovered cells of various sizes have been frequently seen inside the recrystallised grains. These are shown typically in Figures 4.17(a) and (b) in steel 1 and in Figures.4.18 (a) and (b) in steel 2. Steel 3 shows a large number of precipitates of different shapes. These are shown typically in Figures.4.19 (a) to (d).

4.5 Texture results

In this investigation an attempt has been made to determine the effects of a few process variables on texture development in the three steels. In single pass experiments two different soaking temperatures were employed, namely, 1150 ^{o}C and 830 ^{o}C; whereas a soaking temperature of 1150 ^{o}C only was used in multipass experiments. A total of ~ 80% deformation by rolling was given in the single pass experiments at temperatures 800 ^{o}C, 700 ^{o}C, 600 ^{o}C and 500 ^{o}C in the ferrite range. In multipass rolling three different processing schedules involving different amounts of rolling deformation in the γ and α ranges were followed (the total amount of deformation being ~80% in each case) with four different FRT s, such as 800 ^{o}C, 700 ^{o}C, 600 ^{o}C and 500 ^{o}C.All the warm rolled steel

(a) FRT : 800 ^{o}C

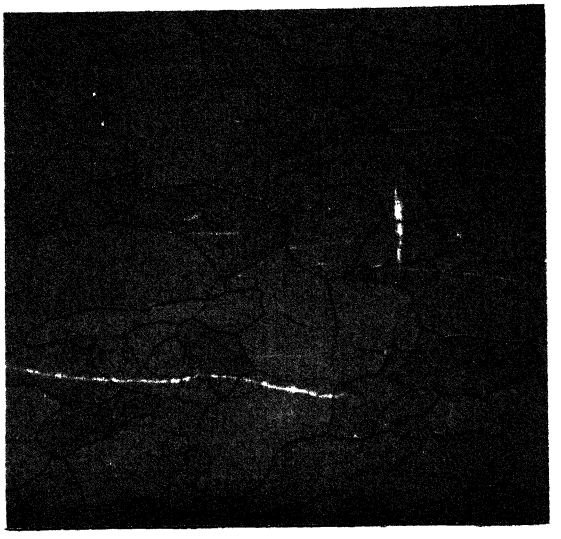

(c) FRT : 600 ^{o}C

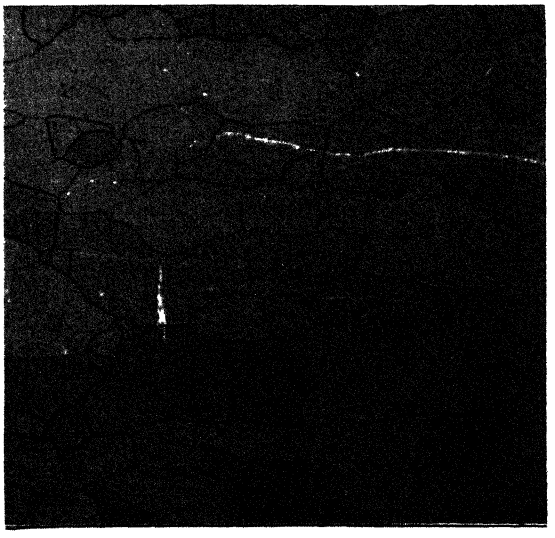

(b) FRT : 700 ^{o}C

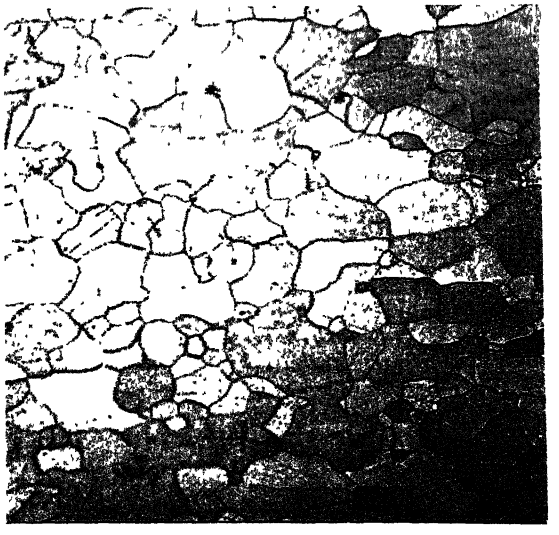

(d) FRT : 500 ^{o}C

100 μm

RD ⟶

Figure 4.15 (a) - (d) : Optical micrographs showing annealed microstructures of steel 1 after single pass rolling (after soaking at 830 ^{o}C).

(a) FRT : 800 ^{o}C

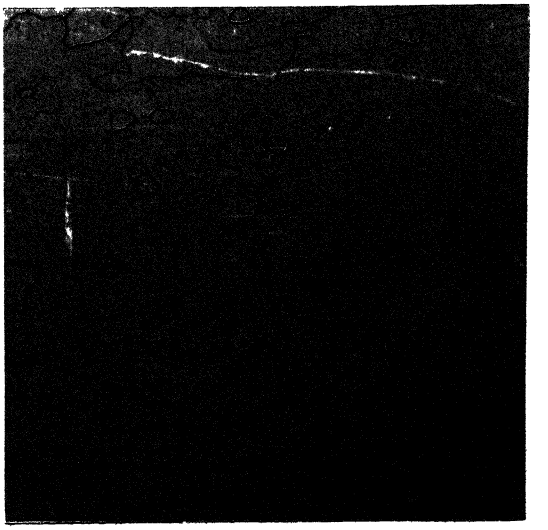

(c) FRT : 600 ^{o}C

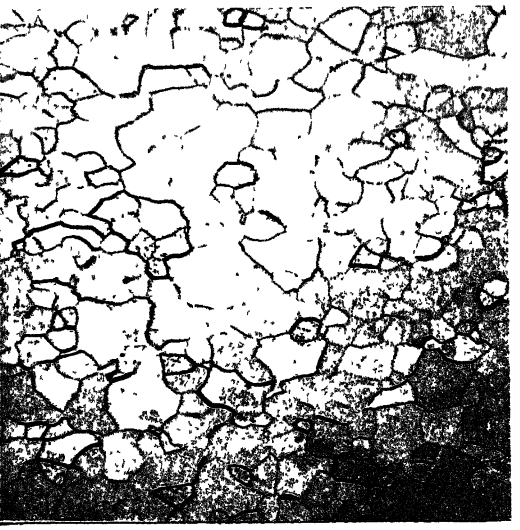

(b) FRT : 700 ^{o}C

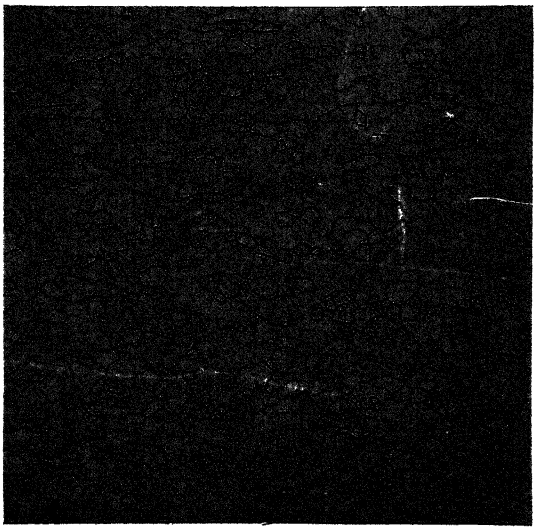

(d) FRT : 500 ^{o}C

100 μm

RD ⟶

Figure 4.16 (a) - (d) : Optical micrographs showing annealed microstructures of steel 2 after single pass rolling (after soaking at 830 ^{o}C).

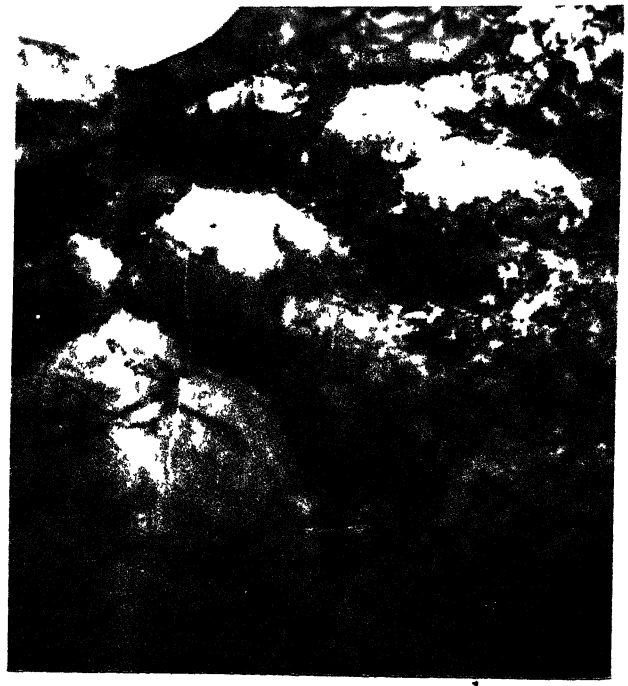

(a) FRT : 500 ^{o}C

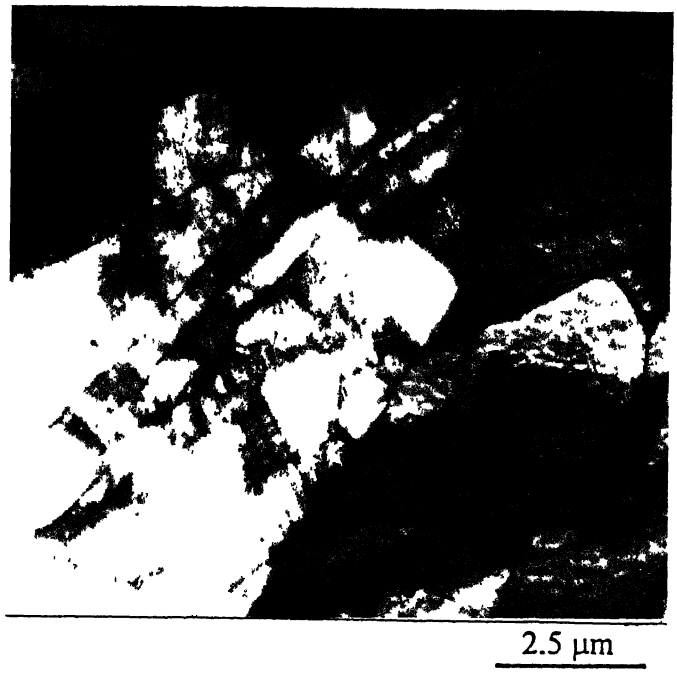

(b) FRT : 500 ^{o}C

Figure 4.17 : TEM micrographs showing the presence of recovered cells in steel 1 after heat treatment [single pass rolling after soaking at 1150 ^{o}C].

(a) FRT : 800 ^{o}C

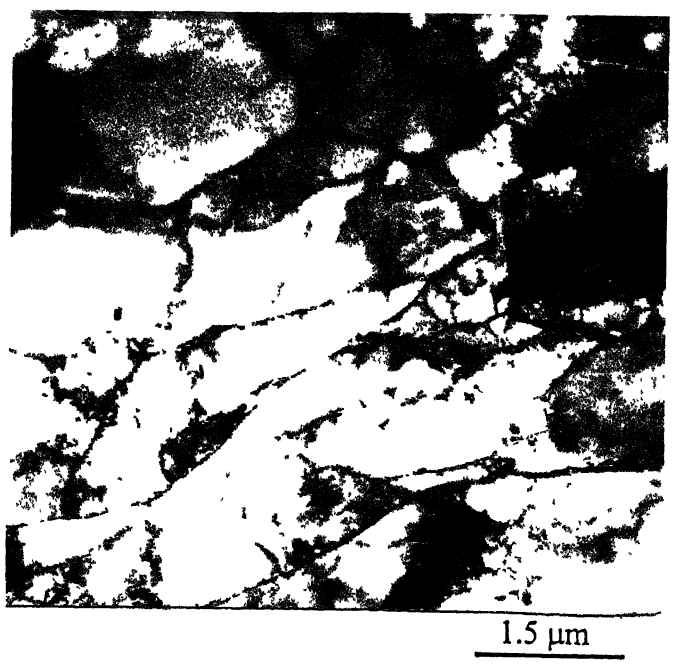

(b) FRT : 500 ^{o}C

Figure 4.18 : TEM micrographs showing the presence of recovered cells in steel 2 after heat treatment (single pass rolling after soaking at 1150 ^{o}C].

samples were subsequently heat treated at 775 ^{O}C for 25 minutes. As mentioned earlier, textures were characterised by evaluating detailed φ_1 section ODFs, $\varphi_2 = 45^{O}$ sections and the different fibre plots.

4.5.1 Steel 1

4.5.1.1. Single pass rolling after soaking at 1150 ^{O}C

(a) Warm rolling textures

The ODF s of the samples rolled at four different FRTs are shown in Figures 4.20 (a) – (d). A rather weak texture was observed in the 800 ^{O}C rolled material [$f(g)_{max} = 3.7$]. Decreasing FRT led to a sharp increase in the texture intensity. The sharpening of the overall texture was accompanied by the formation of clearly delineated fibres running through the different φ_1 sections.

The plots of the α, γ, η, ζ and ε fibres present in the ODFs of Figure 4.20 are shown in Figure 4.21. It is clear from this figure that the sample finish rolled at 800 ^{0}C shows only a weak texture, characterised mainly by a non-uniform α fibre. In addition, there is a rotated cube component $\{001\}< 110 >$ [f (g) = 4.0]. The fibres are of somewhat sharper intensity after finish rolling at 700 ^{O}C. A non-uniform α fibre having its maxima at ~ $\{113\} < 110 >$ is present here along with a weak η fibre. A moderately strong rotated cube component [f (g) = 5] is also seen.

Rather perfect and sharp γ fibres of average f (g) ~ 13 develop after finish rolling at 600 ^{O}C and 500 ^{O}C. While the $\{111\}< 110 >$ component has a higher intensity than the

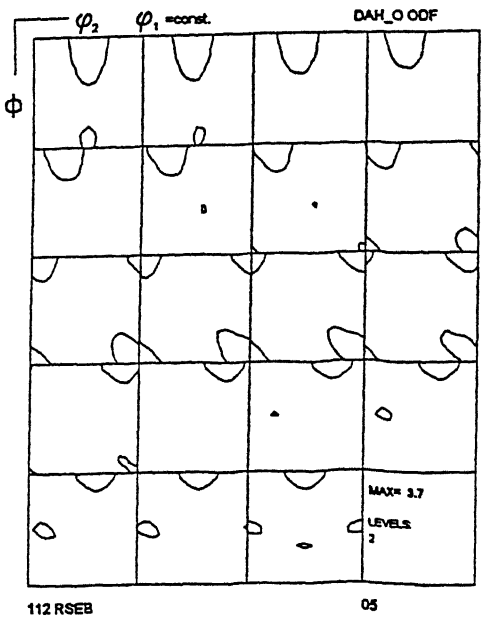

(a) FRT : 800 ^{o}C

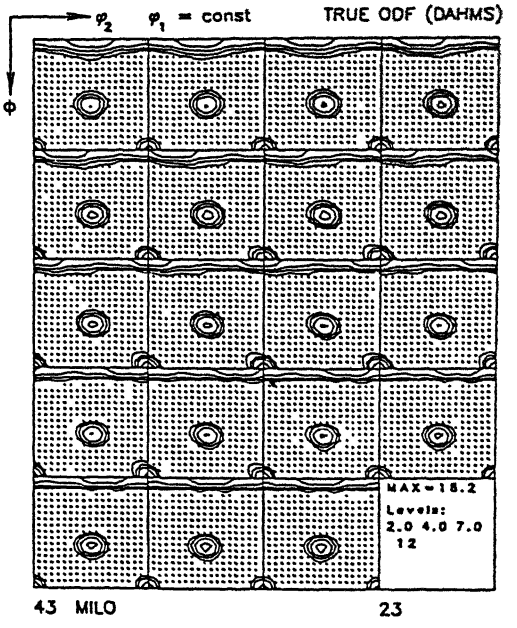

(c) FRT : 600 ^{o}C

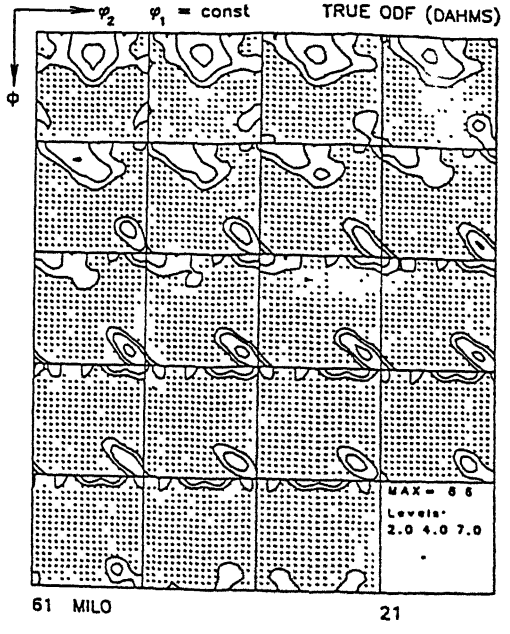

(b) FRT : 700 ^{o}C

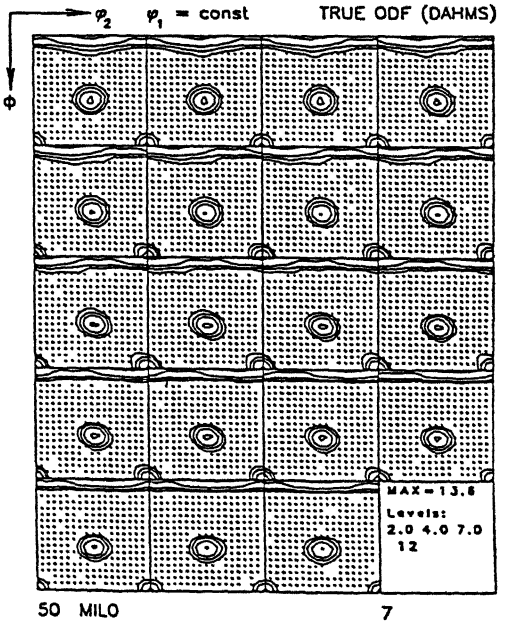

(d) FRT : 500 ^{o}C

Figure 4.20 (a) - (d) : ODF plots (φ_1 sections) for steel 1 after single pass rolling (after soaking at 1150 ^{o}C).

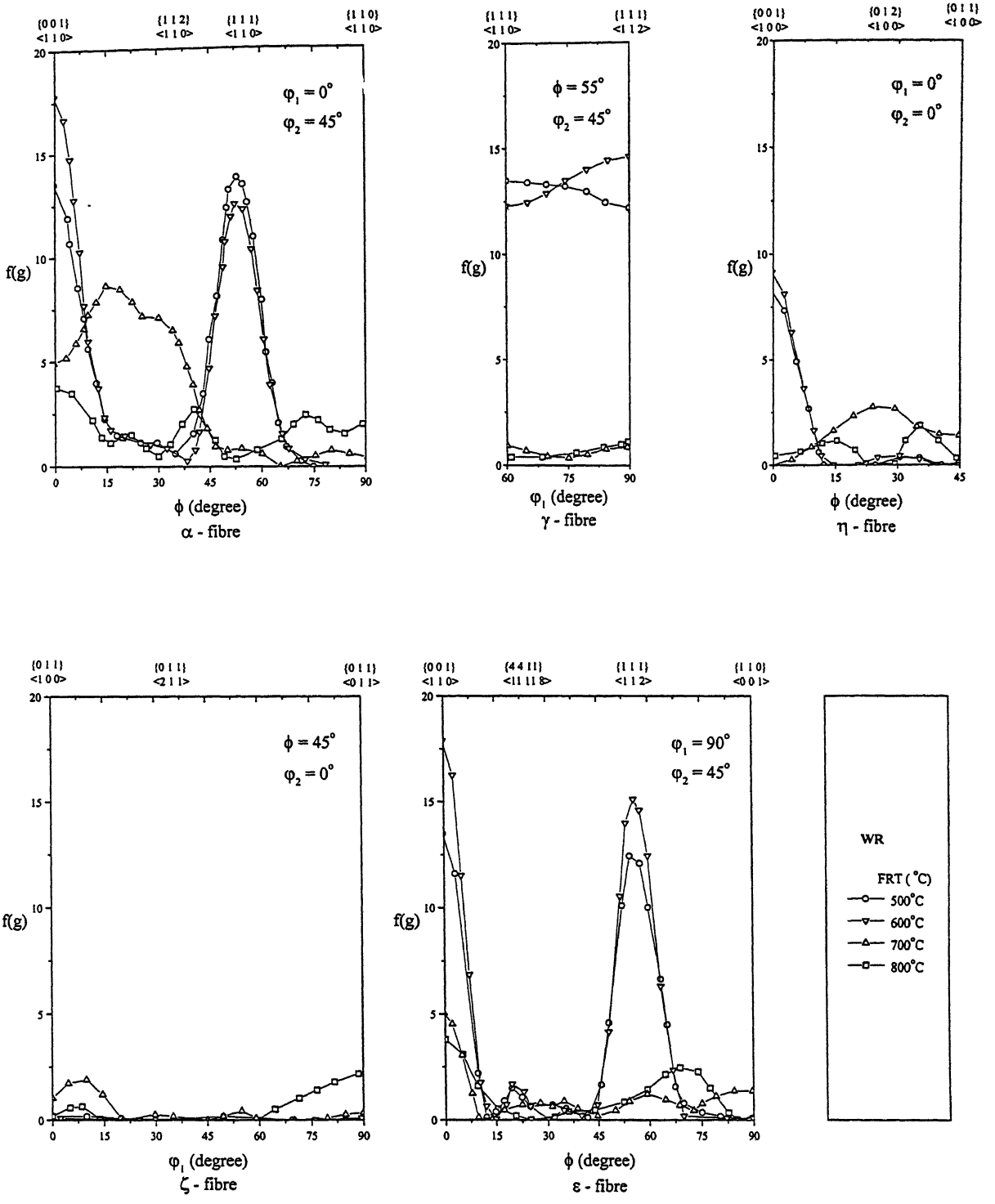

Figure 4.21: Fibre plots for steel 1 after warm rolling (WR) in single pass (after soaking at 1150 °C).

{111}< 112 > in the 600 ^{O}C FRT material, reverse is true in the 500 ^{O}C FRT sample. The cube [f (g) > 8] and the rotated cube components [f (g) > 13] are also quite sharp in these two samples, as seen from the α, η and ε fibre plots. Both these components are a bit sharper in the 500 ^{O}C FRT material than in the 600 ^{O}C FRT sample. Overall, both ODF and fibre plots for the 600 ^{O}C and 500 ^{O}C finish rolled samples exhibit rather sharp intensities for the γ fibre in addition to another equally strong fibre running from $\varphi_2 = 0^{O}$ to 90^{O} in all the φ_1 sections.

The most relevant features of texture development, as described above, can be shown in the appropriate $\varphi_2 = 45^{O}$ sections for the four samples in Figures 4.22(a) - (d). The highly uniform and strong γ fibre, as well as the fibre running from $\varphi_2 = 0^{O}$ to 90^{O} in all φ_1 sections for the 600 ^{O}C and 500 ^{O}C FRT samples are clearly visible in Figures 4.22(c) and (d). By contrast, the 800 ^{O}C and 700 ^{O}C FRT samples show only weak {001}< 100 >, {001}< 110 > and {110}< 110 > components and none of the above fibres.

(b) Textures after heat treatment

The general ODF plots of the rolled samples after heat treatment at 775 ^{O}C for 25 minutes are shown in Figures 4.23(a) – (d). In the 800 ^{O}C FRT sample only a weak texture develops after that treatment. Although the texture intensity here is slightly higher than that of the corresponding rolled sample [Fig. 4.20(a)], the nature of the texture components remain more or less unaltered. Hardly any intensity is observed at the γ fibre orientation location. Heat treatment of the 700 ^{O}C FRT sample reduces the texture intensity by nearly 50% [compare Fig. 4.23(b) with Fig. 4.20 (b)]. Here again the location of the main

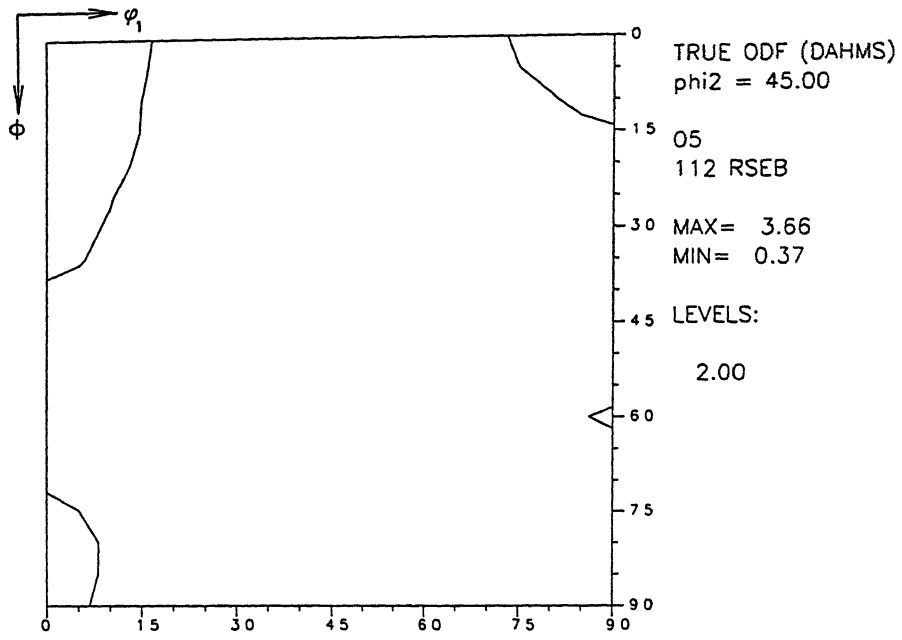

(a). FRT: 800 ^{O}C

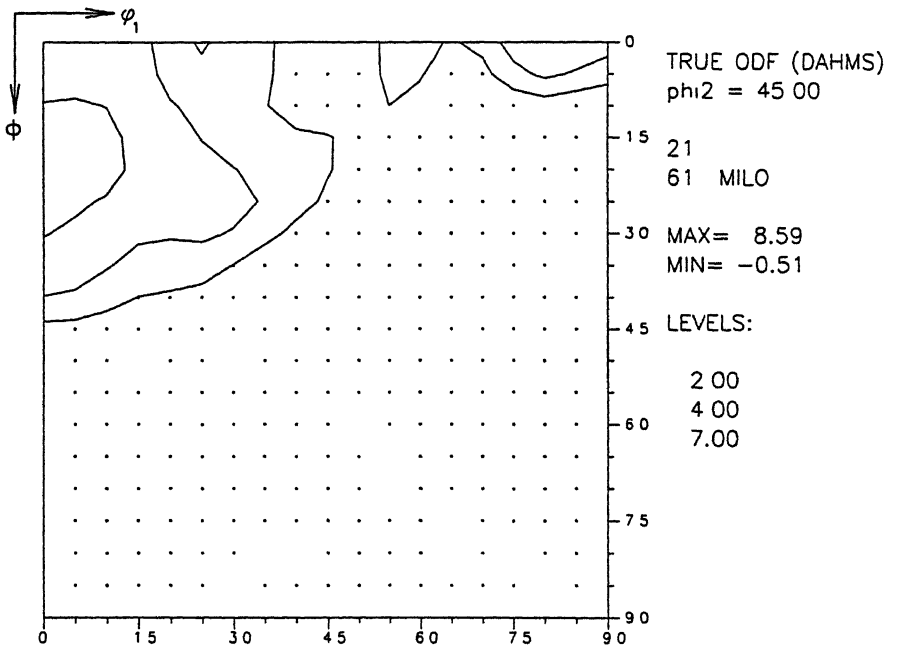

(b). FRT: 700 ^{O}C

Figure 4.22 (a) and (b) : $\varphi_2 = 45^{O}$ sections plots for steel 1 after single pass rolling (after soaking at 1150 ^{O}C).

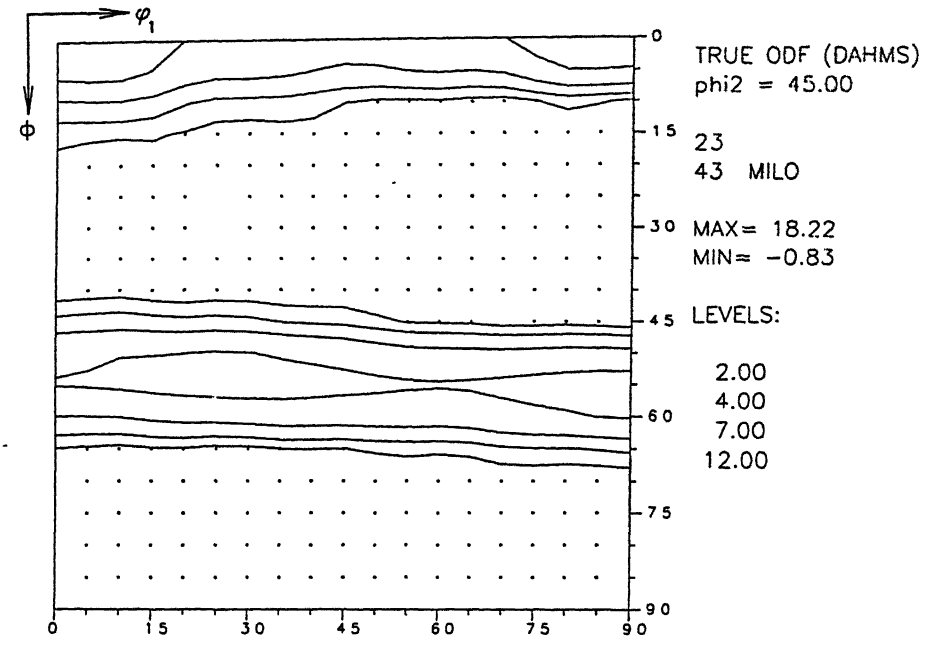

(c). FRT: 600 ^{O}C

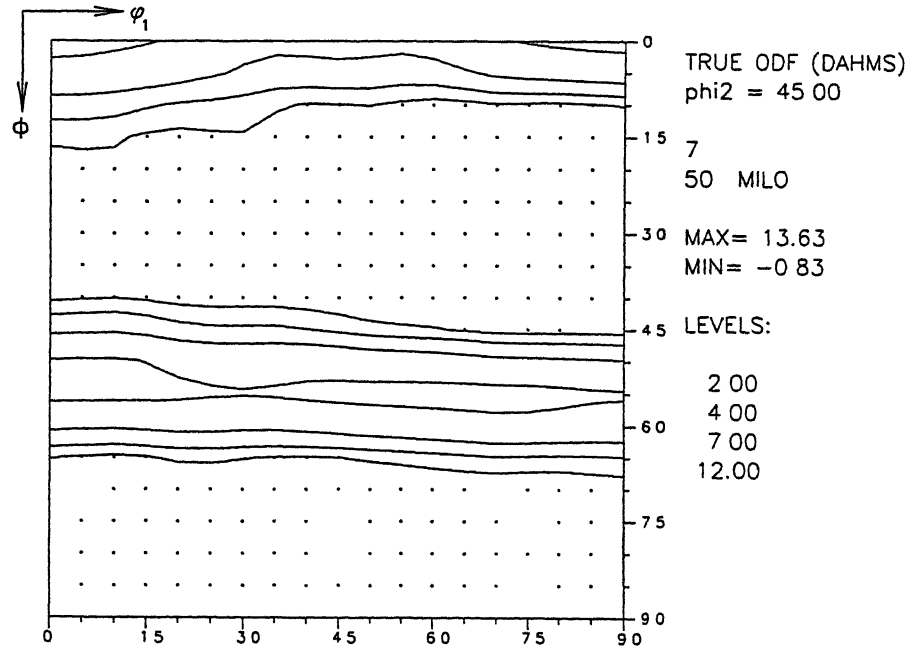

(d). FRT: 500 ^{O}C

Figure 4.22 (c) and (d) : $\varphi_2 = 45^{O}$ sections plots for steel 1 after single pass rolling (after soaking at 1150 ^{O}C).

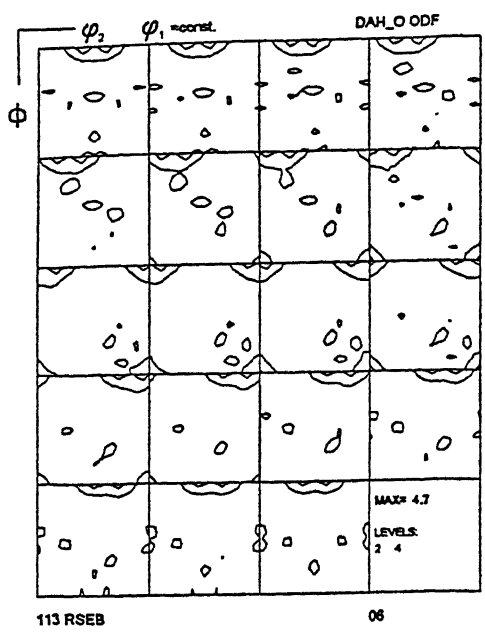

(a) FRT : 800 ^{O}C

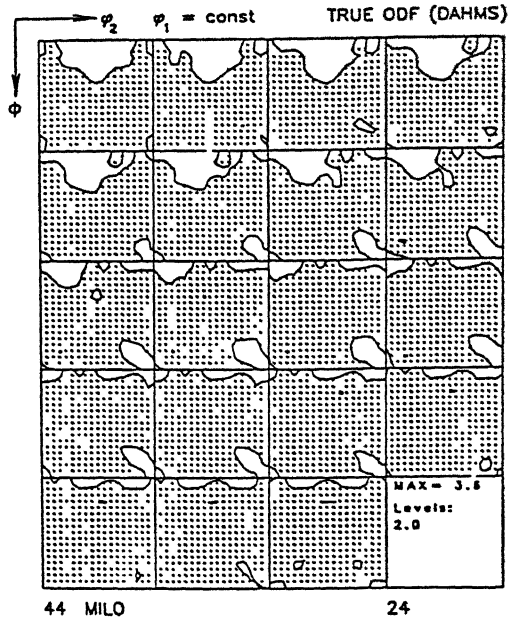

(c) FRT : 600 ^{O}C

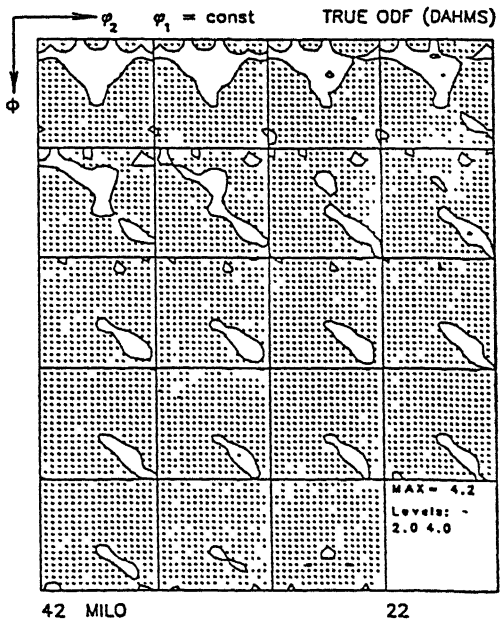

(b) FRT : 700 ^{O}C

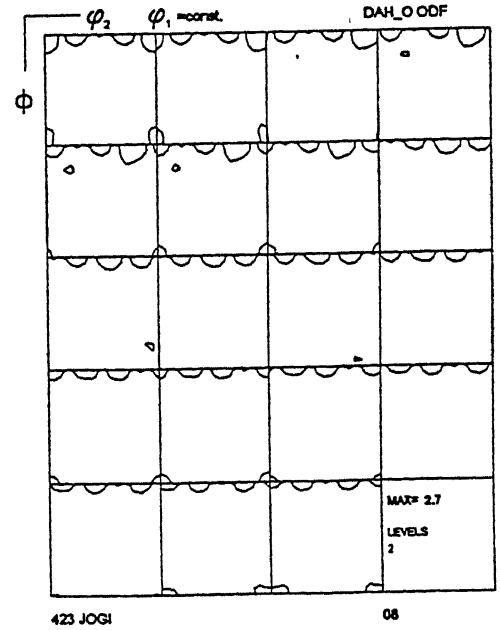

(d) FRT : 500 ^{O}C

Figure 4.23 (a) - (d) : ODF plots (φ_1 sections) for steel 1 after single pass rolling (after soaking at 1150 ^{O}C) and annealing.

intensity peaks remains unaltered before and after the heat treatment. There is a drastic decrement of the sharpness of texture after the 600 ^{o}C and 500 ^{o}C FRT samples are heat treated, as compared with the texture intensities of the original rolled samples [compare Fig. 4.23(c) and (d) with Fig. 4.20(c) and (d)].

Heat treatment seems to have altered the nature of the texture of the rolled samples very significantly. Neither of them shows any perceptible γ fibre in the φ_1 sections of the ODF s. Only rather weak orientations are obtained along the fibre direction running from $\varphi_2 = 0^{o}$ to 90^{o} in all the φ_1 sections.

The various fibre components plotted and shown in Figure 4.24 more or less corroborate the above results. All the five fibres in the four heat treated samples are of rather weak intensity. The γ fibre in the 700 ^{o}C FRT sample is the most intense, although its f(g) value is only about 2.5. All the other three heat treated samples show very weak γ fibres.

The $\varphi_2 = 45^{o}$ sections of the ODF s of the four heat treated samples are shown in Figure 4.25 (a)-(d). It is quite clear from these diagrams that excepting the 700 ^{o}C FRT sample, which shows a weak γ fibre, none of the other three develop the γ fibre at all after heat treatment. All of them, however, show the weak rotated cube component and sometimes a weak cube orientation.

4.5.1.2 Single Pass rolling after soaking at 830 ^{o}C

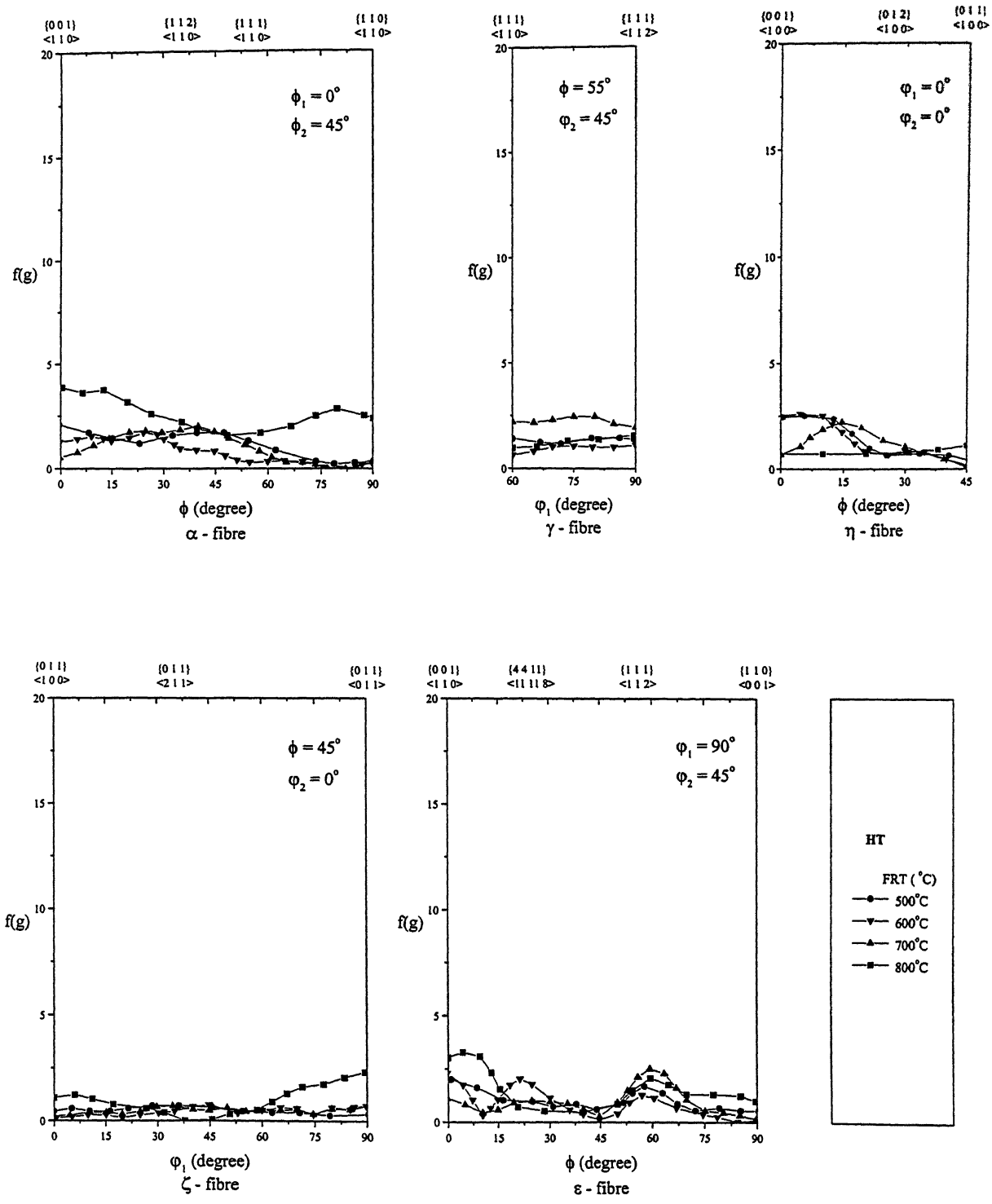

Figure 4.24 : Fibre plots for steel 1 after warm rolling in single pass (after soaking at 1150 °C) and annealing (HT).

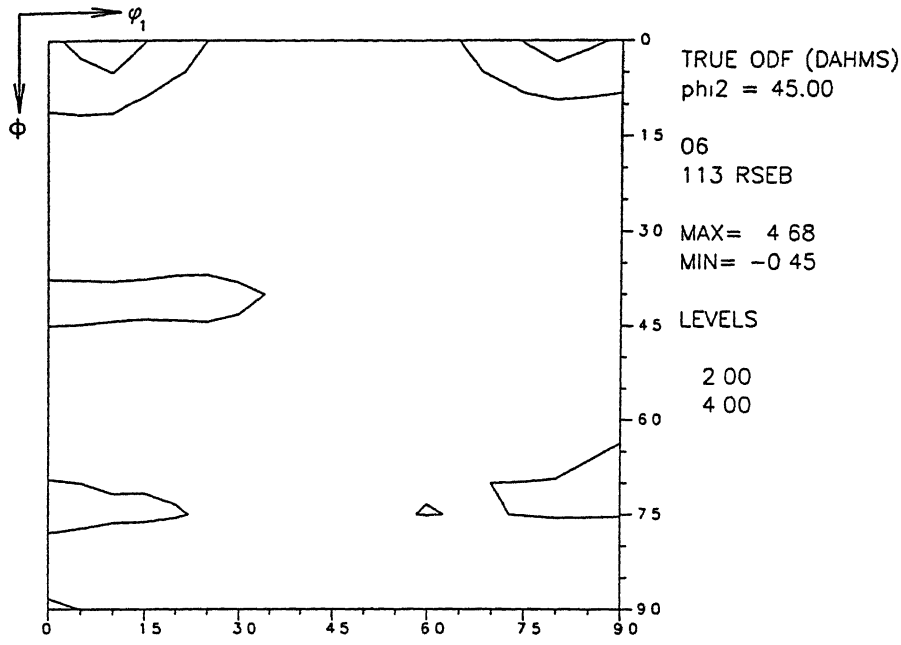

(a). FRT: 800 ^{O}C

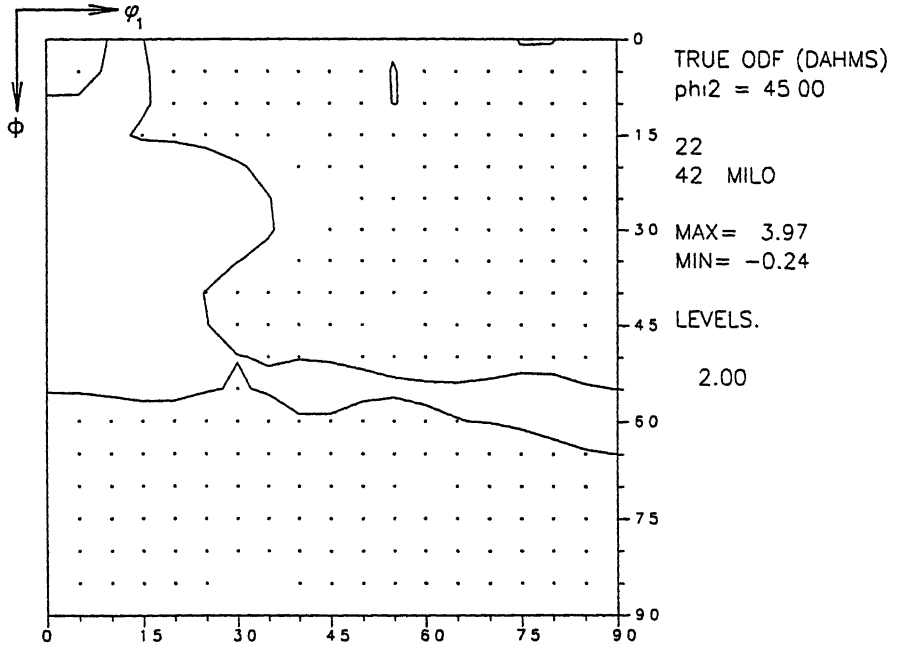

(b). FRT: 700 ^{O}C

Figure 4.25 (a) and (b) : $\varphi_2 = 45^{O}$ sections plots for steel 1 after single pass rolling (after soaking at 1150 ^{O}C) and annealing.

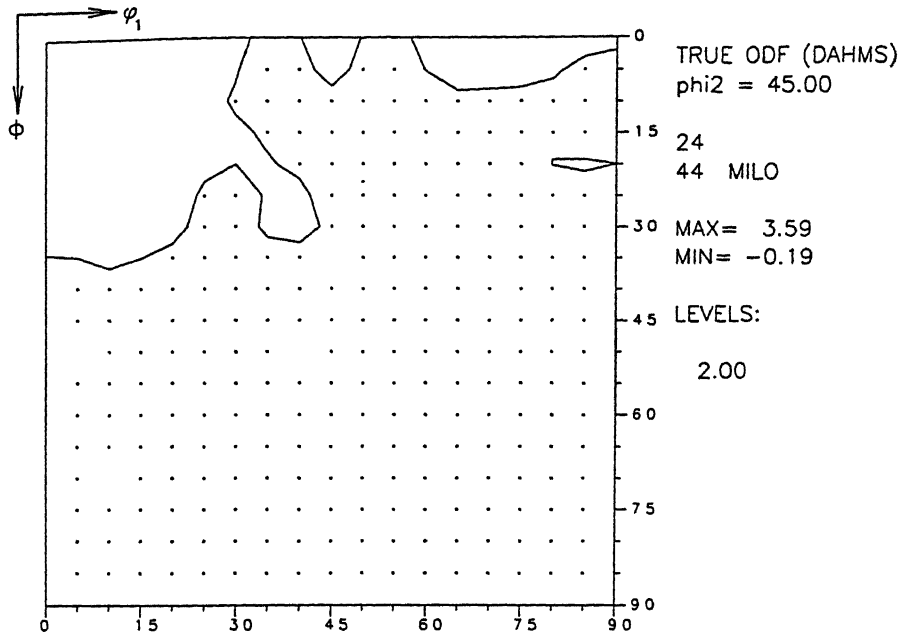

(c). FRT: 600 ^{O}C

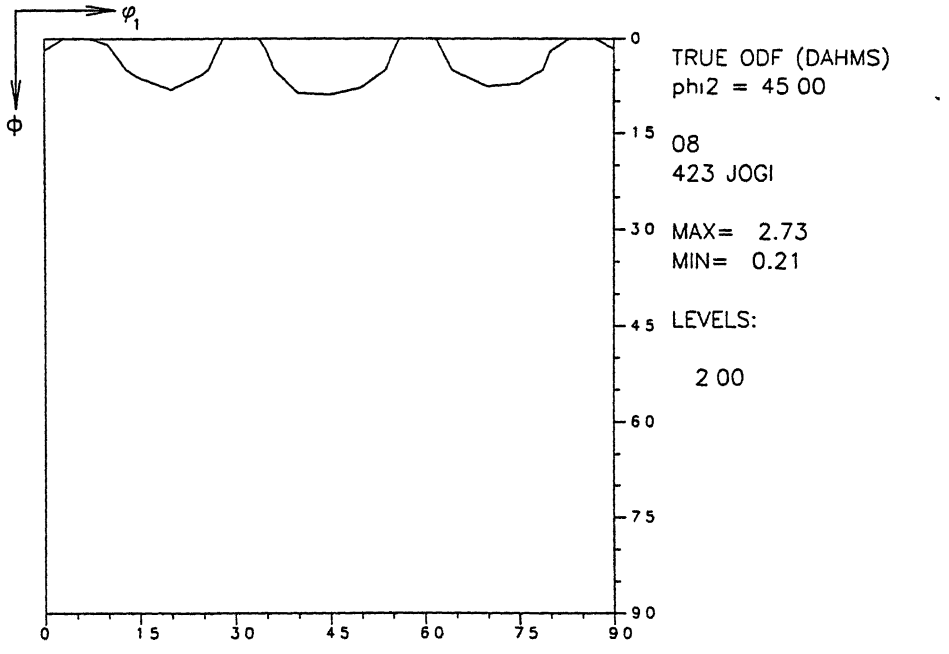

(d). FRT: 500 ^{O}C

Figure 4.25 (c) and (d) : $\varphi_2 = 45^{O}$ sections plots for steel 1 after single pass rolling (after soaking at 1150 ^{O}C) and annealing.

(a) Warm rolling textures

For the soaking temperature of 830 ^{O}C, texture measurements were carried out only on samples finish rolled at 800 ^{O}C and 500 ^{O}C. The general features of the textures in these samples are shown in Figure 4.26 (a) and (b). A moderately strong texture develops in the sample with a FRT of 800 ^{O}C, the maximum intensity being 5.6 times random. Not even a trace of the γ fibre is observed, although reasonably strong intensities at cube and rotated cube locations are found. The overall texture developed at this FRT of 800 ^{O}C is found to be sharper than that developed in the sample with the same FRT but soaked at a higher temperature of 1150 ^{O}C [Fig 4.20(a)]. The texture changes completely when the FRT is lowered to 500 ^{O}C (Fig. 4.26 (b). The overall texture intensity is nearly twice as strong [f(g)max ~ 10.3] as compared to the previous one. A strong γ fibre and a fibre extending from $\varphi 2 = 0^{O}$ to $\varphi_2 = 90^{O}$ in all the φ_1 sections are the two most prominent features of the texture of this sample.

The fibre plots [Fig.4.27] for the 800 ^{O}C FRT sample show the presence of a weak and non- uniform α fibre, with peak at ~ {113} <110>, together with moderate intensities at the {001}< 100> and {001}<110> locations. By contrast, the 500 ^{O}C FRT sample exhibits a rather sharp (~ 8.0 times random) and uniform γ fibre, having nearly equal intensities at {111}<110> and {111} <112> locations. In addition, the texture intensities at the {001} <100> and {001}<110> locations are found to be nearly equally sharp [f(g) ~ 10.0].

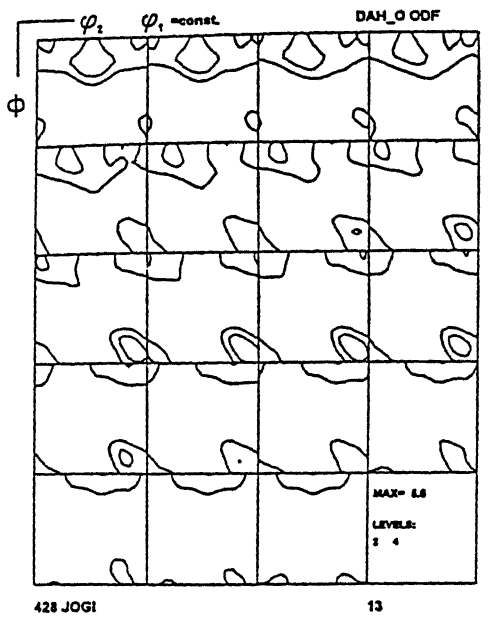

(a) FRT : 800 ^{o}C

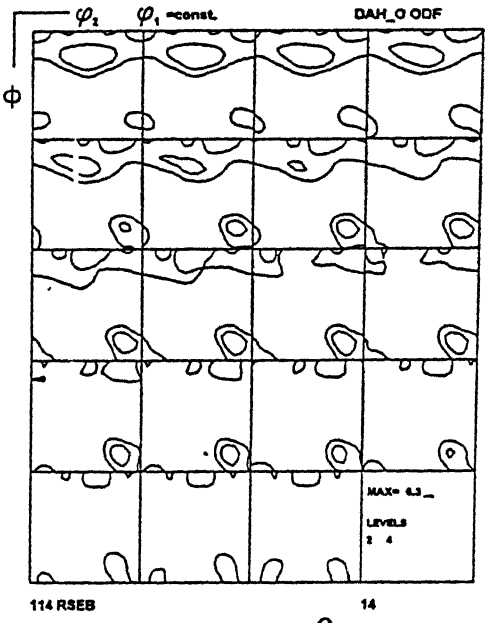

(c) FRT : 800 ^{o}C

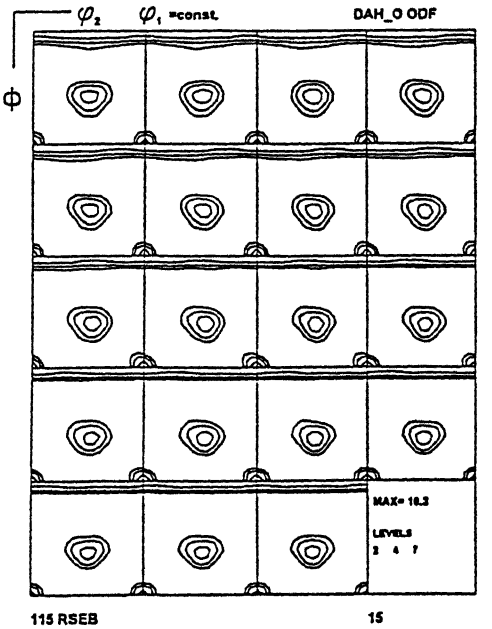

(b) FRT : 500 ^{o}C

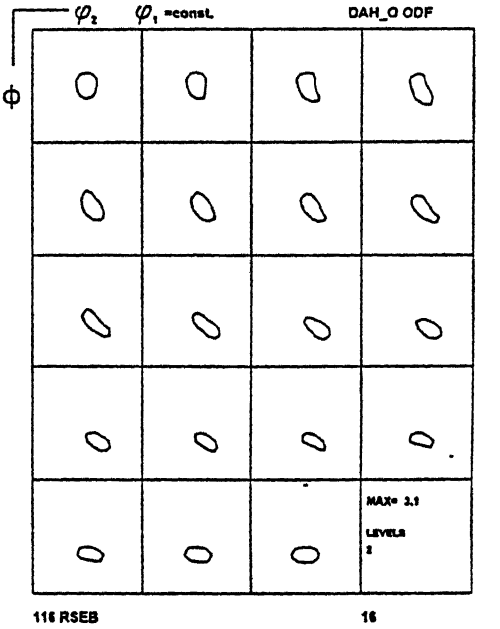

(d) FRT : 500 ^{o}C

Figure 4.26 (a) - (d) : ODF plots (φ_1 sections) for steel 1 after single pass rolling (after soaking at 830 ^{o}C) [(a) and (b)] and annealing [(c) and (d)].

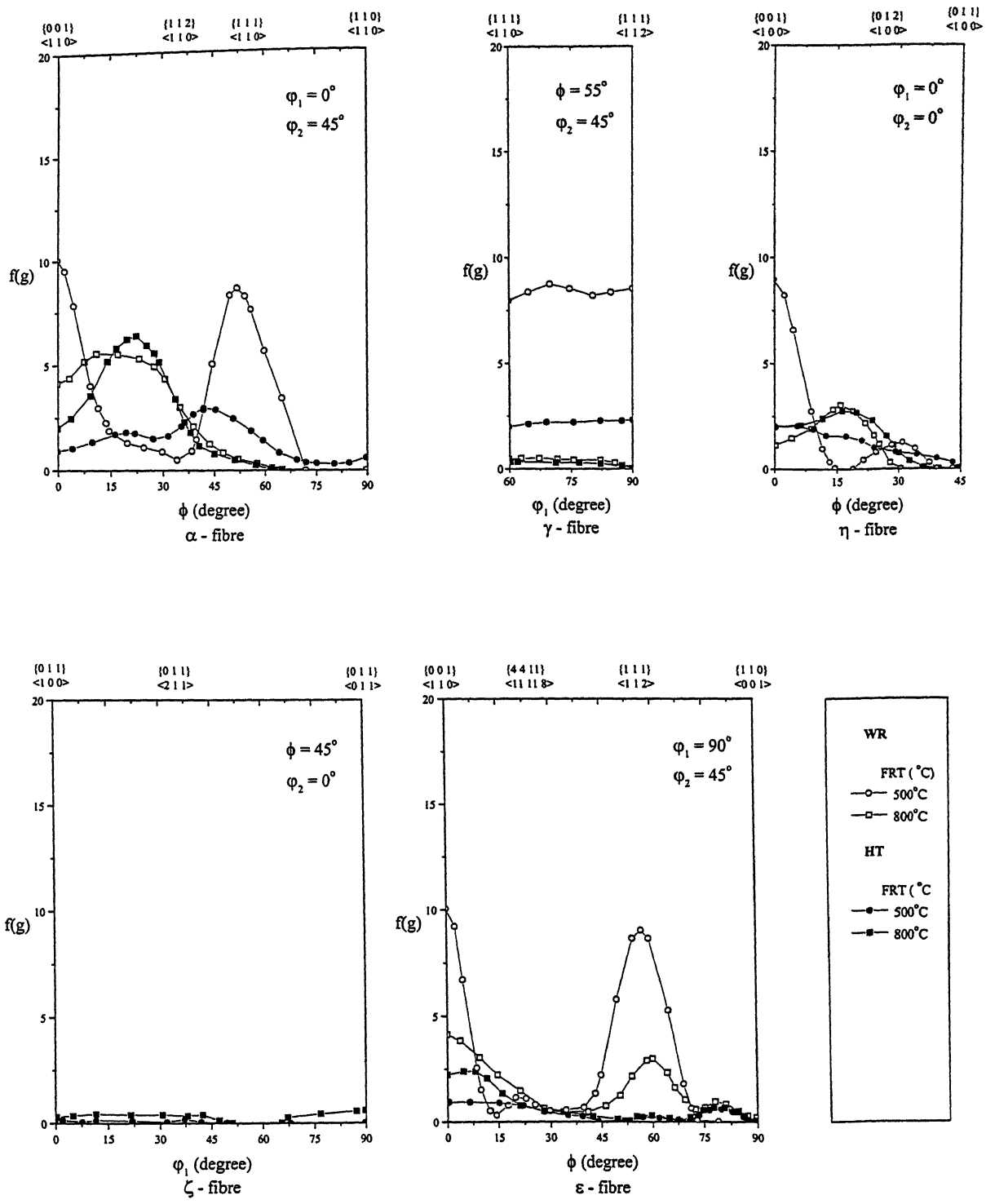

Figure 4.27 : Fibre plots for steel 1 after single pass rolling (after soaking at 830 °C) [WR] and annealing [HT].

The relevant $\varphi_2 = 45^{\circ}$ sections [Fig. 4.28 (a) and (b)] corroborate the above findings. While isolated weak peak intensities are observed at the cube and rotated cube positions for the 800 $^{\circ}$C FRT sample, a sharp and uniform γ fibre along with a sharp and uniform fibre running from $\varphi_2 = 0^{\circ}$ to 90° are clearly observed for the 500 $^{\circ}$C FRT sample.

(b) Textures after heat treatment

The ODFs of the above-mentioned warm rolled samples after heat treatment are shown in Figures 4.26 (c) and (d). Clearly the overall texture seems to sharpen a bit after heat treatment for the 800 $^{\circ}$C FRT sample, although the general features of the texture more or less remain the same. By contrast, heat treatment of the 500 $^{\circ}$C FRT sample appears to change the initial texture completely in addition to bringing down the overall texture intensity very drastically. However the heat treated sample ODF shows the presence of a weak γ fibre only and nothing else. Heat treatment seems to have eliminated the fibre running from $\varphi_2 = 0^{\circ}$ to 90° in all φ_1 sections, which was very prominent in the 500 $^{\circ}$C FRT specimen.

The fibre plots for the two heat treated (HT) samples are again shown in Figure 4.27. The α fibre in the 800 $^{\circ}$C FRT sample,after heat treatment, looks very similar to the same fibre before heat treatment. The maxima of this fibre after heat treatment has now shifted more close to {113}<110>. The α fibre intensity for the 500 $^{\circ}$C FRT sample, after heat treatment, however, has come down to a much lower value. While the 800 $^{\circ}$C FRT and HT sample hardly shows any γ fibre, the 500 $^{\circ}$C FRT and HT sample show a uniform but rather weak [f(g) ~ 2.5] γ fibre. The heat treated samples also show much lower f(g)

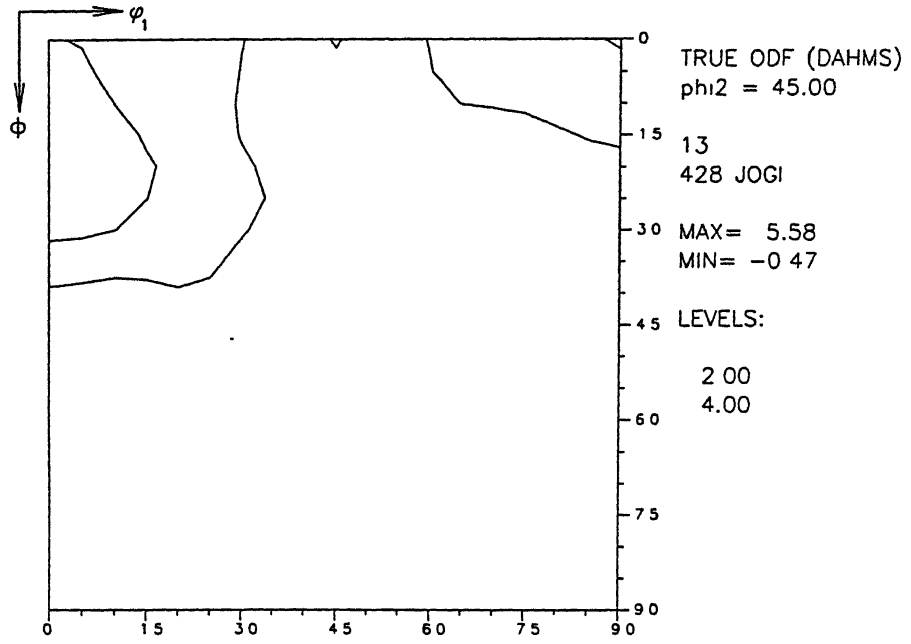

(a). FRT: 800 ^{O}C

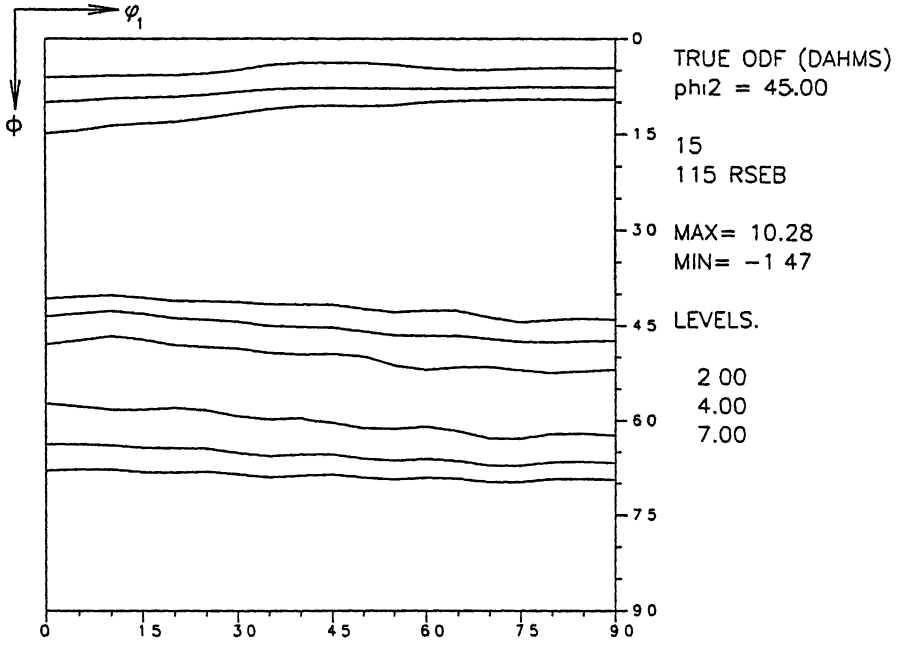

(b). FRT: 500 ^{O}C

Figure 4.28 (a) and (b) : $\varphi_2 = 45^{O}$ sections plots for steel 1 after single pass rolling (after soaking at 830 ^{O}C).

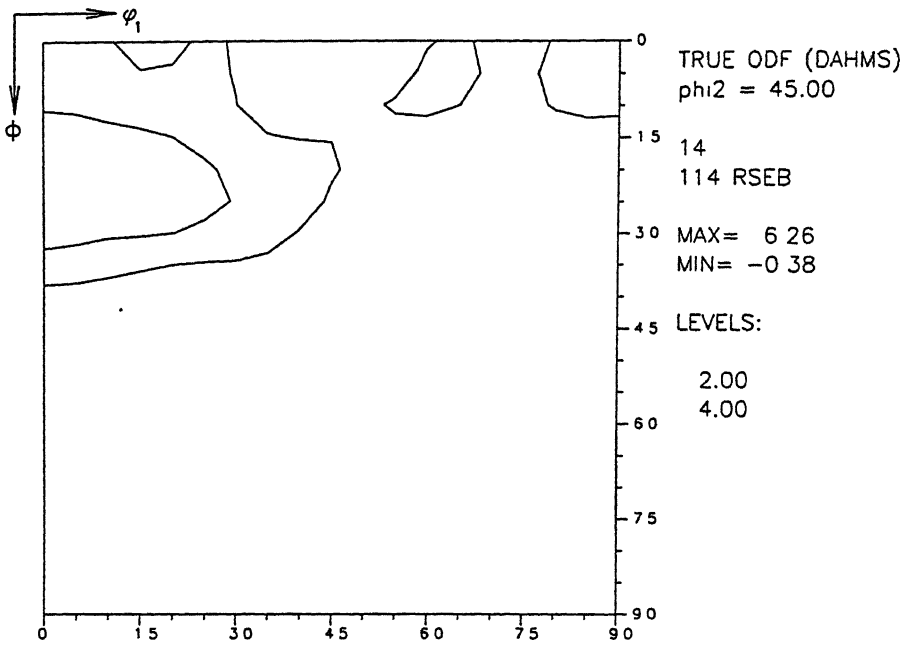

(c). FRT: 800 ^{O}C

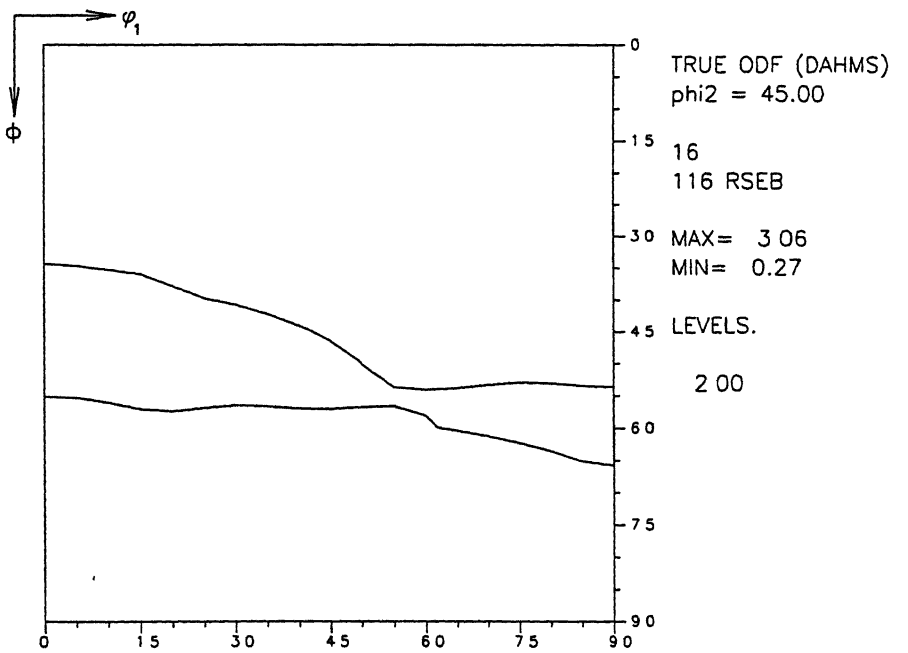

(d). FRT: 500 ^{O}C

Figure 4.28 (c) and (d) : $\varphi_2 = 45^{O}$ sections plots for steel 1 after single pass rolling (after soaking at 830 ^{O}C) and annealing.

values at the cube and rotated cube locations, as compared to the corresponding values in the warm rolled samples.

The $\varphi_2 = 45^O$ sections for the two heat-treated samples fully corroborate the above findings [Fig. 4.28 (c) and (d)].

4.5.1.3 Textures after multipass rolling

(a) Schedule 1

In each of the three schedules of multipass rolling texture measurements were carried out on samples finish rolled at 800 ^{O}C and 500 ^{O}C. The ODF plots of the warm rolled samples of schedule 1 are shown in Figures 4.29 (a) – (b). It is clear that a much sharper (> 2 times) texture develops in the 500 ^{O}C FRT sample as compared to the 800 ^{O}C FRT sample. The plots of the various fibre components [Fig. 4.30] show that all the fibres have developed to rather low intensities in both the samples. The γ fibres are extremely weak in both [f(g). ~ 2.0], while the α fibre is sharper in the 500 ^{O}C FRT sample than in the 800 ^{O}C FRT material. The former also displays sharper intensities at both cube and rotated cube locations. These general features of textures are very well corroborated by the $\varphi_2 = 45^O$ section plots [Fig. 4.31 (a) and (b)].

The overall texture intensities of both the above samples show some increment after heat treatment [Fig. 4.29 (c) and (d)]. Whereas the 800 ^{O}C FRT sample shows only a marginal increase in intensity, the 500 ^{O}C FRT sample sharpens almost 1.5 times after heat treatment. Interestingly enough, the fibre plots [Fig. 4.30] do not show very significant

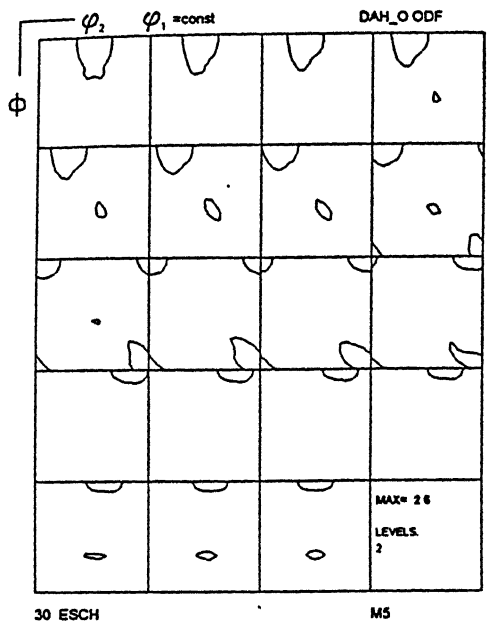

(a) FRT : 800 °C

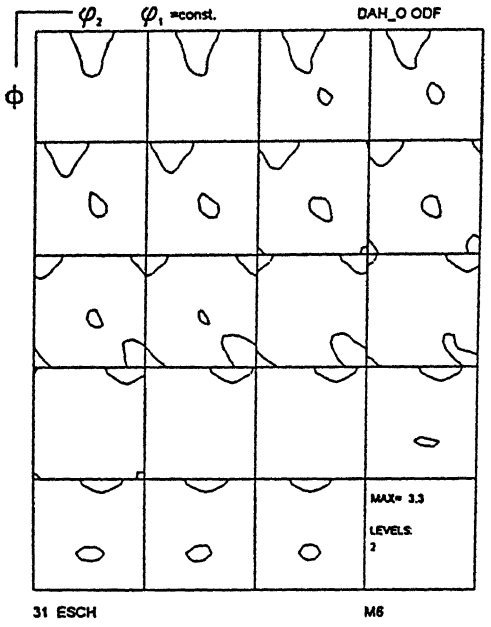

(c) FRT : 800 °C

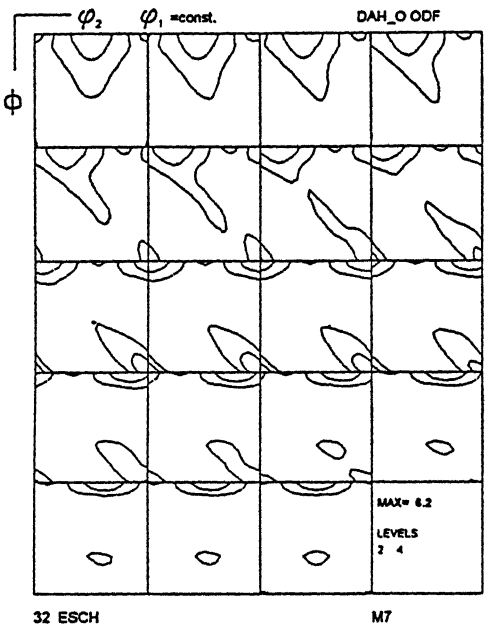

(b) FRT : 500 °C

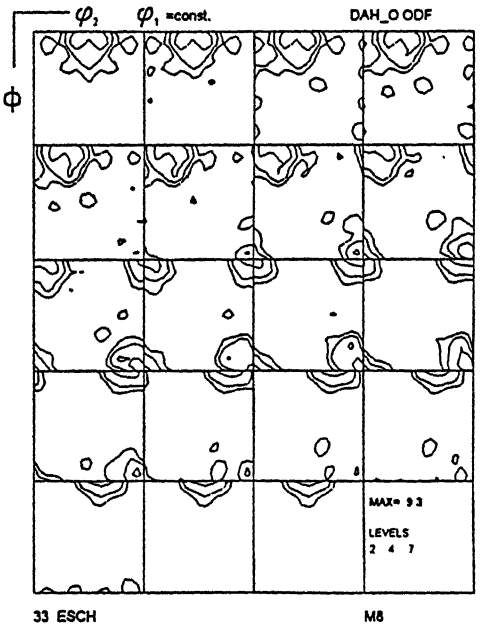

(d) FRT : 500 °C

Figure 4.29 (a) - (d) : ODF plots (φ_1 sections) for steel 1 after multipass rolling under schedule 1 [(a) and (b)] and annealing [(c) and (d)].

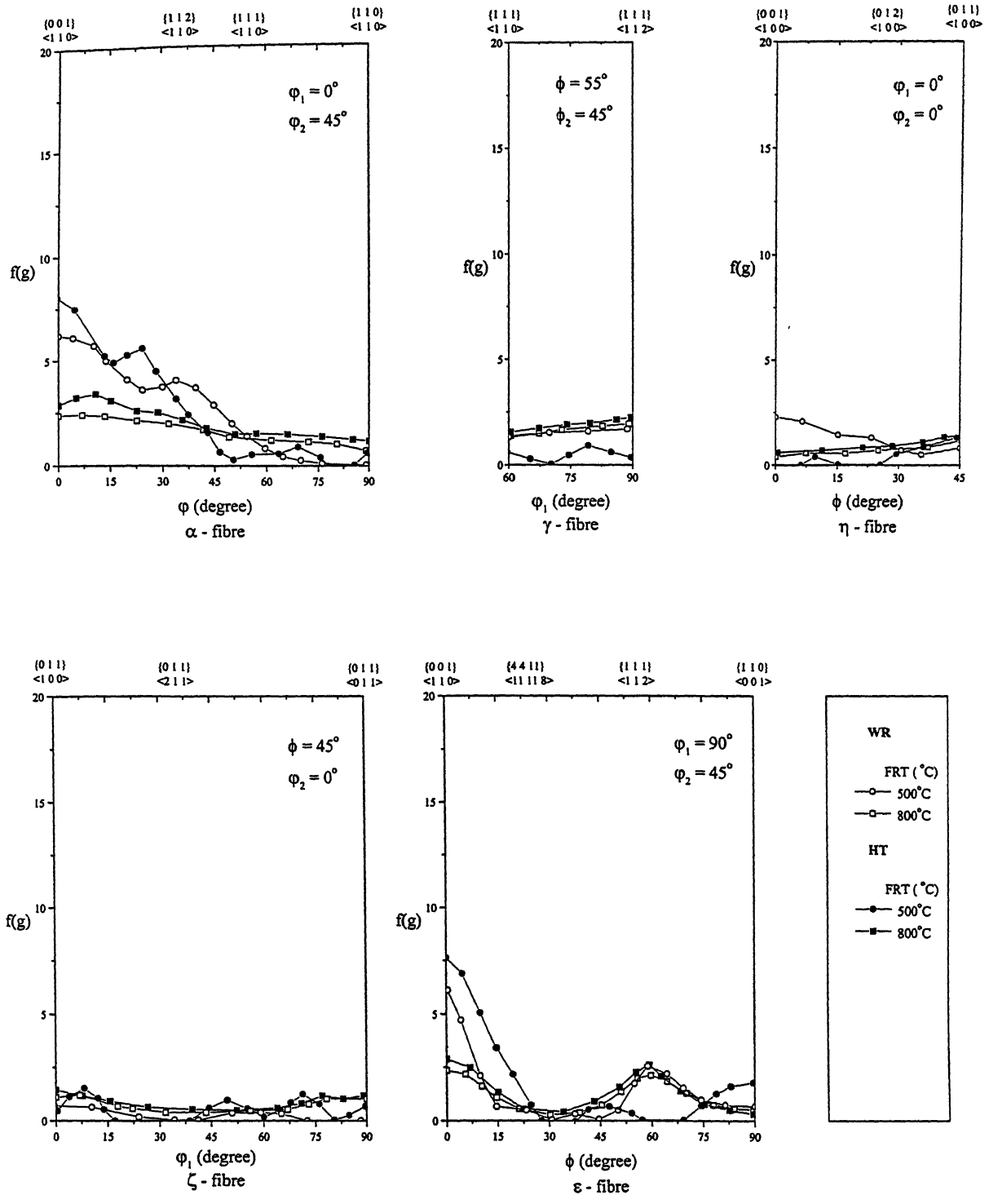

Figure 4.30 : Fibre plots for steel 1 after multipass rolling under schedule 1 (WR) and annealing (HT).

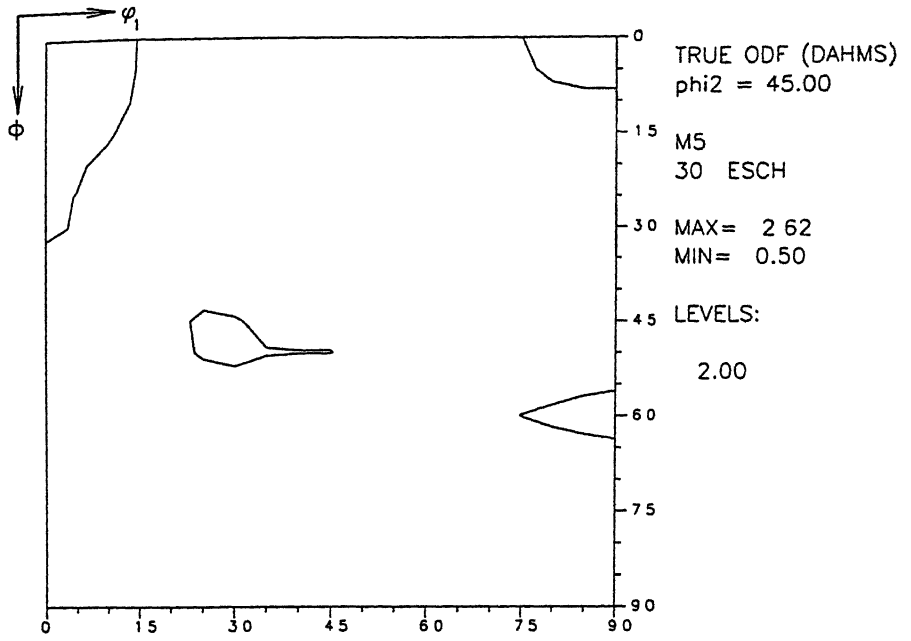

(a). FRT: 800 °C

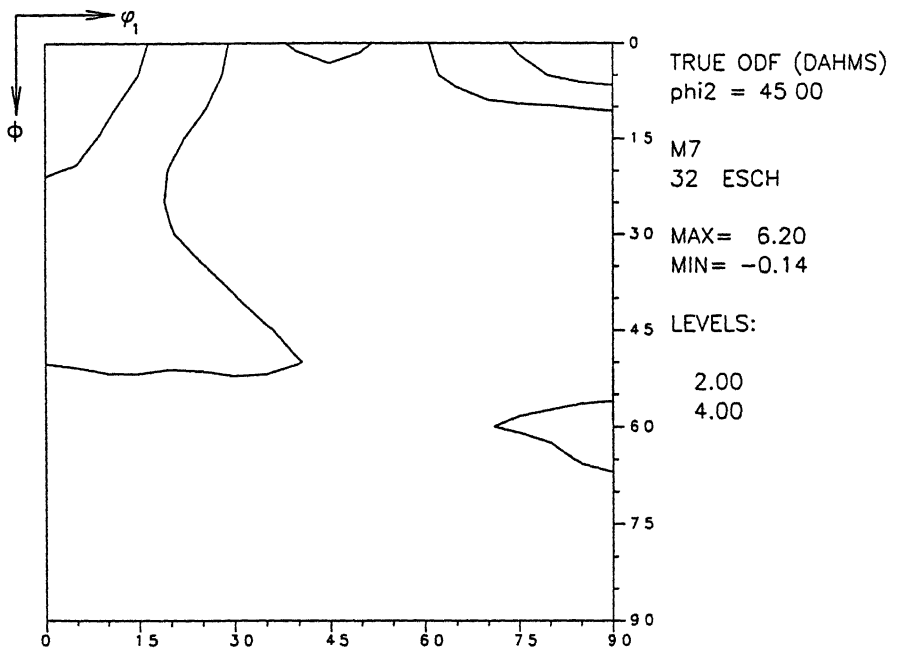

(b). FRT: 500 °C

Figure 4.31 (a) and (b) : $\varphi_2 = 45^{\circ}$ sections plots for steel 1 after multipass rolling under schedule 1.

changes in the locations of the various fibres, although there are changes in intensities after the warm rolled samples are heat treated. For example, the 500 ^{O}C FRT sample shows particularly no γ fibre, while the 800 ^{O}C FRT sample displays a rather weak γ fibre, after heat treatment. The α fibre in both the samples show a similar trend before and after heat treatment. Another noticeable feature is that heat treatment leads to a marginal decrease in the intensity of the cube orientation and an increase in the intensity of the rotated cube component in the texture of the 500 ^{O}C FRT material. The $\varphi_2 = 45^{O}$ sections of the heat treated samples [Fig. 4.31 (c) and (d)] simply corroborate the above findings.

(b) Schedule 2

The ODF plots of the warm rolled samples of schedule 2 with FRT s of 800 ^{O}C and 500 ^{O}C are shown in Figures 4.32(a) and (b) respectively. Although the general nature of the texture in the two cases is quite similar, the texture of the 500 ^{O}C FRT sample is perceptibly sharper than that of the 800 ^{O}C FRT sample. The relevant fibre plots [Fig. 4.33] show that all the five fibres in these two samples are rather weak. The γ fibre in the 500 ^{O}C FRT sample has a maximum intensity of around 2.0, and this is higher than the intensity of the γ fibre in the 800 ^{O}C FRT sample. In a similar manner the α fibre is also marginally sharper in the former than in the latter. Both the cube and the rotated cube component are more intense [f(g) ~ 3 to 4] in the 500 ^{O}C FRT sample than in the other. The above results are also corroborated by the relevant $\varphi_2 = 45^{O}$ section plots [Fig. 4.34(a) and (b)] texture plots.

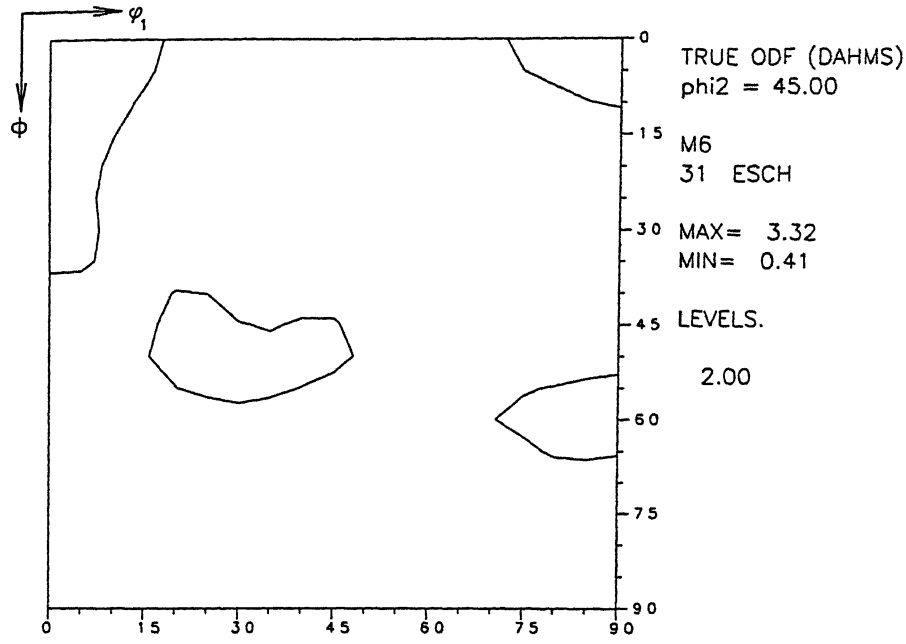

(c). FRT: 800 ^{O}C

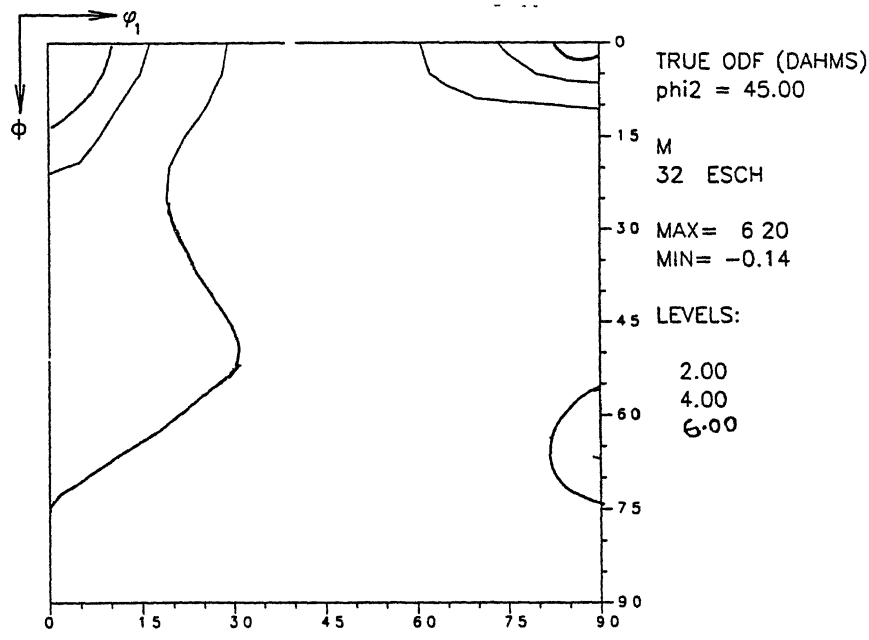

(d). FRT: 500 ^{O}C

Figure 4.31 (c) and (d) : $\varphi_2 = 45^{O}$ sections plots for steel 1 after multipass rolling under schedule 1 and annealing.

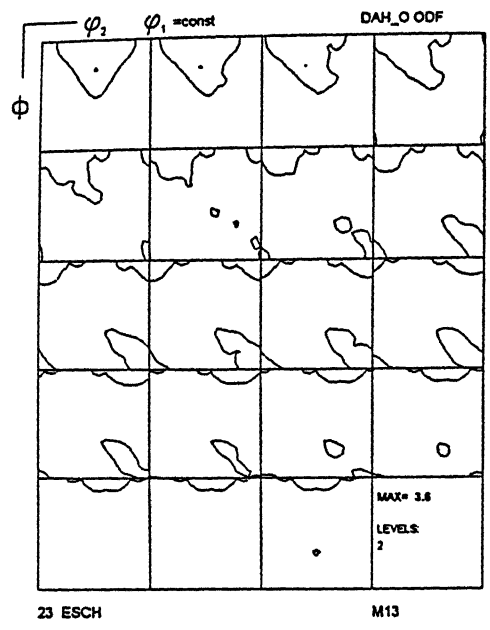

(a) FRT : 800 °C

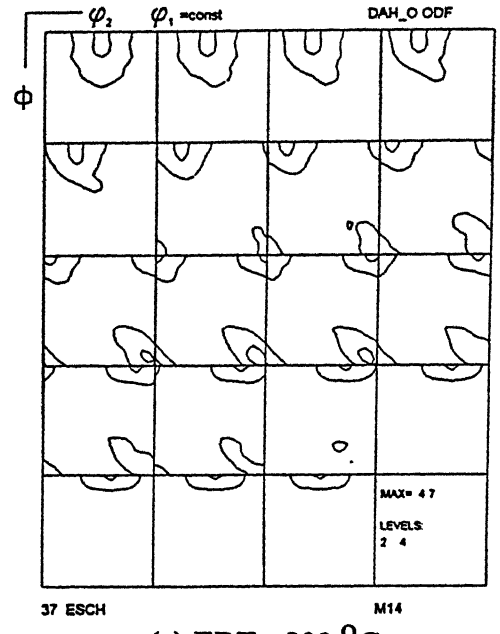

(c) FRT : 800 °C

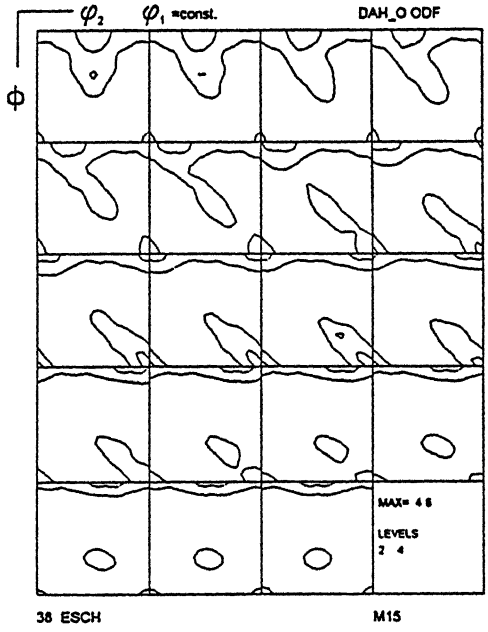

(b) FRT : 500 °C

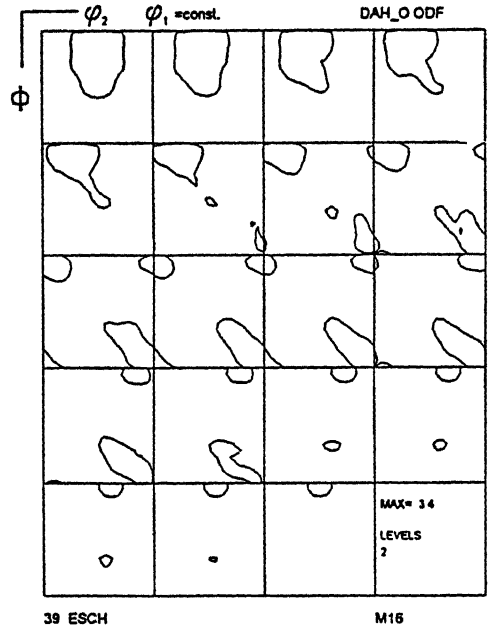

(d) FRT : 500 °C

Figure 4.32 (a) - (d) : ODF plots (φ_1 sections) for steel 1 after multipass rolling under schedule 2 [(a) and (b)] and annealing [(c) and (d)].

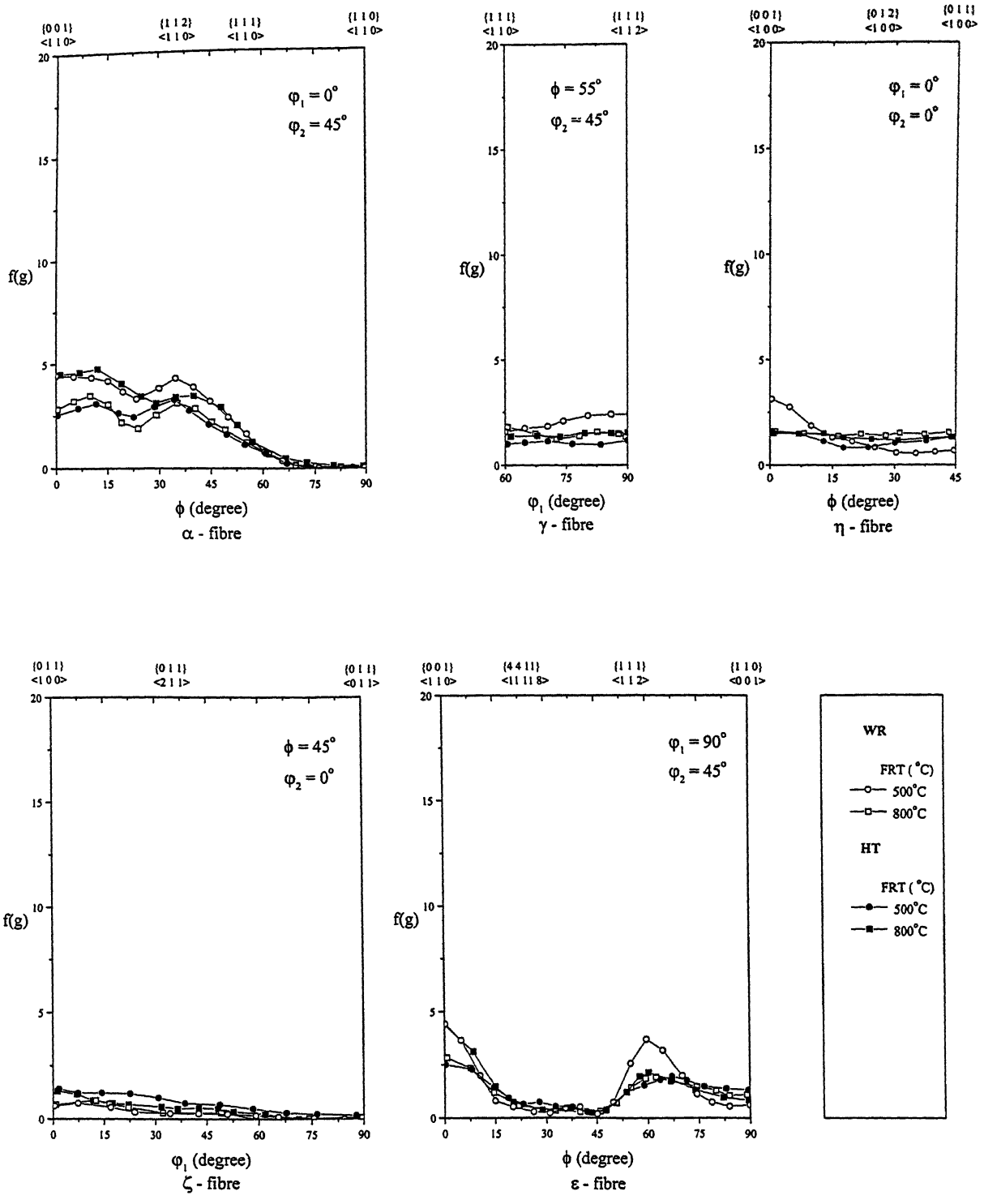

Figure 4.33 : Fibre plots for steel 1 after multipass rolling under schedule 2 (WR) and annealing (HT).

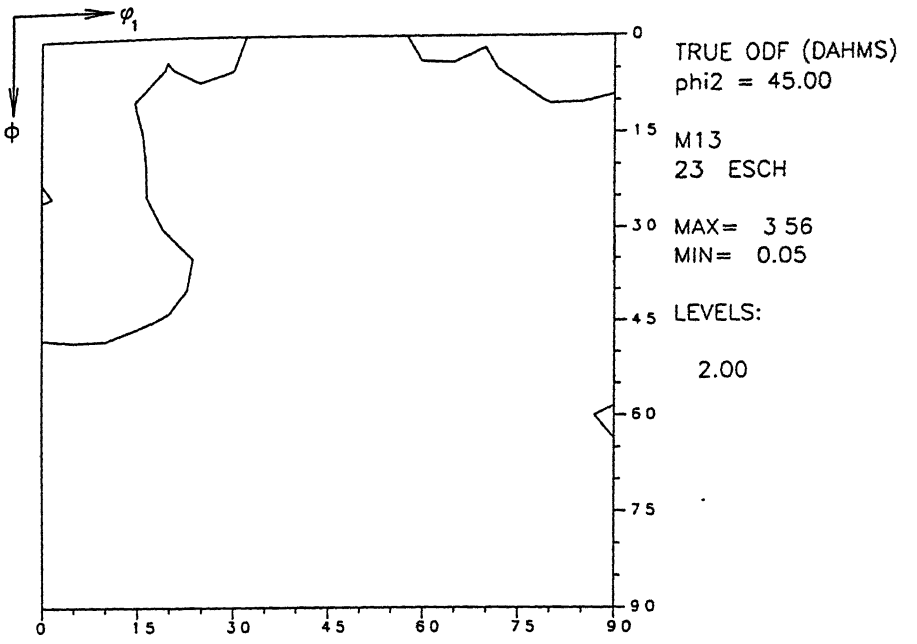

(a). FRT: 800 ^{O}C

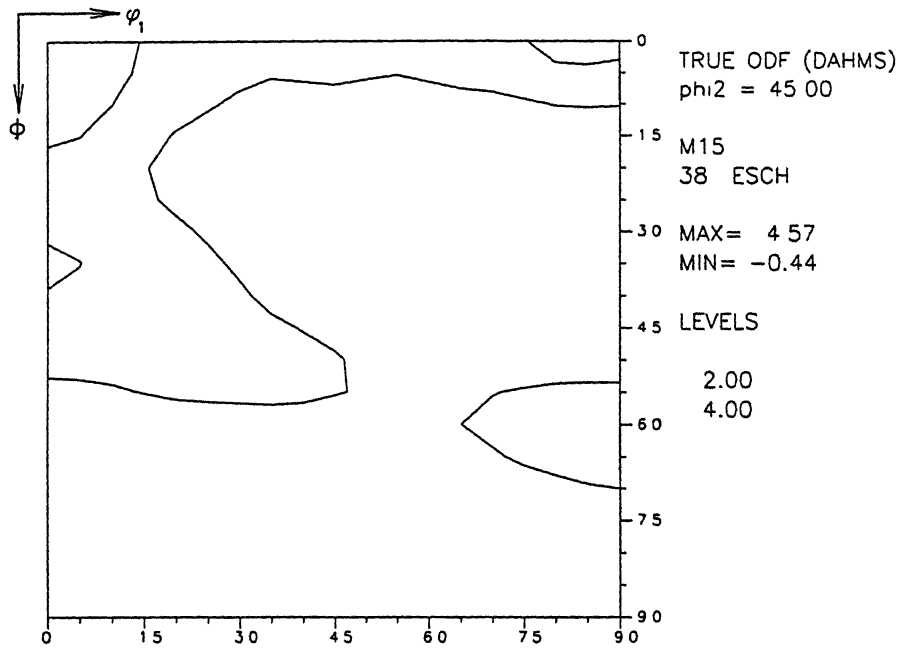

(b). FRT: 500 ^{O}C

Figure 4.34 (a) and (b) : $\varphi_2 = 45^{O}$ sections plots for steel 1 after multipass rolling under schedule 2.

After heat treatment the overall texture intensity improves somewhat for the 800 ^{O}C FRT sample, while it marginally decreases for the 500 ^{O}C FRT sample [Fig. 4.32(c) and (d)]. The nature of the general texture remains more or less unchanged. This is also evident from the relevant fibre plots [Fig. 4.33] and $\varphi_2 = 45^{O}$ sections [Fig. 4.34(c) and (d)].

(c) Schedule 3

The texture of the 800 ^{O}C FRT and 500 ^{O}C FRT samples warm rolled in schedule 3 are shown in the ODF s of Figures 4.35(a) and (b) respectively. The general features and the intensities of the two ODFs are quite similar. The fibre plots of the two samples [Fig. 4.36] also show similarities in many respects. A non-uniform α fibre is obtained in both the samples. The 500 ^{O}C FRT sample shows a high value [f (g) ~ 7.5] at the $\{001\}<110>$ location and another maxima [f (g) ~ 5.0] at the $\{223\}<110>$ position. The non-uniform α fibre in the 800 ^{O}C FRT material shows lower f(g) values all along the fibre. A uniform and weak [f (g) ~ 2.5] γ fibre is present in the 500 ^{O}C FRT sample, and this fibre is practically non-existent in the 800 ^{O}C FRT sample. Both the samples also show some intensity [f (g) ~ 2 – 2.5] at the exact cube location. These results are well corroborated from the $\varphi_2 = 45^{O}$ section plots of the two samples [Fig. 4.37(a) and (b)].

Heat treatment of the above two samples does not seem to change the ODF s of the warm rolled samples by any significant extent [Fig. 4.35(c) and (d)], although there is a slight decrease in the general sharpness. The fibres of the heat treated samples follow the same general pattern of the corresponding warm rolled material [Fig. 4.36]. However, the fibre intensities of the heat treated samples are somewhat weaker as compared to their

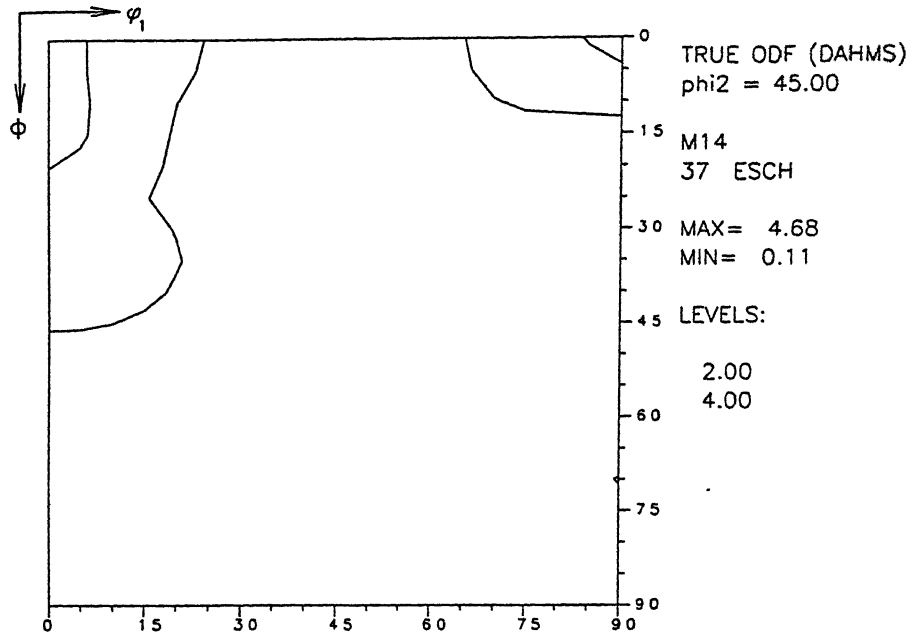

(c). FRT: 800 ^{O}C

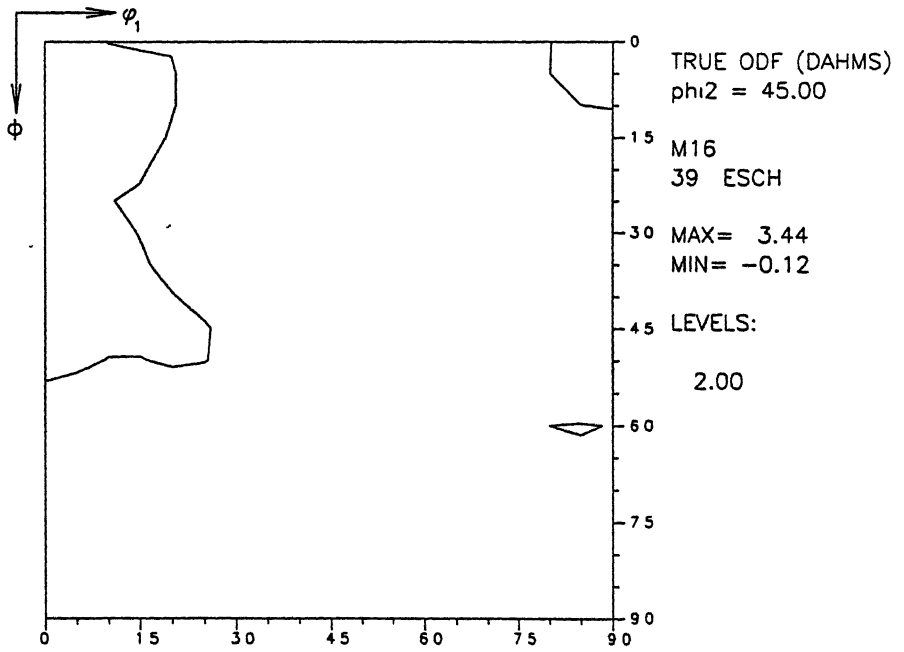

(d). FRT: 500 ^{O}C

Figure 4.34 (c) and (d) : $\varphi_2 = 45^{O}$ sections plots for steel 1 after multipass rolling under schedule 2 and annealing.

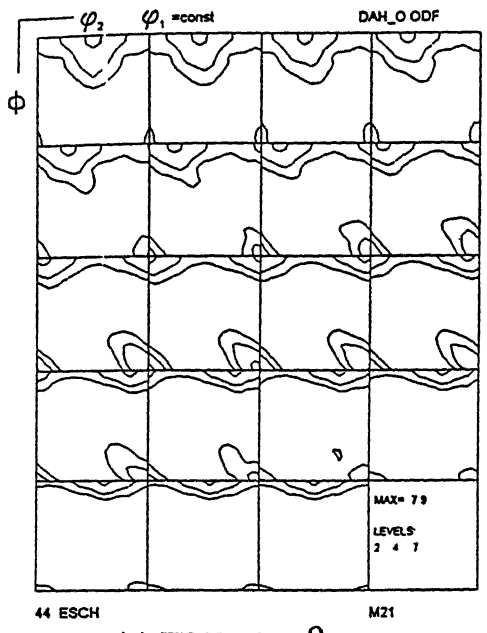

(a) FRT : 800 °C

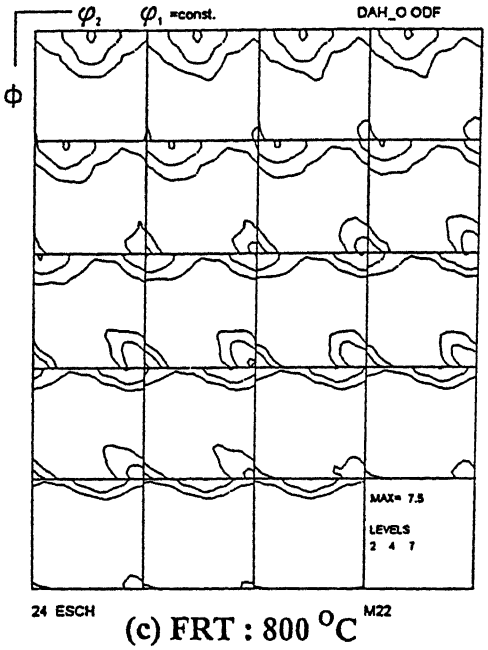

(c) FRT : 800 °C

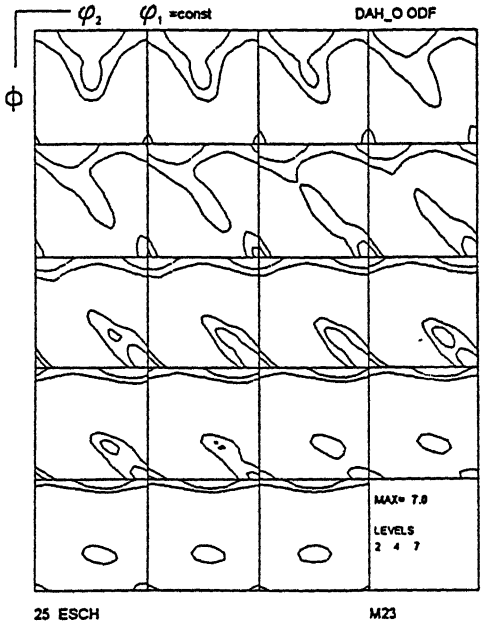

(b) FRT : 500 °C

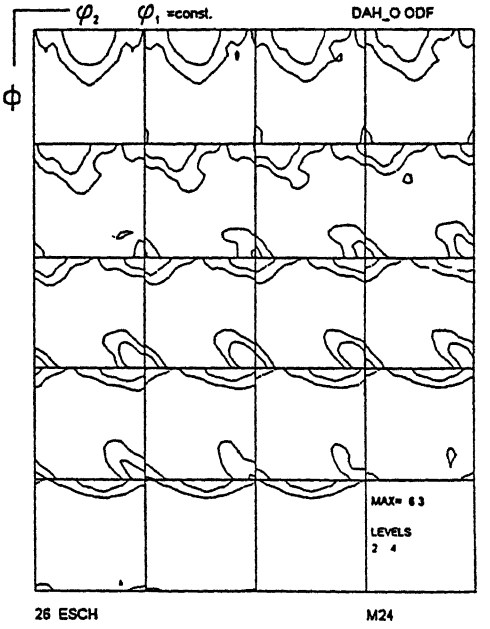

(d) FRT : 500 °C

Figure 4.35 (a) - (d) : ODF plots (φ_1 sections) for steel 1 after multipass rolling under schedule 3 [(a) and (b)] and annealing [(c) and (d)].

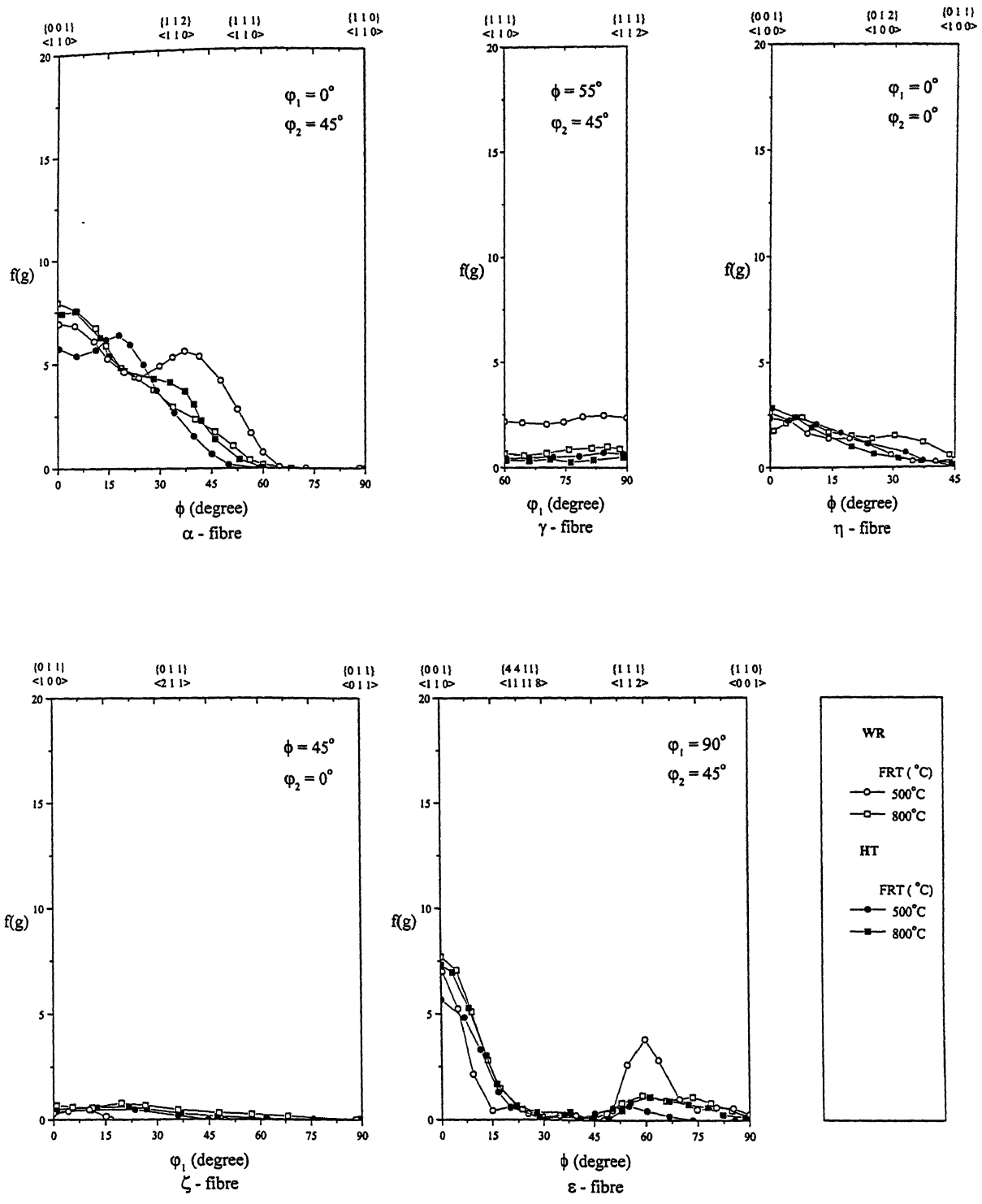

Figure 4.36 : Fibre plots for steel 1 after multipass rolling under schedule 3 (WR) and annealing (HT).

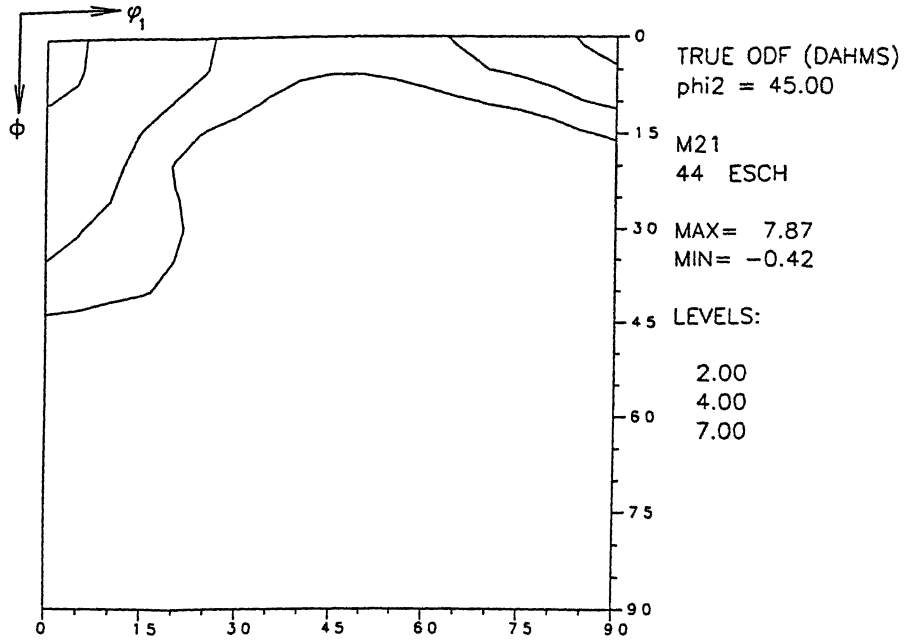

(a). FRT: 800 ^{O}C

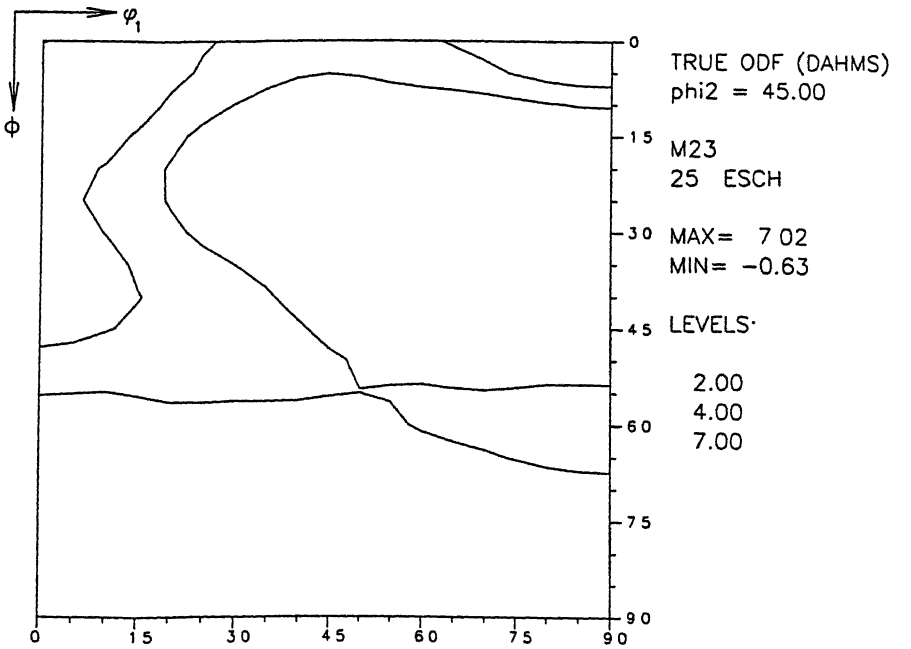

(b). FRT: 500 ^{O}C

Figure 4.37 (a) and (b) : $\varphi_2 = 45^{O}$ sections plots for steel 1 after multipass rolling under schedule 3.

warm rolled counterparts. These results are fully corroborated by the $\varphi_2 = 45^0$ section plots of the samples [Fig. 4.37(c) and (d)].

4.5.2 Steel 2

4.5.2.1 Single pass rolling after soaking at 1150 ^{O}C

(a) Warm rolling textures

The ODFs of steel 2, single pass rolled after soaking at 1150 ^{O}C with FRTs of 800 ^{O}C, 700 ^{O}C, 600 ^{O}C and 500 ^{O}C are shown in Figures 4.38 (a) to (d) respectively. The ODF of the 800 ^{O}C FRT sample displays two distinct fibres — a γ fibre and another running from $\varphi_2 = 0^{O}$ to 90^{O} in every φ_1 section. With the decrease in FRT the texture sharpness increases — from an $f(g)_{max}$ value of 8.0 for the 800 ^{O}C FRT sample to $f(g)_{max}$ of 11.6 for the 600 ^{O}C FRT sample. The ODF of the 500 ^{O}C FRT sample shows an abruptly low texture intensity of $f(g)_{max}$ ~5.6, as shown in Figure 4.38 (d). The general nature of the texture, as observed in these four ODFs, is very nearly the same, each of them showing the presence of the two fibres mentioned above.

The five fibre component plots [Fig. 4.39] show that all the four samples display the presence of two non-uniform fibres, α and ε and a nearly uniform γ fibre. The α fibre intensity is the strongest for the 600 ^{O}C FRT sample and it shows two maxima, at {001}<110> and at {111} <110>. The 700 ^{O}C FRT sample shows a lower value of the maxima at {001}<110> and a singular value of the maxima at {111}<110>. The α fibre in the 800 ^{O}C FRT sample shows just one maxima, somewhat lower in intensity than in the previous two, at near {111}<110>. The α fibre of the lowest intensity is obtained in the

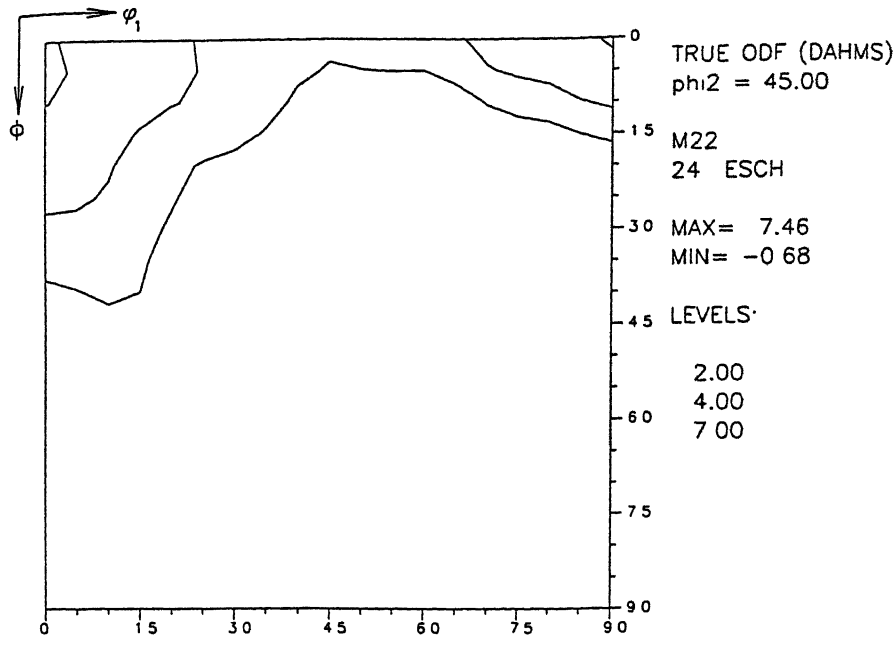

(c). FRT: 800 ^{O}C

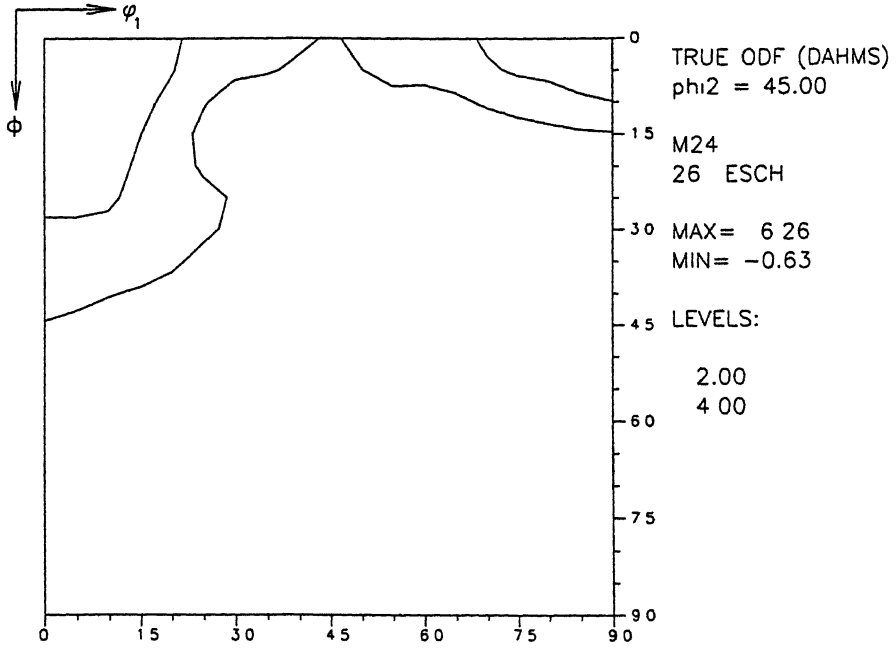

(d). FRT: 500 ^{O}C

Figure 4.37 (c) and (d) : $\varphi_2 = 45^{O}$ sections plots for steel 1 after multipass rolling under schedule 3 and annealing.

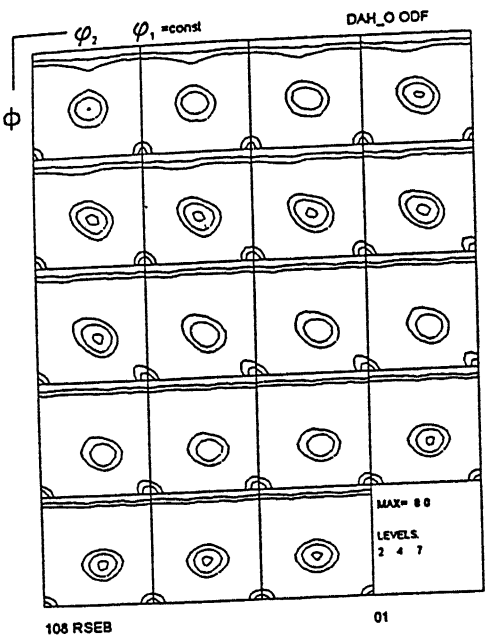

(a) FRT : 800 °C

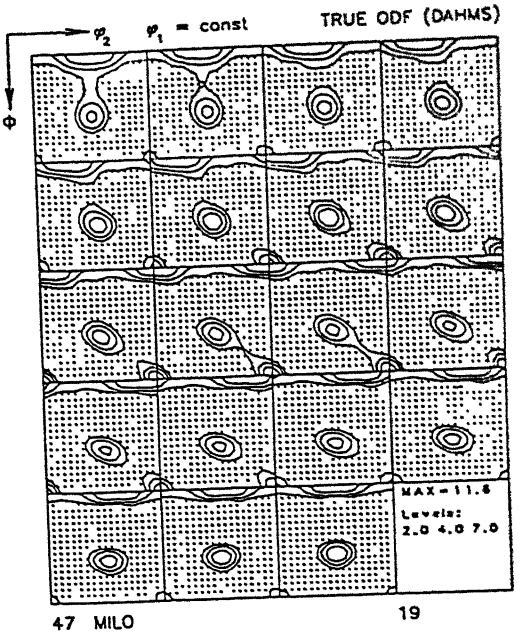

(c) FRT : 600 °C

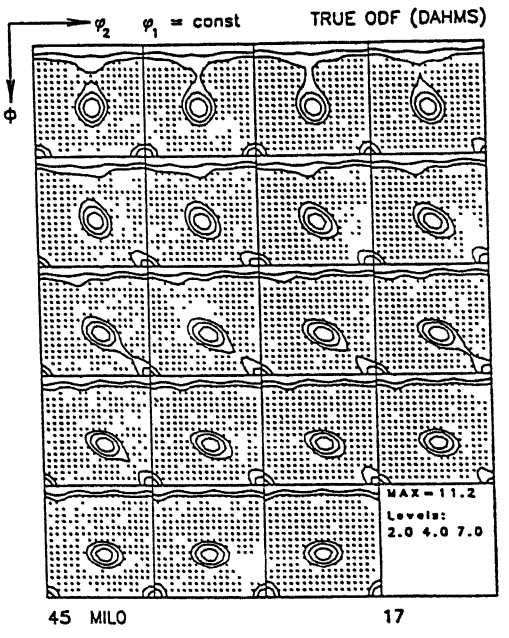

(b) FRT : 700 °C

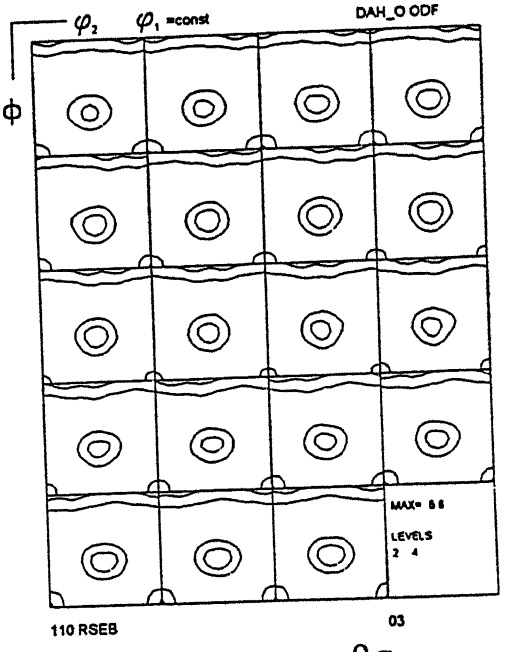

(d) FRT : 500 °C

Figure 4.38 (a) - (d) : ODF plots (φ_1 sections) for steel 2 after single pass rolling (after soaking at 1150 °C).

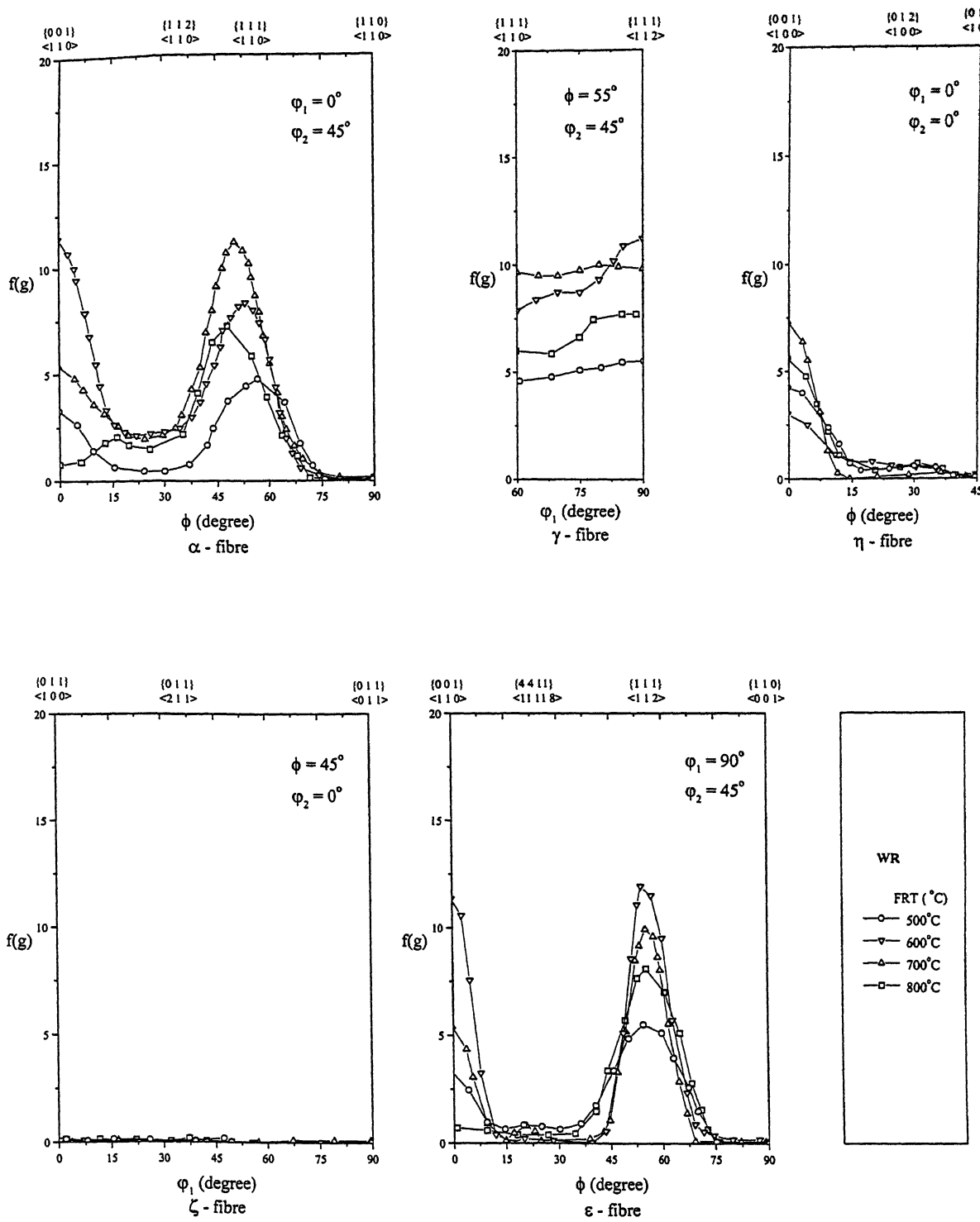

Figure 4.39 : Fibre plots for steel 2 after warm rolling (WR) in single pass (after soaking at 1150 °C).

500 ^{o}C FRT material, again with two maxima at {001}<110> and at {111}<110>. The highest γ fibre intensity is obtained for the 700 ^{o}C FRT sample, followed by the 600 ^{o}C FRT, the 800 ^{o}C FRT and the 500 ^{o}C FRT sample in decreasing order of magnitude. The ε fibre again shows two maxima, at {001}<110> and at {111}<112> and its intensity decreases in the order: 600 ^{o}C FRT, 700 ^{o}C FRT, 800 ^{o}C FRT and 500 ^{o}C FRT. The cube component, {001}<110> is the sharpest in the 700 ^{o}C FRT material, followed by the 800 ^{o}C FRT, 500 ^{o}C FRT and the 600 ^{o}C FRT material, in decreasing order of magnitude.

The $\varphi_2 = 45^{o}$ section texture plots for the above four samples are presented in Figures 4.40(a) to (d). Two clear-cut fibres — a γ fibre and another running down from $\varphi_1 = 0^{o}$ to 90^{o} — are observed for the 800 ^{o}C FRT sample [Fig. 4.40 (a)]. These two nearly uniform fibres are also seen in the relevant plot for the 700 ^{o}C FRT sample [Fig. 4.40 (b)]. The plot for the 600 ^{o}C FRT sample shows a sharp γ fibre, while the second fibre running from $\varphi_1 = 0^{o}$ to 90^{o} shows maxima at the rotated cube orientation, {001}<110>. Finally, the plot for the 500 ^{o}C FRT sample shows a rather uniform γ fibre and the other fibre, mentioned above, centered around the cube {001}<100>.

(b) Textures after heat treatment

The ODFs of the 800 ^{o}C FRT, 700 ^{o}C FRT, 600 ^{o}C FRT and 500 ^{o}C FRT samples, after heat treatment, are displayed in Figures 4.41 (a) to (d). All four of them show primarily the γ fibre running from the $\varphi_1 = 0^{o}$ to $\varphi_1 = 90^{o}$ sections.

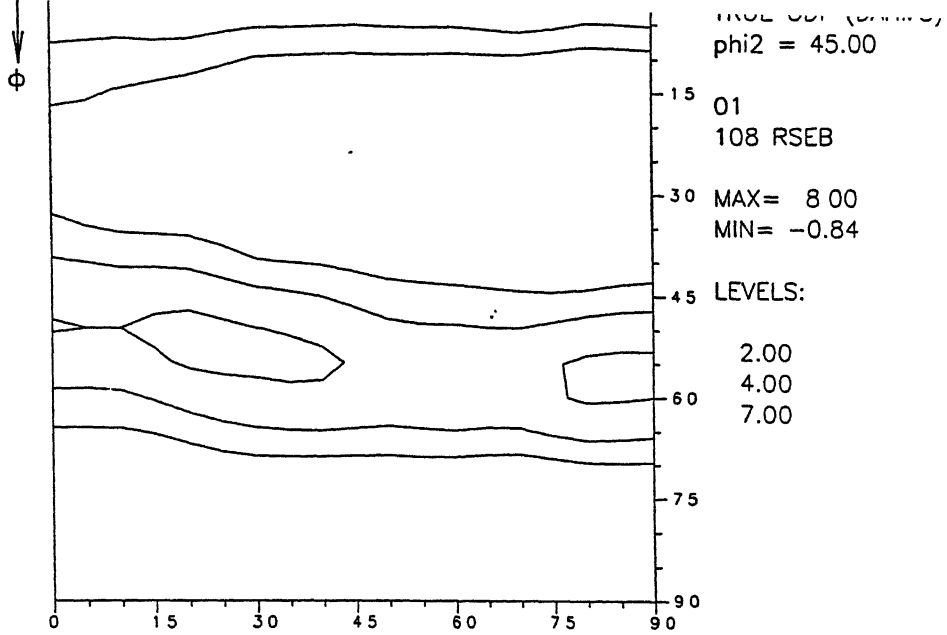

(a). FRT: 800 ^{O}C

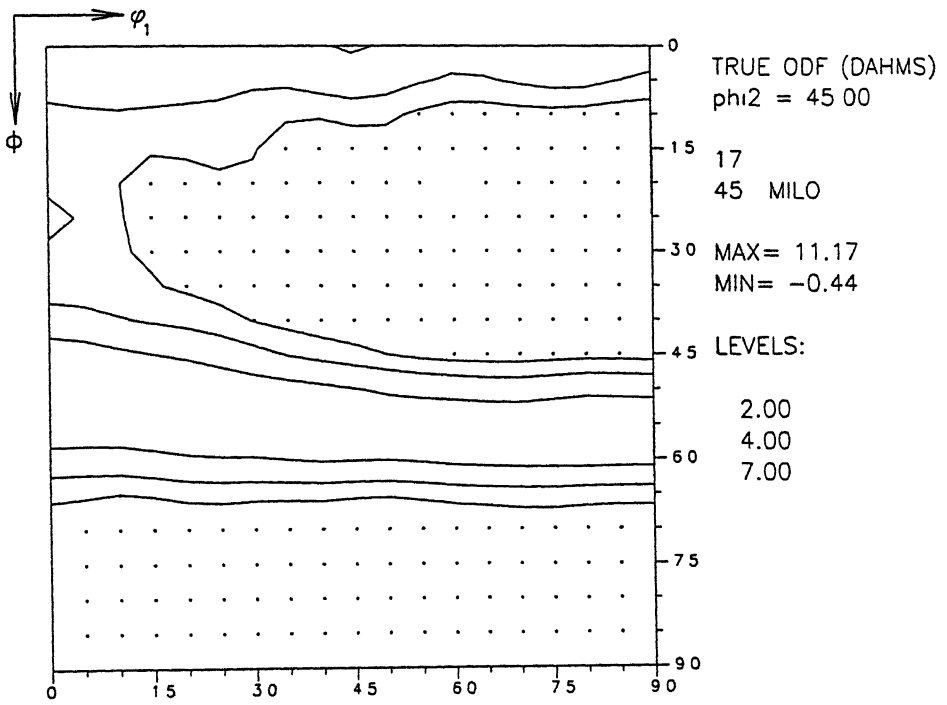

(b). FRT: 700 ^{O}C

Figure 4.40 (a) and (b) : $\varphi_2 = 45^{O}$ sections plots for steel 2 after single pass rolling (after soaking at 1150 ^{O}C).

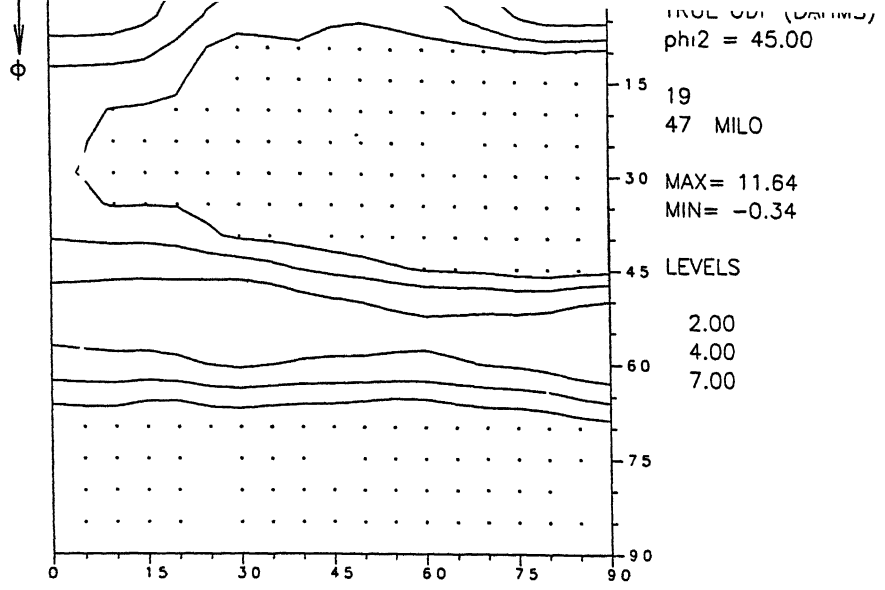

(c). FRT: 600 ^{O}C

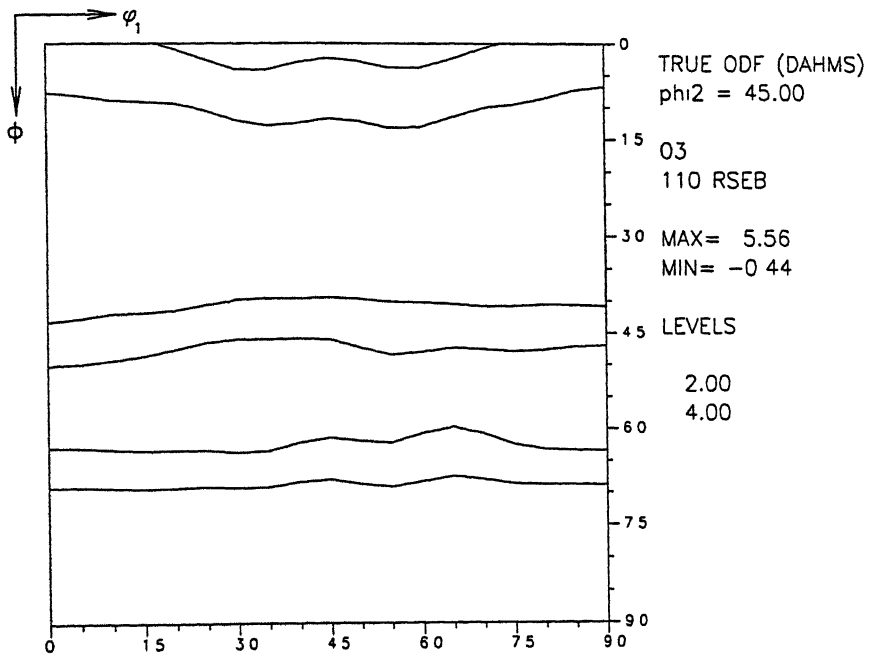

(d). FRT: 500 ^{O}C

Figure 4.40 (c) and (d) : $\varphi_2 = 45^{O}$ sections plots for steel 2 after single pass rolling (after soaking at 1150 ^{O}C).

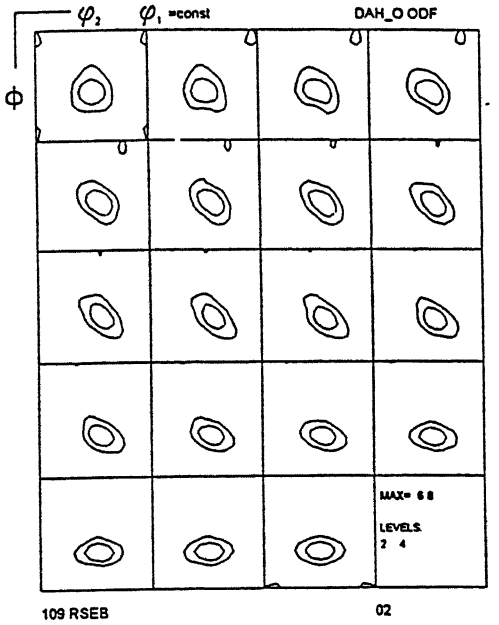

(a) FRT : 800 ^{o}C

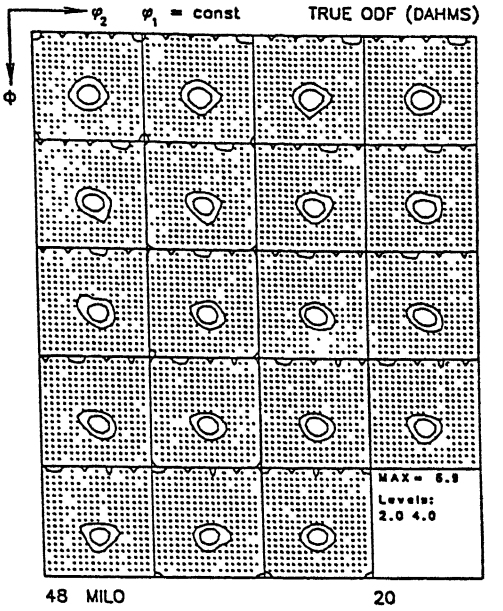

(c) FRT : 600 ^{o}C

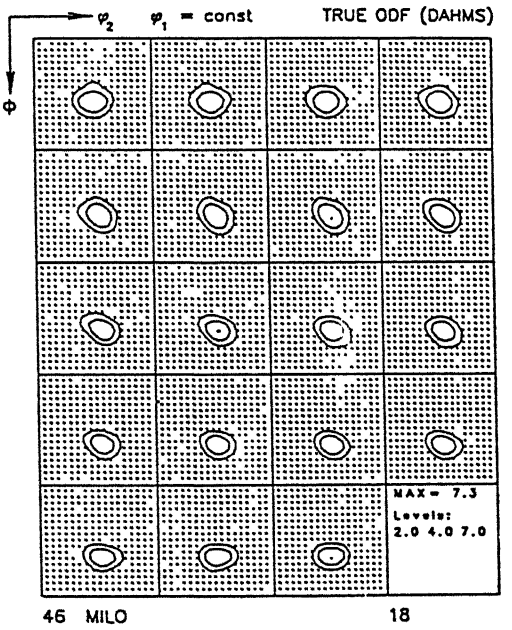

(b) FRT : 700 ^{o}C

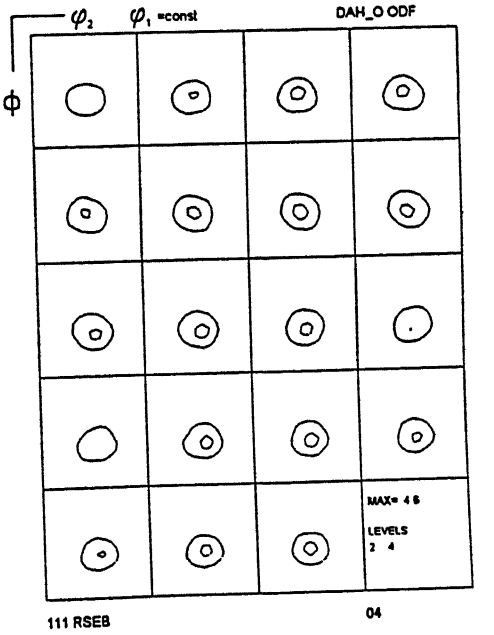

(d) FRT : 500 ^{o}C

Figure 4.41 (a) - (d) : ODF plots (φ_1 sections) for steel 2 after single pass rolling (after soaking at 1150 ^{o}C) and annealing.

The five fibre plots for these heat-treated samples are displayed in Figure 4.42. As in case of the warm rolled samples, the heat treated materials also show the presence of two non-uniform fibres α and ε and a uniform γ fibre. The γ fibre of the 500 ^{o}C FRT and HT sample is of the lowest intensity, while the γ fibres of the 600 ^{o}C and 700 ^{o}C FRT and HT samples show the highest values of the intensity, the γ fibre intensity of the 800 ^{o}C FRT and HT sample coming in between. For any of the samples, the intensity of a fibre decreases after heat treatment, the intensity of the 500 ^{o}C FRT and HT material showing the lowest value in all the three α, γ and ε fibres.

As expected, the $\varphi_2 = 45^{o}$ section plots [Fig. 4.43 (a) to (d)] for all the heattreated samples show primarily reasonably strong γ fibres.

4.5.2.2 Single pass rolling after soaking at 830 ^{o}C

(a) Warm rolling textures

The ODFs of the two samples, single pass rolled after soaking at 830 ^{o}C, with FRTs of 800 ^{o}C and 500 ^{o}C are displayed in Figures 4.44 (a) and (b) respectively. The overall intensity of the former is slightly higher than the latter. The general nature of the textures in the two cases is remarkably similar, showing a γ fibre, in all the φ_1 sections of the Euler Space, and another fibre running from $\varphi_2 = 0^{o}$ to 90^{o} in the φ_1 sections.

The five fibre plots for the above two materials, displayed in Figure 4.45 clearly show the presence of a moderately strong γ fibre in both. The intensities are nearly the same in the two cases. The α fibre in both of them is non-uniform, with maxima at

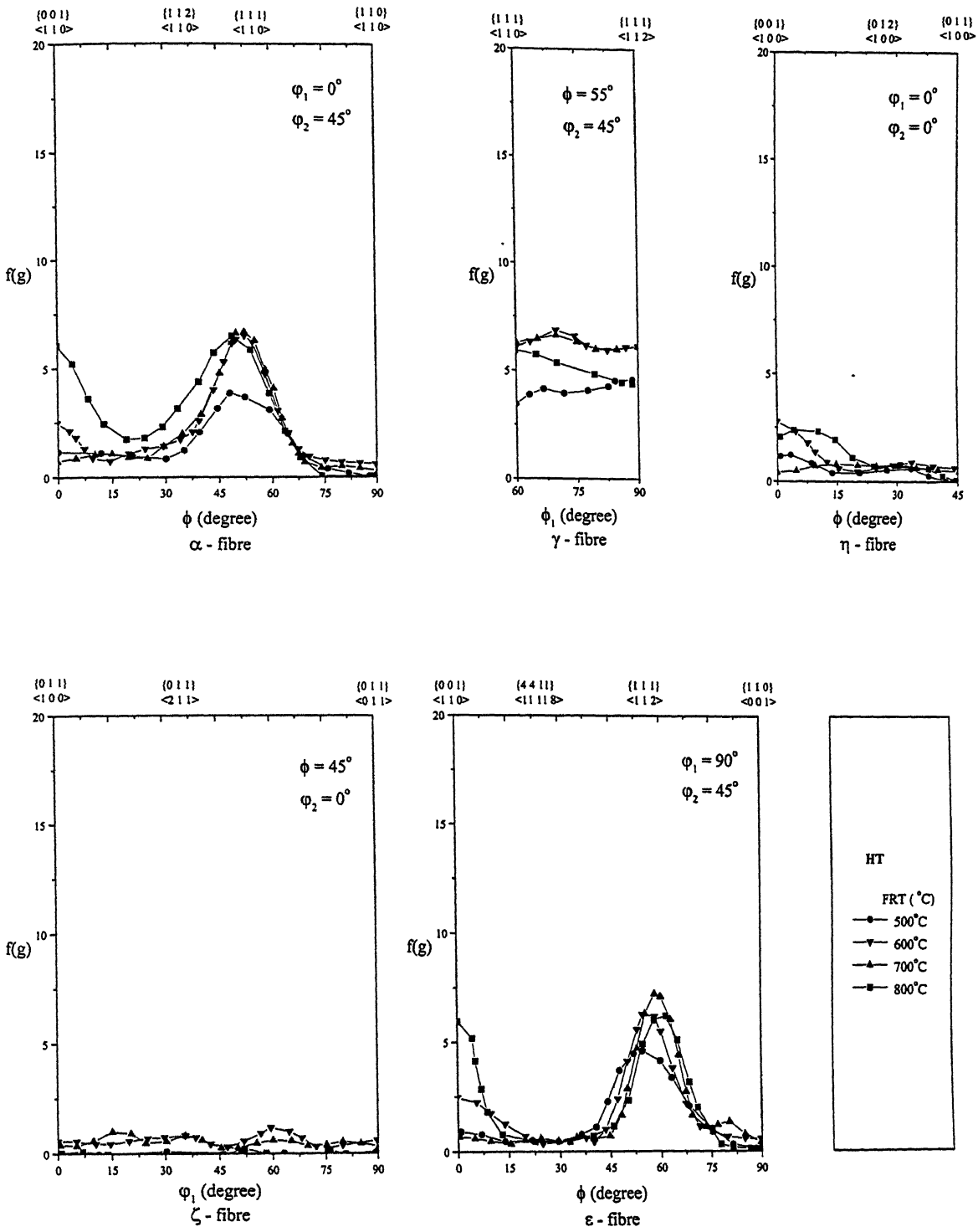

Figure 4.42 : Fibre plots for steel 2 after warm rolling in single pass (after soaking at 1150 °C) and annealing (HT).

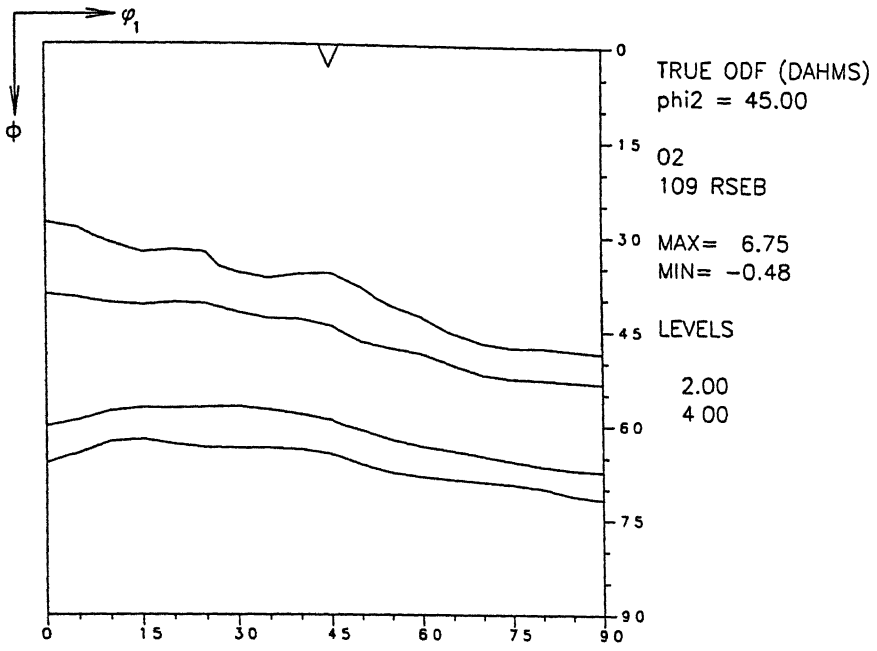

(a). FRT: 800 ^{O}C

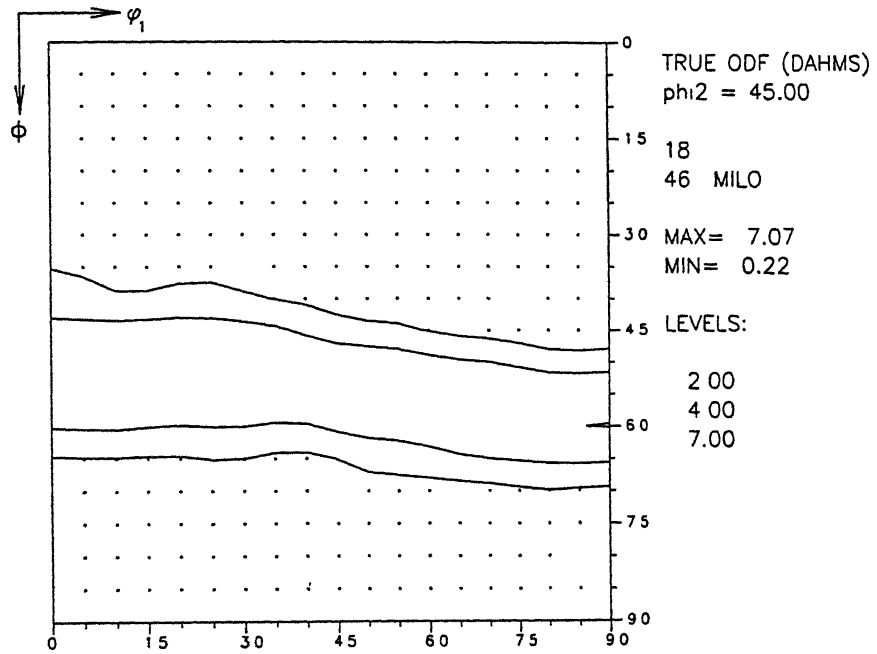

(b). FRT: 700 ^{O}C

Figure 4.43 (a) and (b) : $\varphi_2 = 45^{O}$ sections plots for steel 2 after single pass rolling (after soaking at 1150 ^{O}C) and annealing.

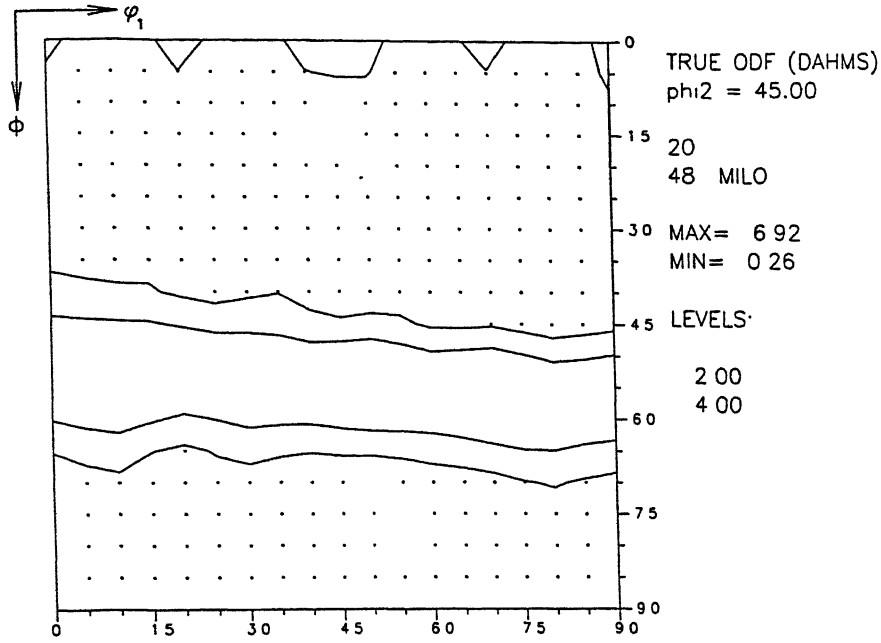

(c). FRT: 600 ^{O}C

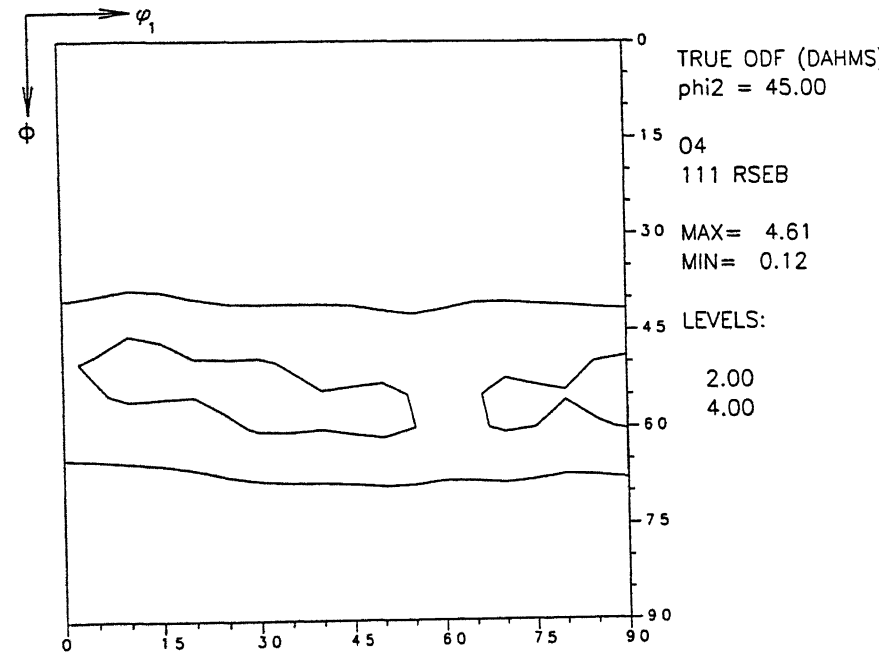

(d). FRT: 500 ^{O}C

Figure 4.43 (c) and (d) : $\varphi_2 = 45^{O}$ sections plots for steel 2 after single pass rolling (after soaking at 1150 ^{O}C) and annealing.

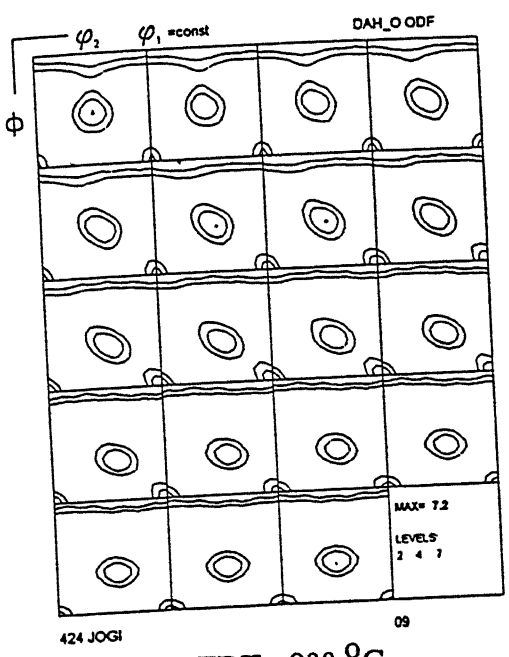

(a) FRT : 800 °C

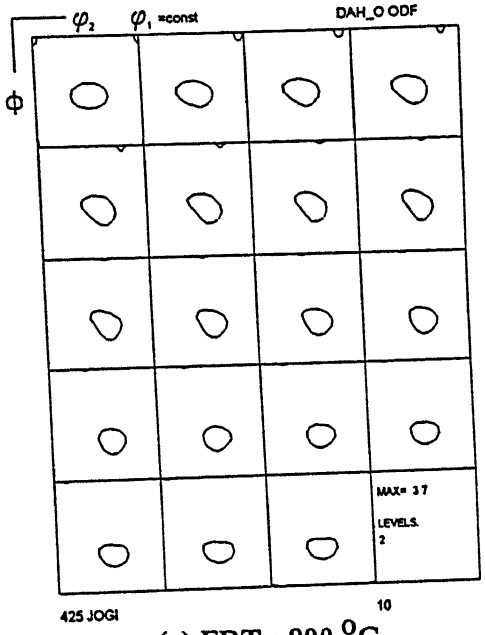

(c) FRT : 800 °C

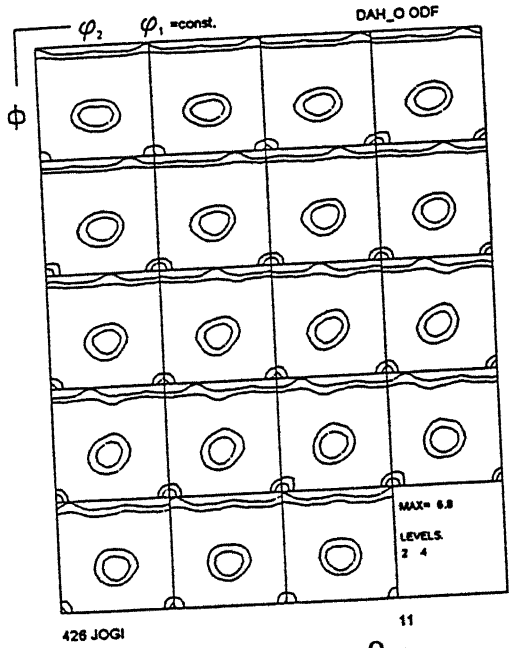

(b) FRT : 500 °C

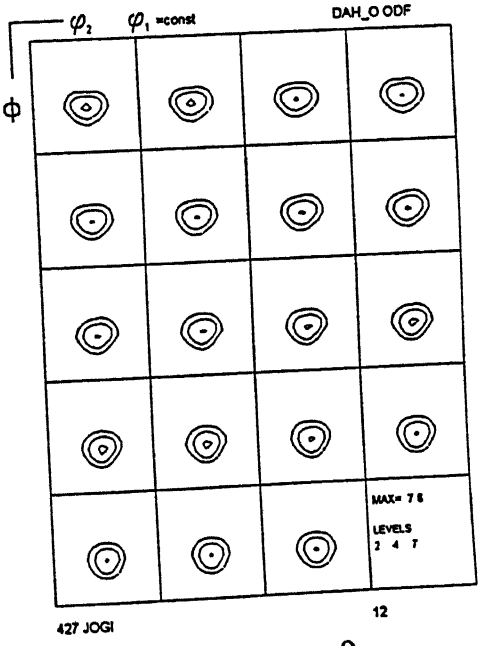

(d) FRT : 500 °C

Figure 4.44 (a) - (d) : ODF plots (φ_1 sections) for steel 2 after single pass rolling (after soaking at 830 °C) [(a) and (b)] and annealing [(c) and (d)].

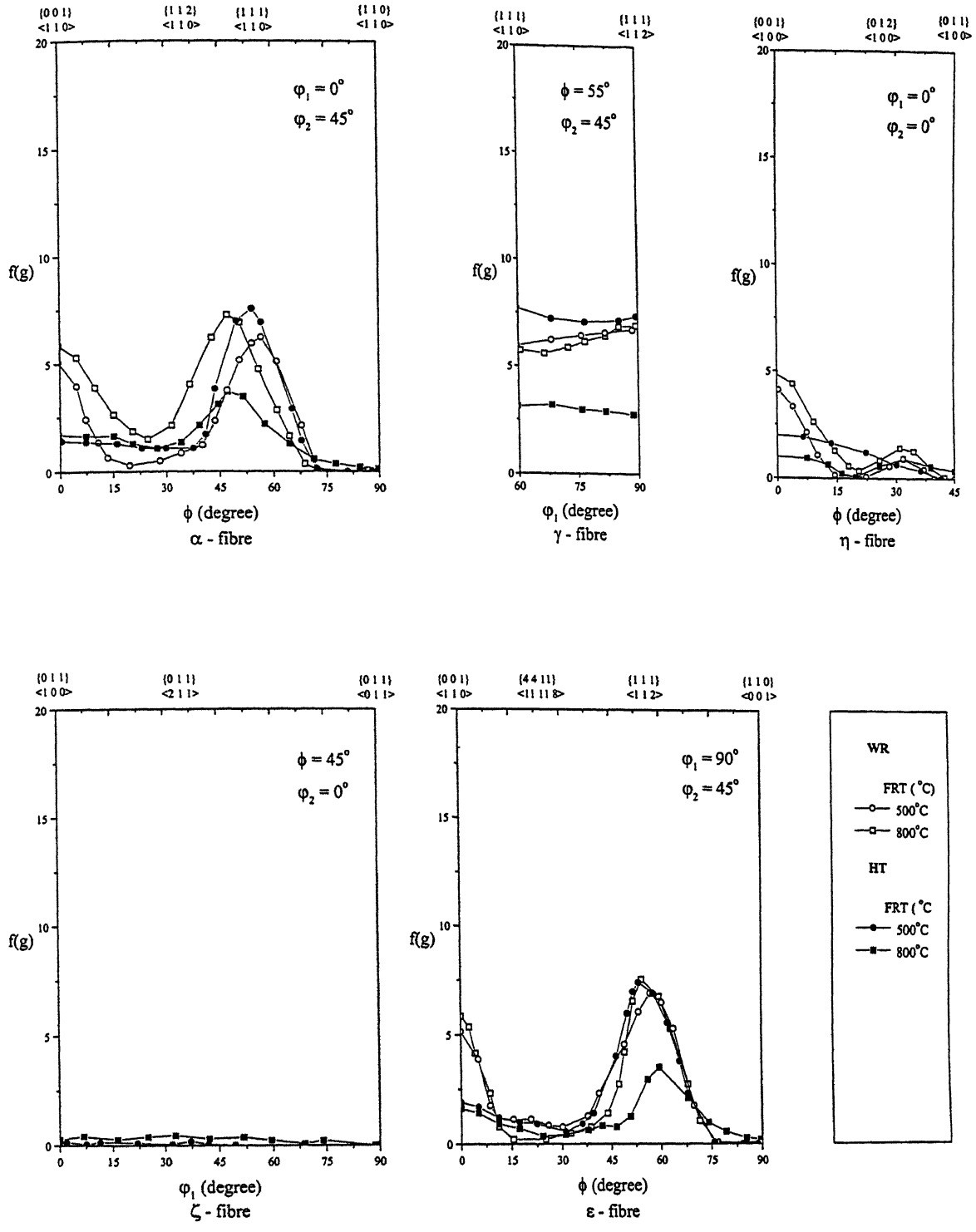

Figure 4.45 : Fibre plots for steel 2 after single pass rolling (after soaking at 830 °C) [WR] and annealing [HT].

{001}<110> and at ~{111}<110>, while the non-uniform ε fibre in both of them shows maxima at the locations {001}<110> and {111}<112>. The textures of both the materials show moderately strong intensities [f(g)~ 5.0] at the cube and rotated cube locations.

As expected, the $\varphi_2 = 45^{\circ}$ section plots for the two samples show two moderately strong fibres, one the γ fibre and the second one running from $\varphi_1 = 0^{\circ}$ to 90° in that section [Fig. 4.46 (a) and (b)].

(b) Textures after heat treatment

The ODFs of the above two materials, after heat treatment, are shown in Figures 4.44 (c) and (d). A comparison of these two plots with the corresponding plots for the warm rolled materials [Fig. 4.44 (a) and (b)] shows a striking difference. The ODF plots for the heat treated materials show primarily the γ fibre and nothing else. In fact, the sharpness of the ODF perceptibly increases after heat treatment in case of the 500 $^{\circ}$C FRT material, while ODF intensity decreases sharply after heat treatment in case of 800 $^{\circ}$C FRT material.

The fibre plots of the heat treated materials [Fig. 4.45] clearly show that the nearly uniform γ fibre in the 500 $^{\circ}$C material is almost twice as strong in intensity as in the 800 $^{\circ}$C FRT material. The non-uniform α and ε fibres also display much stronger intensities for the 500 $^{\circ}$C FRT material than in the 800 $^{\circ}$C FRT sample. The intensities at the cube and the rotated cube positions for both the samples are remarkably less here than in case of the corresponding warm rolled materials.

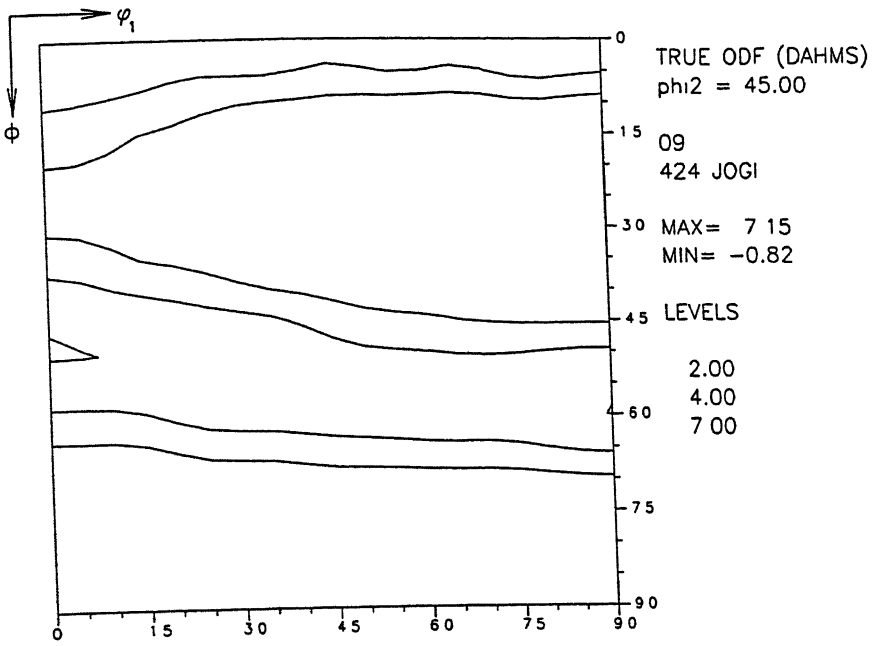

(a). FRT: 800 ^{O}C

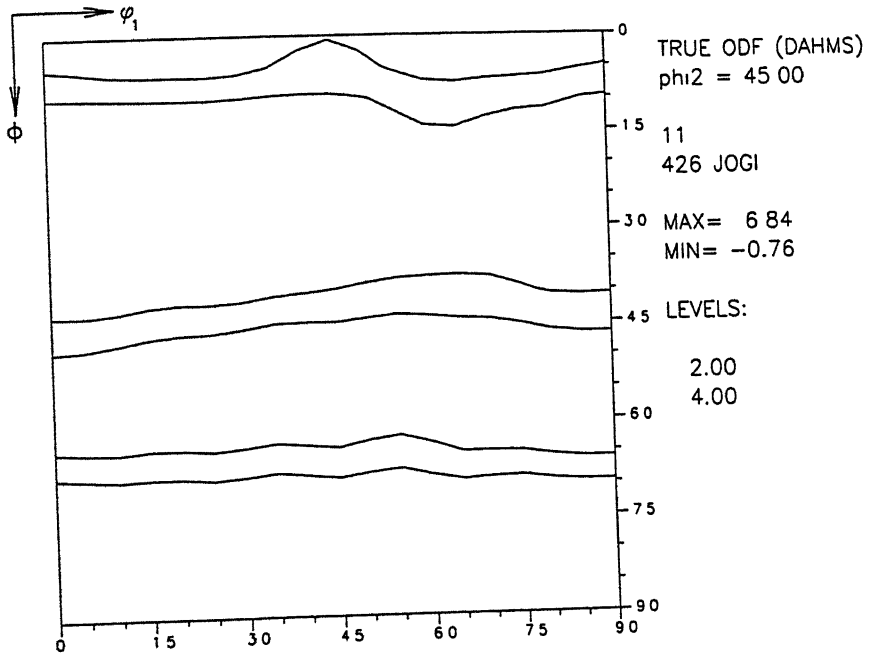

(b). FRT: 500 ^{O}C

Figure 4.46 (a) and (b) : $\varphi_2 = 45^{O}$ sections plots for steel 2 after single pass rolling (after soaking at 830 ^{O}C).

As expected, the $\varphi_2 = 45^{\circ}$ section plots [Fig. 4.46 (c) and (d)] show an almost perfect and moderately strong γ fibre in 500 $^{\circ}$C FRT and HT material and a weak γ fibre only in the 800 $^{\circ}$C FRT and HT sample.

4.5.2.3 Textures after multipass rolling

(a) Schedule 1

Figures 4.47(a) and (b) display the ODFs of the warm rolled samples of schedule 1 which were finish rolled at 800 $^{\circ}$C and 500 $^{\circ}$C respectively. While the former shows a weak texture, the latter is somewhat stronger and definitely shows the presence of a γ fibre. In fact, the fibre plots [Fig. 4.48] bring out the differences between these two textures much more clearly. While the 500 $^{\circ}$C FRT material shows a moderately strong non-uniform α fibre and a moderate and reasonably uniform γ fibre, these are practically absent in the 800 $^{\circ}$C FRT sample. On the other hand, non-uniform η and ζ fibres are present in the 800 $^{\circ}$C FRT material, while these are practically absent in 500 $^{\circ}$C FRT sample. The ε fibre plot shows a moderate peak at ~ {4 4 11}< 11 11 8> for the 800 $^{\circ}$C FRT sample, while a moderately strong peak at {111}<112 > appears for the 500 $^{\circ}$C FRT sample. The $\varphi_2 = 45^{\circ}$ section plots for the two warm rolled samples [Fig. 4.49 (a) and (b)] bring out the differences in their textures in a very striking manner. While the 500 $^{\circ}$C FRT material shows the clear presence of an α and a γ fibre, the 800 $^{\circ}$C FRT sample shows no such fibre at all, but some isolated texture intensities near the cube and the Cu {112}< 111 > location.

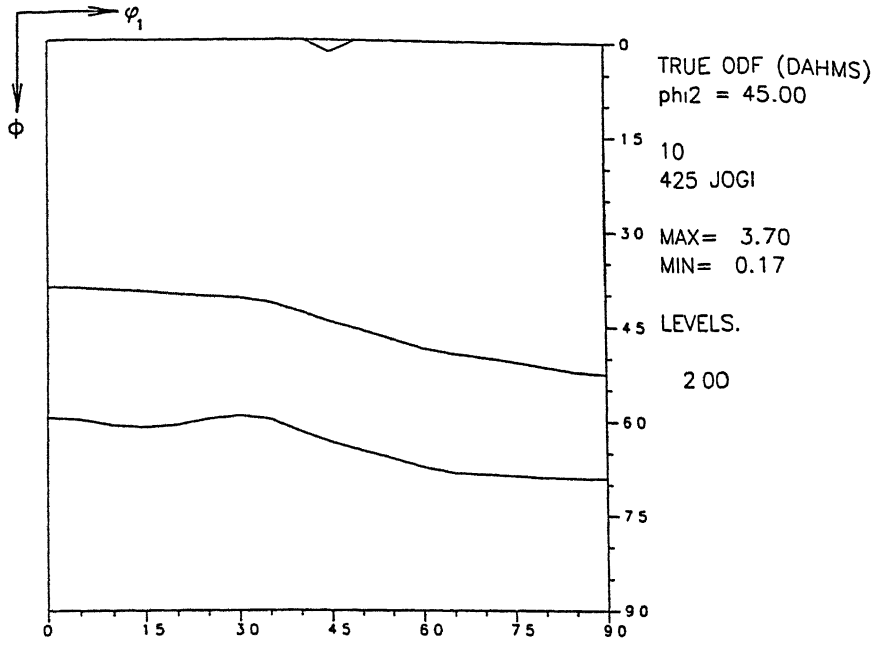

(c). FRT: 800 ^{O}C

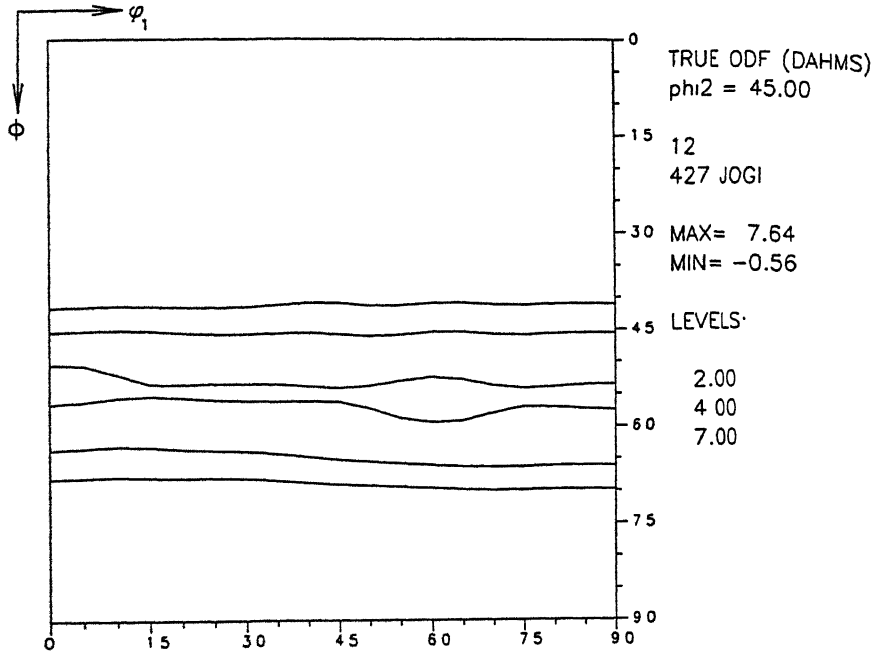

(d). FRT: 500 ^{O}C

Figure 4.46 (c) and (d) : $\varphi_2 = 45^{O}$ sections plots for steel 2 after single pass rolling (after soaking at 830 ^{O}C) and annealing.

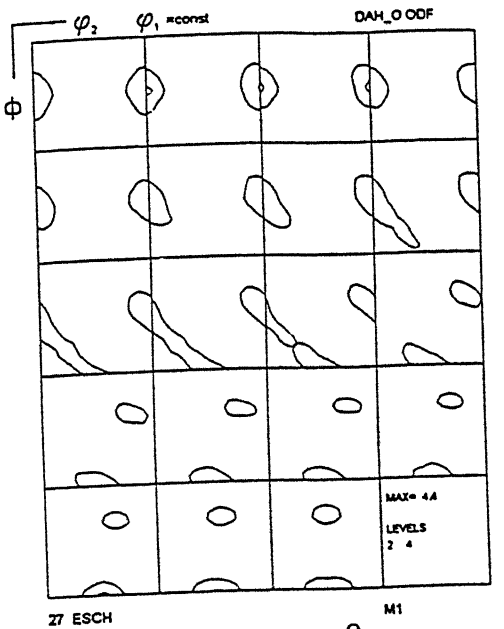

(a) FRT : 800 °C

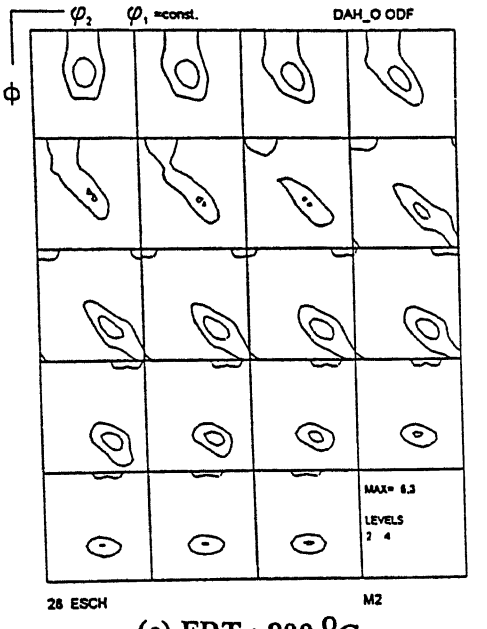

(c) FRT : 800 °C

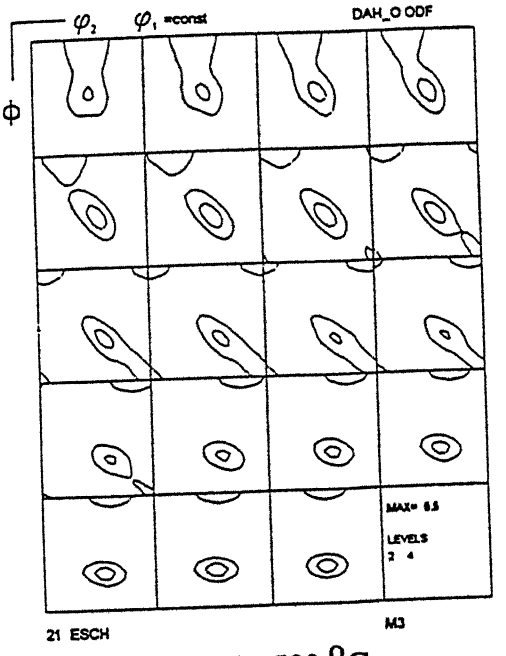

(b) FRT : 500 °C

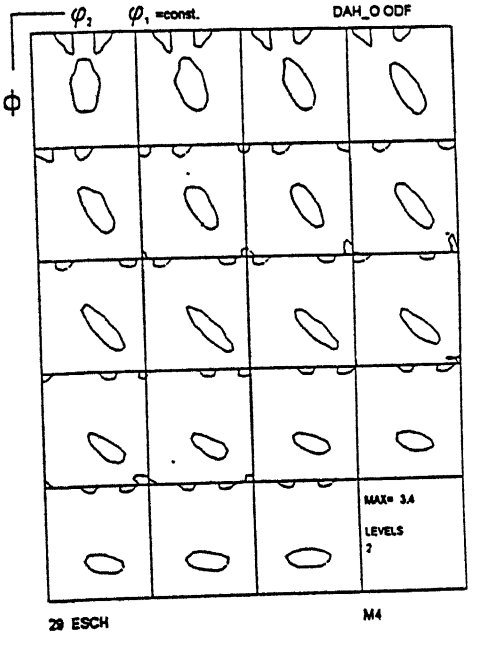

(d) FRT : 500 °C

Figure 4.47 (a) - (d) : ODF plots (φ_1 sections) for steel 2 after multipass rolling under schedule 1 [(a) and (b)] and annealing [(c) and (d)].

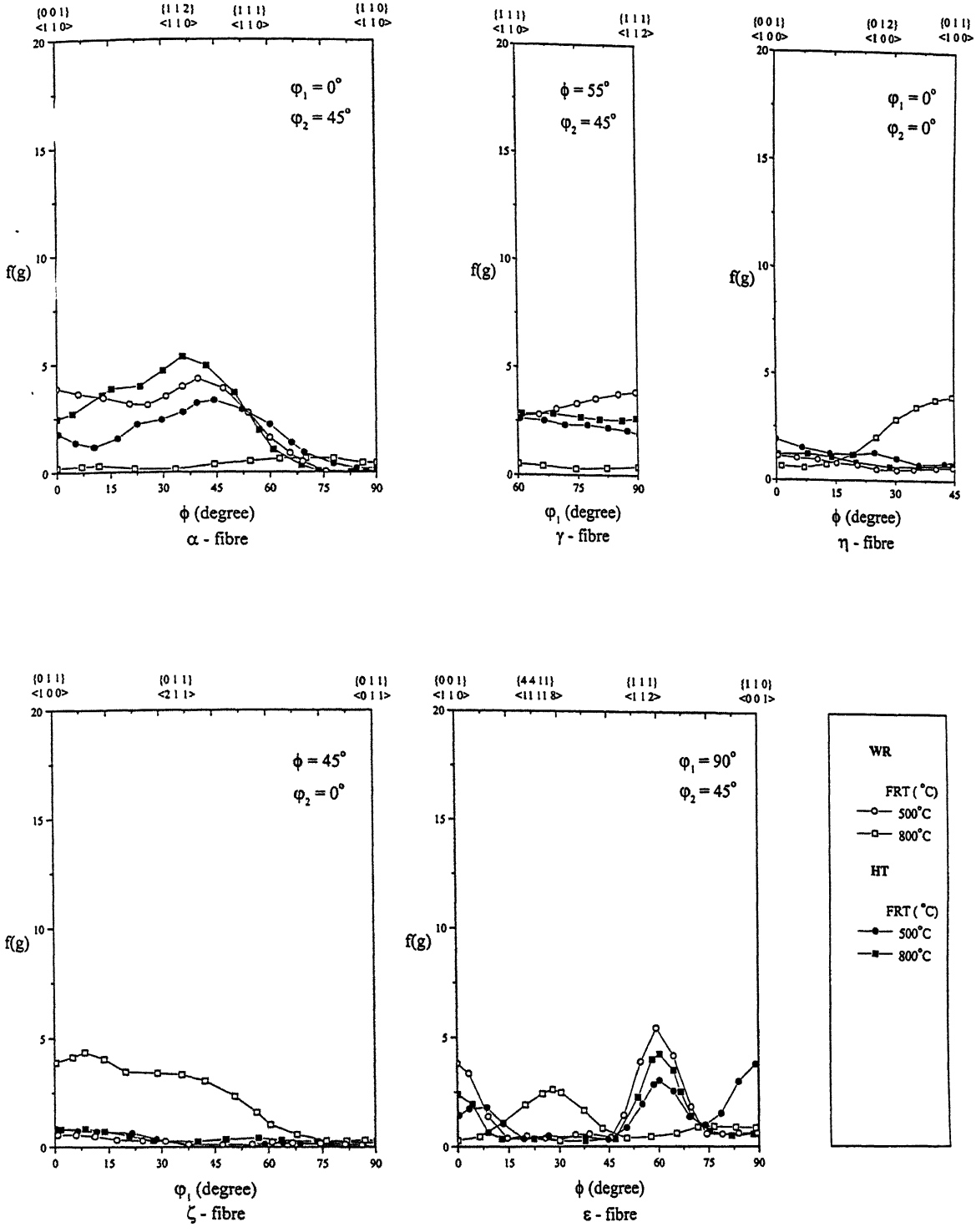

Figure 4.48 : Fibre plots for steel 2 after multipass rolling under schedule 1 (WR) and annealing (HT).

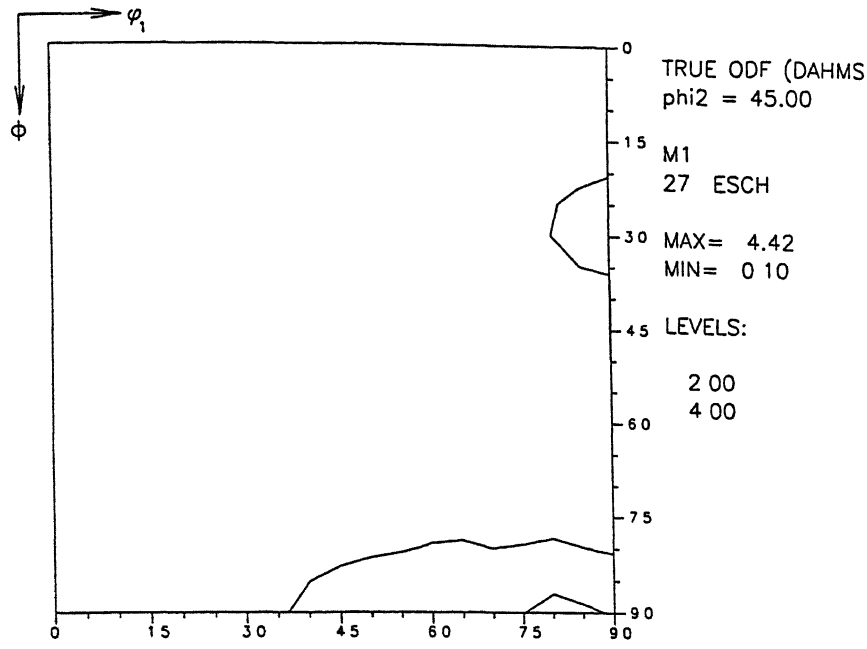

(a). FRT: 800 ^{O}C

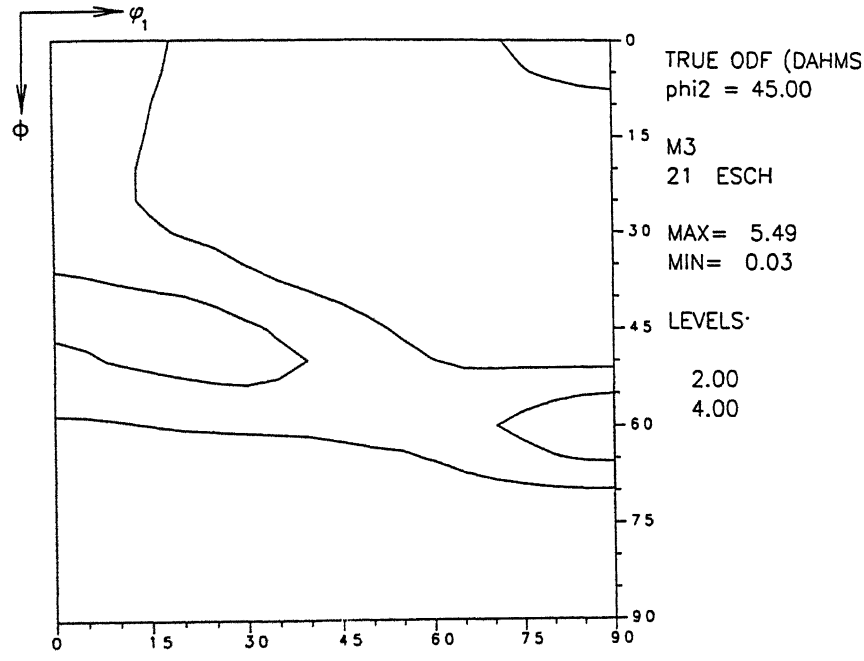

(b). FRT: 500 ^{O}C

Figure 4.49 (a) and (b) : $\varphi_2 = 45^{O}$ sections plots for steel 2 after multipass rolling under schedule 1.

Heat treatment of the 800 ^{o}C FRT sample changes its texture completely. The ODF of this material [Fig. 4.47(c)] clearly shows the presence of a moderately strong γ fibre, which was totally absent in the corresponding warm rolled sample. On the other hand, heat treatment of 500 ^{o}C FRT material leads to a weaker γ fibre as compared to the corresponding warm rolled material [Fig. 4.47 (d)]. The fibre texture plots [Fig. 4.48] show a non-uniform α fibre in both the warm rolled materials, the fibre in the 800 ^{o}C FRT sample being perceptibly stronger than in the 500 ^{o}C FRT sample. The γ fibre is reasonably uniform but weak in both the samples. For both of them intensities at the cube and rotated cube positions are rather low. The $\varphi_2 = 45^{o}$ section plots [Fig. 4.49 (c) and (d)] seem to corroborate the above findings.

(b) Schedule 2

The ODFs of the warm rolled samples of schedule2, which were finish rolled at 800 ^{o}C and 500 ^{o}C [Fig. 4.50 (a) and (b)], look practically the same, having similar texture intensities. Both the samples show a moderate non-uniform α fibre and a moderate γ [Fig. 4.51]. The other fibres also have a similar appearance in the two materials. The $\varphi_2 = 45^{o}$ section plots of the two warm rolled materials [Fig 4.52(a) and (b)] also show the presence of moderately strong to weak γ and α fibres in both of them.

Heat treatment leads to a sharpening of the ODF of the 800 ^{o}C FRT sample [Fig. 4.50 (c)]. For the 500 ^{o}C FRT material, however, the sharpening of the ODF has been only marginal [Fig. 4.50 (d)]. The fibre plots [Fig. 4.51] indicate only a slight improvement in the intensity of the γ fibre in the 800 ^{o}C FRT material and just a slight decrease in the γ

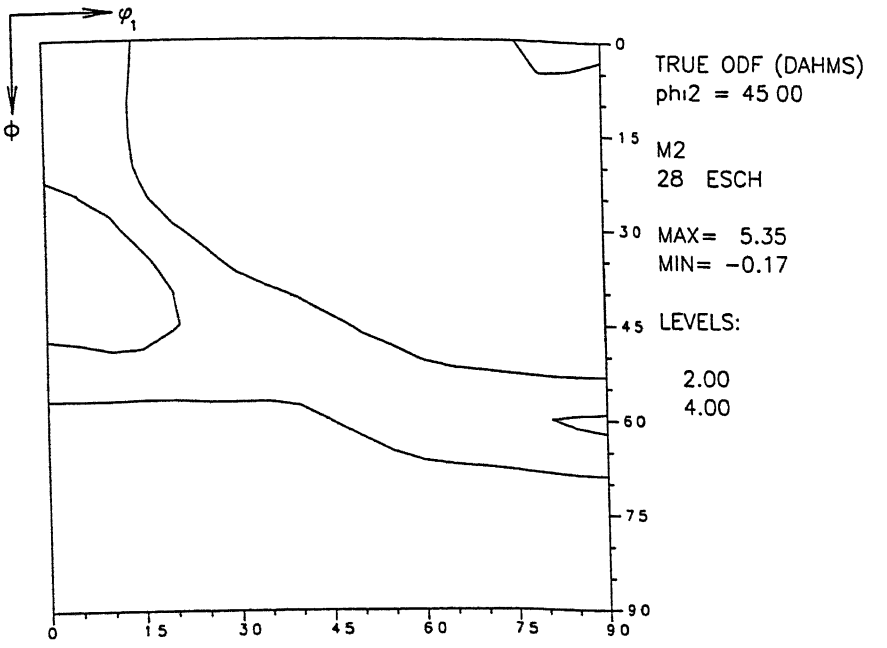

(c). FRT: 800 ^{O}C

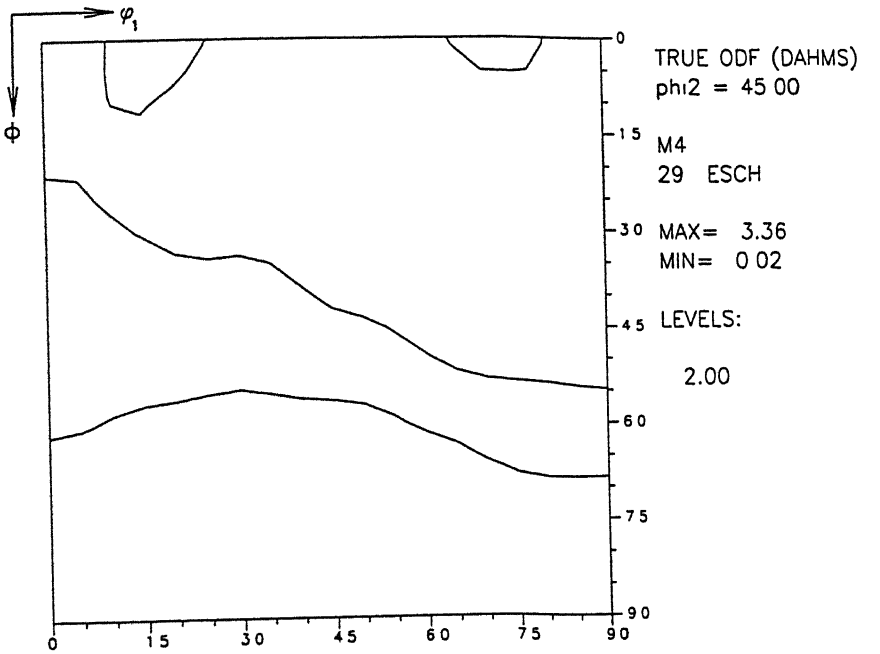

(d). FRT: 500 ^{O}C

Figure 4.49 (c) and (d) : $\varphi_2 = 45^{O}$ sections plots for steel 2 after multipass rolling under schedule 1 and annealing.

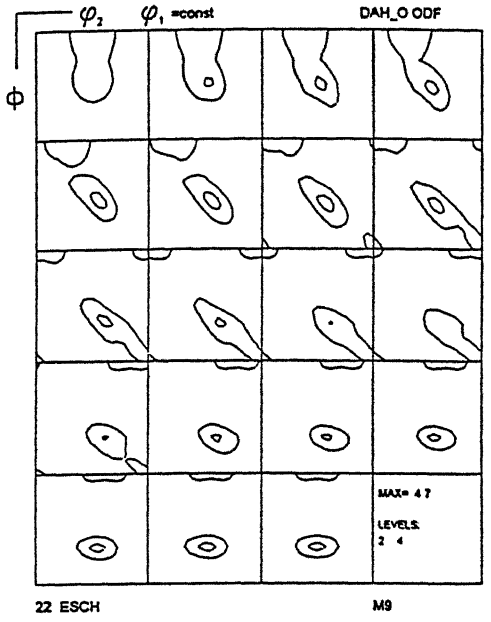

(a) FRT : 800 °C

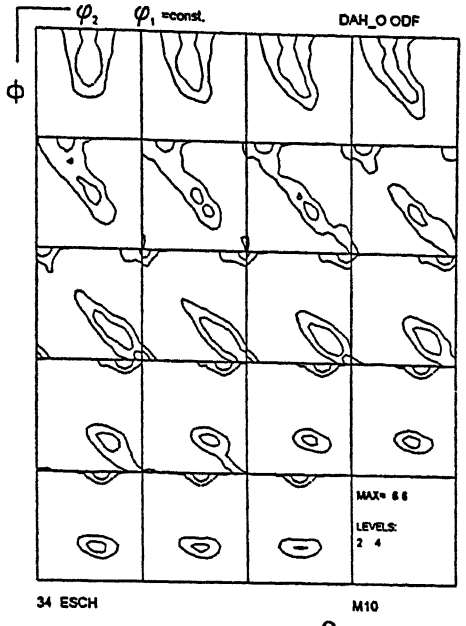

(c) FRT : 800 °C

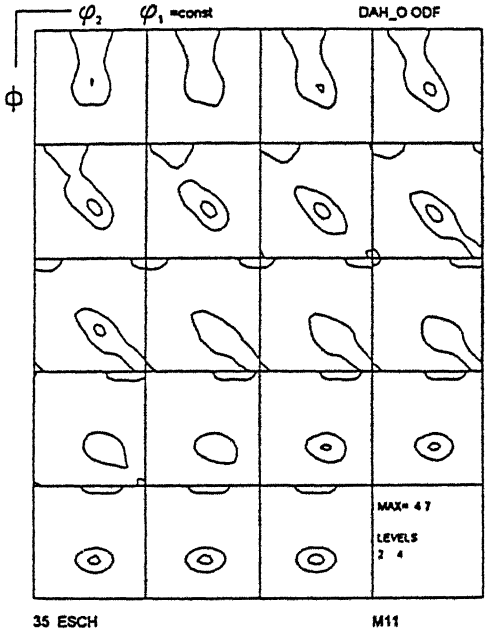

(b) FRT : 500 °C

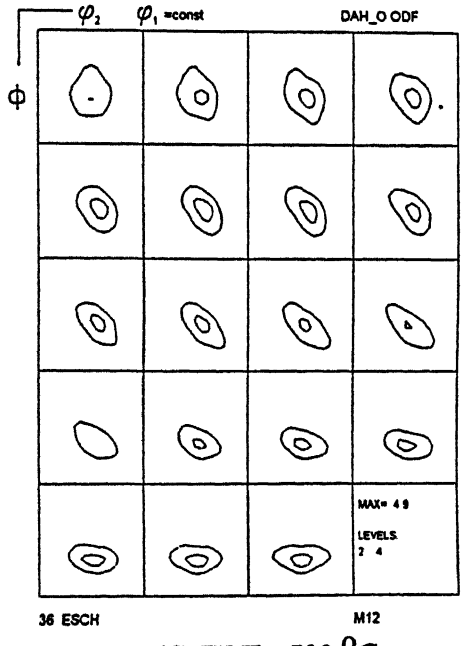

(d) FRT : 500 °C

Figure 4.50 (a) - (d) : ODF plots (φ_1 sections) for steel 2 after multipass rolling under schedule 2 [(a) and (b)] and annealing [(c) and (d)].

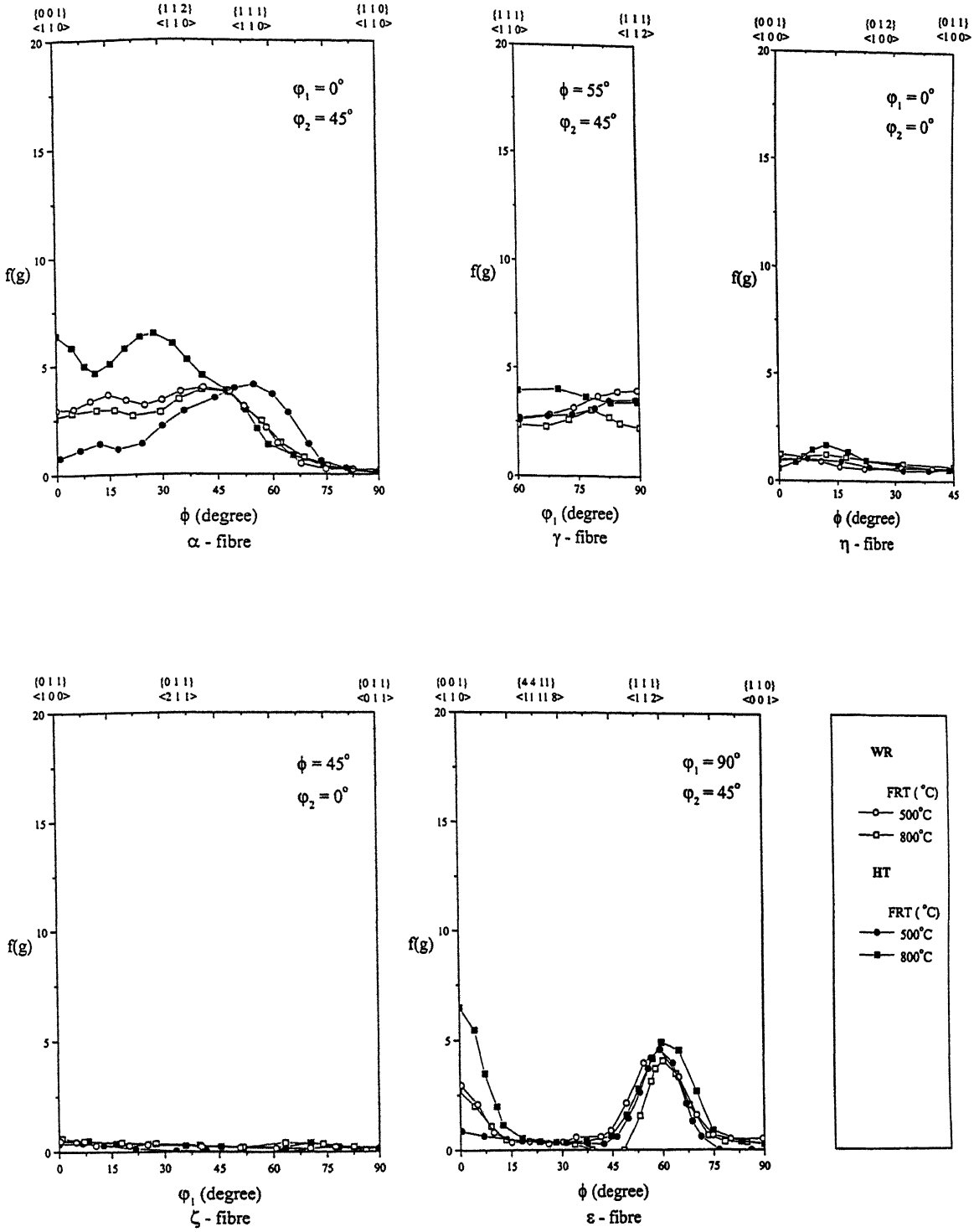

Figure 4.51 : Fibre plots for steel 2 after multipass rolling under schedule 2 (WR) and annealing (HT).

fibre intensity of the 500 ^{o}C FRT sample. Heat treatment also leads to an increase in the intensity of the α fibre of the 800 ^{o}C FRT sample, and a decrease in the intensity of the same fibre in the 500 ^{o}C FRT sample. Heat treatment also leads to an increment in the intensity at the {001}<110> location for the 800 ^{o}C FRT sample. The $\varphi_2 = 45^{o}$ section plots for the heat treated samples [Fig. 4.52 (c) and (d)] show the presence of a moderate γ fibre and α fibre as well as a texture peak at the rotated cube position for the 800 ^{o}C FRT sample; on the other hand, the 500 ^{0}C FRT material shows only a moderate γ fibre.

(c) Schedule 3

The ODFs of the two warm rolled samples of schedule 3 are displayed in Figures 4.53 (a) and (b). Both the ODFs show the clear presence of the γ fibre. The fibre plots [Fig. 4.54] show non-uniform α fibres in both the samples, however, the intensity of the α fibre is nearly twice as strong in the 800 ^{o}C FRT sample than in the 500 ^{o}C FRT material. The nearly uniform and moderately strong γ fibre is also sharper in the former than in the latter. In addition, the 800 ^{o}C FRT sample also shows a higher intensity in the rotated cube position than the 500 ^{o}C FRT sample. The findings are also corroborated by the plots of the $\varphi_2 = 45^{o}$ sections for both the materials [Fig. 4.55 (a) and (b)].

Heat treatment of the above two warm rolled materials leads to significant changes in their textures. The ODFs of the 800 ^{o}C FRT and HT sample and the 500 ^{o}C FRT and HT sample are displayed in Figures 4.53 (c) and (d) respectively. Both these ODFs show the presence of a strong γ fibre. The fibre plots [Fig. 4.54] show the presence of reasonably strong α and γ fibres in both the materials, the fibres being stronger in intensity in the 800

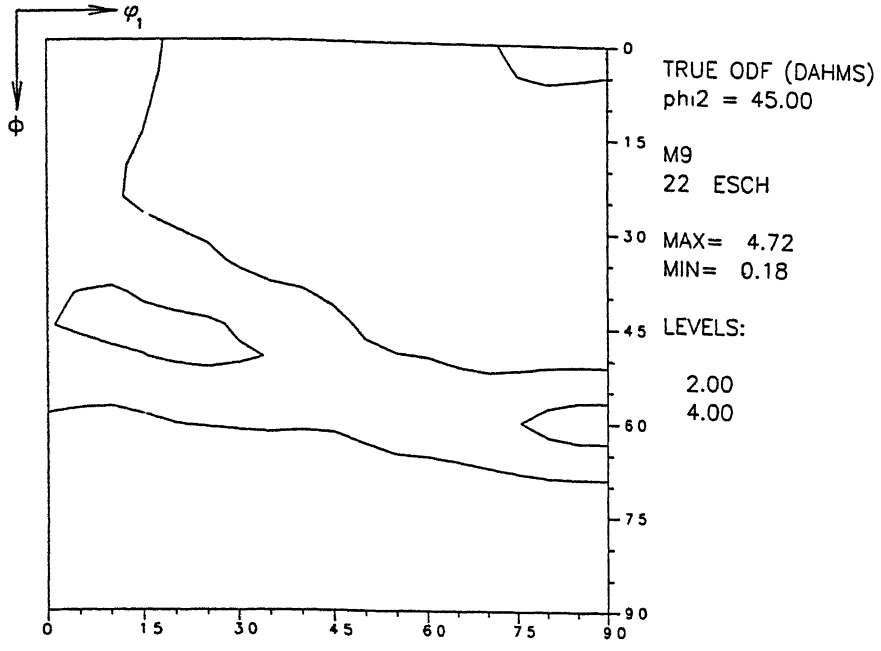

(a). FRT: 800 ^{O}C

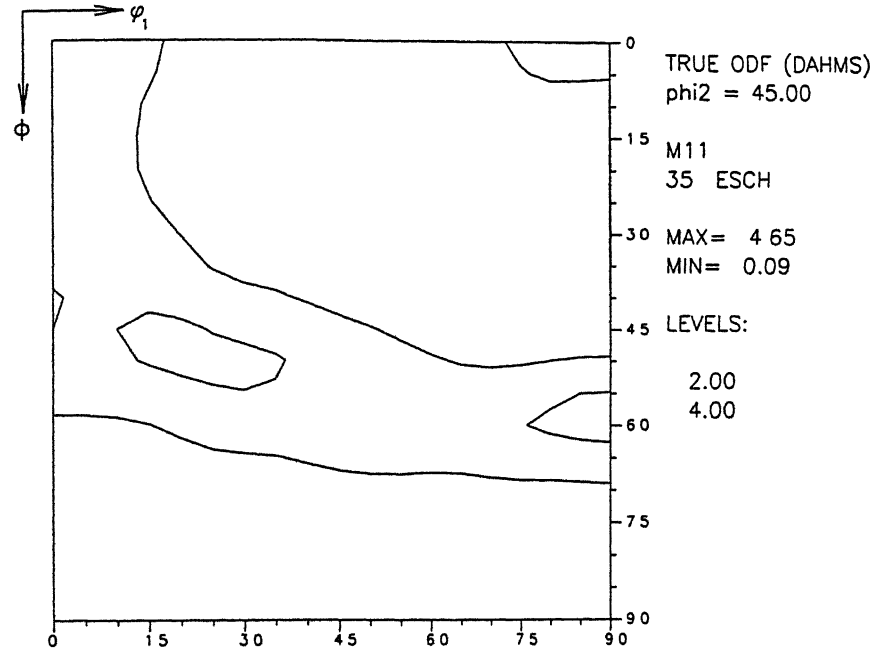

(b). FRT: 500 ^{O}C

Figure 4.52 (a) and (b) : $\varphi_2 = 45^{O}$ sections plots for steel 2 after multipass rolling under schedule 2.

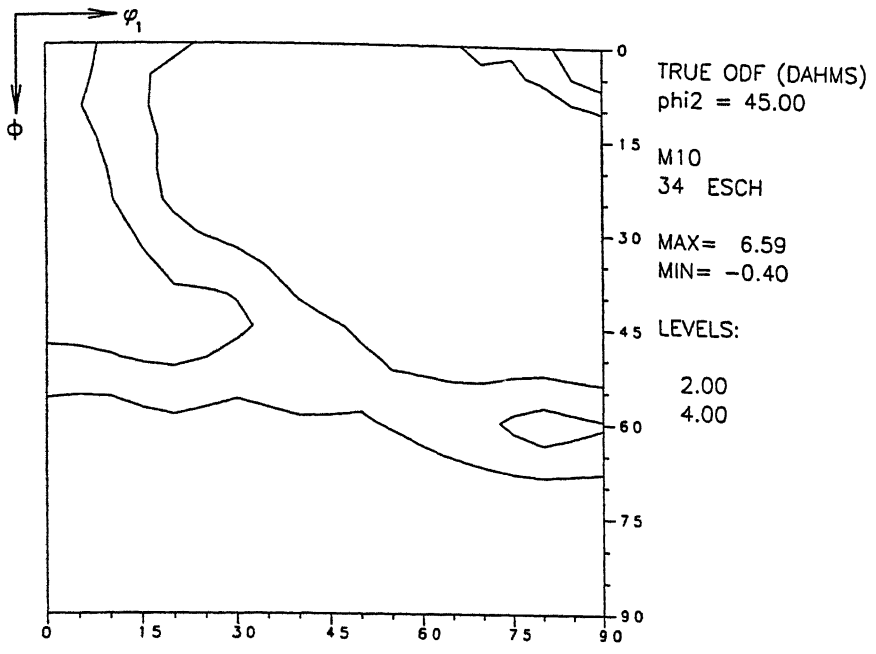

(c). FRT: 800 ^{O}C

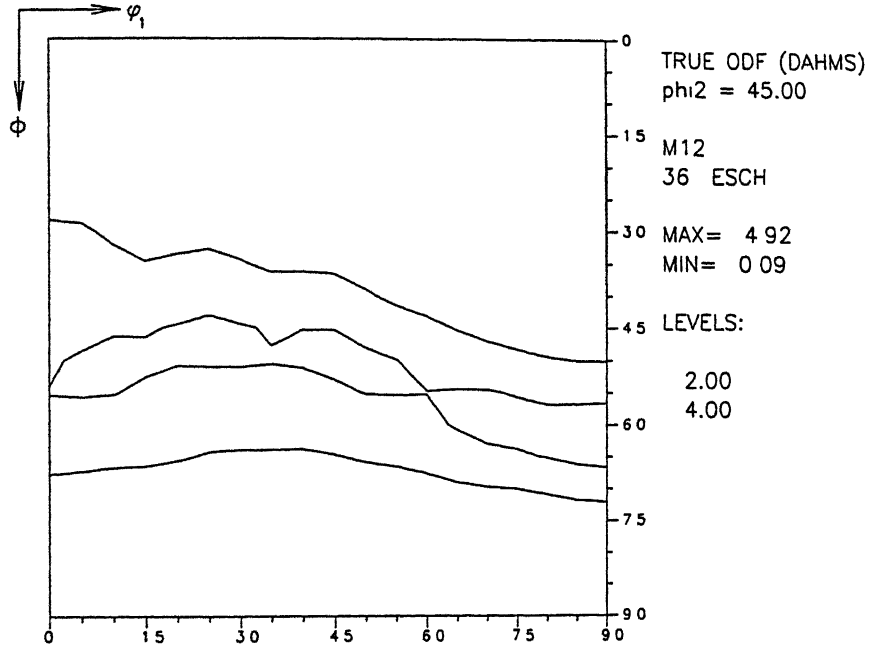

(d). FRT: 500 ^{O}C

Figure 4.52 (c) and (d) : $\varphi_2 = 45^{O}$ sections plots for steel 2 after multipass rolling under schedule 2 and annealing.

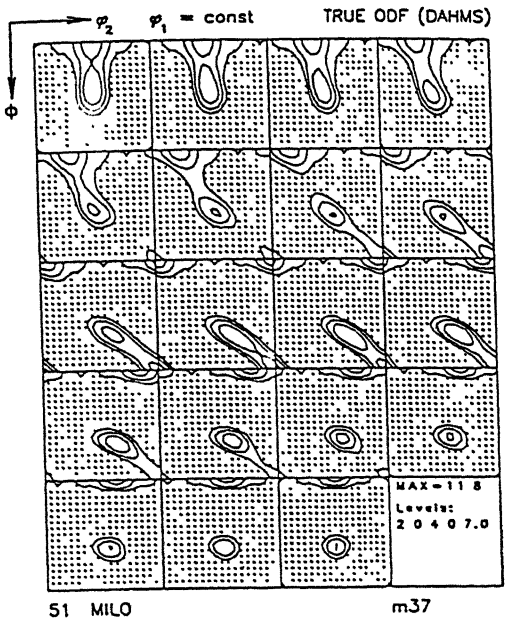

(a) FRT : 800 °C

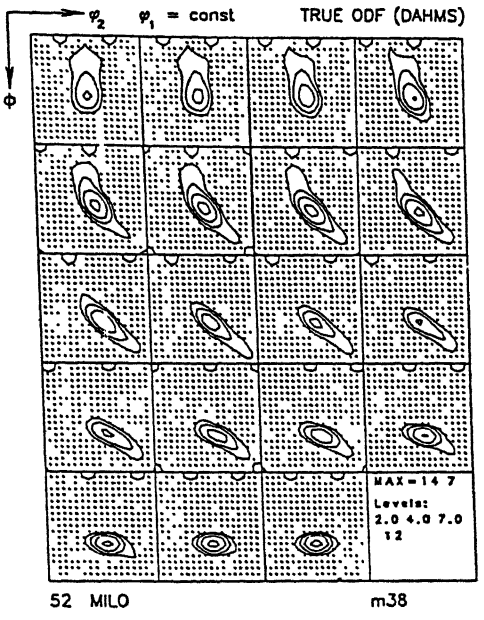

(c) FRT : 800 °C

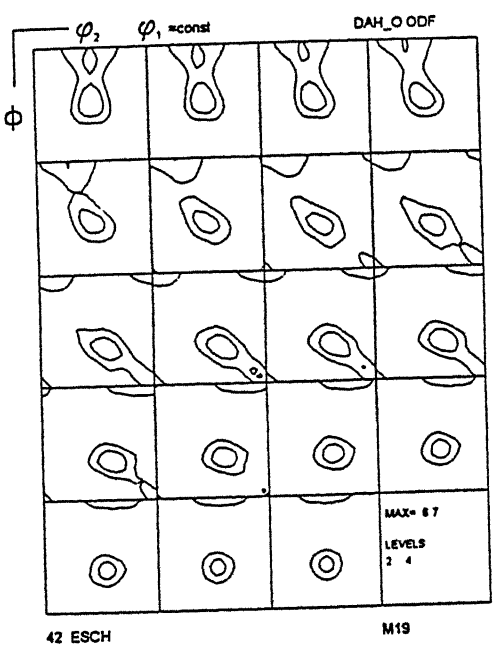

(b) FRT : 500 °C

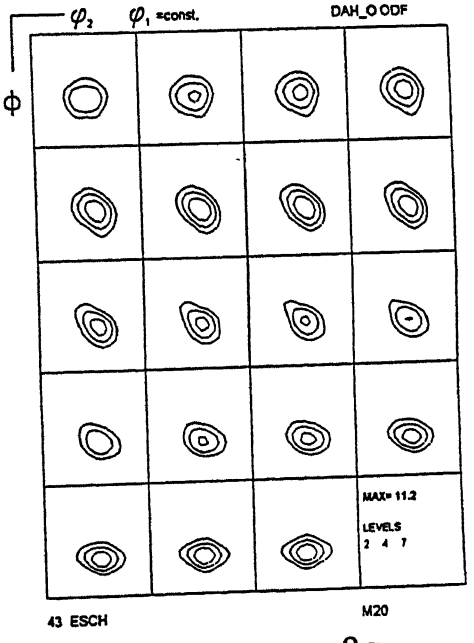

(d) FRT : 500 °C

Figure 4.53 (a) - (d) : ODF plots (φ_1 sections) for steel 2 after multipass rolling under schedule 3 [(a) and (b)] and annealing [(c) and (d)].

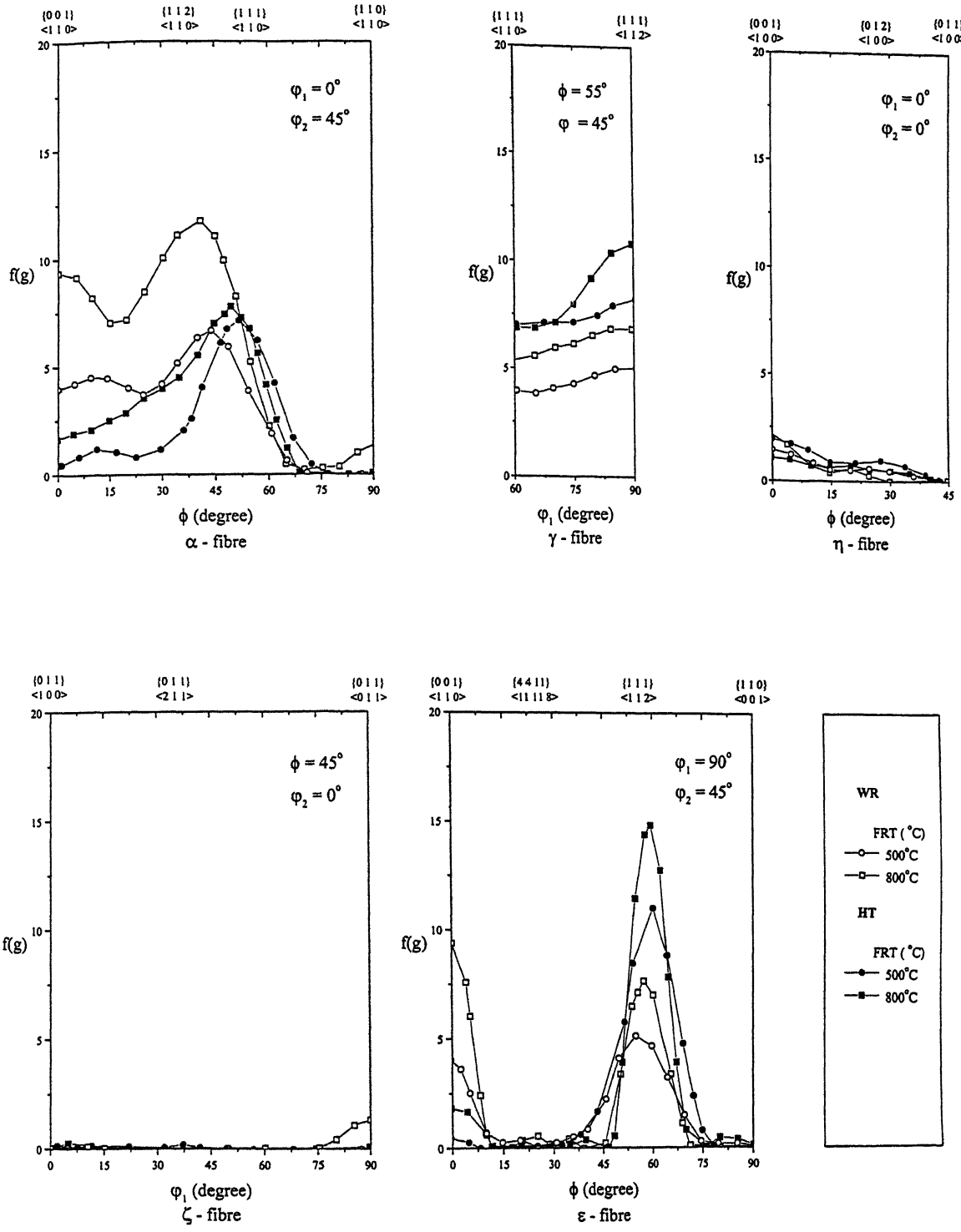

Figure 4.54 : Fibre plots for steel 2 after multipass rolling under schedule 3 (WR) and annealing (HT).

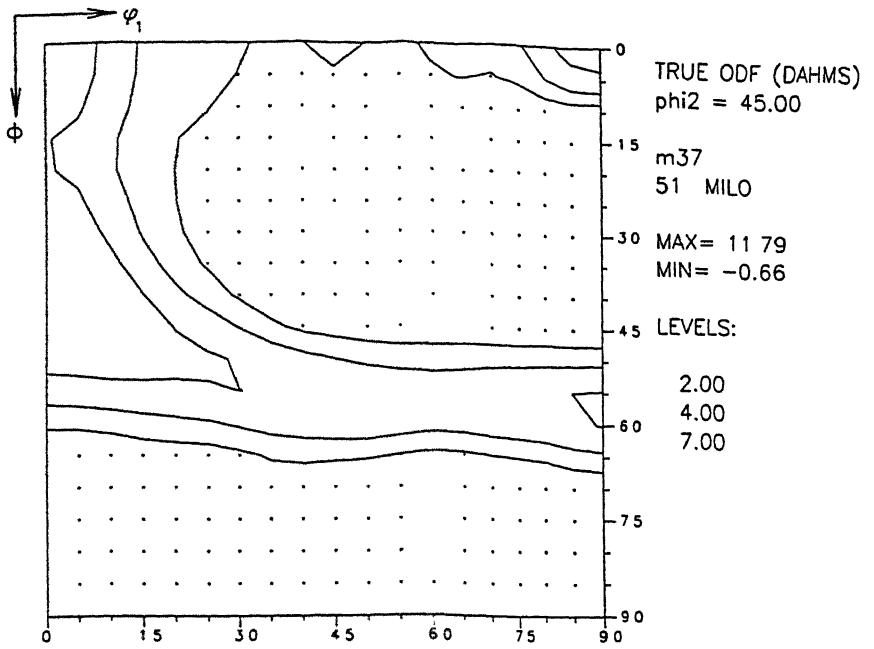

(a). FRT: 800 ^{O}C

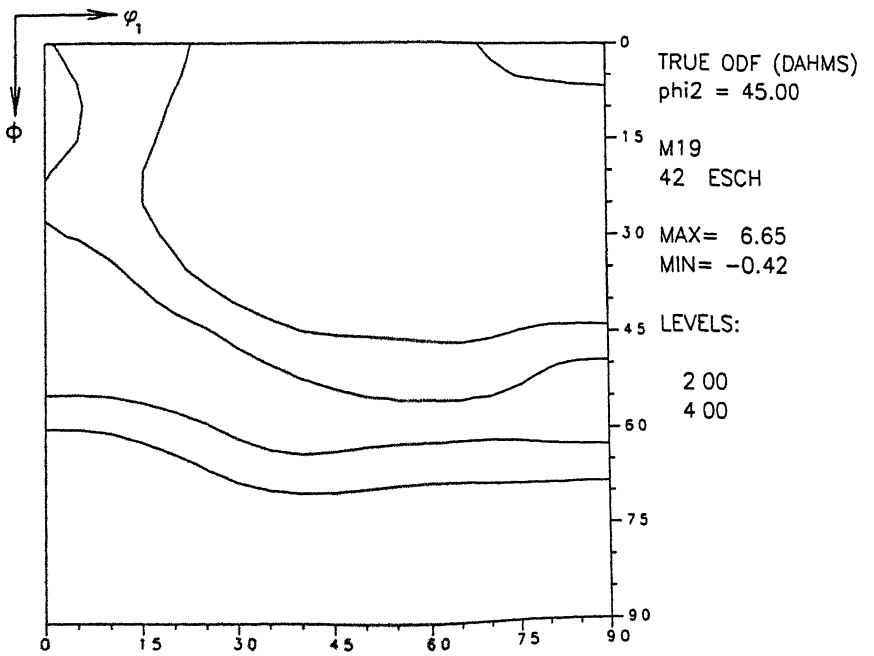

(b). FRT: 500 ^{O}C

Figure 4.55 (a) and (b) : $\varphi_2 = 45^{O}$ sections plots for steel 2 after multipass rolling under schedule 3.

^{O}C FRT sample. For both, the peak of the α fibre appears at {111}<110>. The γ fibre in both the samples shows a higher intensity in the {111}<112> than in the {111}<110> location. Heat treatment also significantly brings down the intensity at the rotated cube {001}<110> position, as compared to the warm rolled materials. Reasonably strong γ fibres are also found in the $\varphi_2 = 45^{O}$ section plots of the above two samples [Fig. 4.55 (c) and (d)].

4.5.3 Steel 3

4.5.3.1 Single pass rolling after soaking at 1150 ^{O}C

(a) Warm rolling textures

The ODFs of samples single pass rolled after soaking at 1150 ^{O}C are displayed in Figures 4.56(a) to(d). All the four ODFs appear very similar in nature; the overall texture intensity, however, increases with the decrease in FRT. Thus, f(g) max = 6.3 for the 800 ^{O}C FRT sample, while it is equal to 10.5 for the 500 ^{O}C FRT sample. The presence of a reasonably strong γ fibre is clearly discernible in all these ODFs.

The five fibre plots [Fig 4.57] again clearly show that the γ fibre is indeed quite strong in all the four materials, the 500 ^{O}C FRT sample showing the strongest γ fibre and the 800 ^{O}C FRT sample showing the weakest γ fibre among all. All these four samples also show non-uniform but strong α fibres. Excepting the 800 ^{O}C FRT sample, all the others show two maxima for the α fibre – one at the rotated cube {001}<110> location and the other one at ~ {111}<110> position. The α fibre of the 800 ^{O}C FRT sample shows a single peak at near {111}<110>. The ε fibre plot clearly shows that all four samples have

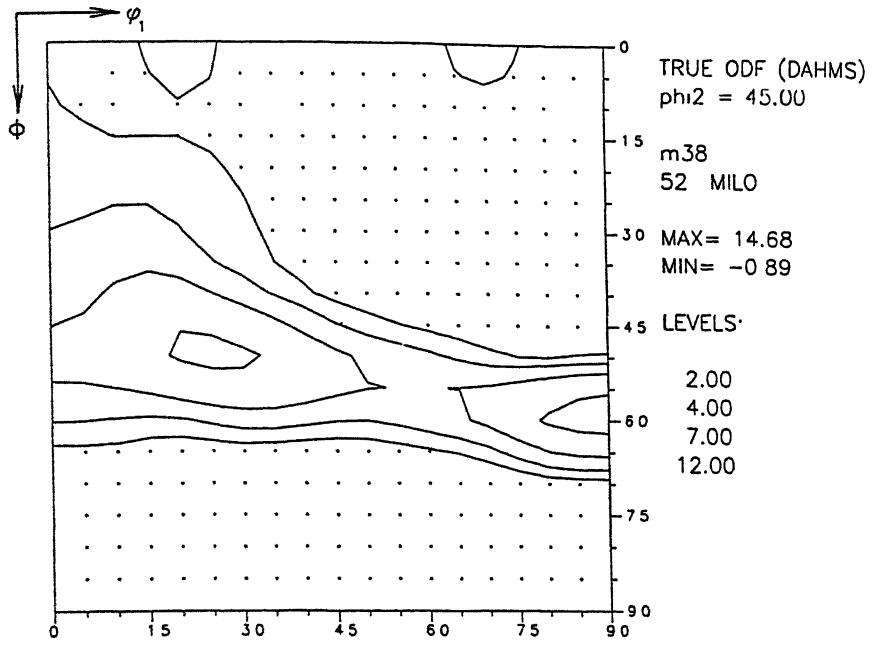

(c). FRT: 800 ^{O}C

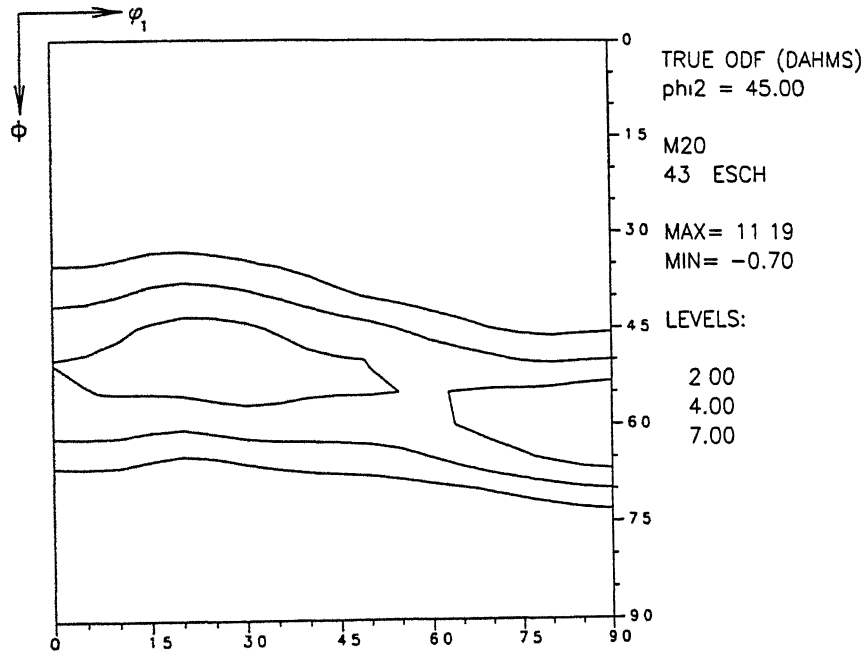

(d). FRT: 500 ^{O}C

Figure 4.55 (c) and (d) : $\varphi_2 = 45^{O}$ sections plots for steel 2 after multipass rolling under schedule 3 and annealing.

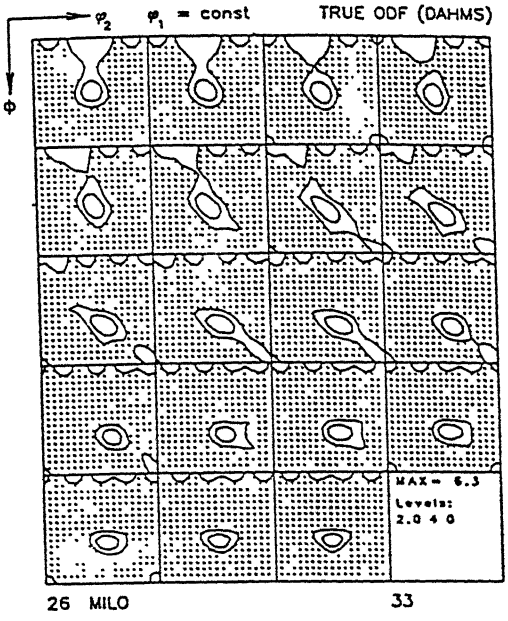

(a) FRT : 800 ^{O}C

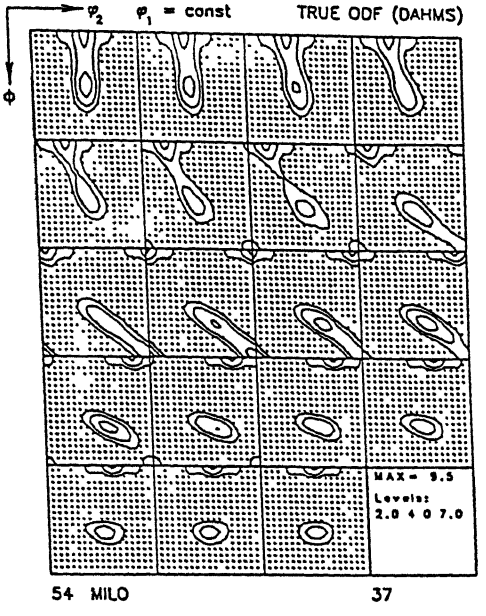

(c) FRT : 600 ^{O}C

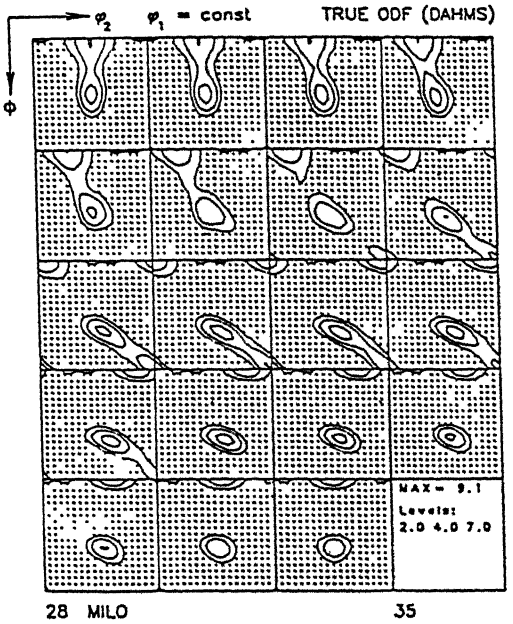

(b) FRT : 700 ^{O}C

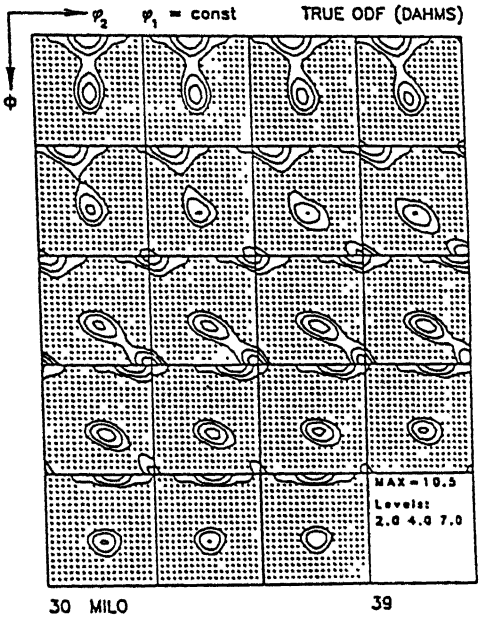

(d) FRT : 500 ^{O}C

Figure 4.56 (a) - (d) : ODF plots (φ_1 sections) for steel 3 after single pass rolling (after soaking at 1150 ^{O}C).

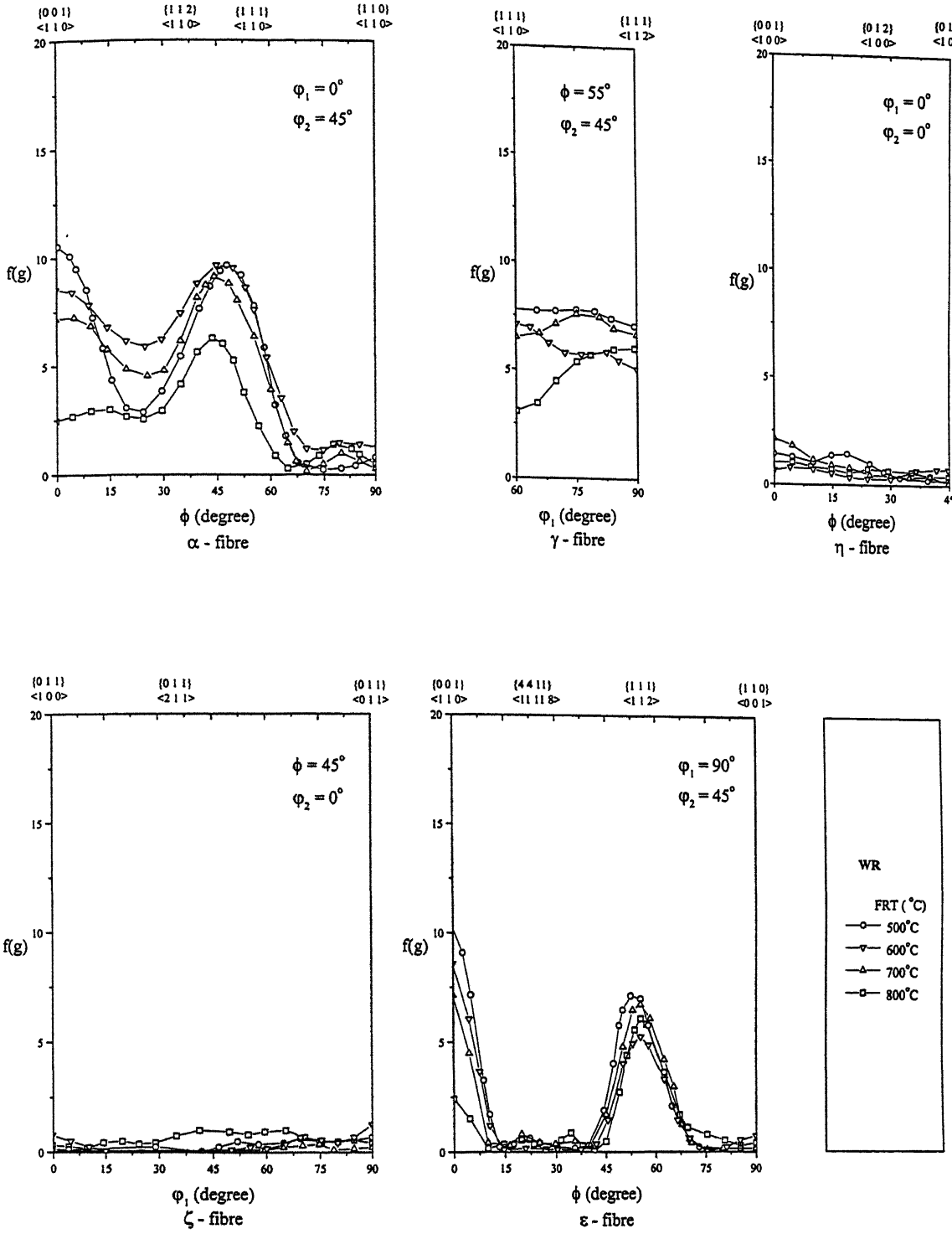

Figure 4.57 : Fibre plots for steel 3 after warm rolling (WR) in single pass (after soaking at 1150 °C).

reasonably strong intensities at the {111}<112> location. Excepting the 800 ^{o}C FRT sample, all the other three also show sharp intensities at the rotated cube {001}<110> location.

All the above findings are also corroborated by the $\phi_2 = 45^{o}$ section plots [Fig. 4.58(a) to (d)].

(b) Textures after heat treatment

Heat treatment appears to sharpen the textures of the warm rolled materials. Figures 4.59(a) to (d) display the ODFs of the four warm rolled samples after heat treatment. The ODF of the 800 ^{o}C FRT sample shows the presence of a moderately strong γ fibre, in addition to some other components. By contrast, the textures of all three other samples show the presence primarilyof the γ fibre alone. An increase in intensity of the overall texture with the lowering of the warm rolling temperature is also discernible.

The fibre plots presented in Figure 4.60 clearly show that the γ fibre is quite strong in all the four samples; it is the strongest in the 500 ^{o}C FRT sample and the weakest in the 800 ^{o}C FRT material. In general, the γ fibre intensity shows a higher value at the {111}<112> location and a lower value at the {111}<110> position. The α fibre has a moderately strong intensity from {001}<110 > through {112}<110> to {111}<110> in the 800 ^{o}C FRT sample. The α fibres in all the other three samples show peak values only at {111}<110> location and rather low intensities at other positions along the fibre. While heat treatment has led to a sharpening of the intensity at the rotated cube position

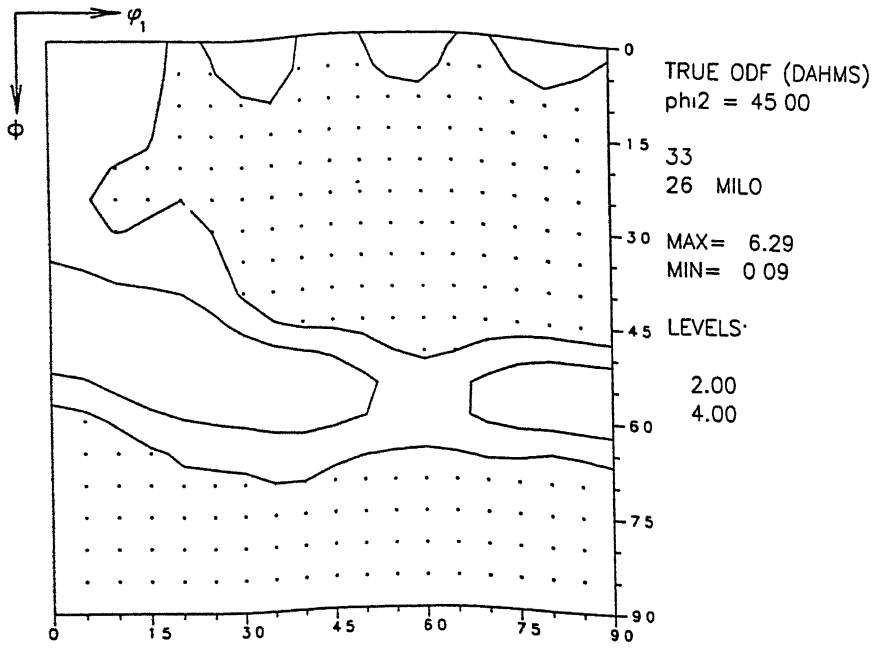

(a). FRT: 800 ^{O}C

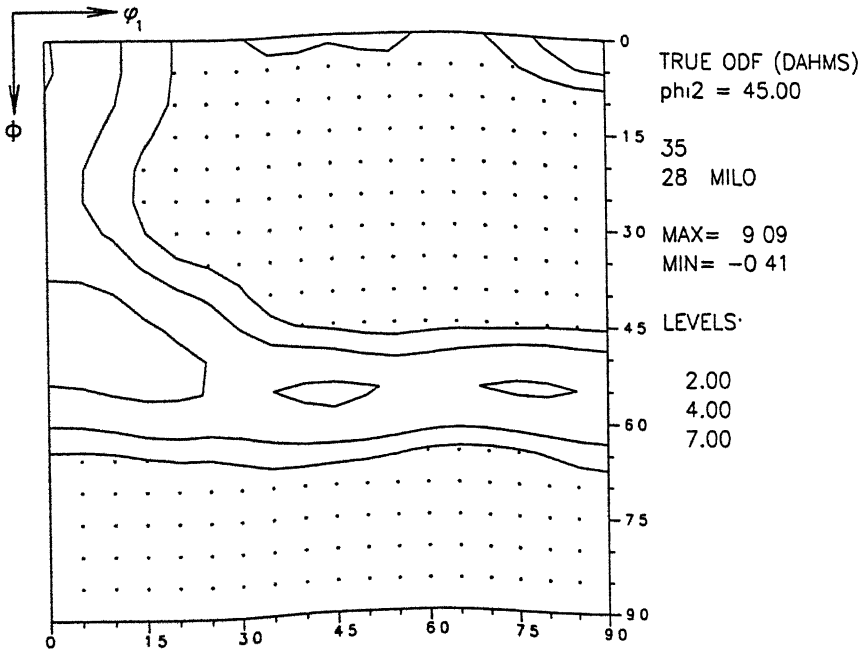

(b). FRT: 700 ^{O}C

Figure 4.58 (a) and (b) : $\varphi_2 = 45^{O}$ sections plots for steel 3 after single pass rolling (after soaking at 1150 ^{O}C).

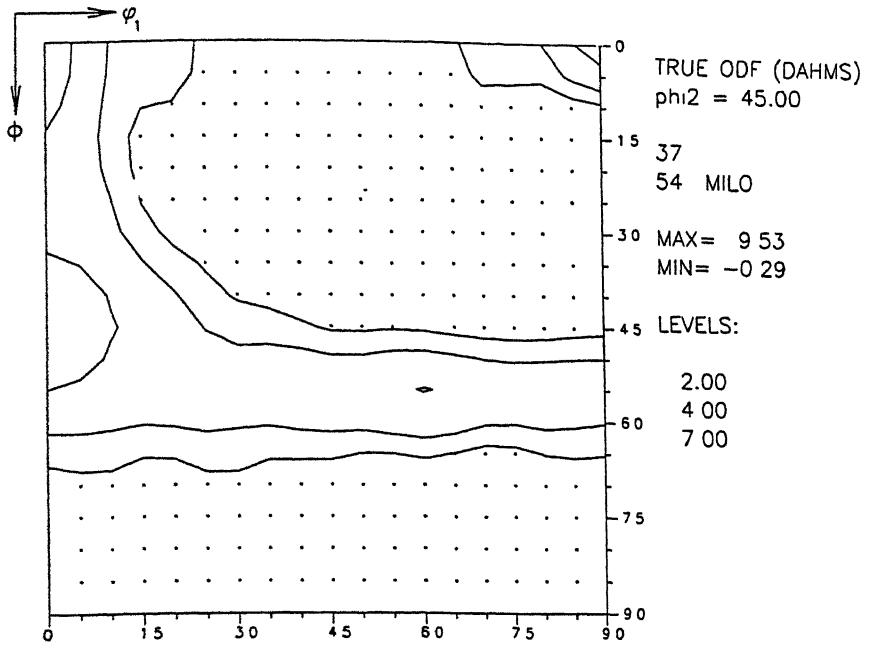

(c). FRT: 600 ^{O}C

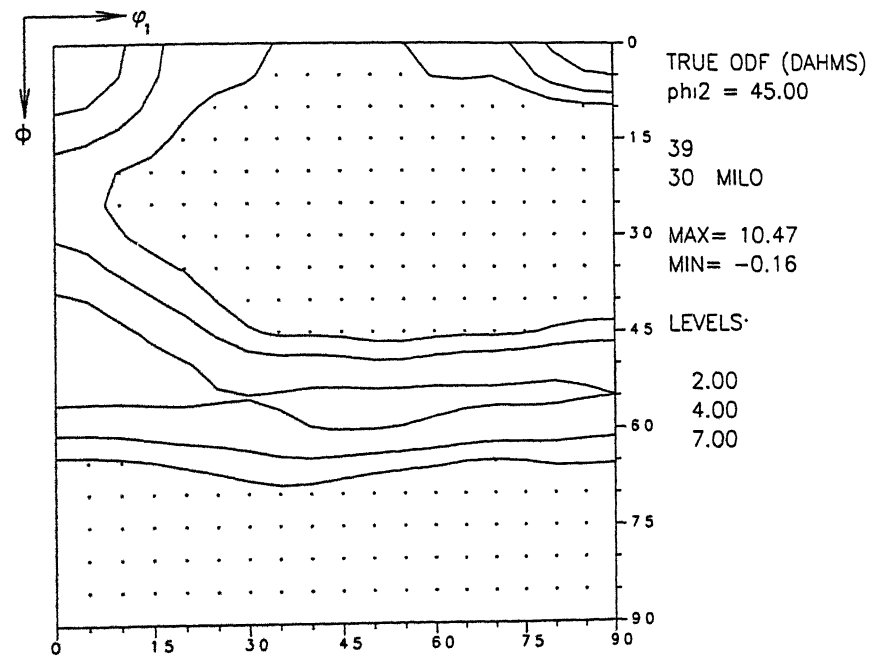

(d). FRT: 500 ^{O}C

Figure 4.58 (c) and (d) : $\varphi_2 = 45^{O}$ sections plots for steel 3 after single pass rolling (after soaking at 1150 ^{O}C).

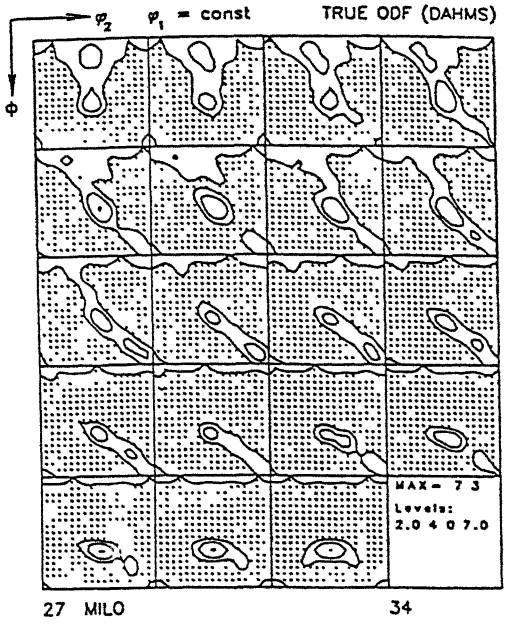

(a) FRT : 800 °C

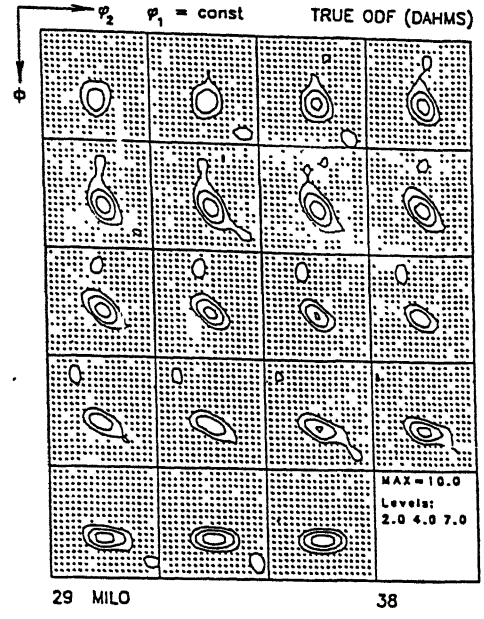

(c) FRT : 600 °C

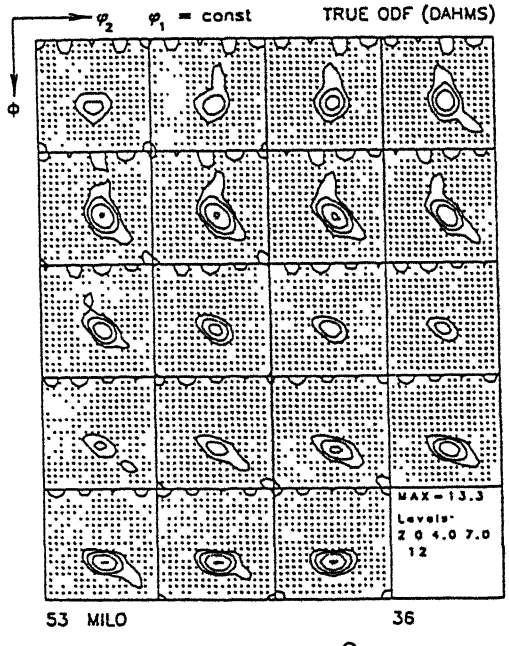

(b) FRT : 700 °C

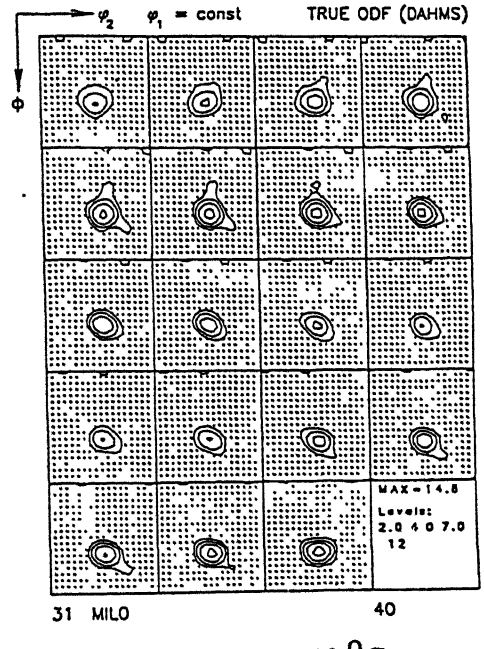

(d) FRT : 500 °C

Figure 4.59 (a) - (d) : ODF plots (φ_1 sections) for steel 3 after single pass rolling (after soaking at 1150 °C) and annealing.

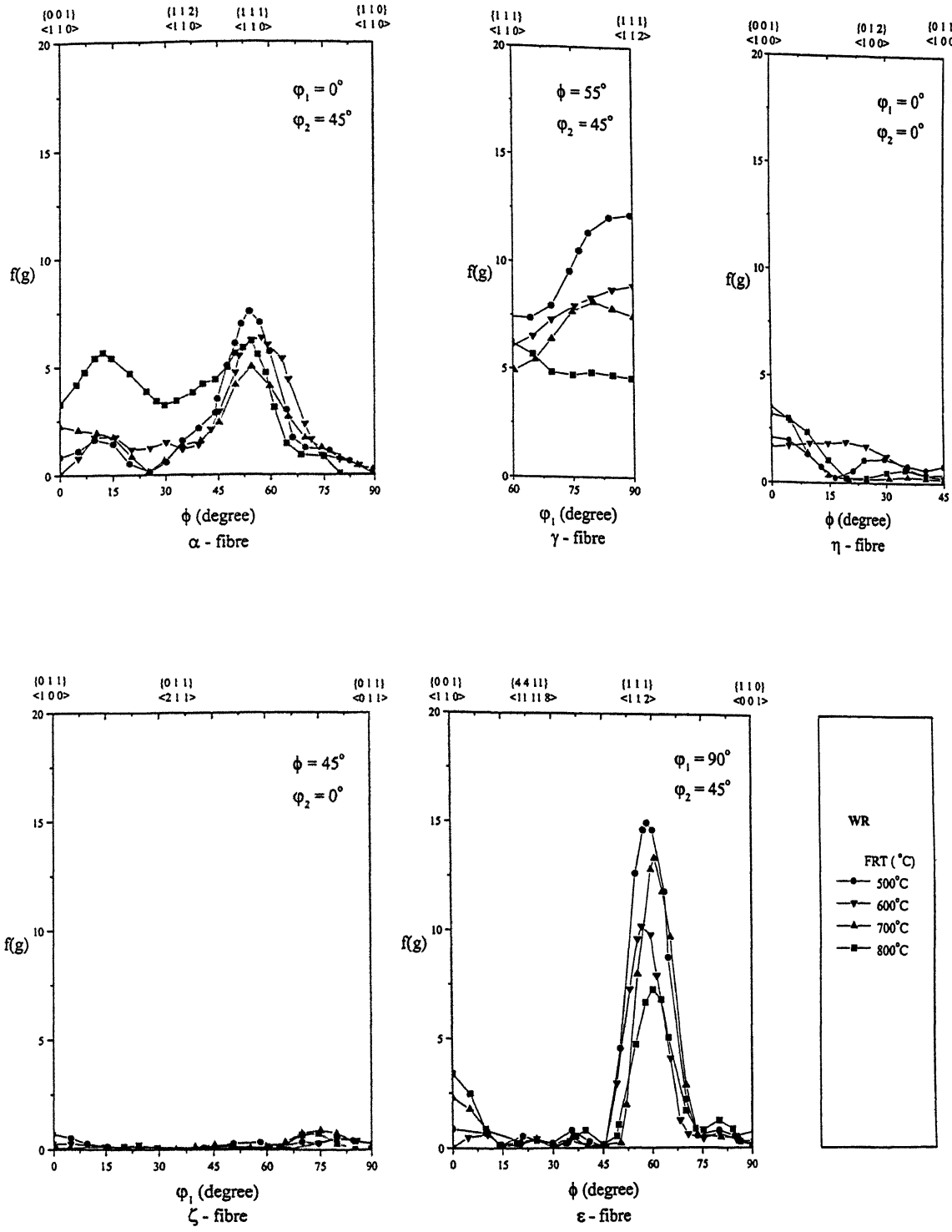

Figure 4.60 : Fibre plots for steel 3 after warm rolling in single pass (after soaking at 1150 °C) and annealing (HT).

{001}<110> in case of the 800 ^{O}C FRT sample, the intensities at this location in fact decreased for other three samples after heat treatment.

The φ_2 = 45^{O} section plots [Figs 4.61(a) to (d)] show clearly that while a moderately strong γ fibre and a weak α fibre are present in the texture of the 800 ^{O}C FRT sample, the textures of the other three samples exhibit reasonably strong γ fibre only.

4.5.3.2 Single pass rolling after soaking at 830 ^{O}C

(a) Warm rolling textures

Figures 4.62 (a) and (b) represent the ODFs of single pass rolled 800 ^{O}C FRT and 500 ^{O}C FRT materials, respectively, after soaking at 830 ^{O}C. These two ODFs show quite a bit of similarity, although the overall intensity of the former is slightly more than that of the latter.

The fibre plots of the above two samples [Fig.4.63] clearly indicate the presence of nearly uniform γ fibres in both. A prominent non-uniform but strong α fibre is present in the texture of the 800 ^{O}C FRT material, having two peaks located at {001}<110> and ~{223}<110> positions. On the other hand, the α fibre in the 500 ^{O}C FRT sample shows a single but strong peak at {111}<110> location. The ε fibre plots show strong peaks at the {111}<112> position for both the samples. Again, the 800 ^{O}C FRT sample shows a rather high value at the rotated cube {001}<110> location, while this component is nearly half in intensity in the 500 ^{O}C FRT material. The $\varphi_2 = 45^{O}$ section plots of the above two samples are displayed in Figures 4.64 (a) and (b) respectively. Both these figures show the presence

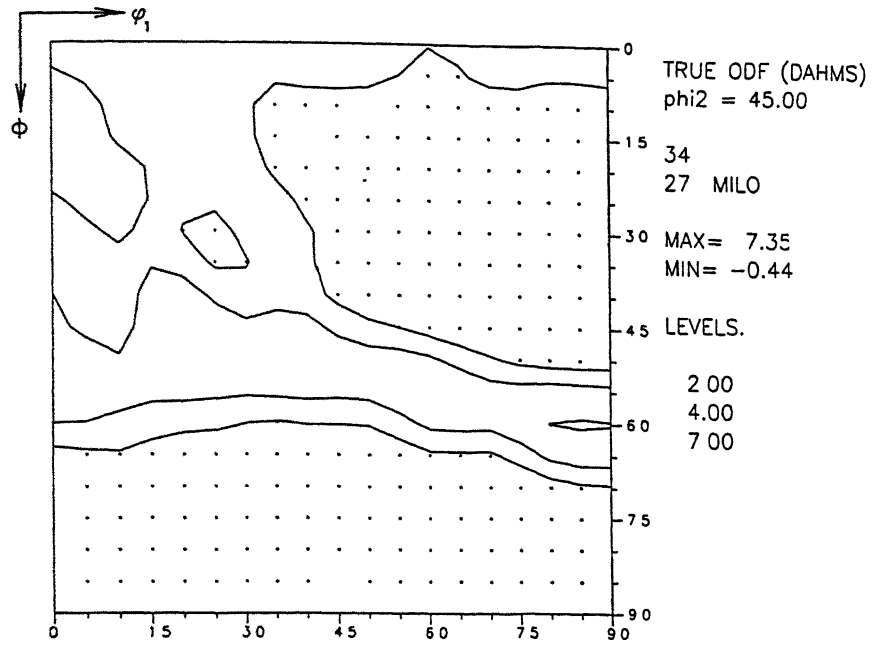

(a). FRT: 800 ^{O}C

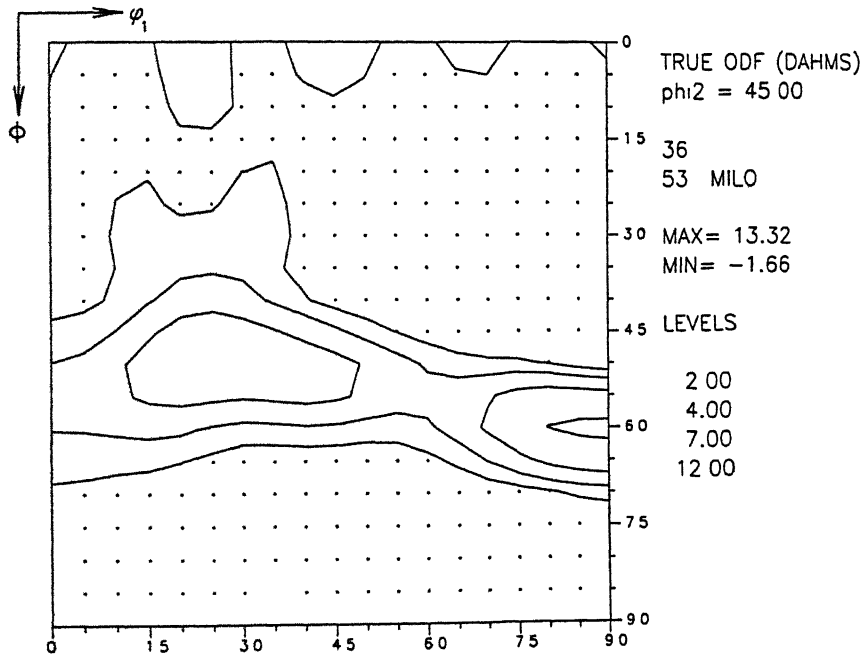

(b). FRT: 700 ^{O}C

Figure 4.61 (a) and (b) : $\varphi_2 = 45^{O}$ sections plots for steel 3 after single pass rolling (after soaking at 1150 ^{O}C) and annealing.

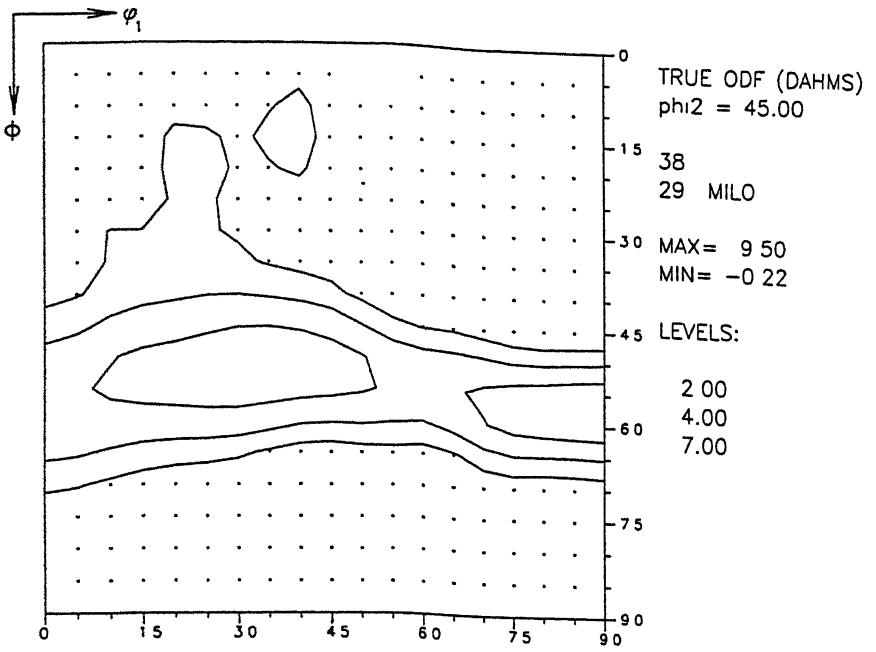

(c). FRT: 600 ^{O}C

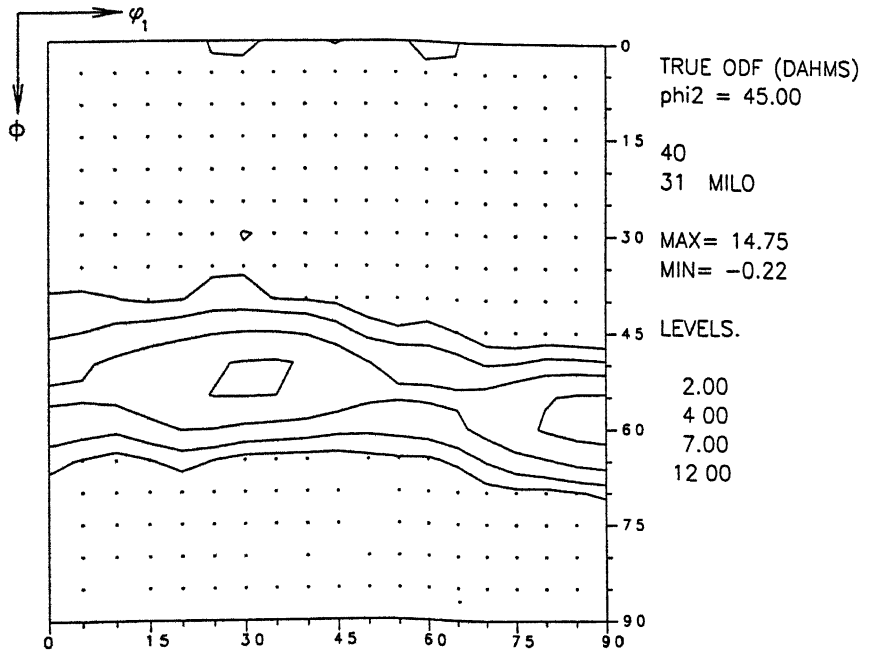

(d). FRT: 500 ^{O}C

Figure 4.61 (c) and (d) : $\varphi_2 = 45^{O}$ sections plots for steel 3 after single pass rolling (after soaking at 1150 ^{O}C) and annealing.

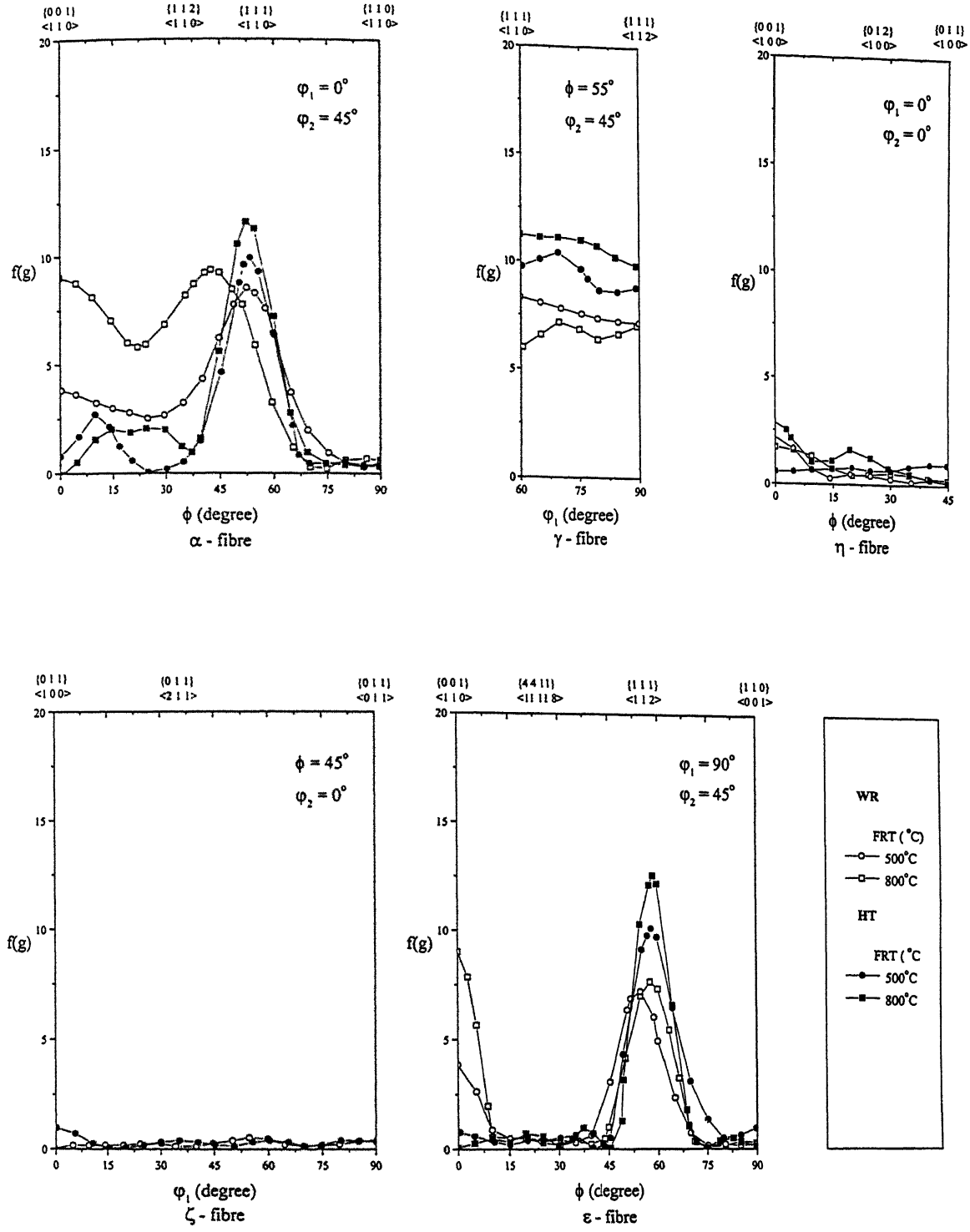

Figure 4.63 : Fibre plots for steel 3 after single pass rolling (after soaking at 830 °C) [WR] and annealing [HT].

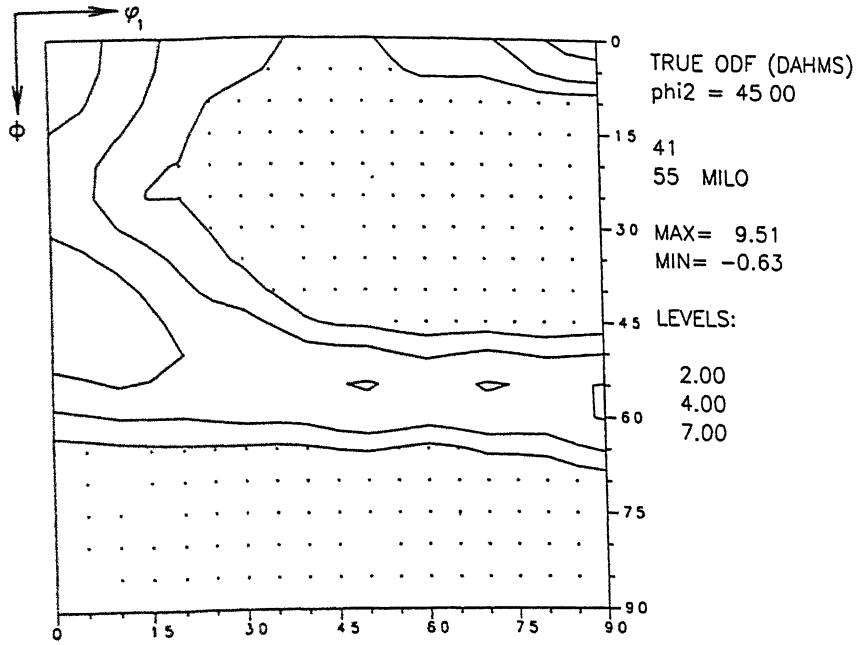

(a). FRT: 800 ^{O}C

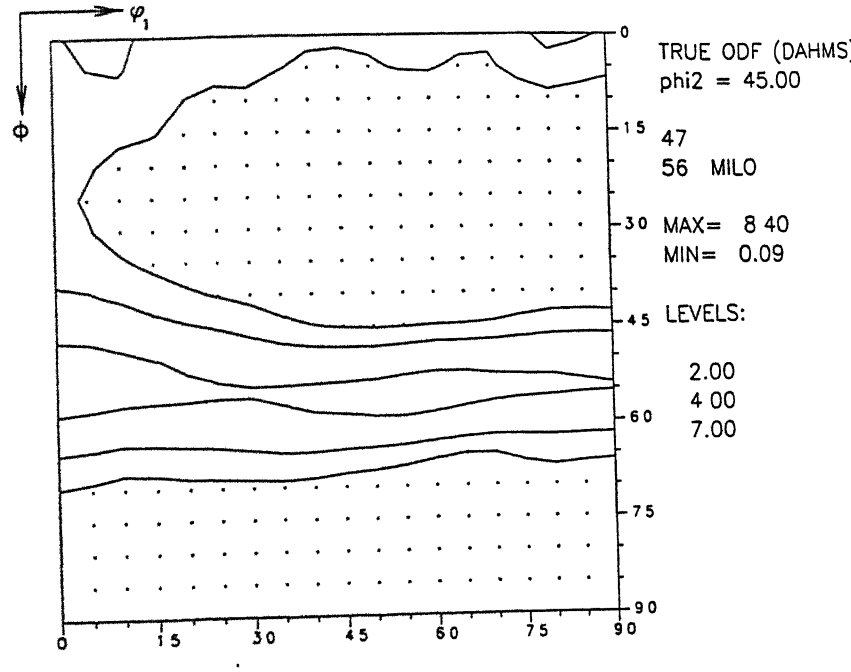

(b). FRT: 500 ^{O}C

Figure 4.64 (a) and (b) : $\varphi_2 = 45^{O}$ sections plots for steel 3 after single pass rolling (after soaking at 830 ^{O}C).

of reasonably strong γ fibres and α fibres, together with strong intensities at the rotated cube positions.

(b) Textures after heat treatment

Heat treatment of the above two warm rolled samples leads to perceptible increase in the overall texture intensities, as is evident from the relevant ODFs [Figs. 4.62(c) and (d)]. Both the figures show primarily the presence of the γ fibre.

The fibre plots [Fig. 4.63] indicate perceptible sharpening of the γ fibres in both the samples. Heat treatment also leads to significant sharpening of the α fibre peaks at ~ {111}<110>, at the same time the high intensities along the α fibre from the {001}<110> to near {111}<110> diminish for both the samples. The ε fibre plot clearly indicates a drastic decrease of the intensities at the rotated cube {001}<110> position due to heat treatment The peaks at near {111}<112> location are quite sharp in both the heat treated materials.

The $\varphi_2 = 45^{\circ}$ section plots for the heat treated materials show primarily the presence of strong γ fibres only [Fig. 4.64 (c) and (d)].

4.5.3.3 Textures after multipass rolling

(a) Schedule 1

The ODFs of the 800 $^{\circ}$C FRT and 500 $^{\circ}$C FRT samples, multipass rolled in schedule 1 after soaking at 1150 $^{\circ}$C, are shown in Figures 4.65 (a) and (b) respectively.

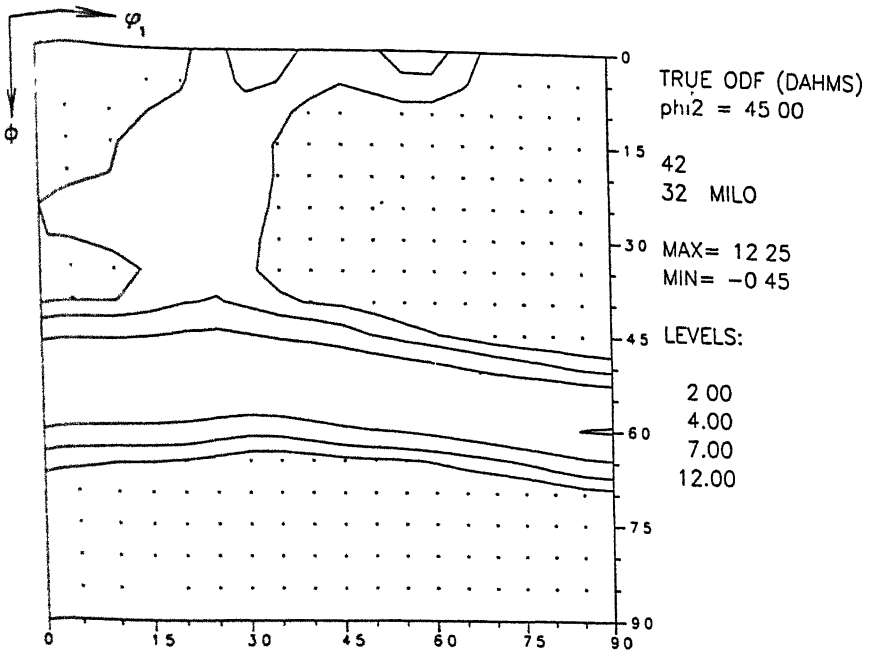

(c). FRT: 800 ^{O}C

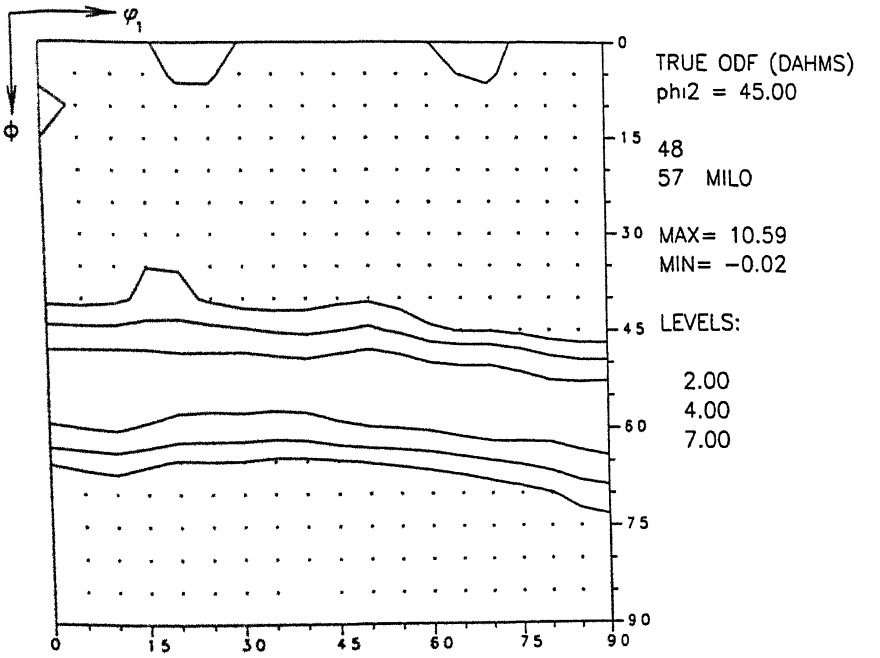

(d). FRT: 500 ^{O}C

Figure 4.64 (c) and (d) : $\varphi_2 = 45^{O}$ sections plots for steel 3 after single pass rolling (after soaking at 830 ^{O}C) and annealing.

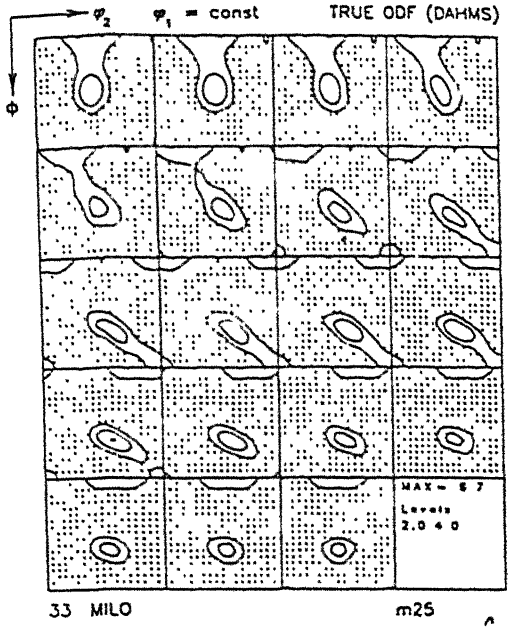

(a) FRT : 800 °C

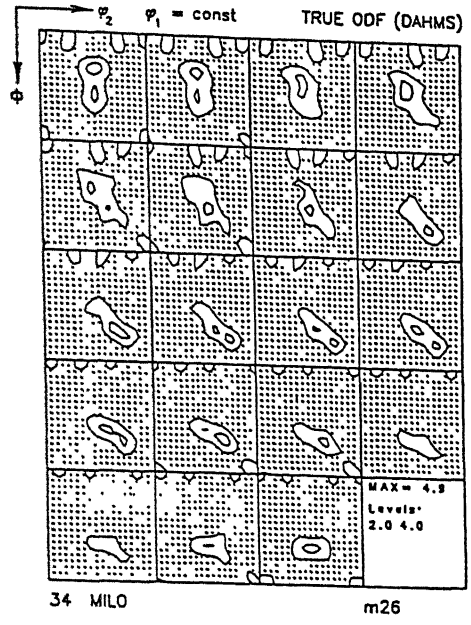

(c) FRT : 800 °C

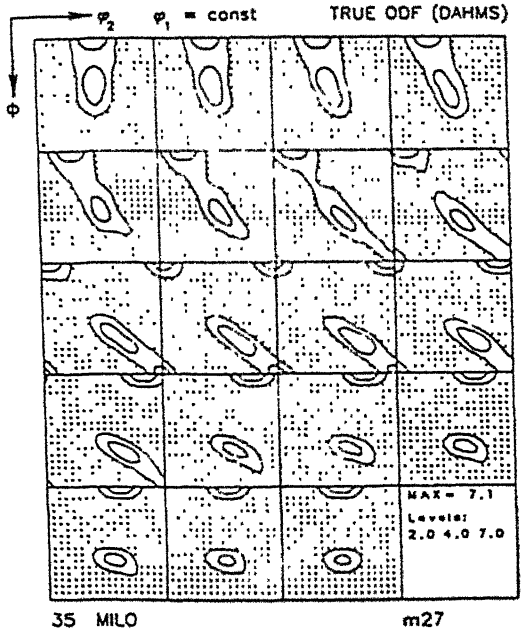

(b) FRT : 500 °C

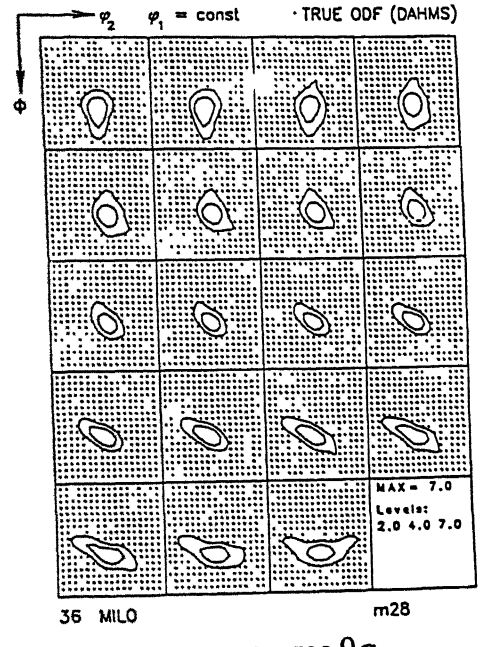

(d) FRT : 500 °C

Figure 4.65 (a) - (d) : ODF plots (φ_1 sections) for steel 3 after multipass rolling under schedule 1 [(a) and (b)] and annealing [(c) and (d)].

Although apparently both the ODFs look quite similar, the 500 ^{o}C FRT material has slightly higher texture intensity. The presence of the moderately strong γ fibres can be seen in both the ODFs. The fibre plots [Fig.4.66] indicate the presence of non-uniform α fibres of similar intensity in both the samples. While the α fibre in the 500 ^{o}C FRT sample shows a maxima at {112}<110>, the corresponding maxima for the 800 ^{o}C FRT sample is obtained at ~ {223}<110>. The γ fibres in both the samples are rather uniform and are of nearly equal intensities (~ 5.0). Both the samples also show some intensity at the rotated cube location. The presence of an α and a γ fibre are also clearly visible in the $\varphi_2 = 45^{o}$ section plots [Fig. 4.67(a) and (b)].

Heat treatment of the warm rolled 800 ^{o}C FRT sample leads to a significant decrease of the overall texture intensity, as is evident from the corresponding ODF [Fig. 4.65 (c)]. On the other hand, the ODF of the heat treated 500 ^{o}C FRT sample [Fig. 4.65(d)] shows practically no change in intensity from that of the warm rolled sample; however, the presence of a sharp γ fibre component only becomes quite apparent from this ODF. The fibre plots [Fig. 4.66] clearly show that heat treatment leads to sharpening of the γ fibre in the 500 ^{o}C FRT material and weakening of the γ fibre in the 800 ^{o}C FRT sample. Heat treatment also lowers texture intensities at the rotated cube orientations. A weak γ fibre and a moderately strong and uniform γ fibre in the 800 ^{o}C FRT and HT and 500 ^{o}C FRT and HT materials, respectively, are also clearly seen in the corresponding $\varphi_2 = 45^{o}$ sections [Fig. 4.67(c) and (d)].

(b) Schedule 2

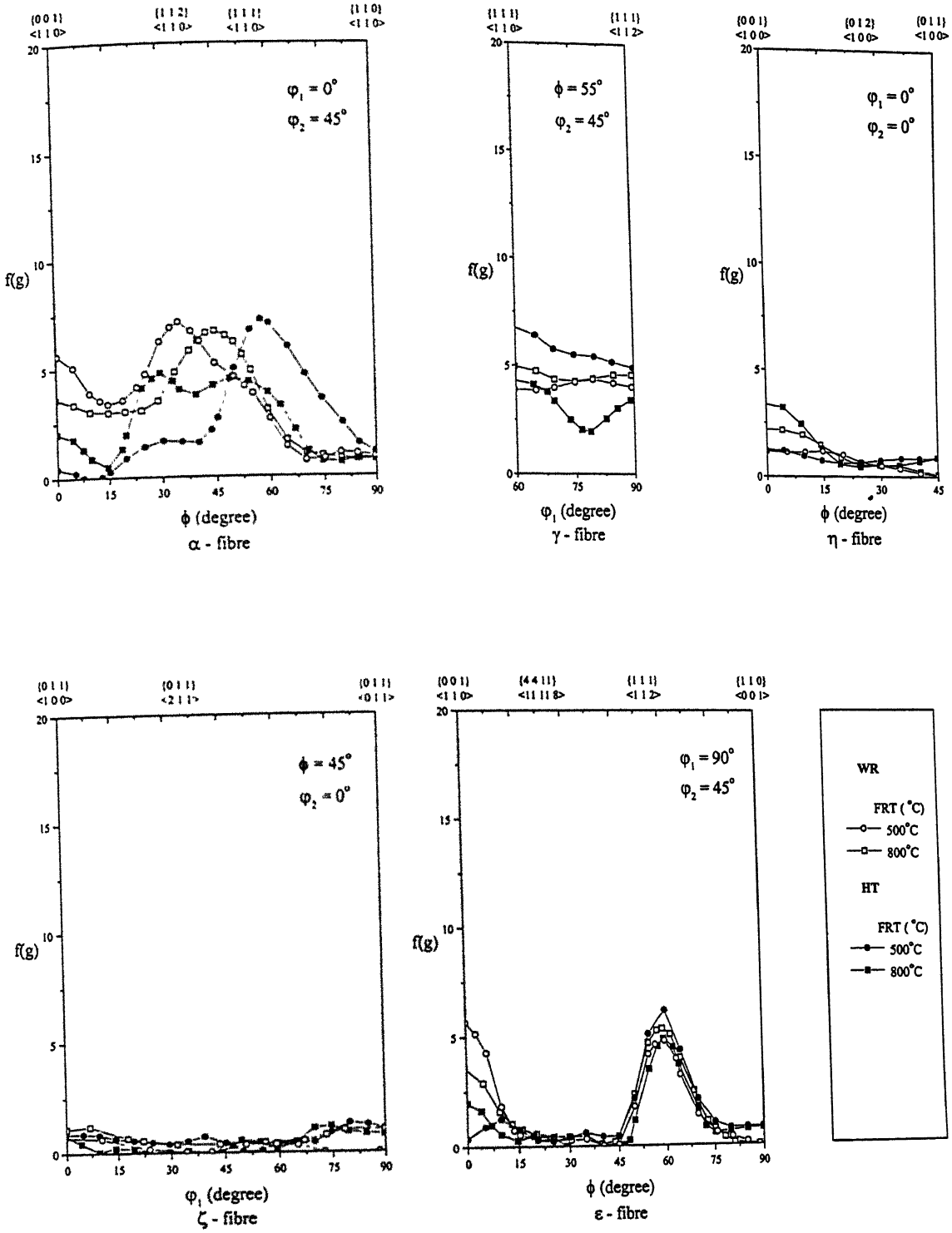

Figure 4.66 : Fibre plots for steel 3 after multipass rolling under schedule 1 (WR) and annealing (HT).

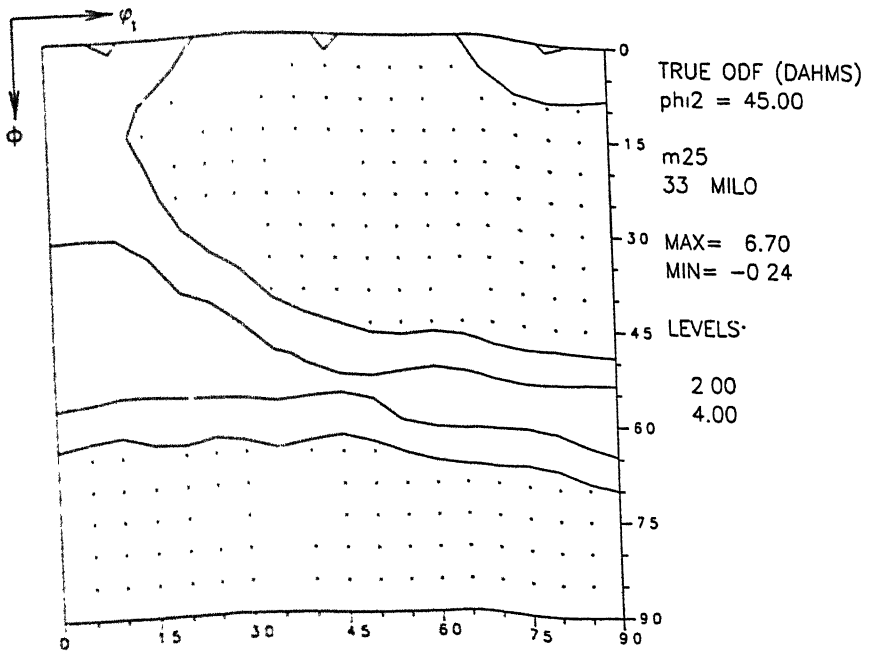

(a). FRT: 800 °C

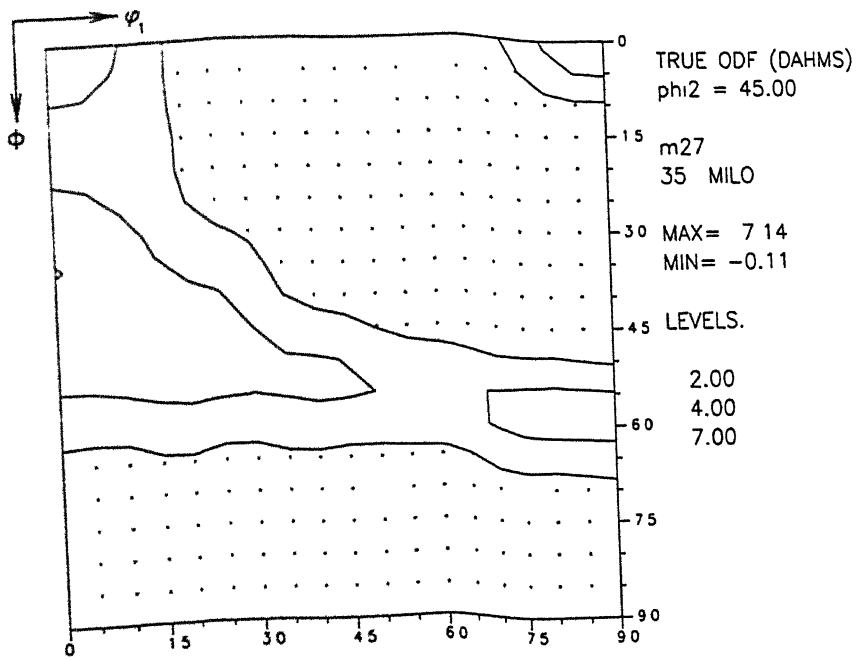

(b). FRT: 500 °C

Figure 4.67 (a) and (b) : $\varphi_2 = 45^{\circ}$ sections plots for steel 3 after multipass rollin under schedule 1.

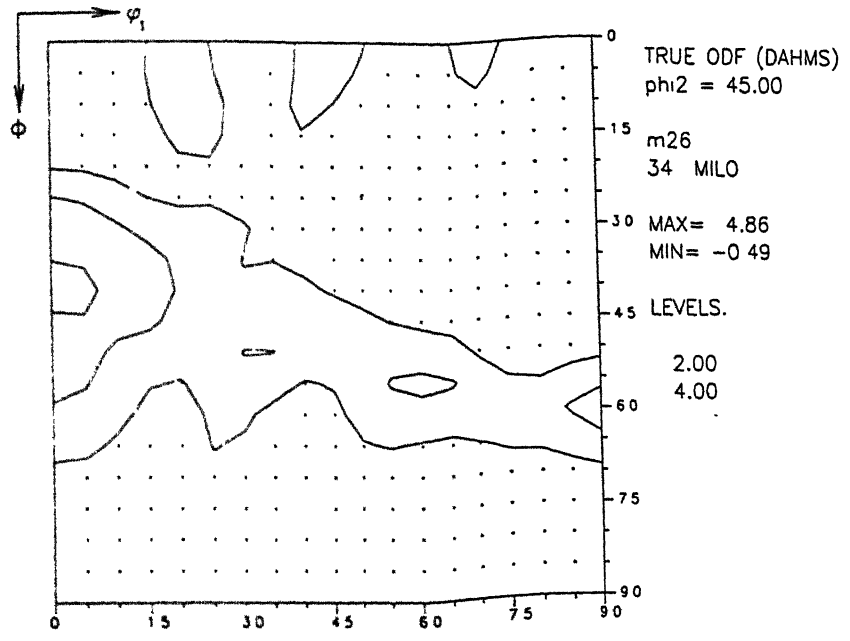

(c). FRT: 800 °C

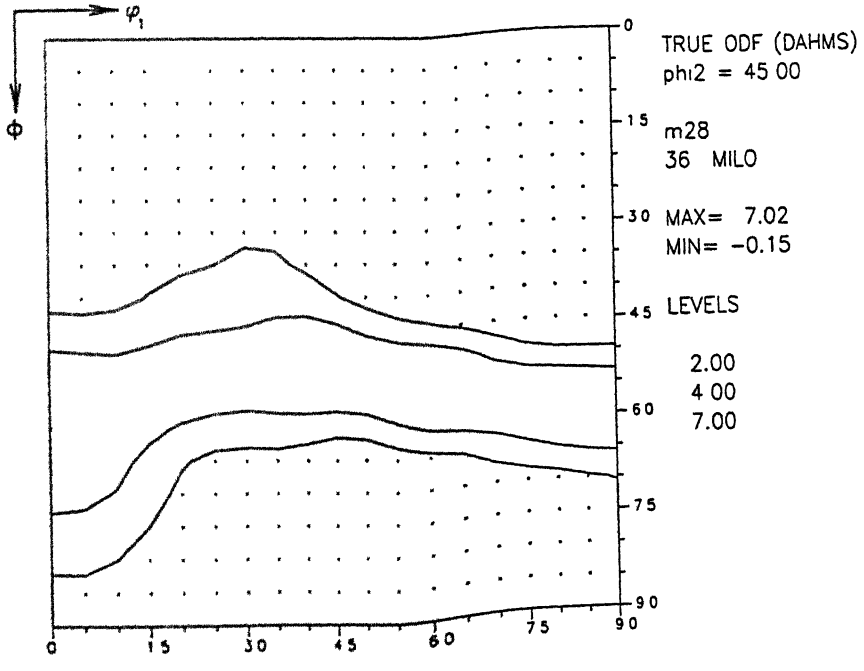

(d). FRT: 500 °C

gure 4.67 (c) and (d) : $\varphi_2 = 45^{\circ}$ sections plots for steel 3 after multipass rolling under schedule 1 and annealing.

Figures 4.68 (a) and (b) show the ODF plots of the 800 ^{o}C FRT and 500 ^{o}C FRT samples, respectively, which were multipass rolled in schedule 2 after soaking at 1150 ^{o}C. The overall intensity of the latter sample is just twice that of the former. In both of them presence of a γ fibre is quite apparent. The fibre plots [Fig. 4.69] show a strong non-uniform α fibre, with maxima at the {112}<110> location, in the 500 ^{o}C FRT sample, which also shows a moderately strong and nearly uniform γ fibre. The α and γ fibre intensities in the 800 ^{o}C FRT sample are nearly half of those in the 500 ^{o}C FRT material. The 500 ^{o}C FRT sample also shows a rather strong intensity at the rotated cube position. The intensity at this location for the 800 ^{o}C FRT sample is quite low. The $\varphi_2 = 45^{o}$ section plots [Fig. 4.70(a) and (b)] show rather weak α and γ fibres in the 800 ^{o}C FRT material and moderately strong α and γ fibres in the 500 ^{o}C FRT sample.

After heat treatment almost perfect γ fibre develops in both the samples, as is evident from the corresponding ODFs [Fig. 4.68 (c) and (d). The overall intensity of texture improves substantially after heat treatment in both the materials. The fibre plots [Fig.4.69] show reasonably strong γ fibres in both the samples, the intensities of the fibres being more at the {111}<112> location than at the {111}<110>. The non-uniform α fibres in both the materials show peak values at {111}<110>, but show very low values elsewhere along the fibre. Heat treatment of both the materials has brought down the intensities at the rotated cube position by a substantial amount. The almost perfect and rather strong γ fibres in these two heat treated materials are quite apparent in the corresponding $\varphi_2 = 45^{o}$ section plots also [Fig. 4.70 (c) and (d)].

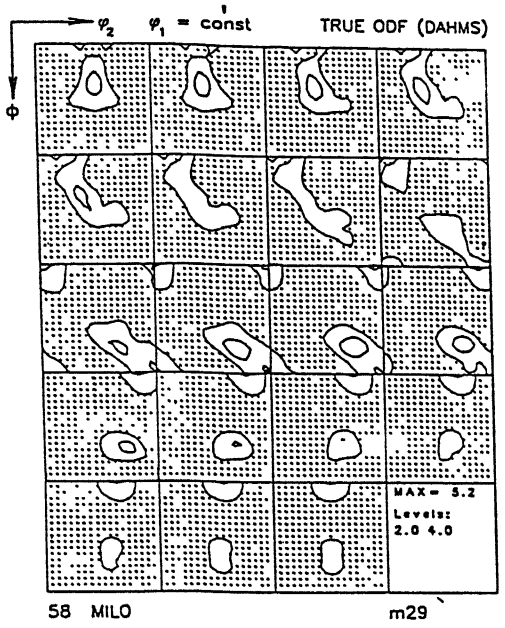

(a) FRT : 800 ^{O}C

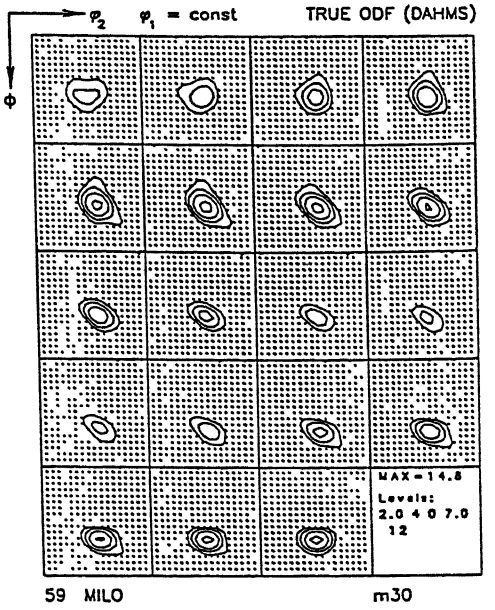

(c) FRT : 800 ^{O}C

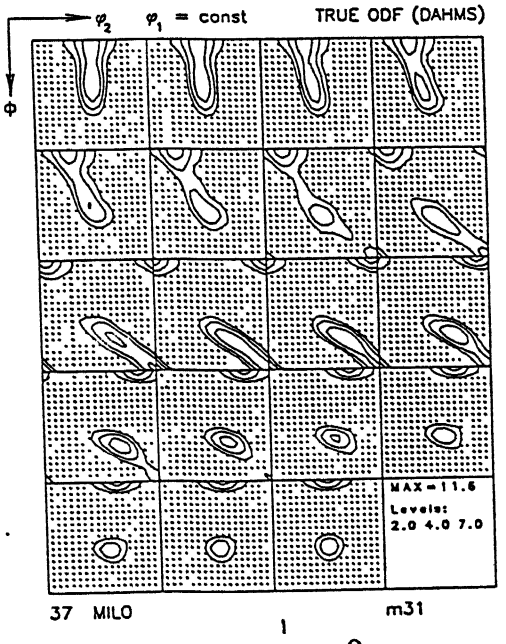

(b) FRT : 500 ^{O}C

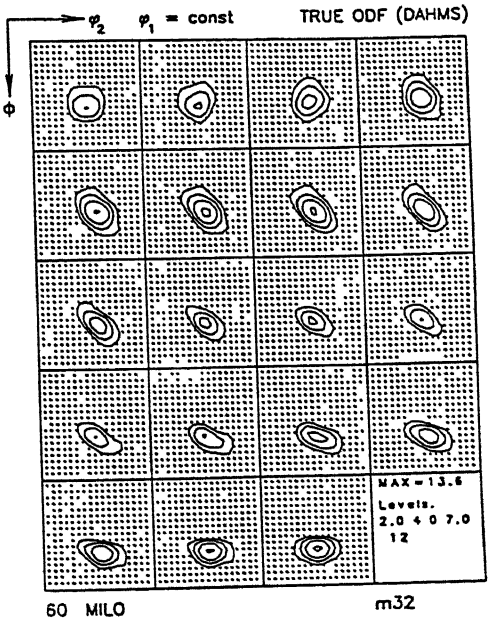

(d) FRT : 500 ^{O}C

Figure 4.68 (a) - (d) : ODF plots (φ_1 sections) for steel 3 after multipass rolling under schedule 2 [(a) and (b)] and annealing [(c) and (d)].

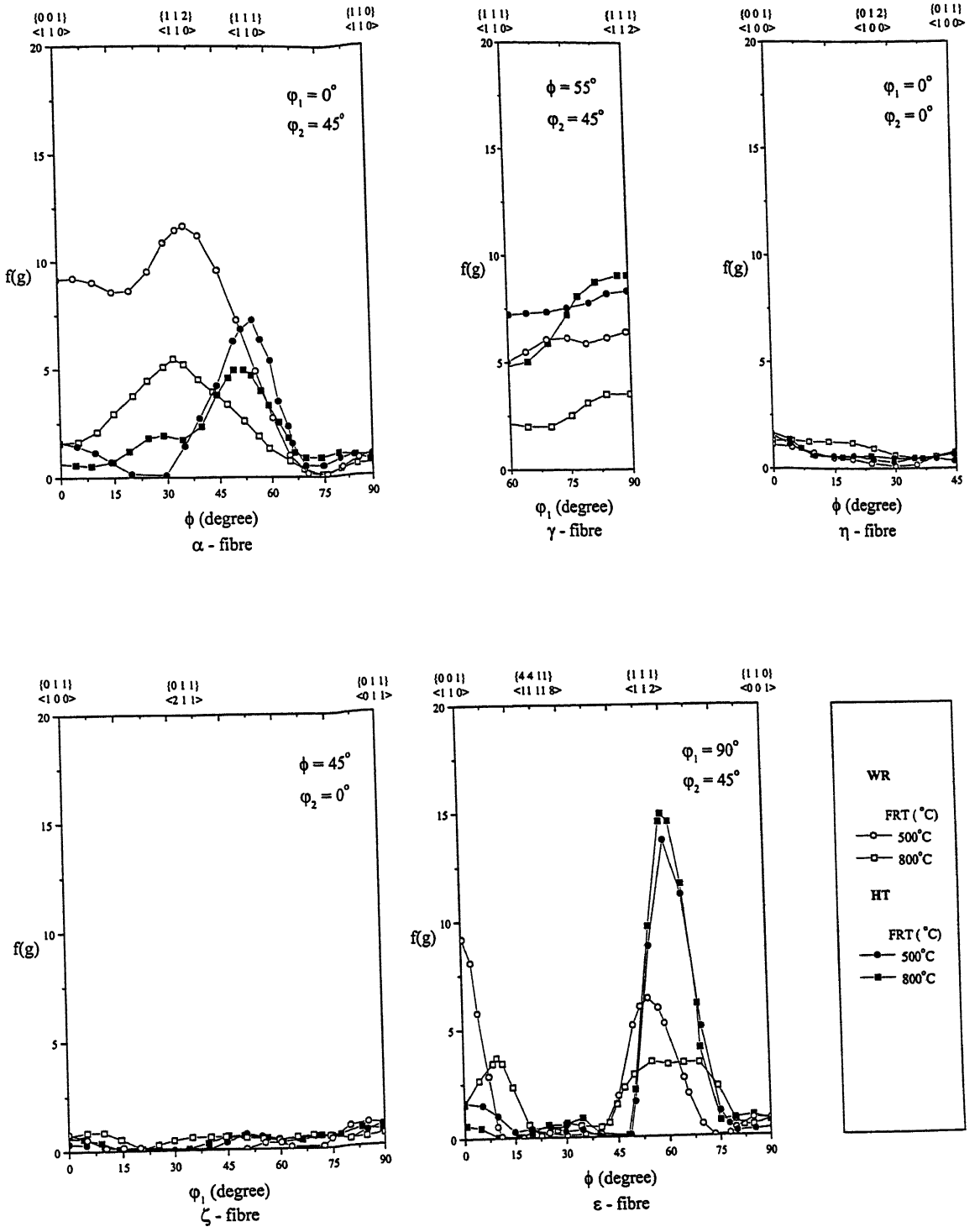

Figure 4.69 : Fibre plots for steel 3 after multipass rolling under schedule 2 (WR) and annealing (HT).

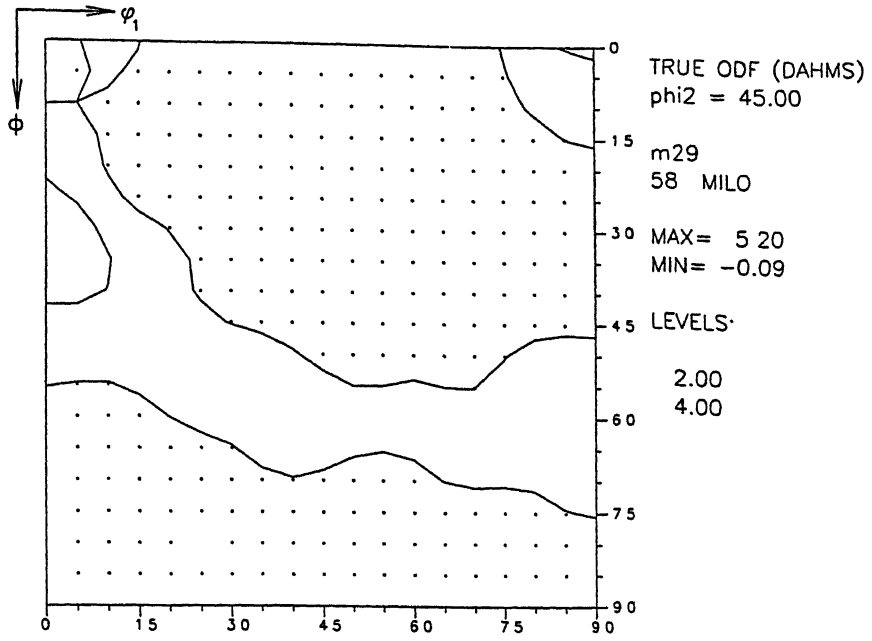

(a). FRT: 800 °C

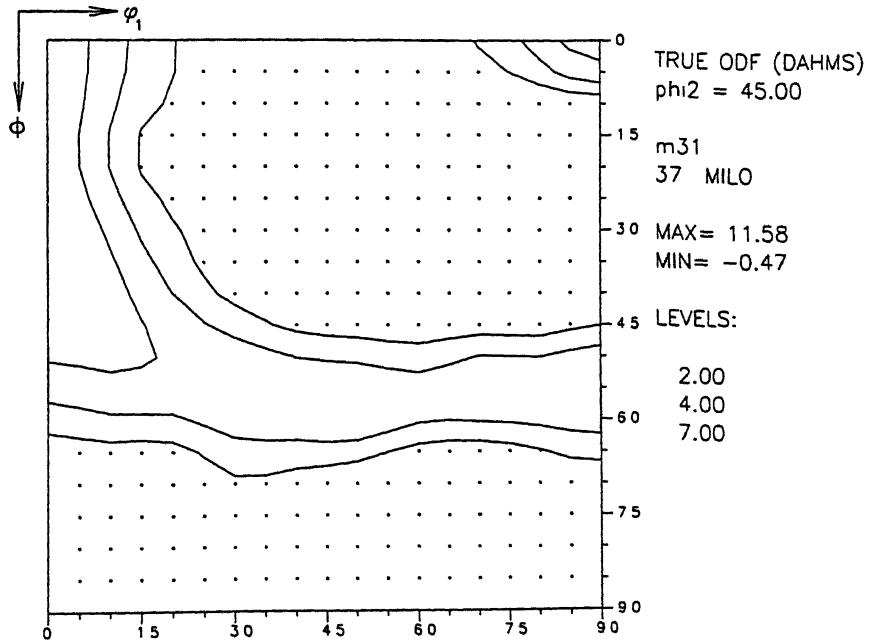

(b). FRT: 500 °C

Figure 4.70 (a) and (b) : $\varphi_2 = 45^{\circ}$ sections plots for steel 3 after multipass rolling under schedule 2.

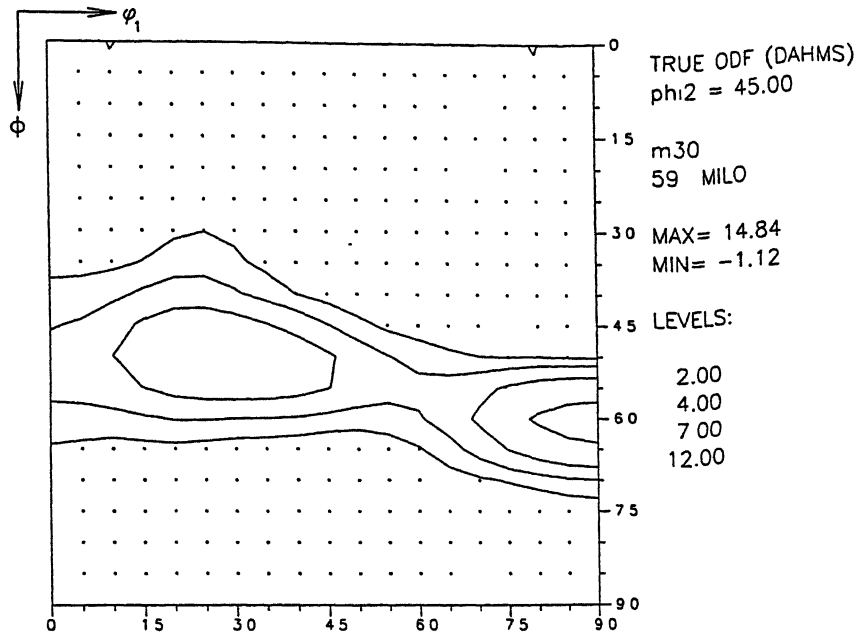

(c). FRT: 800 ^{o}C

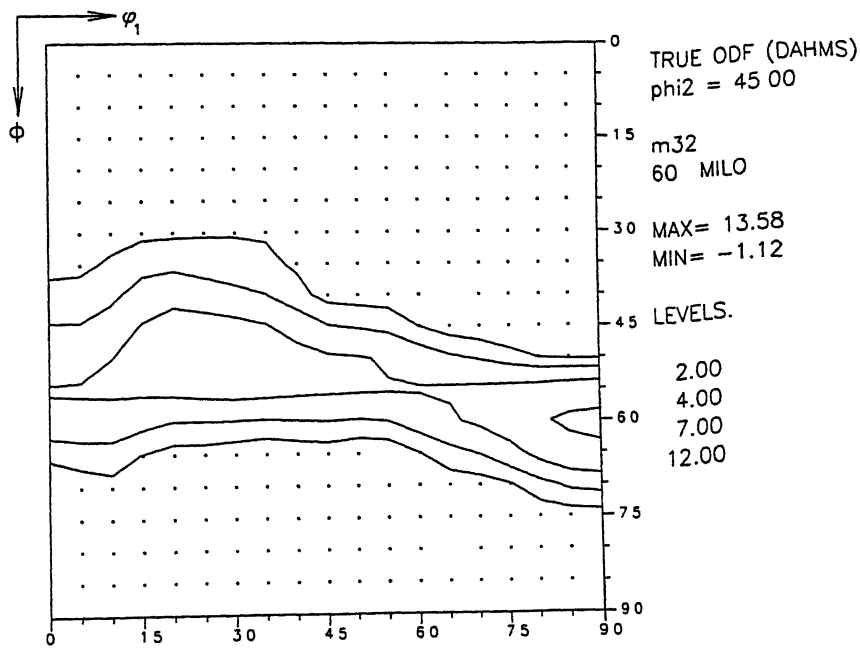

(d). FRT: 500 ^{o}C

Figure 4.70 (c) and (d) : $\varphi_2 = 45^{o}$ sections plots for steel 3 after multipass rolling under schedule 2 and annealing.

(c) Schedule 3

Figures 4.71 (a) and (b) display the ODFs of the 800 ^{O}C FRT and 500 ^{O}C FRT materials, respectively, of schedule 3. Both these ODFs look quite similar, although the latter one is perceptibly sharper than the former. The fibre plots [Fig.4.72] clearly show the presence of reasonably strong γ fibres in both the materials, the fibre in the 500 ^{O}C FRT sample being somewhat stronger. The two samples also show non-uniform α fibres, both having their maxima at ~ {111}<110>. The α fibre intensity in the 500 ^{O}C FRT sample is nearly twice as strong as in the 800 ^{O}C FRT material. The ε fibre plots show peaks at ~{111}<112>, the 800 ^{O}C FRT sample showing a marginally sharper value than the 500 ^{O}C FRT sample. Both the samples also exhibit substantial intensities at the rotated cube position. The $\varphi_2 = 45^{O}$ section plots from the above two samples [Fig.4.73 (a) and (b)] show the presence of both sharp γ fibre and α fibres, as expected.

Heat treatment of the above two samples leads to substantial sharpening of their ODFs [Fig. 4.71 (c) and (d)]. In fact, the increase in the texture intensity is much higher in case of the 500 ^{O}C FRT and HT sample than in the 800 ^{O}C FRT and HT material. The ODFs of both the heat treated materials primarily show sharp γ fibres only. The fibre plots [Fig. 4.72] show a very sharp γ fibre in the 500 ^{O}C FRT and HT samples, with an intensity of ~ 10.0 at {111}<110> and ~ 20.0 at {111}<112>. The γ fibre in the 800 ^{O}C FRT and HT sample is much less sharp and somewhat more uniform in intensity. The α fibres of the heat treated materials show sharp peaks at ~ {111}<110>, the intensities at other locations along this fibre are quite low. The ε fibre plot shows very sharp intensities at ~ {111}<112> for both the samples. Heat treatment has also been effective in reducing the

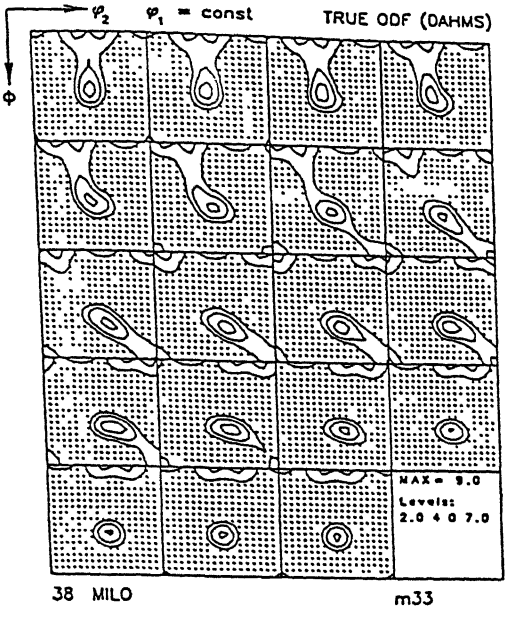

(a) FRT : 800 ^{o}C

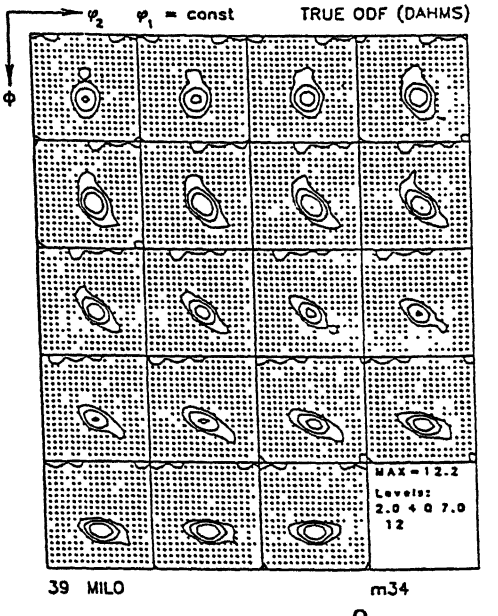

(b) FRT : 500 ^{o}C

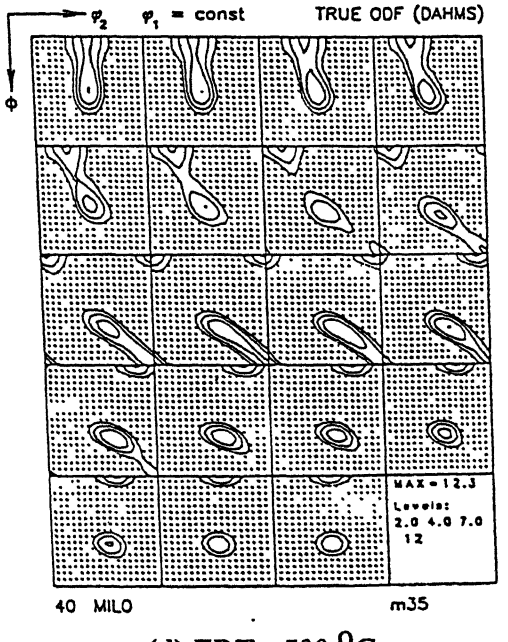

(d) FRT : 500 ^{o}C

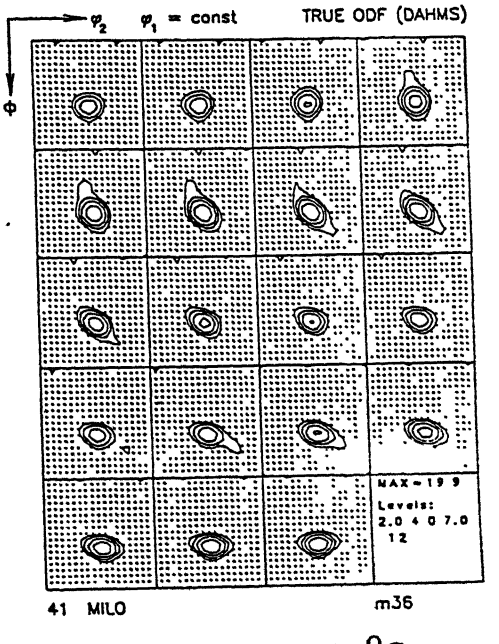

(d) FRT : 500 ^{o}C

Figure 4.71 (a) - (d) : ODF plots (φ_1 sections) for steel 3 after multipass rolling under schedule 3 [(a) and (b)] and annealing [(c) and (d)].

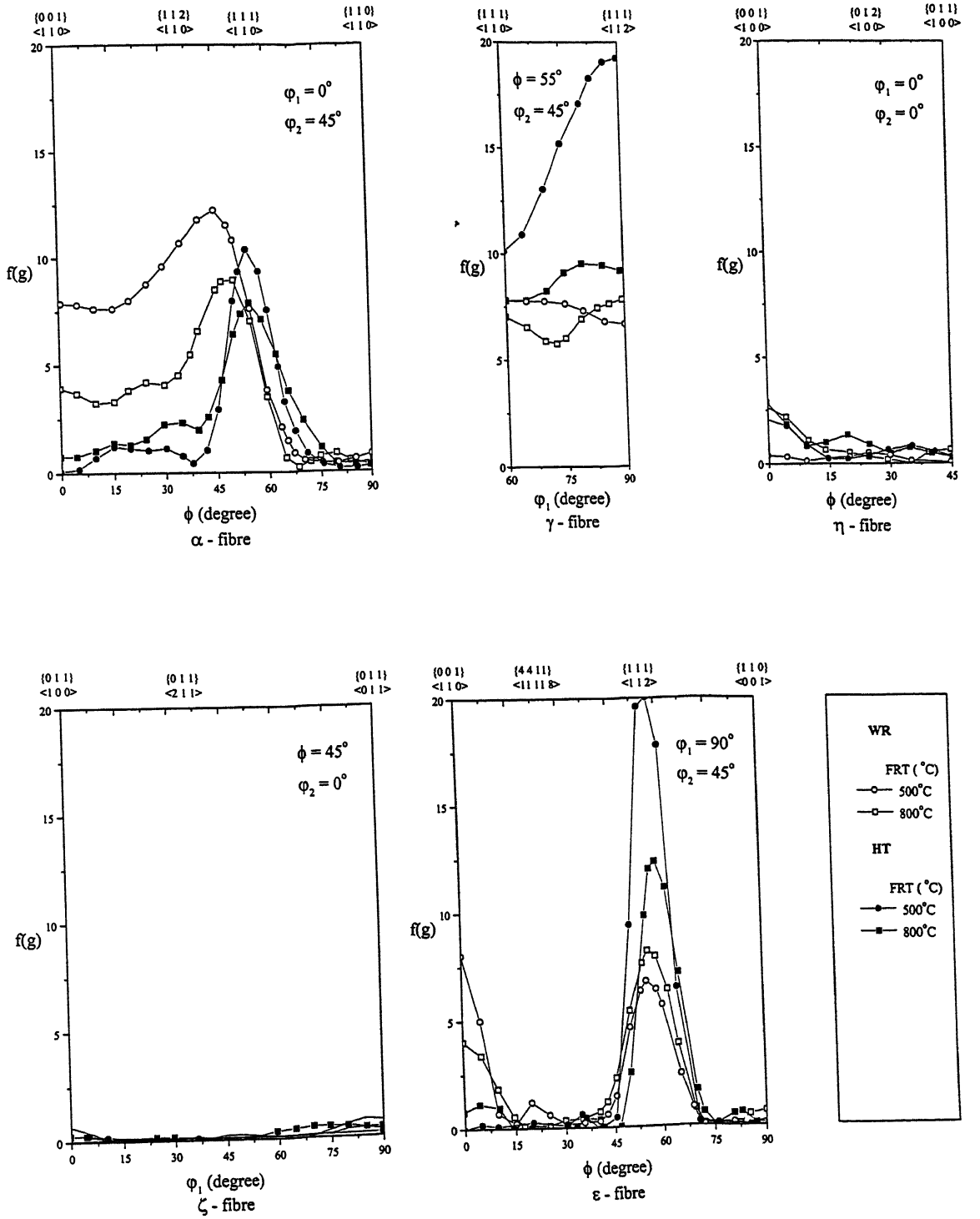

Figure 4.72 : Fibre plots for steel 3 after multipass rolling under schedule 3 (WR) and annealing (HT).

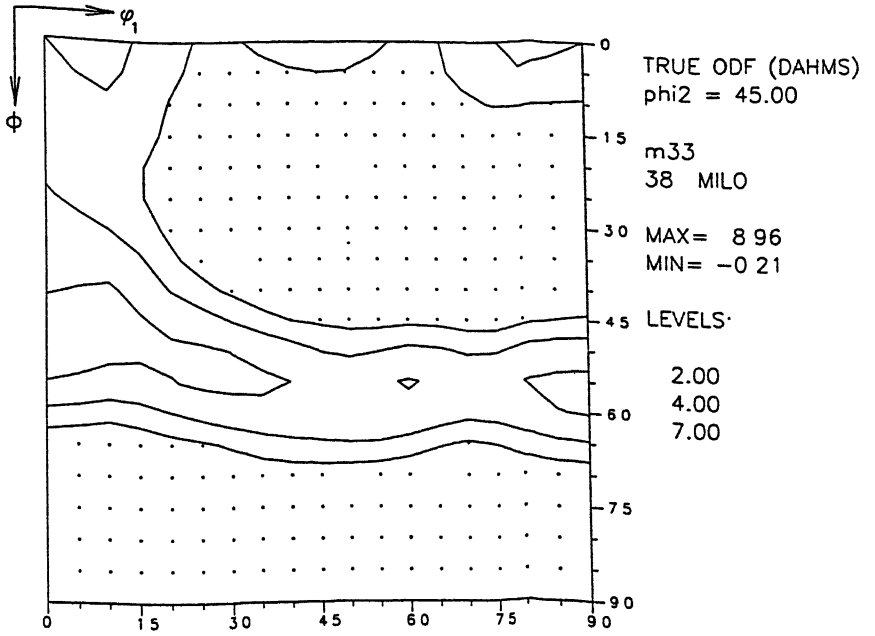

(a). FRT: 800 ^{O}C

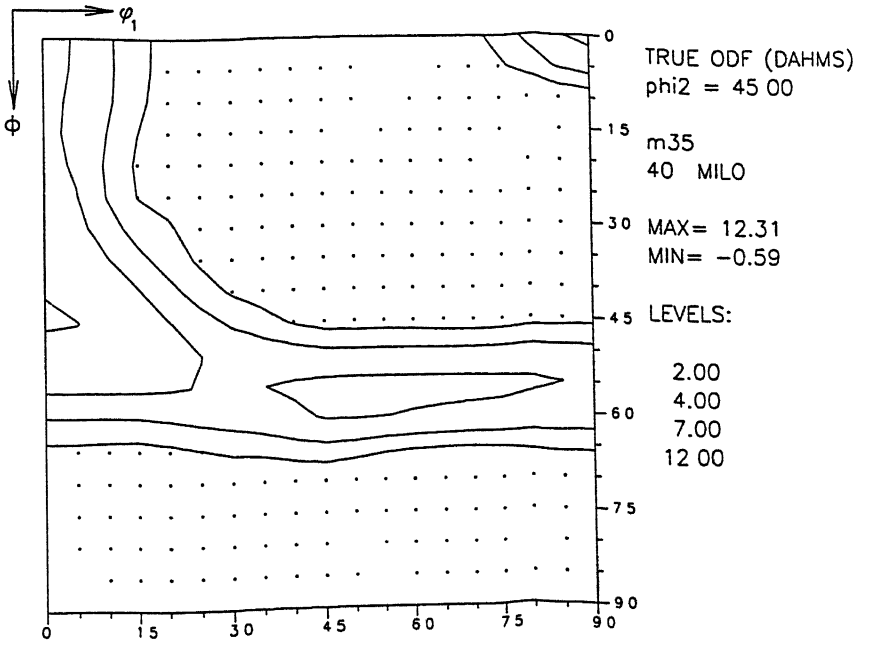

(b). FRT: 500 ^{O}C

Figure 4.73 (a) and (b) : $\varphi_2 = 45^{O}$ sections plots for steel 3 after multipass rolling under schedule 3.

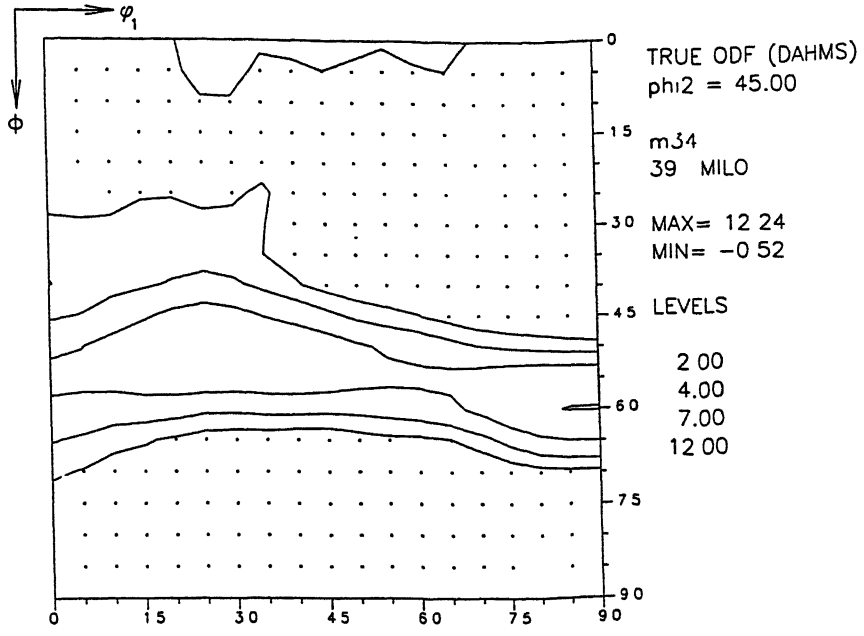

(c). FRT: 800 ^{O}C

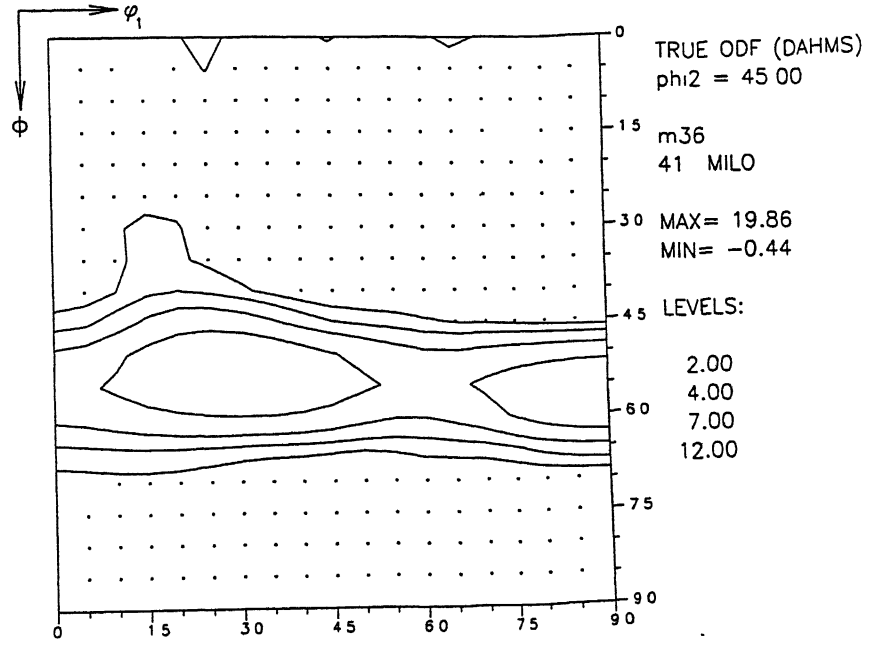

(d). FRT: 500 ^{O}C

Figure 4.73 (c) and (d) : $\varphi_2 = 45^{O}$ sections plots for steel 3 after multipass rolling under schedule 3 and annealing.

intensities at the rotated cube positions to insignificant values in both the samples. As expected, the $\varphi_2 = 45^{O}$ section plots for both the materials [Fig. 4.73 (c) and (d)] show the presence of very sharp γ fibres only.

CHAPTER 5
DISCUSSION

5. Discussions

Attempts have been going on, over the last decade or so, to produce thin gauges of good quality deep drawable steels right from the hot rolling mill. This will necessitate bringing down the finish rolling temperature to within the upper α range. The process generally goes by the name of Warm rolling or Ferritic rolling. These warm rolled steels are to replace the conventional hot rolled and cold rolled grades. The obvious benefits of these new products will be in terms of energy savings, cost effectiveness and productivity. Although some amount of research has been carried out on the physical metallurgical aspects of warm rolling, not much is really known about the details of this process. This leaves room for further work in this area. The present work was undertaken to determine how optimum deep drawability can be achieved in low carbon warm rolled steels by varying the compositional and processing parameters such as (i) steel composition, (ii) soaking temperature, (iii) rolling schedule and (iv) finish rolling temperature (FRT).

Three steel compositions – one extra low carbon (ELC) and two interstitial free (IF) steels were used for this purpose. Since good deep drawability is achieved only in those steels where a strong <111> || ND (γ fibre) texture forms during processing, detailed textural studies have been carried out under different processing conditions. Since, these products are industrially used in soft condtion, the warm rolled steels were subjected to recrystallisation annealing. Microstructural information from the different steel compostions, after warm rolling operation as well as annealing, was gathered in the form of densities of dislocation and deformation bands, grain size etc. and attempt was made to

correlate these structural features with the corresponding textures. No conscious effort was however, made to study the effects of precipitation, if any, on textural aspects.

The results of this investigation clearly indicate that the best <111>||ND (γ fibre), beneficial for good deep drawability, develops in the IF steel (steel 3) after final processing. Development of the γ fibre in the other IF steel (steel 2) after final processing was not very satisfactory. Both these IF steels contain Ti and Nb, steel 3 containing more Ti than Nb while reverse was the case with steel 2. For convenience the former will be called a Ti enriched IF steel while the latter will be referred to as a Nb enriched IF steel.In comparison to the behaviours of these two IF steels , the ELC steel showed only a poorly developed γ fibre after final processing.

In this chapter an attempt will be made to correlate the textural results with the corresponding microstructural observations. This will be followed by a critical discussion of the major experimental findings.

5.1 Microstructures of the warm rolled steels

5.1.1 Deformation band density

The major microstructural features observed in all the three steels, after warm rolling, were profusion of deformation bands (in-grain shear bands) within individual grains. The densities of the bands, as functions of steel composition, rolling schedule soaking temperature and FRT have already been given in Figure 4.8. Side by side a plot o normalized dislocation densities, as functions of the above mentioned parameters, hav

also been presented in Figure 4.11. The dislocation density plots give an idea about the relative amounts of stored energy present due to warm rolling in the different materials.

The deformation bands have been found to make widely different angles to the rolling direction. Akbari et al. (41), from their work on a warm rolled Ti containing IF steel, have reported that the majority of the bands (microbands, according to Akbari et al.) made nearly the same average angle of $\pm 35^{o}$ to the rolling direction. Hatherly and malin (43) have reported that the inclinations of such bands with the rolling direction in rolled brasses vary between $\sim 20^{o}$ - $\sim 40^{o}$. Several other workers (42-54) also reported wide angular ranges for band formation in different materials after cold rolling. Barnett and Jonas (9) from their work on warm rolled LC and IF steels, found out that these bands (in-grain shear bands, according to them) are inclined within two different angular ranges, 30^{o} - 35^{o} and 17^{o} - 20^{o}, with the rolling direction. The present work has shown that the deformation band inclinations in the three steels vary widely, as seen in Tables 4.3 and 4.4. Some representative cumulative frequency plots of deformation band angles [Fig 4.10] in the present work clearly shows that the majority of bands (80-85%) lie within a band angle of $\pm 25^{o}$. These plots and the data in Tables 4.3 and 4.4 also show that the angles of inclination of deformation bands do not show any significant dependence on steel composition, soaking temperature, rolling schedule or FRT.

Unfortunately, the question of deformation band formation has not been treated that extensively and critically as yet and, therefore, a final word can not be said in this matter. The controversies in this area can be very well illustrated by quoting the observation made

by Akbari et al. (41) and by Lee et al. (42). While according to the former the formation of these bands is not primarily dependent on crystallographic orientation, but should be determined by the stress system and geometrical requirements imposed by the deformation, the latter authors have suggested that the criteria for deformation band formation are grain orientation (most important), grain size and strain.

Figure 5.1 Shows a comparison of the density of deformation bands for the three steels during single pass and multipass rolling at different FRTs. These figures have been obtained by replotting the data in Figure 4.8 in a different manner. It is quite apparent from this figure that the deformation band densities in the ELC steel are significantly lower than those of the two IF steels in all the three schedules of multipass rolling. There is not a very wide variation in deformation band densities between the two IF steels for multipass rolling. Neither is there a very marked difference in DB density between the two IF steels during single pass rolling also. On the other hand the DB densities for the ELC steel, for soaking at 1150 ^{o}C as well as at 830 ^{o}C, show a steep decline from a high value at 500 ^{o}C FRT to a significantly low value at 800 ^{o}C FRT.

The observed variation of the DB density with FRT in ELC and IF steels is very similar to the case reported by Barnett and Jonas (9). There are, however, some basic differences between the present results and the results of Barnett and Jonas, who had plotted the deformation band density after single pass rolling over a range of temperatures varying between 70 ^{o}C to 700 ^{o}C for their steels. In the present case, measurements were done over a temperature range of 500^{o} C to 800^{o} C keeping in mind the practical industrial

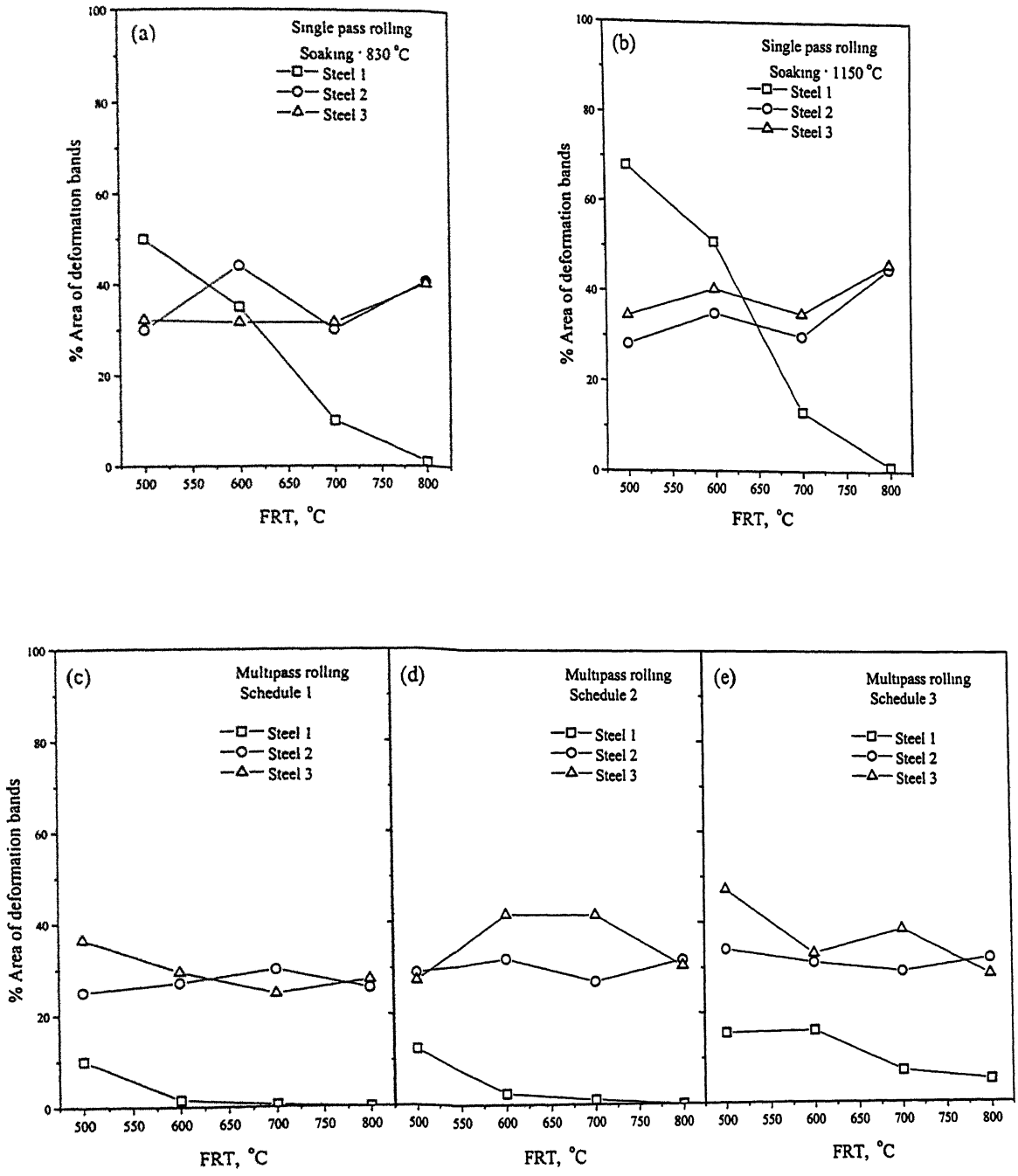

Figure 5.1 : Comparison of % area of deformation bands for three steels during single pass (a, b) and multipass (c, d, e) rolling at different FRTs.

aspects of warm rolling. Although the DB density in their LC steel had a much higher value than that of the IF steel at lower temperatures, the curves crossed over at a temperature of about 450 ^{o}C, beyond which the LC steel showed a much lower value of DB density than the IF steel. The cross over temperature in the present investigation, however, is 600^{o} C, which is about 150^{o} C higher than what they had obtained. The reason for these differences could arise from the factors that i) the initial grain size (30-40 μm) of the steels used by Barnett and Jonas was nearly half of the initial grain size (50-80 μm) in the present case, ii) the amount of rolling deformation in their steels was 65%, whereas in the present case, all the three steels were given a rolling reduction of ~80% in single pass, and iii) the carbon levels in the steels used by Barnett and Jonas were almost twice as much as their amounts in the corresponding steels in the present investigation. Hence a direct one-to-one comparison between their results and the present ones is not possible.

5.1.2 Normalised dislocation density

Figure 5.2 shows a comparison of normalised dislocation density (which is a measure of the total stored energy) for the three steels during single and multipass rolling at different FRTs. These plots were produced by replotting the data in Figure 4.11. In most of the cases here the dislocation density is higher in the ELC steel for the FRT of 500 ^{o}C and then it decreases steeply with FRT and reaches values lower than these for the two IF steels. The comparatively less decrease of dislocation densities in the IF steels at higher FRTs, as compared to those of the LC steel, is very much likely to be due to the retarded softening in the IF steels due to the presence of Ti and Nb and possible precipitation of Ti and Nb bearing compounds. The variation of dislocation density with FRT for all the three

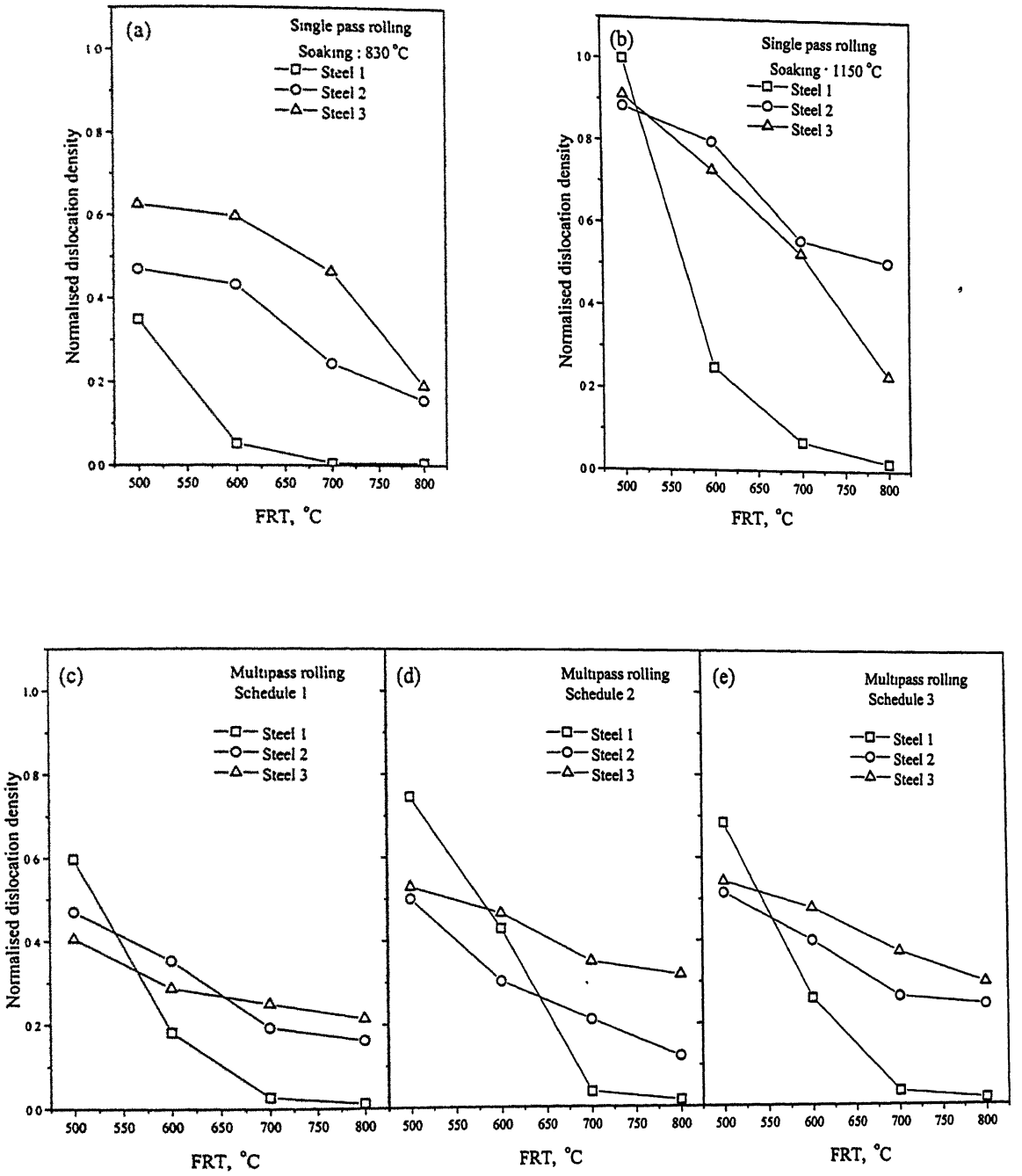

Figure 5.2 : Comparison of normalised dislocation density for three steels during single pass (a, b) and multipass (c, d, e) rolling at different FRTs.

steels here appear similar to what Barnett and Jonas (9) observed in their steels, within comparable FRT range. The general decrease of the normalised dislocation density with increasing FRT in any particular steel is related to dynamic relaxation processes (in single pass) and dynamic and static relaxation processes (in multipass) which occur at higher temperatures. The tendency for dynamic recovery at higher FRTs is quite apparent for all the three steels from their relevant flow stress curves [Fig. 4.2, 4.4 and 4.5]. During multipass rolling the steels will undergo some amount of static relaxation processes (post dynamic) during the interpass holding times. This will lead to even greater decrease of the normalised dislocation density at higher FRTs for the multipass rolled materials. This indeed is the case as displayed in Figure 5.2.The normalised dislocation density assumes very low values in both the single pass and multi pass rolled ELC steel after finish rolling at 700 ^{o}C and 800 ^{o}C. There is some evidence to show that at these stages the ELC steel recrystallizes completely, giving a ploygonal grain structure [Fig. 4.6].

5.1.3 Transmission electron microstructures

It is quite apparent from the TEM micrographs of Figures 4.12, 4.13 and 4.14 that all the three experimental steels show clear signs of recovery (presence of subgrains) within the ranges of FRTs used. These micrographs were taken from single pass rolled materials only. Therefore, it can be safely assumed that recovery (dynamic and post dynamic) will be more prominent in the multipass rolled samples where holding during interpass will add to the relaxation processes.

5.2 Warm rolling textures

A comparison of the γ fibre intensities of the 1150 °C soaked and single pass rolled ELC and IF steels at different FRTs is shown in Figures 5.3 (a-d). The maximum intensity [f(g) ≈ 13] of the γ fibre has been obtained for the ELC steel at FRTs of 500 °C and 600 °C; the γ fibre is practically absent for the 700 °C and 800 °C FRT materials.

The two IF steels also show moderately strong γ fibers at all FRTs, but their intensities are much less than the intensities of the γ fibres obtained in the ELC steel. The intensities of the α fibres in all three steels show a simialr trend - these are quite strong in all the cases.

In general, the γ fibre intensities in the ELC and the Ti enriched steels show a decrease with increase in FRT. However, in Nb enriched steel the sharpest γ fibre are obtained at the FRTs of 600 °C and 700 °C. Here the 500 °C FRT material shows the weakest γ fibre. The general characteristics of the warm rolled textures in all the three steels are quite similar to those of cold rolled LC and IF steels which normally show a strong γ fibre and a non-uniform α fibre (5). The general trend of obtaining sharper γ fibres at lower FRTs is presumably due to higher accumulated strain coupled with less chance of any restoration process. An interesting observation is that the sharpness of the γ fibre can be correlated with the corresponding deformation band densities reasonably well [see Fig 5.1]

A comparison of the texture results here with those of Barnett and Jonas (9) shows some interesting differences. They observed much higher intensity of the γ fibre in the LC

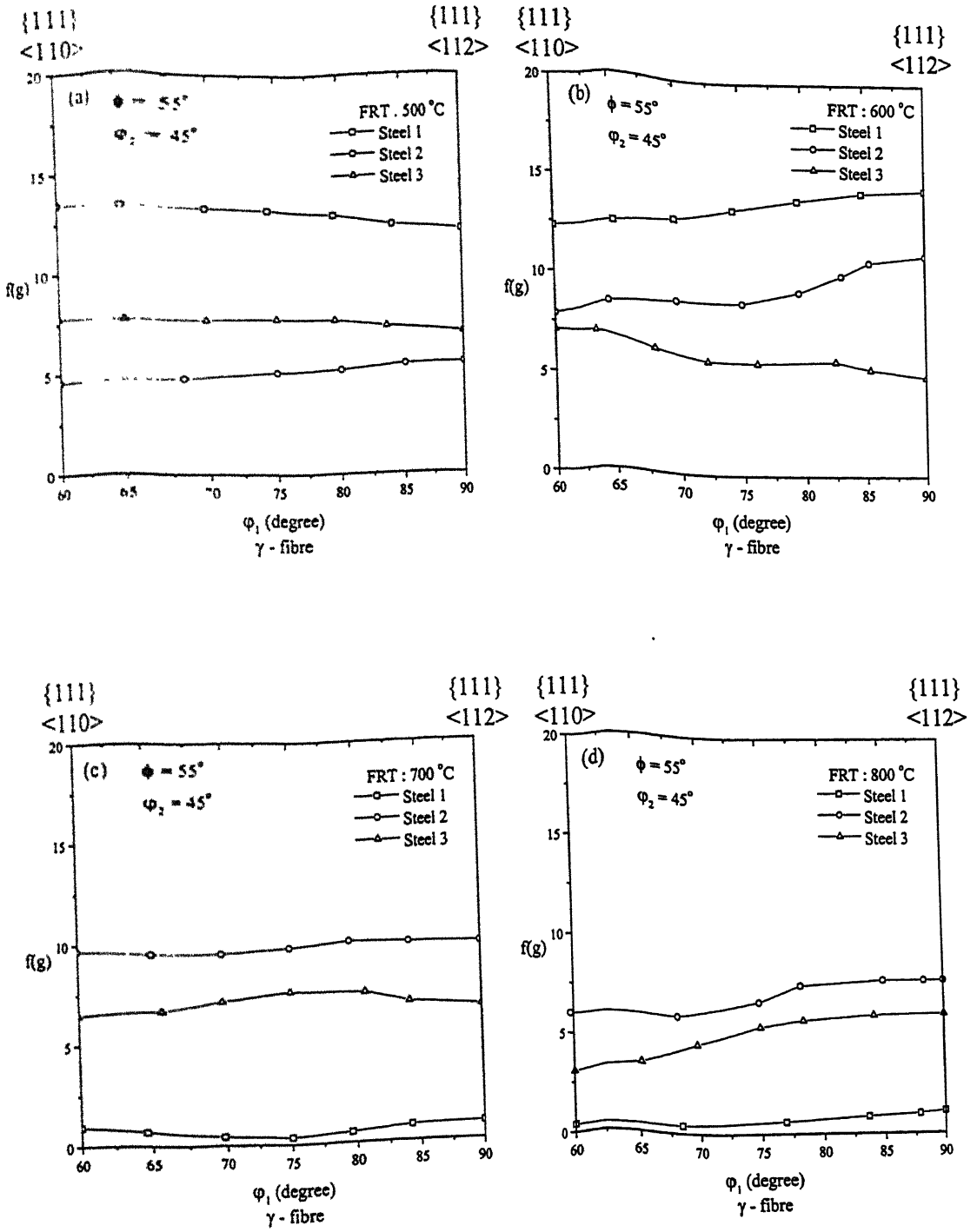

Figure 5.3 : Comparison of γ fibres for three steels after single pass rolling (soaking at 1150 °C)

steel than in the IF steel, finish rolled at 700 ^{o}C. On the other hand, in the present work the γ fibre is found to be non-existent in the ELC steel at FRT of 700 ^{o}C and above. It has also been seen that at these temperatures of deformation there is a substantial amount of dynamic restoration processes operating in the present ELC steel. Of course, the ELC steel here also shows very strong (stronger than in the two IF steels) values of the γ fibre intensity, but only at the lower FRTs of 500 ^{o}C and 600 ^{o}C. On the other hand, the present results seem to tally with the texture results of Tomitz and Kaspar (58) on their ELC steel.

A comparison of the γ fibre intensities in the 830 ^{o}C soaked and single pass rolled steels at the FRTs of 500 ^{o}C and 800 ^{o}C is displayed in Figures 5.4 (a, b). For the ELC steel, the γ fibre intensity here is found to be drastically reduced from that in the 1150 ^{o}C soaked material at 500 ^{o}C FRT. For the two IF steels, however, there is hardly any marked change in the γ fibre intensities for the two soaking temperatures. The changes in the intensities of the α fibre in the 830 ^{o}C soaked samples follow a trend similar to that for the γ fibre. Apparently, the changes in the initial grain size do not have a very significant effect on the textures of the IF steels, but affect the texture intensities (both α and γ fibres) of the ELC steel to a large extent.

A comparison of the γ fibre intensities of the three steels, multipass rolled (all schedules) at the FRTs of 500 ^{o}C and 800 ^{o}C is shown in Figures 5.5 (a) and (b), 5.6 (a) and (b) and 5.7 (a) and (b). It is clear that the γ fibre intensities in the ELC and the Nb enriched steel are quite comparable and pretty low for both schedules 1 and 2. The Ti enriched steel shows a perceptibly sharper γ fibre for both the schedules. [Fig. 5.7] sho

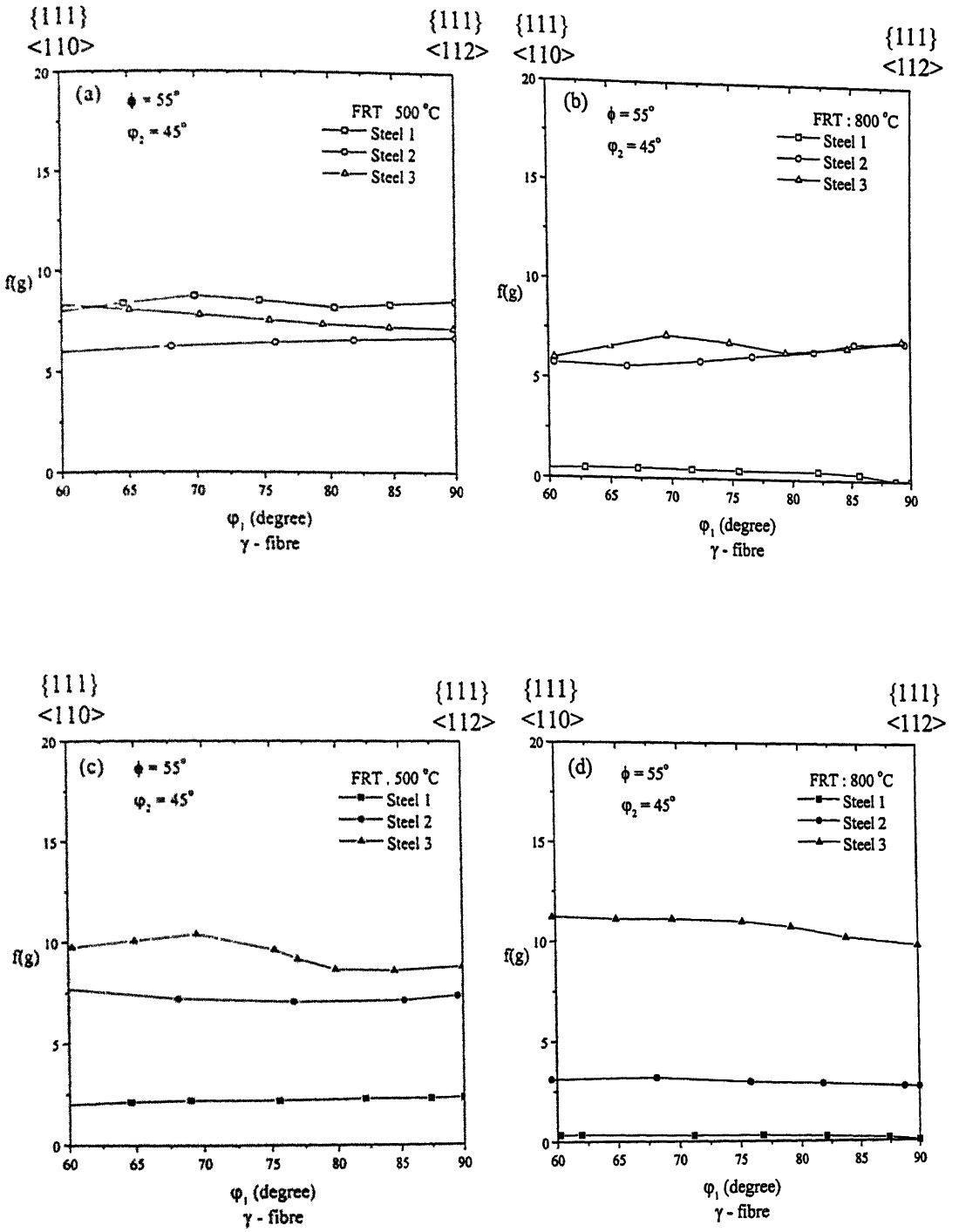

Figure 5.4 : Comparison of γ fibres for three steels after single pass rolling (soaking at 830 °C) (a, b) and annealing (c, d)

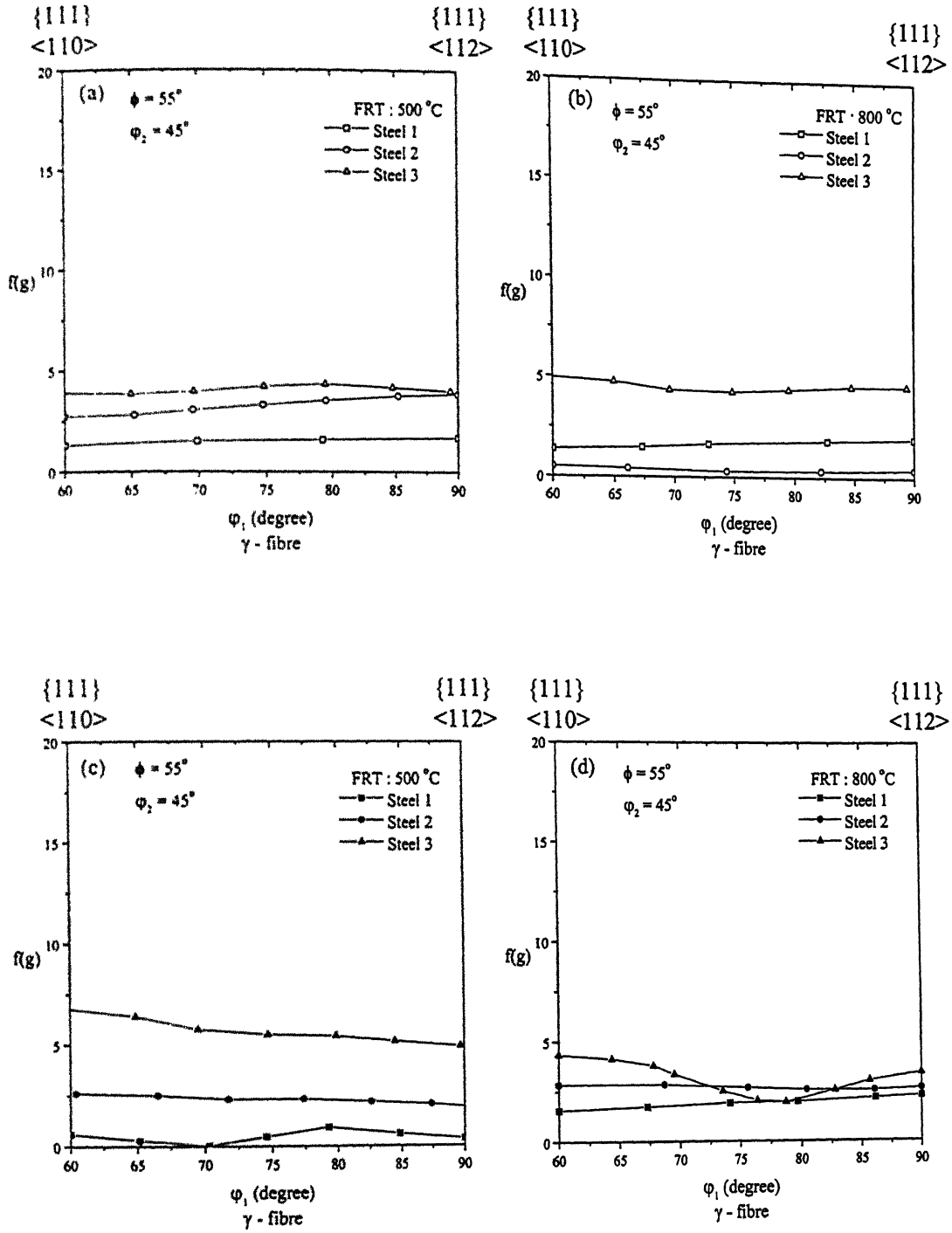

Figure 5.5 : Comparison of γ fibres for three steels after multipass (schedule 1) rolling (a, b) and annealing (c, d)

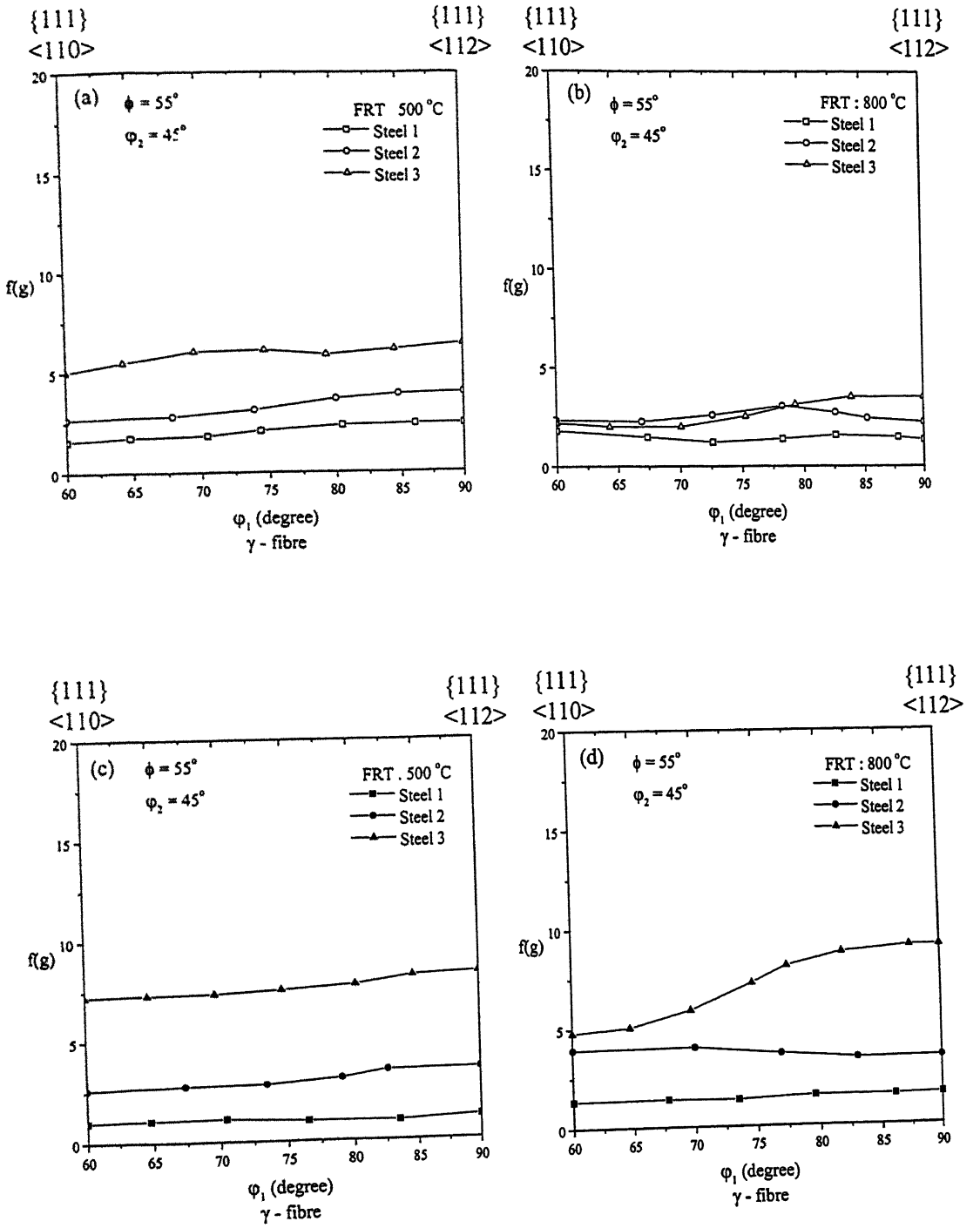

Figure 5.6 : Comparison of γ fibres for three steels after multipass (schedule 2) rolling (a, b) and annealing (c, d)

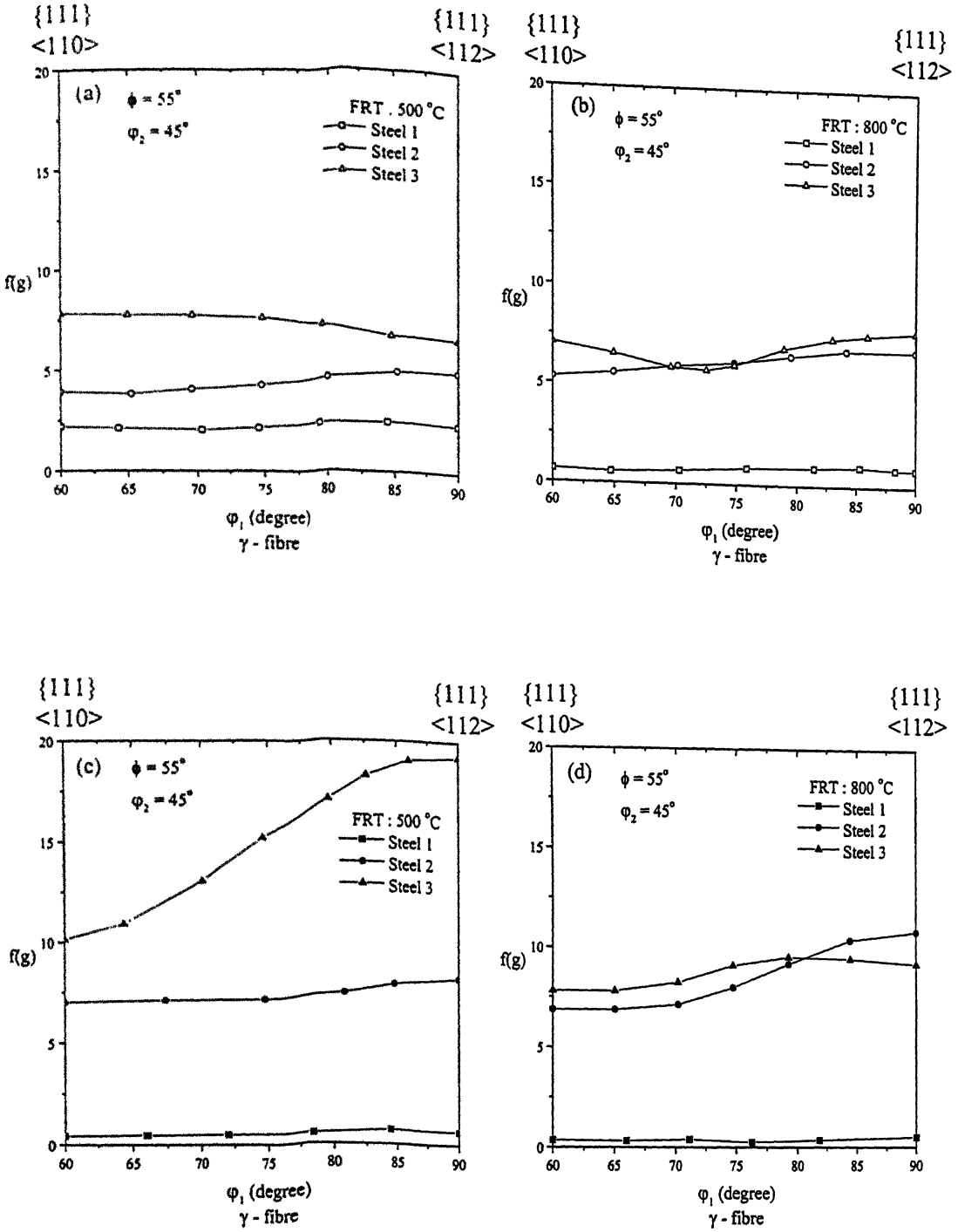

Figure 5.7 : Comparison of γ fibres for three steels after multipass (schedule 3) rolling (a, b) and annealing (c, d)

that the general value of the γ fibre intensity in schedule 3 increases in the order Ti enriched steel → Nb enriched steel → ELC steel. A comparison of all the γ fibres in the three schedules clearly indicates that γ fibre sharpens if larger amount of deformation is given to the steels in the α regime than in the γ regime. Among the three steels, the two IF steels are much more amenable to improved in the γ fibre intensity by this process than the LC steel.

Overall, the present result clearly indicate that among the three steels warm rolling imparts the best results in terms of γ fibre development in the Ti enriched steel. The ELC steel, although it shows sharp γ fibres in single pass rolled materials at lower FRTs, in general, develops rather poor γ fibre during warm rolling. The behaviour of the Nb enriched steel comes in between these two extremes. An interesting point to note in this particular steel is that very often the higher FRT material shows a sharper γ value as compared to a lower FRT material. This indicates that in this particular steel finish rolling in the upper α range is more beneficial than in the lower α range.

5.3 Textures of heat treated materials

A comparison of the γ fibre intensities in the three steels, 1150 ^{o}C soaked and single pass rolled, after heat treatment is shown in Figures 5.8 (a)-(d). It is clear from this figure that recrystallization annealing improves the intensities of the γ fibre in the warm rolled Ti enriched steel by about 1.5 times. At the same time the intensities of the α fibres at the rotated cube locations also come down drastically. By contrast, in the Nb enriched steel both the γ and α fibres weaken by a factor of nearly 2 after heat treatment. The fall in

γ and α fibre intensities, after heat treatment, is the most drastic in the case of the ELC steel.

Figures 5.4 (c) and (d) Shows the γ fibre plots for the three steels, 830 ^{o}C soaked and single pass rolled after heat treatment. As in the preceding case, recrystallisation annealing seems to improve the intensities of γ fibres of steel 3 by a factor of nearly 1.5, although the γ fibre intensity of the 500 ^{o}C FRT material in steel 2 shows only a marginal improvement. In both the cases the strong intensities at the rotated cube location came down drastically after heat treatment. In the ELC steel, on the other hand, γ fibre intensity decreases drastically after heat treatment.

A comparison of the γ fibre plots of the multipass rolled steels (all three schedules), after heat treatment is shown in Figures 5.5 (c) and (d), 5.6 (c) and (d) and 5.7 (c) and (d). It is clear from these diagrams that there is no improvement in the γ fibre intensities in the ELC or the Nb enriched IF steel in schedule 1; γ fibre of the 500 ^{o}C FRT material in the Ti enriched IF steel, however, shows only a marginal improvement. In schedule 2 there is marked improvement of the γ fibre of the Ti enriched IF steel, heat treatment also brings down the intensities at the rotated cube location in this steel. On the other hand, the two other steels hardly show any change in their γ fibre profiles. In schedule 3, as in the two previous schedules , no change in the γ fibre profiles takes place in the ELC steel after heat treatment. In Nb enriched steel there is a marked and in the Ti enriched steel there is a drastic improvement of the γ fibre intensities due to

recrystallisation annealing. Side by side the intensities of α fibres at the rotated cube location also come down quite heavily.

Thus one thing is very clear. If the γ fibre intensity is quite high in the warm rolled IF steels, these intensities can only improve after recrystallisation annealing, the improvement is more marked in case of the Ti enriched IF steel than in the Nb enriched IF steel. On the other hand, whatever may be the γ fibre intensity, high or low, in the ELC steel, their intensities decrease drastically after annealing.

In this connection it would not be out of place to discuss here the roles played by Ti and Nb in the two IF steels in tying up with the interstitial solute carbon and nitrogen. In the ELC steel the Al added will take care of the nitrogen. The equilibrium solubility of nitrogen in ferrite can be given as (92):

$$N\ (wt\ \%) = 12.3 \exp (-4177 / T) \quad \ldots\ldots(5.1)$$

The critical amount of Al needed to tie up with the N will be 27/14 N(wt %). Therefore, the unreacted Al will be equal to Al(wt%) in steel –27/14 N (wt %), equals to 0.033 (wt %) for the ELC steel, which will remain in solid solution. Therefore, theoretically in the ELC steel the only interstitial that will be left in solution in ferrite during warm rolling will be carbon. The equilibrium solubility of C in ferrite is given by (93)

$$C\ (wt\ \%) = 2.55 \exp (-4850/T) \quad \ldots\ldots(5.2)$$

According to this relationship, the equilibrium C concentration in solution within the ferrite will be 0.027(wt %) at 800 ^{o}C and 0.005 (wt %) at 500 ^{o}C. This shows that the equilibrium carbon concentration is quite high at 800 ^{o}C. It may be recalled that, in general, the warm rolling textures (in most cases) and annealing textures (in all cases) in the ELC steel are rather poor. Obviously, principally C has played an important role in both the cases.

In the Ti – Nb steels, the common practice is to add sufficient amount of Ti to react with N to form TiN, leaving Nb to scavange C as NbC. In the absence of Ti, Al reacts with N to form AlN. However, Ti will also tie up with S and C, if added in sufficient amount. Therefore, individually if only Ti is used to stabilise the steel fully, the minimum amount of Ti (wt %) should be greater than 48/14 N (wt %) + 48/32 S (wt %) + 48/12 C (wt %).

In the Nb enriched steel (Steel 2), the minimum amount of Ti required for full stabilisation for the particular composition of steel, will be 0.037 (wt %). Since the amount of Ti present in this steel is only 0.02 (wt %), it can be shown that theoretically it can take care of the whole of N and only a part of S (~ 0.0064 wt %) present in the steel. Obviously the remaining amount of S will combine with Mn to form MnS. This will lead Nb to take care of the entire carbon in the steel. Calculations show that the amount of Nb present in the steel 2 is sufficient to take care of the entire C, leaving 0.0137 (wt %) Nb free in solution in ferrite.

In the Ti enriched steel (Steel 3), it appears that Ti added was sufficient to take care of N, S and C so as to fully stabilise the steel. Calculations show that the amount of free Ti left after combining with all the N, S and C is 0.0175 (wt %). In this steel, theoretically at least, the entire amount of Nb will be left as free solute in the ferrite matrix.

Reecent work by several authors (62, 63, 66), has however emphasised the importance of formation of Ti carbo-sulphides, $Ti_4C_2S_2$ for fully stabilising the carbon. These studies have clearly indicated that C is principally removed from solid solution by the formation of $Ti_4C_2S_2$. The removal of C by way of precipitation of MC particles (e.g., TiC, NbC) which form epitaxially on the $Ti_4C_2S_2$, represents only a small fraction of carbon bearing precipitates. $Ti_4C_2S_2$ has been found to form exclusively from TiS particles, produced during reheating, by an internal transformation mechanism.

Assuming that C, S and N will be fixed by Ti in the form of $Ti_4C_2S_2$ and TiN, calculations show that in the Nb enriched steel (steel 2), the total amount of Ti needed is 2x1.5 S (wt %) + 3.42 N (wt %), which is equal to 0.040 (wt %). However, the amount of Ti present in this steel is only 0.02 (wt %), i.e., half of the total requirement for full stabilisation. Similar calculations indicate that if the above criteria for C removal is taken into account, the amount of Ti left free in the Ti enriched steel (steel 3) after full stabilisation will be 0.016 (wt %). On this basis it is clear that the Nb enriched steel may not be fully stabilised with respect to the interstitials (C, N), while the Ti enriched steel is. It may be mentioned here that the latter criterion is more suited to the modern day IF steels, while the previous criterion is best suited for conventional HSLA steels (63).

The observed superior γ fibre development in the Ti enriched steel, in comparison to the Nb enriched IF steel, can be due to the absence of required amount of stabilising Ti in the latter. In other words, a larger concentration of free carbon in solution in the ferrite matrix of the Nb enriched steel will be primarily responsible for its poorer γ fibre development after the processing. However, being an IF steel it, of course, displays better texture development than the ELC steel.

5.4 Role of deformation bands in the development of warm rolling and annealing textures

It has been emphasised time and again by the early workers investigating the warm rolling process that the deformation bands produced during warm rolling play a very significant role in texture development during deformation as well as after annealing. In rolled bcc steel, the orientations constituting the γ fibre are the ones with high Taylor factors (5). Therefore, significant amounts of deformation bands are expected to be produced within grains of these orientations during warm rolling. This indeed has been observed by EBSD orientation measurement technique on γ fibre grains of LC and IF steels by Barnett (56). He further reported that the deformation bands in the IF steel are much more fragmented than in the LC grade.

A very important discrepancy has emerged between the present work and that by Barnett and Jonas (6,9) on the role of deformation bands on warm rolling texture development, especially in the LC steel. They have shown that the LC grade displays a higher intensity of overall texture (γ fibre also) with increasing warm rolling temperatur

and shows the sharpest texture at 700 ^{o}C. The intensity of this texture is much higher than the texture of the IF steel, deformed at the same temperature. They ascribed this result to the absence of deformation bands in the microstructure of the LC steel, at the same time arguing that a higher degree of fragmentation of deformation bands present in the IF steel is responsible for this effect.

The present results also demonstrate that the ELC grade does develop a very intense texture (strong γ fibre also) after warm rolling at 500 ^{o}C and 600 ^{o}C. In contrast to the observations of Barnett and Jonas (9) substantial densities of deformation bands could be seen in the corresponding microstructures [Fig. 4.6 (b)]. Thus it is difficult to agree with the contentions of those authors that an intense texture in the ELC grade is due to the absence of deformation bands. In the present work it has been found out that dynamic restoration processes [recovery and recrystallisation (?)] are quite active at warm rolling temperatures of 700 ^{o}C and above. In fact a very weak overall texture (and practically no γ fibre) have been observed after warm rolling at 700 ^{o}C and 800 ^{o}C in the present investigation. An analysis of the present result suggest that the development of warm rolling textures in the ELC and the two IF steels takes place in a manner similar to that in conventional LC and IF steels. However, since warm rolling occurs at temperatures much higher than room temperature, depending on the rolling schedule used, dynamic and (post dynamic) static relaxation processes will come into play and modify the final textures. Since relaxation processes will be much more difficult in the two IF steels due to the presence of Ti and Nb, the warm rolling textures in these steels will not be affected that significantly by the deformation temperature. The effect of deformation temperature will,

however, be most pronounced in the ELC steel where the relaxation processes will come about more easily. The ease or difficulty involved in the operation of relaxation processes to some extent appears to determine the relative density of deformation bands in a particular steel for a particular warm rolling temperature. The presence of higher amount of free solute carbon in the ELC steel is likely to produce a higher density of the bands in that steel, at lower warm rolling temperatures, where the effects of the relaxation processes will be not that significant.

In conventional cold rolled and annealed low carbon and IF steels it is known that γ fibre grains nucleate at grain boundaries whereas grains of other orientations, especially the Goss nucleate at deformation bands (5). Thus, formation of deformation bands is considered deleterious for the attinment of a high γ fibre density.

The present results suggest that the absence or near absence of deformation bands in warm rolled steels, specially at higher temperatures of deformation as in case of the ELC steel, causes a drastic decrement of the γ fibre intensity in the annealed materials. It therefore appears that a reasonable density of deformation bands in warm rolled steels is necessary for achieving a sharp γ fibre in the subsequently annealed material. Barnett (56) also suggested that the deformation bands (in-grain shear bands) play a large role in the nucleation of γ fibre grains during the recrystallisation of warm rolled IF steel.

The question now arises as to how to reconcile these two apparently opposite roles of deformation bands in the warm rolled and annealed vis-a-vis conventionally cold rolled

and annealed materials. The nature of the deformation bands probably plays an important part in this respect. The most prevalent orientation that readily forms deformation bands in steel is the {111} <112> (5). In general it is believed that the deformation bands having a 20° - 35° inclination to the rolling direction are present in the warm rolled steels (41,9). This has also been corroborated by the present results. On the basis of his Taylor simulation of shear in the deformation bands inclined at 20° and 35° to the rolling direction, Barnett (56) observed that the deformation bands in {111}<112> do not always give rise to the Goss orientation by lattice rotation. In fact, lattice rotation to both Goss and near γ fibre orientations are possible, depending on the conditions under which the deformation bands form. He further suggested that the rotation to the Goss are more likely to occur in 35° than in 20° deformation bands. For Goss orientation to be formed, the deformation conditions are much more likely to arise in materials where the driving force for flow localisation is particularly high, as in case of say, conventional cold rolling. The present results [Fig 4.10] have consistently shown that there is a high proportion (more than 60-70%) of the 20-25 $^{\circ}$C deformation bands among all the bands produced in the ELC and the two IF steels during warm rolling. This possibly could be the reason why the grains nucleating at the deformation bands in warm rolled steels contribute to the high intensity of the γ fibre after recrystallisation annealing. It is apparent that much more detailed work is needed to fully characterise the deformation bands produced in the warm rolled steels during deformation. This might hold the key to a much better understanding of the development of annealing textures in these materials.

CHAPTER 6
SUMMARY AND CONCLUSIONS

6. Summary and Conclusions

Three industrially produced steels, an ELC, a Nb enriched IF and a Ti enriched IF steel were investigated to evaluate their microstructural and textural changes after warm rolling and after subsequent recrystallisation annealing.

All the three steels were soaked at two different temperatures – 1150 ^{o}C (in the γ range) and 830 ^{o}C (in the α range) – followed by single pass rolling (~ 80% reduction) with four different FRTs, 800 ^{o}C, 700 ^{o}C, 600 ^{o}C and 500 ^{o}C. Wedge-shaped specimens were used for this purpose. Bar shaped specimens were also subjected to multipass rolling after soaking at 1150 ^{o}C. For this purpose three different rolling schedules were chosen in which different amounts of reduction were given in the γ and in the α range, keeping the total amounts of reduction in the three schedules nearly the same (~ 80%). The following conclusions have been drawn after analysing the results of the present investigation.

1. Flow stress curves generated by hot compression tests indicate that the high temperature γ phase undergoes dynamic restoration processes like recovery and recrystallisation. Dynamic recovery is very much operative when the ferrite is warm rolled within the upper α range such as at 800 ^{o}C and 700 ^{o}C. Post-dynamic static relaxation processes occur during interpass holding times in multipass rolling. The above observations are also corroborated by the relevant SEM and TEM microstructures of the steels.

2. The microstructures of the warm rolled steels display the presence of a high density of deformation bands (DB). After single pass rolling, the ELC steel shows the highest density of DB at the FRT of 500 ^{o}C, which decreases drastically with increasing FRT, assuming nearly zero value at an FRT of 800 ^{o}C. Samples soaked at the higher temperature (1150 ^{o}C) have slightly higher DB densities than the ones soaked at the lower temperature (830 ^{o}C). The DB densities in the multipass rolled steel are rather low, the samples subjected to the schedule 3 showing higher DB density than those subjected to the two other schedules. The microstructures of the 800 ^{o}C and 700 ^{o}C FRT materials also show predominantly signs of recovery and some recrystallisation.

3. The deformation band densities in the two IF steels, after single pass as well as multipass rolling, do not show much variation with composition, soaking temperature or FRT. Their values are slightly on the lower side in the multipass rolled than in the single pass rolled materials.

4. The deformation bands make a series of angles with the rolling direction, starting from rather low angles going up to ~ ± 35^{o}. Deformation bands with angles up to ± 25^{o} constitute nearly 80 to 90 percent of the cumulative frequency. The band angles do not show any significant correlation with steel composition, soaking temperature, FRT and relative amounts of deformation given in the γ and α regions during multipass rolling.

5. The normalised dislocation density values in all the three steels, single pass as well as multipass rolled, have the highest value at 500 ^{o}C FRT, decreasing rapidly with

increasing FRT. The rate of this decrease is slower in the two IF steels than in the ELC grade. In general, the levels of normalised dislocation densities are somewhat higher in the single pass rolled than in the multipass rolled materials.

6. Sharp overall texture and high intensity of the γ fibre are obtained in the ELC steel after single pass rolling at the FRTs of 500 ^{o}C and 600 ^{o}C. However, the γ fibre intensity reduces to near zero at higher FRTs of 700 ^{o}C and 800 ^{o}C. Moderately strong γ fibres develop in both the IF steels after single pass rolling at all the four FRTs. A high value of the γ fibre intensity appears to be related to the presence of a high deformation band density.

7. Post warm rolling annealing, in general, sharpens the γ fibre intensities in both the IF steels; by contrast, annealing drastically reduces the γ fibre intensities in the ELC steel.

8. In general, multipass rolling does not produce as sharp overall textures and high intensities of γ fibre as are obtained after single pass rolling. Among the three steels, the ELC grade shows the least sharp texture. Slight improvements in γ fibre intensities after post warm rolling annealing occurs in both the IF steels; the effect of annealing is insignificant in case of the ELC steel. The maximum improvement in γ fibre intensity on annealing is obtained in schedule 3 and minimum in schedule 1 of the multipass rolling process.

9. Out of the two IF steels, the Ti enriched steel develops stronger γ fibres, specially after single pass rolling, which further improve in intensity after post warm rolling annealing. Stoichiometric calculations indicate that out of these two steels, the Nb enriched one may not be fully stabilised with respect to carbon, while the Ti enriched steel very much is. This will allow a higher amount of free solute carbon atoms in the ferrite matrix in the Nb enriched steel, and this could be responsible for the attainment of poorer γ fibres in that steel. The ELC steel, without any Ti or Nb, is expected to have a very large concentration of free solute carbon atoms in the ferrite and this is supposed to be largely responsible for the development of very poor γ fibres in this alloy, specially after recrystallisation annealing.

10. In an attempt to rationalise the seemingly contradictory roles played by deformation bands in the development of γ fibres in conventional cold rolled and annealed low carbon steels and in warm rolled and annealed ELC and IF grade steels, a suggestion is made here that, among deformation bands, those which make angles of $\sim 20 \pm 5^{o}$ with the rolling direction may be responsible for the nucleation of γ grains in them. The higher angle deformation bands may be preferred sites for the nucleation of grains with orientations other than the γ. Evidently further detailed work is necessary in this direction.

REFERENCES

References

1. A. tomitz and R.Kasper Steel research, 71 (2000), p. 233.
2. S. Mishra and C. Darmann, Int. Met. Rev., 27 (1982), p. 307.
3. W.B. Hutchinson, Int. Met. Rev., 29 (1984), p. 25.
4. R.K. Ray and J.J. Jonas, Int. Mater. Rev., 35 (1990), p. 1.
5. R.K. Ray, J.J. Jonas and R.E. Hook, Int. Mater. Rev., 39 (1994), p. 129.
6. M.R. Barnett and J.J. Jonas, ISIJ Int., 39 (1999), p. 856.
7. T. Senuma and H. Yada: Int. Conf. on Thermomechanical Processing of Steels and Other Materials (THERMECH'88), ed. by I. Tamura, TMS-AIME, Warrendale, PA (1988), p. 386.
8. T. Senuma, H. Yada, R. Shimizu and J. Harase, Acta Metall. Mater., 38 (1990), p. 2673.
9. M. R. Barnett and J. J. Jonas, ISIJ Int., 37 (1997),p. 697.
10. M. R. Barnet and J. J. Jonas, ISIJ Int., 37 (1997), p. 706.
11. M. Unemoto, A. Hiramatsu, A. Moriya, T. Watanabe, S. Nanba, N. Nakajima, G. Anan and Y. Higo: ISIJ Int., 32, (1992), p. 306.
12. H. Langner and W. Bleck, 40th MSWP Conf. Proc. ISS, Vol XXXV (1998), p. 345.
13. P. Harlet, F. Beco, P. Cantinieaux, D. Bouquegneau, P. Messien and J. C. Herman, Int. Symp. On Low C Steels for the 90's ed. by R. Asfahani and G. Tither, TMS-AIME, Warrendale, PA, (1993), p. 389.
14 P. A. Bagshaw and R. J. Kimber: Int. Conf. on Thermo-mechanical Processing of Steels and Other Materials (THERMEC'97), ed. by T. Chandra and T. Sakai, TMS-AIME, Warrendale, PA, (1998), p. 147.

15 Y. Saito, Trans. ISIJ, 27 (1987), p. 419.

16. A. Laasraoui and J. J. Jonas, Metall. Trans. A, 22A (1991), p. 1545.

17. S.B. Davenport, N.J. Silk, C.N. Sparks and C.M. Sellars, Mater. Sci. and Technol., 16 (2000), p. 539.

18. A.S. Keh and S. Weissmann, Electron Microscopy and the Strength of Crystals, ed. by G. Thomas and J. Washburn, Interscience, New York, (1963), p. 231.

19. J. D. Baird and A. Jamieson, J. Iron Steel Inst., (1966), p. 793.

20. M. R. Barnett, Modern LC and ULC Sheet Steels for Cold Forming: Processing and Properties, ed. by W. Bleck, Verlag Mainz, Aachen, (1998), p. 61.

21. M. R. Barnett, Materials '98, ed. by M. Ferry, IMEA, Wollongong, (1998), p. 167.

22. J. Glen, J. Iron Steel Inst., (1957), p. 21.

23. G. Glover and C. M. Sellars, Metall. Trans., 4 (1973), p. 765.

24. R. D. Doherty, D. A. Hughes, F. J. Humphreys, J. J. Jonas, D. Juul Jensen, M. E. Kassner, W. E. King, T. R. McNelly, H.J. McQueen and A.D. Rollet, Mater. Sci. Eng., A238 (1997), p. 219.

25. E. Bull Simsonsen and J.M. Dossin, J. Iron Steel Inst., 203 (1965), p. 380.

26. Y. Matsubara, N. Tsuji and Y. Saito, Int. Conf. on Thermomechanical Processing of Steels and Other Materials (THERMECH'97), ed. by T. Chandra and T. Sakai, TMS-AIME, Warrendale, PA, (1997), p. 653.

27 A. Najafi-Zadeh, J. J. Jonas and S. Yue, Metall. Trans. A, 23A, (1992), p. 2607.

28. R. Z. Wang and T. C. Lei, Scr. Met Mater., 31 (1994), p. 1193.

29. S. Gohda, K. Watanabe and Y. Hashimoto, Trans. ISIJ, 21 (1981), p. 6.

30. Y. Ishida, C.Y. Cheng and J.E. Dom, Trans TMS - AIME, 236 (1966), p. 964.

31. H.W. Wagenaar, Iron and Steel Inst., London, spec. Report No. 108, (1968), p. 38.

32. A. Belyakov, R. Kaibyshev and T. Sakai, Metall. Trans A, 29A (1998), p. 161.

33. N. Tsuji, Y. Matsubara and Y. Saito, Scripta Materialia, 27 (1997), p. 477.

34. J. Baczynski and J. J. Jonas, Metall. Trans. A, 29A (1998), p. 447.

35. S. Gourdet and F. Monthelliet, J. Phys., 5 (1994), p. 255.

36. G. E. Dieter, Mechanical Metallurgy, McGraw-Hill, London, (1988).

36. A.S. Keh, Y. Nakada and W.C. Leslie, Dislocation dynamics, ed. by A.R. Rosenfield, G.T. Hahn, A.L. Bemment and R.I. Jaffee, Mc Graw - Hill, New York, (1967), p. 381.

38. T. Takeyama and H. Takahashi, Trans. ISIJ, 13 (1973), p. 293.

39. R. J. McElroy and Z. C. Szkopiak, Int. Met. Rev. 17 (1972), p. 175.

40. J. J. Jonas, C. M. Sellars and W. J. McG. Tegart, Metall. Rev., Review 130, (1969), p.1.

41. G. H. Akbari, C. M. Sellars and J. J. Whiteman, Acta Metall. Mater., 45 (1997), p. 5047.

42. C.S. Lee, B.J.Duggan and R.E. Smallman, Acta Metall. Mater., 41(1993), p. 2265.

43. M. Hatherly and A.S. Malin, Scripta Metallurgica, 18 (1984), p. 449.

44. C.S. Lee and B.J. Duggan, Acta Metall. Mater., 30 (1993), p. 2691.

45. C.S. Lee and B.J. Duggan, Acta Metall. Mater., 41 (1993), p. 2265.

46. C.S. Lee, R.E. Smallman and B.J. Duggan, Scripta Metal Mater.,33 (1995), p. 727.

47. D.A. Hughes, and N. Hansen, Mettall. Trans A, 24A (1993), p. 2021.

48. J.H. Cairns, J. Clough, M.A.P Dewey and J. Nutting, J. of Inst. of Metals, 99 (1971), p. 93.

49. S. Horiuchi, K. Asaura, G. Wassermann and Grewen, J. of Texture., 2 (1975), p. 17.

50. A.S.Malin and M.hatherly, Metal Science, 8 (1979), p. 463.

51. A.N. Beyakov and R.O. Kaibyshev, Phys. Met. Metallogr.,76 (1993), p. 162.

52. G.A. Salishchev, R.G. Zaripova, A.A. Zakirova and H.J. McQueen, Hot Workability of Steels and Light Alloys - Composites, ed by H.J. McQueen, E.V.Konopleva and N.D. Reyan, TMS - CIM, Montreal, (1996), p. 217.

53. S. Dymek and M. Bilcharski, Z. Metallkd.,76 (1985), p. 777.

54. C.S. Barrett, Trans. AIME, 135 (1939), p. 296.

55. S. L. Semiatin and J. J. Jonas: Formability and Workability of Metals-Plastic Instability and Flow Localisation, ASM, Metals. Park, Ohio (1984 , p. 43.

56. M. R. Barnett: ISIJ Int., 38,1 (1998), p. 78.

57. S. Matsouoka, K. Sakata, S. Satoh and T. Kato:,Textures Microstruct., 22 (1993), p. 113.

58. A. Tomitz and R. Kasper, Steel Reaearch, 71, (2000), p. 497.

59. T. Sakai, Y. Saito and K. Kato, Trans. ISIJ, 28 (1988), p. 1037.

60. Y. Shimizu, Y. Ito and Y. Iida, Metall. Trans. A, 17A (1986), p. 1323.

61. M. R. Barnett: BHP Steel, unpublished work, (1998).

62. M.Hua, C.I. Garcia and A.J.DeARDO, Metall. Trans A, 28A (1997), p. 1769.

63. C. Huang, E.B. Hawbolt and T.R. Meadowcroft, Can. Met. Quarterly, 39 (2000), p. 369.

64. S.V. Subramanian and M. Prikryl, Developments in the Annealing of Sheet Steels, ed. by R. Pradhan and I. Gupta, The Minerals, Metals and Materials Society, (1992), p. 219.

65. D.O. Wilshynsky - Dresler, G.Krauss and D.K. Matlock, Developments in the Annealing of Sheet Steels, ed. by R. Pradhan and I. Gupta, The Minerals, Metals and Materials Society, (1992), p. 191.

66. G. Dupuis, R.A. Hubert and R. Tailard, 40th MSWP Conference Proc. ISS, Vol XXXV (1998), p. 117.

67. P. R. Cetlin, S. Yue, J. J. Jonas and T. M. Maccagno, Metall, Trans, A, 24A (1993), p. 1543.

68. B.Dutta and C.M. Sellars, Mater. Sci.Technol., 3, (1987), p. 197.

69. D. Vanderschueren, N. Yoshinaga and K. Koyama, ISIJ Int., 36 (1996), p. 1046.

70. T. Senuma, Modern LC and ULC Sheet Steels for Cold Forming: Processing and Properties, ed. by W. Bleck, Verlag Mainz, Aachen, (1998), p. 157.

71. B. J. Duggan, H. Ning and L. X. Zhang, Int. Conf. On Thermomechanical Processing of Steels and Other Materials (THERMECH'97), ed. by T. Chandra and T. Sakai, TMS, Warrendale, PA, (1998), p. 157.

72. W. Truszkowski, J. Krol and B. Major, Metall. Trans A, 11A (1980), p. 749.

73. B. Major, Material, Mater. Sci.Technol., 8 (1992), p. 515.

74. D. Raabe, J. Mater. Sci., 30 (1995), p. 47.

75. M.Y. Huh, C.J. Park and S.Lee, Metal and Mater, 2 (1996), p. 141.

76. M.Y. Huh, Y.S. Cho and O. Engler, Mater. Sci. Eng., A 247 (1998), p. 152.

77. Y.B. Park, D.N. Lee and G. Gottstein, Mater. Sci. Technol., 13 (1997), p. 289.
Y.B. Park, D.N. Lee and G. Gottstein, Acta Metall. Mater., 44 (1996), p. 3421.

78. M.Y. Huh, Y.S. Cho, J.S. Kim and O. Engler, Z. Metallkd., 90 (1999), p. 2.

79. M.Y. Huh, H.C. Kim and O. Engler, Steel Research, 71. (2000), p. 239.

80. S. Matsuoka, M. Morita, O. Furukimi and T. Obara, ISIJ Int., 38 (1998), p. 633.

81. T. Senuma and K. Kawasaki, ISIJ Int., 34 (1994), p. 51.

82. P. Messien and J. Herman , Int. Symp. On Low C Steels for the 90's, Ed. by R. Asfahani and G. Tither, TMS-AIME, Warrendale, PA, (1993), p. 383.

83. S. Matsuoka, K. Sakata, O. Furukimi and T. Obara, Modern LC and ULC Sheet Steels for Cold Forming: Processing and Properties, ed. by W. Bleck, Verlag Mainz, Aachen, (1998), p. 85.

84. K. M. Browne, J. Dryden and M. Assefpour, Recent Advances in Heat Transfer and Micro-Structure Modelling for Metal Processing, , ed. by R-M. Guo and J. J. M. Too, ASME, New York, MD-Vol. 67 (1995), p. 187.

85. W. H. Parks, C. S. Haggerty and T. R. Rock, Iron Steel Eng., (1997), p. 35.

86. A.D. Paepe and J.C. Herman, 41st MSWP Conference Proc. ISS, Vol XXXVII (1999), p. 951.

87. K. Eloot, K. Okuda, K. Sakata and T. Obara, ISIJ Int., 38 (1998), p. 602.

88. A. Tomitz and R. Kasper, Steel Research, 71 (2000), p. 504.

89. J. G. Sevillano , P. van Houtte and E. Aernoudt, Prog. Mater. Sci., 25 (1980), p. 69.

91. H.J. Bunge "Texture analysis in Materials Science", Butterworths, (1982).

90. J.D. Fast, Interaction of Metals and Gases, Academic press, New York, (1965).

92. C.A. Wert, Trans AIME, 188(1950), p. 1242.